

**CASSON-WHITNEY UNKNOTTING, DEEP SLICE
KNOTS AND GROUP TRISECTIONS OF KNOTTED
SURFACE TYPE**

Dissertation

zur

Erlangung des Doktorgrades (Dr. rer. nat.)

der

Mathematisch-Naturwissenschaftlichen Fakultät

der

Rheinischen Friedrich-Wilhelms-Universität Bonn

vorgelegt von

BENJAMIN MATTHIAS RUPPIK

aus

Aachen

BONN 2022

Angefertigt mit Genehmigung der Mathematisch-Naturwissenschaftlichen Fakultät der Rheinischen Friedrich-Wilhelms-Universität Bonn

Gutachter: Prof. Dr. Peter Teichner
Gutachter: Dr. Daniel Kasprowski
Gutachter: Assoc. Prof. Dr. Mark Powell

Tag der Promotion: 07.06.2022
Erscheinungsjahr: 2022

SUMMARY

In this thesis, we study knotted surfaces in 4-dimensional manifolds from three different but interconnected perspectives.

In the first part, we introduce a measure of ‘distance’, or rather ‘length’, between regularly homotopic knotted surfaces in 4-manifolds via the minimal length of a regular homotopy. For knotted surfaces in the 4-sphere, it is natural to consider the smallest number of finger moves and Whitney moves in such a regular homotopy to an unknotted surface, which is defined to be the *Casson-Whitney number*. This number is closely related, but not equal, to the stabilization number of a surface. We give lower bounds on this unknotting number coming from the fundamental group of the complements and construct explicit regular homotopies for ribbon surfaces. The Casson-Whitney number of surfaces arising from rim surgery is related to the classical unknotting number of the pattern knot. We close the section by considering the Casson-Whitney number of a family of knotted surfaces, each with trefoil knot group, that was originally constructed by Suci.

In the second part, we move to the relative setting and study surfaces with knotted boundaries properly embedded in non-closed 4-manifolds. We then distinguish such knots in the boundary which have slice disks embedded in a collar (so called *shallow slice knots*) from knots which are slice in the 4-manifold, but the slice disks always need to go far away from the 3-manifold boundary (so called *deep slice knots*). In 4-dimensional 1-handlebodies, every slice knot is automatically shallow slice. On the other hand, every 4-dimensional 2-handlebody which is not the 4-ball contains deep slice knots in the boundary.

In addition, we compare topological and smooth shallow and deep sliceness. We construct infinitely many non-local null-homotopic knots in the boundary of the (-1) -trace of the left-handed trefoil which are topologically shallow slice, but smoothly deep slice. For this result, topological constructions employing Casson towers and a result of Freedman are contrasted with smooth sliceness obstructions in products of a 3-manifold with an interval. We recall the immersed curve language for bordered Heegaard Floer homology, and use it to reprove special cases of the formulas for the τ -invariants for Whitehead doubles and cables. Various generalizations to links are discussed as well, in particular constructing examples of links for which every proper sublink is shallow slice but the link as a whole is deep slice.

Then we consider 4-manifolds where every knot in the boundary bounds an embedded disk in the interior. On the contrary, we show that every compact oriented topological 4-manifold V^4 with $\partial V = \mathbb{S}^3$ contains a knot in its boundary that does not bound a null-homologous embedded disk in V , i.e there exists a knot which is not topologically H -slice in V .

In the third part, we define *group trisection of knotted surface type* for bridge trisected surfaces in the 4-sphere. This is a decomposition of the fundamental group of the complement of the surface into three group epimorphisms from a punctured sphere group onto three free groups, with a pairwise compatibility condition. This datum not only allows recovering the group, but also the whole bridge trisection of the knotted surface, and we give many examples together with a computer implementation.

ACKNOWLEDGEMENTS

First and foremost, I want to thank my thesis advisors Arunima Ray and Peter Teichner of the Max-Planck-Institute for Mathematics in Bonn. Thank you for guiding me through this journey! I always knew that I could come to you with questions about my research and writing, and for advice about academia and daily life. Dear Aru, I've learned a lot from our weekly meetings (both virtually and in person), and thoroughly enjoyed the puns. I cannot imagine having a better advisor and mentor!

My studies were funded by the Max Planck Institute for Mathematics in Bonn, which provided office space and perfect working conditions, with a very welcoming administration and library staff.

I want to thank Peter Teichner, Wolfgang Lück, Daniel Kasproski, Mark Powell, and Albrecht Klemm for agreeing to be my committee members, and our IMPRS Coordinator Christian Kaiser for his help.

The exposition benefited from detailed referee reports I received after submitting parts of this thesis to journals.

Working with my coauthors Jason Joseph, Daniel Kasproski, Michael Klug, John Nicholson, Mark Powell and Hannah Schwartz was fun and refreshing, and even though we were separated by a pandemic for most of the time, it could not have gone better.

It was a pleasure to participate (virtually) in various trisection-themed workshops organized by Jeffrey Meier and Alexander Zupan. This led to exciting collaborations with Sarah Blackwell, Patricia Cahn, Rob Kirby, Vincent Longo, and Gordana Matic. Thank you Maggie Miller and Puttipong Pongtanapaisan for making me laugh and teaching me about U.S. culture. I have benefited enormously from David Gay's and Rob Schneiderman's advice and guidance.

Dear Bertram Arnold, Daniel Brüggemann, Julian Brüggemann, Fabian Henneke, Hyeonhee Jin, Danica Kosanović, Luuk Stehouwer, Simona Veselá, you were great office-mates and colleagues! Thank you Danica for sharing your \LaTeX -template and answering all of my questions! Thank you Anthony Conway, Sashka Kjuchukova, Filip Misev, Sümeyra Sakallı, Rachael Boyd, Thorben Kastenholz for organizing interesting seminars and always generously sharing your knowledge.

I thank Wenzhao Chen, Matthew Hedden, Tom Hockenhull, Jen Hom, Katherine Raoux for comments on the Heegaard Floer calculations. I am grateful to Marc Kegel for teaching me how to use SnapPy and for very helpful comments on computations with contact surgery diagrams. Visiting Regensburg and talking to Stefan Friedl and Lukas Lewark was always inspiring, thank you for the invitations!

Kevin Li, José Pedro Quintanilha, Yuqing Shi, thank you for being great friends, it was a wonderful time with you together in Bonn!

Danke Annika, Barbara, Wolfgang und Vincent, dass ihr immer für mich da seid!

February, 2022

CONTENTS

<i>List of Figures</i>	vii
<i>List of Tables</i>	ix

INTRODUCTION

1 Overview of parts	4
2 Statements of the new results	13

I CASSON-WHITNEY UNKNOTTING

3 Regular homotopies of surfaces and stabilization	19
3.1 The Casson-Whitney length 19	
3.2 The stabilization number 22	
3.3 Fundamental group calculations 23	
3.4 Algebraic lower bounds 26	
4 Rim surgery and Casson-Whitney length	29
4.1 Twist rim surgery and the accordion homotopy 29	
5 Stabilization length versus Casson-Whitney length	41
6 Ribbon knots and Casson-Whitney length	46
6.1 Fusion number upper bound on Casson-Whitney length 46	
6.2 Handle ribbon 2-knots and Casson-Whitney length 50	
6.3 Suciu's family of ribbon 2-knots and Casson-Whitney length 53	

II DEEP AND SHALLOW SLICE KNOTS IN 4-MANIFOLDS

7 Definition of deep slice knots	66
7.1 First examples 68	
7.2 Concordances in non-orientable 3-manifolds 69	
8 Deep slice knots in 2-handlebodies	71
8.1 Deep slice knots in 2-handlebodies with simply connected boundary 71	
8.2 Obstructing topological shallow sliceness with genus bounds 73	
8.3 Overview: The Schneiderman-Wall μ -invariant 75	
8.4 Deep slice knots in 2-handlebodies with non-simply connected boundary 76	
9 Comparing smooth and topological deep and shallow sliceness	78
9.1 Relation to previous work 79	
9.2 Knot Floer homology in integral homology 3-sphere L-spaces 80	
9.3 Construction of topological shallow and smooth deep slice knots 98	
9.4 An infinite family of examples 112	
10 Deep slice links	122
10.1 Existence of deep slice links 122	
10.2 Topological shallow versus smooth deep slice for links 126	
11 The Norman-Suzuki-trick and universal slicing problems	129
12 Conclusion and open questions related to deep sliceness	131

III TRISECTING GROUPS OF KNOTTED SURFACE COMPLEMENTS

13	Group trisections of closed 4-manifolds and bridge trisections	134
13.1	Definition of group trisections of knotted surface type	135
13.2	The free group characterizes unlinks	139
14	Trivial tangles in the 3-ball from group epimorphisms	141
14.1	Stallings folding	145
15	Computing epimorphisms from triplane diagrams	148
15.1	Choosing Wirtinger generating meridians for trivial tangles	148
15.2	Documentation of the SageMath module	154
16	Group trisections of twist-spun torus knots	157
16.1	Bridge trisections of twist spun 2-bridge torus knots	158
16.2	Bridge trisections of twist spun 3-bridge torus knots	161
17	Suciu's trefoil group	164
17.1	Bridge trisections of Suciu's knots	164
17.2	Group trisections of Suciu's knots	165
18	Conclusion and further directions for studying group trisections of knotted surface type	167
18.1	Appendix: Group trisection data	168
	<i>References</i>	171
	<i>Index</i>	183
	<i>Curriculum Vitae</i>	185

LIST OF FIGURES

1	<i>Finger and Whitney move</i>	20
2	<i>Unknotted projective plane</i>	20
3	<i>Regular homotopy</i>	22
4	<i>Stabilization of a surface</i>	23
5	<i>Meridians and guiding arcs</i>	24
6	<i>Boundary twist</i>	25
7	<i>Fundamental group after stabilization and finger move</i>	25
8	<i>Schematic illustration of rim surgery</i>	30
9	<i>Local situation close to the curve $\alpha \subset F$ before and after rim surgery</i>	31
10	<i>Accordion homotopy</i>	32
11	<i>After the accordion homotopy</i>	33
12	<i>Schematic for the spin $\tau^0 k$ and the twist spins $\tau^n k$ of a 1-knot k</i>	34
13	<i>Finger moves on twist spins</i>	35
14	<i>Tubing an immersed surface along an arc</i>	41
15	<i>Local pictures of the spheres U_g and K given by Whitney moves on the immersion Σ</i>	43
16	<i>Trefoil 3_1 and figure eight 4_1 as plumbings of Hopf bands</i>	45
17	<i>Genus 1 cobordism between the trefoil 3_1 and figure eight 4_1</i>	45
18	<i>Miyazaki's proof that $u_{st}(K) \leq \text{fus}(K) - g$ for ribbon surfaces K</i>	47
19	<i>Proof of the fusion number upper bound</i>	49
20	<i>Regular homotopy and the Tube map</i>	51
21	<i>Saddle moves for Suciu's knot R_2</i>	55
22	<i>Banded unlink diagram of Suciu's knot R_3</i>	55
23	<i>R_3 stabilized between the minima c and d</i>	56
24	<i>Isotopy from stabilization between c and d to unknotted torus</i>	57
25	<i>Isotopy of the immersion after a finger move with relation $[c, d]$ on $R_k \# \mathbb{RP}^2$ for k odd</i>	62
26	<i>Isotopy of the immersion after a finger move with relation $[c, d]$ on $R_k \# \mathbb{RP}^2$ for k even</i>	63
27	<i>Topological shallow and deep sliceness</i>	67
28	<i>Smooth shallow and deep sliceness</i>	67
29	<i>Punctured genus 1 surface as movie in non-orientable 3-manifold</i>	70
30	<i>Schematic of surface in 2-handlebody</i>	73
31	<i>Pattern of the (a, b)-shake satellite, here for $(a, b) = (2, 3)$</i>	74
32	<i>Topological deep slice knot in a bounded punctured $\mathbb{S}^2 \times \mathbb{S}^2$</i>	75
33	<i>t-twisted positively clasped Whitehead pattern $\text{Wh}_+(U, t)$ in the solid torus</i>	76
34	<i>Whitehead double of framed meridian</i>	77
35	<i>Track of a homotopy from Whitehead double to unknot</i>	77
36	<i>Schematic of the 4-manifold $(Y \times [0, 1]) - \nu(a)$ after drilling out an open tubular neighborhood of an arc a on a concordance</i>	80
37	<i>Doubly pointed bordered genus one Heegaard diagram of the Whitehead pattern</i>	82
38	<i>Immersed curve for the cable $K = (T_2, -3)_{2,5}$</i>	88
39	<i>Bordered Heegaard diagram for the 0-twisted Whitehead pattern</i>	90
40	<i>Pairing diagram for the Whitehead double pattern</i>	91
41	<i>Pairing diagram in universal cover</i>	91
42	<i>Pairing diagram in universal cover with single lifts</i>	92
43	<i>Pairing diagram with Alexander filtration and first Whitney moves of filtration difference zero</i>	92

44	<i>After Whitney moves with filtration difference 1</i>	93
45	<i>Eleven intersection points remaining</i>	93
46	<i>Alexander filtration of remaining intersection point encodes the τ-invariant</i>	94
47	<i>Cancellations of intersections in the case where the companion has $\tau(Y, C) > 0$</i>	96
48	<i>Cancellations of intersections in the case where the companion has $\tau(Y, C) < 0$</i>	97
49	<i>Different ways of drawing the dual curve in the Poincaré homology sphere in a surgery diagram of $\mathbb{S}_{-1}^3(T_{2,-3})$.</i>	99
50	<i>Longitudes of the dual curve in the surgery diagram $\mathbb{S}_{-1}^3(T_{2,-3})$.</i>	99
51	<i>Whitehead double of a knot in the boundary of a 4-manifold</i>	102
52	<i>Null-homotopy of the t-twisted Whitehead double $\text{Wh}_+(l, t)$</i>	102
53	<i>Iterated doubles of the dual curve \tilde{K} in $\mathbb{S}_{-1}^3(T_{2,-3})$</i>	106
54	<i>Schematic of a height 3 Casson tower</i>	108
55	<i>Dual curve in contact surgery diagrams of the tight contact structure on the Poincaré homology sphere</i>	111
56	<i>(+1)-parallel and positive Whitehead double of the dual curve in $Y = \mathbb{S}_{-1}^3(T_{2,-3})$.</i>	111
57	<i>($p, 1$)-pattern in the solid torus</i>	112
58	<i>Bordered Heegaard diagram with β-curve for ($p, 1$) cable pattern, in the case $p = 5$</i>	114
59	<i>Pairing diagram of the β-curve of the ($5, 1$)-pattern with the immersed curve for $T_{2,3}$ in the universal cover</i>	115
60	<i>Single lift of the β-curve of the ($5, 1$)-pattern and the immersed curve for $T_{2,3}$</i>	116
61	<i>Cancellations of intersection points with filtration difference 1, followed by cancellation with difference 2, then 3 and then 4</i>	117
62	<i>Final Whitney move removing a pair of intersection points with filtration difference 5</i>	118
63	<i>Remaining intersection point with Alexander filtration for $\tau \neq 0$ and $\varepsilon \neq 0$ of the companion</i>	119
64	<i>Remaining intersection point for $\tau(Y, C) > 0$ and $\varepsilon(Y, C) = +1$</i>	120
65	<i>Remaining intersection point for $\tau(Y, C) < 0$ and $\varepsilon(Y, C) = -1$</i>	120
66	<i>Initial and final position of the β-curve for the ($p, 1$)-pattern</i>	121
67	<i>Bing double of meridian</i>	123
68	<i>Fusion band from Bing to Whitehead</i>	123
69	<i>Disjoint Seifert surfaces with a choice of basis for the components of $J = \text{Wh}_{+,1}(\text{BD}(\alpha, 0), 0)$</i>	125
70	<i>Double branched cover over the component L_1</i>	128
71	<i>Pieces of a (parameterized) trisection</i>	134
72	<i>Pieces of a (parameterized) b-bridge trisection</i>	135
73	<i>Sphere with $2b$ marked points p_1, \dots, p_{2b} and generators of π_1</i>	136
74	<i>Seifert-van Kampen cube associated to bridge trisection</i>	137
75	<i>Definition of a group trisection of knotted surface type.</i>	138
76	<i>Bridge disk and bubble disk</i>	141
77	<i>Shadow arcs and dual loops</i>	143
78	<i>Intersection point signs and Wirtinger relation</i>	143
79	<i>Cutting along bridge disks</i>	144
80	<i>Setup for Stallings folding</i>	145
81	<i>Step and goal of Stallings folding</i>	146
82	<i>Meridians of a trivial tangle</i>	150
83	<i>Unsuccessful Wirtinger seed strands</i>	150
84	<i>Wirtinger process with seed strands at the maxima</i>	151
85	<i>Stallings folding sequence for the images of x_0 and x_1</i>	152
86	<i>Stallings folding sequence for the images of x_0 and x_3</i>	152

87	<i>Stallings folding sequence for the images of x_1 and x_2</i>	152
88	<i>Stallings folding sequence for the images of x_2 and x_3</i>	153
89	<i>Triplane diagram of a 4-bridge trisection of an 1-twist spin of the $(2, n)$-torus knot, $\tau^1 T_{2,n}$</i>	158
90	<i>Triplane diagram of a 4-bridge trisection of the 3-twist spin of the $(2, 5)$ torus knot, $\tau^3 T_{2,5}$</i>	159
91	<i>$(3, 5)$ torus knot as a 3-bridge plat closure</i>	161
92	<i>Triplane diagram of a 7-bridge trisection of an 1-twist spin of the $(3, n)$ torus knot, $\tau^1 T_{3,n}$</i>	162
93	<i>Triplane diagram of a 7-bridge trisection of the 2-twist spin of the $(3, 5)$ torus knot, $\tau^2 T_{3,5}$</i>	162
94	<i>Final pushout of 7-bridge group trisection of knotted surface type of $\tau^2 T_{3,5}$</i>	163
95	<i>Simplification isomorphism of the group presentation for $\pi_1(\mathbb{S}^4 - \tau^2 T_{3,5})$</i>	163
96	<i>Banded bridge position of Suciu's knot R_3</i>	164
97	<i>Triplane diagram of 7-bridge trisection of Suciu's knot R_3</i>	165
98	<i>Alternative banded bridge position for Suciu's knot R_k</i>	166

LIST OF TABLES

1	<i>Trivial_tangle.add_crossing() method</i>	153
2	<i>Trivial_tangle.group() method</i>	156
3	<i>Relations for the α-tangle in the group trisection of Suciu's R_3</i>	168
4	<i>Relations for the α-tangle in the group trisection of Suciu's R_3, continued.</i>	169
5	<i>Relations for the α-tangle in the group trisection of Suciu's R_3, continued.</i>	170

INTRODUCTION

In this thesis, we study different notions of measuring the ‘complexity’ of embedded and immersed surfaces living in ambient 4-manifolds. We develop a length between homotopic embeddings, distinguish properly embedded surfaces which reside in a collar of the boundary from those which go deep into the 4-manifold, and lastly define a group-theoretic analogue of bridge trisections in the 4-sphere. Before we outline the motivation and content of each part in more detail, we want to advertise the study of knotted surfaces in 4-manifolds by introducing two typical paradigms of the field; these are the dichotomy of the smooth and topological settings, and classification questions.

Comparing the smooth and topological categories. In contrast to 1-, 2- and 3-dimensional manifolds, for which the topological and smooth categories are ‘essentially equivalent’, from dimension 4, they start to exhibit very different behavior. More precisely, the slogan that the categories are ‘essentially equivalent’ means that for $n = 1, 2, 3$, every topological n -manifold can be given a smooth structure, and every homeomorphism between smooth n -manifolds is isotopic to a diffeomorphism. Thus for these dimensions n , the smooth structure of a topological n -manifold is unique up to diffeomorphism.

The difference between topological and smooth 4-dimensional topology manifests itself in various different ways: The *smooth 4-dimensional Poincaré conjecture* (SPC4) proposes that every closed smooth 4-manifold Σ that is homotopy equivalent to \mathbb{S}^4 is diffeomorphic to the standard \mathbb{S}^4 . A closed smooth 4-manifold Σ that is homotopy equivalent to \mathbb{S}^4 is called a *smooth homotopy 4-sphere*. If such a Σ is not diffeomorphic to the 4-sphere equipped with the standard smooth structure, it is called *exotic*. In general, we call a pair of smooth 4-manifolds *exotic* if they are homeomorphic, but not diffeomorphic. The existence of an exotic homotopy 4-sphere is equivalent to the existence of a smooth contractible compact manifold with \mathbb{S}^3 boundary which is not diffeomorphic to the standard 4-ball [Mil65, p. 113], henceforth called an *exotic homotopy 4-ball*.

By work of Freedman [Fre82], it is known that if a closed topological 4-manifold Σ is homotopy equivalent to \mathbb{S}^4 , then Σ is in fact homeomorphic to \mathbb{S}^4 . Additionally, Freedman-Quinn [FQ90, Ch. 10.1] obtained a topological classification of closed simply connected topological 4-manifolds. Thus while the *topological 4-dimensional Poincaré conjecture* (TPC4) has a positive solution, the SPC4 remains open. In stark contrast to the SPC4, it might be the case that every compact smooth 4-manifold admits infinitely many distinct smooth structures. The classification question of smooth structures can be split into two sub-tasks:

- **Geography:** Which smooth 4-manifolds M admit an exotic smooth structure?
- **Botany:** If there exist exotic structures on M , how many of them are there and what invariants can be used to distinguish them?

The *smooth unknotting conjecture* proposes that every smoothly embedded 2-sphere $K: \mathbb{S}^2 \hookrightarrow \mathbb{S}^4$ in the 4-sphere with $\pi_1(\mathbb{S}^4 - K, *) \cong \mathbb{Z}$ is smoothly unknotted. This conjecture is wide open. By contrast, removing the smoothness condition, Freedman-Quinn [FQ90, Thm. 11.7A] showed the topological unknottedness of topologically embedded knotted 2-spheres in \mathbb{S}^4 with fundamental group \mathbb{Z} . Analogous problems can be considered for embedded positive genus surfaces, see [CP20] for recent progress in the topological category.

In low ambient dimensions, including four, it is usually a hard problem to represent second homology classes via topologically or smoothly embedded surfaces with minimal genus. Given a smooth 4-manifold X^4 and an integral class $\alpha \in H_2(X; \mathbb{Z})$, we can ask about the minimal genus of an oriented closed embedded surface $\iota: S \hookrightarrow X$ such that the image of the fundamental class $\iota_*[S]$ is equal to α . The answer often depends on whether one is looking for topologically or smoothly embedded surfaces. We will be interested in a relative version of the setting, where the manifold X has non-empty boundary ∂X , and we are looking for surfaces with boundary a prescribed knot $k: \mathbb{S}^1 \hookrightarrow \partial X$. In particular, we are interested in finding embedded genus zero surfaces with boundary k which represent the trivial relative homology class in $H_2(X, \partial X; \mathbb{Z})$. We give multiple examples in which the solutions differ in the topological and smooth world. Our upcoming comparison of topological and smooth deep and shallow sliceness fits into the long history of results showing that the categories behave in very different ways.

Homotopy classification of 4-manifolds. Closed oriented topological 4-manifolds are homotopy equivalent to finite oriented Poincaré 4-complexes, which are finite CW-complexes that satisfy a version of Poincaré duality. A first step in a classification program for topological 4-manifolds could be

a homotopy classification of the 4-dimensional Poincaré complexes which occur for a given finitely presented fundamental group. Since every finitely presented group appears as the fundamental group of a closed smooth orientable 4-manifold, we usually fix a fundamental group at the beginning and consider the classification problems for each isomorphism class of group separately. For example, for the trivial group, results of Whitehead and Milnor [Mil58] imply that the homotopy type of finite oriented simply connected Poincaré 4-complexes is determined by their intersection form. Additionally, we know that all unimodular symmetric bilinear forms on finitely generated free \mathbb{Z} -modules are realizable by finite oriented simply connected Poincaré 4-complexes.

Inspired by work of Hambleton-Kreck [HK88; HK18], there has been some recent progress in the homotopy classification of 4-dimensional Poincaré complexes with certain finite fundamental groups. The *quadratic 2-type* of a finite connected oriented Poincaré 4-complex X is the collection $[\pi_1(X, *), \pi_2(X, *), k_X, \lambda_X]$ of the following invariants.

Here, $\pi_2(X, *)$ is a $\mathbb{Z}[\pi_1(X, *)]$ -module over the integral group ring of the fundamental group $\pi_1(X, *)$, $k_X \in H^3(\pi_1(X, *); \pi_2(X, *))$ is the Postnikov k -invariant and $\lambda_X: \pi_2(X, *) \otimes \pi_2(X, *) \rightarrow \mathbb{Z}[\pi_1(X, *)]$ is the equivariant intersection form on 2-spheres in X . This intersection form records a signed sum of double point loops, with one summand for each intersection point between immersed 2-spheres representing the second homotopy classes. In other words, it records the intersections between all pairs of immersed spheres in the complex.

The quadratic 2-type is a collection of natural algebraic-topological invariants that one is led to compute for a given complex. In fact, in various known settings, the homotopy type of a finite oriented Poincaré 4-complex is determined by the isometry class of its quadratic 2-type. For example, the author obtained such classification results for finite connected oriented Poincaré 4-complexes X for $\pi_1(X, *) \cong \mathbb{Z}/n \times \mathbb{Z}/m$ with Daniel Kasprowski and Mark Powell [KPR20], and for $\pi_1(X, *) \cong \text{Dih}_{2n}$ with Daniel Kasprowski and John Nicholson [KNR21]. The statements are slightly stronger, as this remains true for finite fundamental groups if their Sylow 2-subgroup is of the mentioned form.

This is again evidence that understanding the surfaces and their intersections in an ambient 4-manifold can tell us a lot about the space, and, supplemented with additional invariants, can determine the homotopy type of the associated 4-complex. In practice, it is usually very hard to algebraically classify all possible quadratic 2-types up to isometry, and to determine which of these are realizable by 4-manifolds. One approach to this is attempting a stable classification of 4-manifolds first, where we allow connected sums with copies of $\mathbb{S}^2 \times \mathbb{S}^2$, and consider the cancellation problem in a separate step. For a stable classification of closed connected spin 4-manifolds see [KPT21].

Outline. In [Section 1](#), we give a quick overview over the contents of [Parts I to III](#). At the end of the introduction in [Section 2](#), we highlight the new results of this thesis, which contain individual work of the author that did not appear in the published articles [JKRS20] and [KR21]. Each part of the thesis starts with a more detailed overview of upcoming topics, together with further references and conventions for that particular part.

1 OVERVIEW OF PARTS

In [Part I, Section 3](#), we introduce the *Casson-Whitney length* as a notion of ‘distance’ between surfaces in 4-manifolds defined in terms of the length of a regular homotopy. We will avoid the word ‘distance’ in the upcoming discussion to prevent confusion with previous usage of this word as measuring the width of regular homotopies and sequences of stabilizations and destabilizations [[JZ18](#); [Sin20](#)].

We explain our motivation by considering the case of classical 1-dimensional knots in 3-space. The *classical unknotting number* of a knot $k: \mathbb{S}^1 \hookrightarrow \mathbb{S}^3$ can be defined diagrammatically as the minimal number of crossing changes which transform a diagram of k into a diagram of the unknot. This minimum does not depend on whether we allow isotopies of the diagrams between each crossing change step. We take a perspective on the classical unknotting number which does not employ diagrams, but rather thinks of a crossing change as a certain isolated time in a generic homotopy. At this point, one strand of the knot passes through another part of the knot, creating a self-intersection in a single time step. In codimension two, there are two ways of resolving the singularity by pushing the strand either in the positive or negative time direction, leading to the two ways of choosing the type of crossing in the diagram.

Let us turn to smoothly knotted surfaces in the 4-sphere, and consider regular homotopies to the unknot in particular. The analogue of the classical unknotting number we consider in the 4-dimensional setting is the minimal number of Whitney moves needed in a regular homotopy taking an oriented smoothly knotted surface $K: \Sigma_g \hookrightarrow \mathbb{S}^4$ to the unknot. In regular homotopies of surfaces in 4-manifolds, double points are introduced by a finger move and removed by a Whitney move. We call the minimal number of Whitney moves the *Casson-Whitney number* $u_{\text{CW}}(K)$ of the knot K , since techniques for manipulating finger moves (the inverse homotopy to a Whitney move) were pioneered by Casson [[Cas86](#)].

The *stabilization number* $u_{\text{st}}(K)$ has traditionally been called the “unknotting number” of a smoothly knotted surface $K: \Sigma_g \hookrightarrow \mathbb{S}^4$. It records the minimal number of stabilizations of K required to obtain a smoothly embedded surface that bounds a solid handlebody [[HMS79](#)]. In classical knot theory, this is analogous to the number of band attachments to a 1-knot needed to obtain an unknot, or alternatively an unlink, see [[JMZ20a](#)] for different variations. The comparison of stabilizing surfaces and stabilizing 1-manifolds is slightly flawed, as stabilizations of knotted surfaces never increase the number of connected components. In contrast, an oriented band attachment on a classical link from a component to itself always splits this component into two. Nevertheless, the band unknotting and unlinking numbers are bounded above by twice the classical unknotting number, but generally this estimate is not an equality. We propose that the Casson-Whitney number is a complexity measure for knotted surfaces which is a better analogue of the classical unknotting number than the stabilization number.

The Casson-Whitney number can be generalized further to a *Casson-Whitney length* between a pair K_0, K_1 of regularly homotopic knotted surfaces in a smooth 4-manifold X^4 . The regular homotopy can be decomposed into a sequence of finger moves introducing pairs of double points, followed by a sequence of Whitney moves which remove pairs of double points. Then the *Casson-Whitney length*

$$\text{length}_{\text{CW}}(K_0, K_1) \in \mathbb{Z}_{\geq 0}$$

is the minimal length of such a regular homotopy from K_0 to K_1 , where length is the number of finger moves, or equivalently the number of Whitney moves.

Whenever we find an explicit regular homotopy between a pair of surfaces, this gives us an upper bound on the Casson-Whitney length. This constructive approach also allows us to bound the Casson-Whitney number of certain families of knotted surfaces in the 4-sphere in terms of other invariants related to their construction.

A *rim surgery* on a locally flat surface $F^2 \subset X^4$ is constructed by replacing an embedded annulus, usually described as the neighborhood of simple closed curve $\alpha \subset F$, by a knotted version of itself with the same boundary; see [Figure 8](#). For example, we can tie a pattern knot $J: \mathbb{S}^3 \hookrightarrow \mathbb{S}^3$ into each arc segment of the annulus, potentially with additional twisting τ^m in the gluing map, which produces the new knotted surface $F_{\tau^m}(\alpha, J) \subset X$. Crossing changes on the pattern knot J can be realized by a finger and Whitney move pair on the surface, which we call the *accordion homotopy* between the rim surgeries in [Section 4](#).

THEOREM (4.2). *Fix $m \in \mathbb{Z}$ and an embedded smoothly knotted surface $F^2 \subset X^4$. Let J_1 and J_2 be classical knots which differ by c crossing changes. Then there is a regular homotopy of length c between the m -twist rim surgeries $F_{\tau^m}(\alpha, J_1)$ and $F_{\tau^m}(\alpha, J_2)$. In other words, the Casson-Whitney length between twist rim surgeries is bounded above by the Gordian distance¹ between the pattern knots,*

$$\text{length}_{\text{CW}}(F_{\tau^m}(\alpha, J_1), F_{\tau^m}(\alpha, J_2)) \leq \text{dist}_{\text{Gord}}(J_1, J_2).$$

The regular homotopy is supported in a neighborhood of the rim surgery curve $\alpha \subset F$.

As a special case, this shows that the classical unknotting number of a 1-knot in the 3-sphere is an upper bound on the Casson-Whitney number of any of its twist spins.

COROLLARY (4.4). *Let $k: \mathbb{S}^1 \hookrightarrow \mathbb{S}^3$ be a classical knot. For any twist spin $\tau^n k: \mathbb{S}^2 \hookrightarrow \mathbb{S}^4$ of k , the Casson-Whitney number $u_{\text{CW}}(\tau^n k) \leq u(k)$ is bounded by the classical unknotting number $u(k)$ of k .*

Refer to [Section 2](#) for an extended overview and comparison with our previously published results. An interesting switch in perspective is thinking of this as an algebraic lower bound

$$\text{alg}_{\text{CW}}(\tau^n k) \leq u_{\text{CW}}(\tau^n k) \leq u(k)$$

for the classical unknotting number of k in terms of 4-dimensional quantities. Here the *algebraic Casson-Whitney number* $\text{alg}_{\text{CW}}(K)$ of a knotted surface K in the 4-sphere records the minimal number of finger move relations which are necessary to abelianize the knot group $\pi_1(\mathbb{S}^4 - K, *)$.

We compare the stabilization and Casson-Whitney length in [Section 5](#). Both the stabilization and Casson-Whitney number have algebraic relatives, which are defined as the minimal number of stabilization or finger move relations that need to be introduced to make the fundamental group of the complement into a cyclic group. Obviously, these give lower bounds for the geometric quantities, but they are in general hard to compute. Finger moves have a slightly weaker effect on the fundamental group of a surface's complement than stabilizations: Attaching a stabilization tube allows the meridian at one of the feet of the tube to travel along the guiding arc to the other end, setting these meridians to be equal in the fundamental group. In an immersion resulting from a finger move, meridians of the two sheets coming together at an intersection point lie on a Clifford torus, which shows that they commute in the fundamental group of the complement of the immersion. Both for stabilizations and finger moves, the precise pair of based meridians which are identified in the resulting quotient of the knot group is determined by the guiding arc of the move. From the minimal number of generators of the Alexander module – the *Nakanishi index* – we obtain the same lower bound for both the Casson-Whitney number and the stabilization number.

Nevertheless, we can detect the subtle difference between the types of relations and show that the stabilization number and Casson-Whitney number are not equal.

THEOREM (2.2). *There are infinitely many 2-knots $K: \mathbb{S}^2 \hookrightarrow \mathbb{S}^4$ with $u_{\text{st}}(K) = 1$ and $u_{\text{CW}}(K) = 2$.*

¹ The *Gordian distance* between two classical knots $k_1, k_2: \mathbb{S}^1 \rightarrow \mathbb{S}^3$ is defined as the minimal number of crossing changes which relates a diagram of k_1 to a diagram of k_2 , where we minimize over all possible diagrams.

The main idea is to work in quotients of the knot group coming from a coloring of the knot, and considering the image of a finger move relation. If the quotient cannot be abelianized via a single relation of finger move type, we know that the group of the original is immune to this as well, and then the algebraic and geometric Casson-Whitney number is at least two. For a pair of 2-knots, both with non-trivial determinants, the algebraic Casson-Whitney number of their connected sum is strictly greater than one. This theorem and its proof goes beyond the abelian invariants such as the Alexander module; the group theory tool used is a Freiheitssatz on free products of finite groups [FHR88]. Miyazaki found 2-knots K_1, K_2 with $u_{\text{st}}(K_i) = 1$ but $u_{\text{st}}(K_1 \# K_2) = 1$ as well [Miy86]. Since his knotted spheres have nontrivial determinants, these examples together with the above theorem imply that the Casson-Whitney number is different from the stabilization number.

For sequences leading to the unknotted oriented surface in the 4-sphere, the stabilization number is bounded by one more than the Casson-Whitney number.

THEOREM (5.6). *For a smoothly knotted oriented surface $K: \Sigma_g \hookrightarrow \mathbb{S}^4$,*

$$u_{\text{st}}(K) \leq u_{\text{CW}}(K) + 1.$$

This observation is a consequence of Singh's work [Sin20]. Singh compares related invariants that record the minimal 'width' of a sequence of stabilizations and destabilizations of a regular homotopy, which is the maximum number of stabilizations or double points that occur *simultaneously*. The geometric techniques in the proofs of Theorems 5.6 and 5.7 are inspired by Singh, Gabai [Gab20] and Schneiderman-Teichner [ST19]. For knotted 2-spheres, a careful manipulation of 'simple' regular homotopies to the unknot gives settings in which this inequality is always strict:

THEOREM (5.7). *Every smoothly knotted 2-sphere $K: \mathbb{S}^2 \hookrightarrow \mathbb{S}^4$ with $u_{\text{CW}}(K) = 1$ also has $u_{\text{st}}(K) = 1$.*

We dedicate Section 6 to the study of ribbon surfaces in the 4-sphere. A *ribbon surface* $K: \Sigma_g \hookrightarrow \mathbb{S}^4$ is the result of stabilizing an unlink of 2-spheres in \mathbb{S}^4 until we obtain a connected surface. This unlink of 2-spheres corresponds to the minima of K with respect to the standard Morse function of the ambient 4-sphere, and the minimal number of stabilizations necessary in the construction of K is called the *fusion number* $\text{fus}(K)$ of the ribbon surface. We find that the fusion number of a ribbon surface is an upper bound for the Casson-Whitney number.

THEOREM (6.3). *In the 4-sphere, the Casson-Whitney number of an oriented ribbon surface $K: \Sigma_g \hookrightarrow \mathbb{S}^4$ is bounded above by the fusion number minus the genus g of the surface,*

$$u_{\text{CW}}(K) \leq \text{fus}(K) - g.$$

This is proved via an inductive argument in which, after a natural collection of finger moves, we can unlink the fusion tubes from the minima 2-spheres of the ribbon presentation of K one after another. The analogous result $u_{\text{st}}(K) \leq \text{fus}(K) - g$ for the stabilization number is due to Miyazaki [Miy86].

By modifying the monodromy of the fibration of the spun trefoil, Suciuc constructed an infinite family of mutually non-isotopic knotted 2-spheres $R_l: \mathbb{S}^2 \hookrightarrow \mathbb{S}^4$, $l \in \mathbb{N}$, each with $\pi_1(\mathbb{S}^4 - R_l, *)$ isomorphic to the trefoil knot group. We recall their construction and reproduce fusion number two ribbon presentations in Section 6.3, where we also investigate them from the perspective of Casson-Whitney unknotting. Their stabilization number is equal to one, and we realize the isotopy from a stabilization $R_k + h^{(1)}$ to an unknotted torus via an explicit manipulation of a banded unlink diagram. Thus R_l is an infinite family of distinct ribbon 2-knots with isomorphic groups that all admit a single stabilization to an unknotted torus. Supplemented by our computer implementation [Rup21a] in SageMath and GAP, we determine that the algebraic Casson-Whitney number $\text{alg}_{\text{CW}}(R_l)$ for $l = 1, 2, 3$ is equal to one.

Taking a connected sum with an unknotted $\mathbb{RP}^2 \subset \mathbb{S}^4$, we are able to produce upper bounds on the geometric Casson-Whitney length of the resulting knotted projective planes to an unknotted projective plane. Results of Kanenobu-Sumi [KS20] on the representation theory of the commutator subgroup of $\pi_1(\mathbb{S}^4 - R_l \# \mathbb{RP}^2)$ imply that for $l \in \mathbb{N}$, the knotted projective planes $R_l \# \mathbb{RP}^2$ are pairwise not smoothly isotopic. We show that $R_i \# \mathbb{RP}^2$ and $R_j \# \mathbb{RP}^2$ are related by a single finger-Whitney move pair. Thus the members of this infinite family are Casson-Whitney length one away from the unknotted projective plane:

THEOREM (6.19). *The Casson-Whitney length between any of Suciu's associated \mathbb{RP}^2 -knots $R_l \# \mathbb{RP}^2$, $l \in \mathbb{N}$, and the standard unknotted projective plane $\mathbb{RP}^2 \subset \mathbb{S}^4$ is*

$$\text{length}_{\text{CW}}(R_l \# \mathbb{RP}^2, \mathbb{RP}^2) = 1.$$

For this, we consider a specific finger move between two of the minima of the ribbon summand R_l , which results in an immersion whose complement has cyclic fundamental group. The relations in the group of the immersion complement can be used to untangle the ribbon fusion bands, so that we can recognize it as a finger move on an unknotted projective plane.

In **Part II**, we move to the relative setting of surfaces in 4-manifolds bounded by knots in the 3-manifold boundary. We investigate the difference between *shallow slice disks* that live in the collar of the boundary and *deep slice disks* which necessarily use other parts of the 4-manifold.

Our motivation for studying the difference between these notions comes from the following: One possible approach to proving that a proposed smooth homotopy 4-ball \mathcal{B} is in fact exotic is to find a knot $K \subset \mathbb{S}^3 = \partial\mathcal{B}$, such that there is a smooth properly embedded disk $\mathbb{D}^2 \hookrightarrow \mathcal{B}$, with $\partial\mathbb{D}^2$ mapped to K , but where K is **not** smoothly slice in the usual sense in the standard 4-ball \mathbb{D}^4 .

Let X^4 be a smooth compact 4-manifold with non-empty boundary ∂X . We call a knot $K \subset \partial X$ *topologically/smoothly slice* in X if there is a locally flat/smooth properly embedded disk in X with boundary K . A knot is topologically/smoothly slice in \mathbb{D}^4 if and only if it is topologically/smoothly null-concordant in $\mathbb{S}^3 \times [0, 1]$, i.e. there is a properly embedded locally flat/smooth cylinder $\mathbb{S}^1 \times [0, 1] \hookrightarrow \mathbb{S}^3 \times [0, 1]$ whose oriented boundary is $K \subset \mathbb{S}^3 \times \{0\}$ together with the unknot $U \subset \mathbb{S}^3 \times \{1\}$. So, another way of thinking about the strategy in the previous paragraph is that we want to find a knot K in $\mathbb{S}^3 = \partial\mathcal{B}$ that bounds a smooth properly embedded disk in \mathcal{B} , but does not bound any such disk that is contained in a collar $\mathbb{S}^3 \times [0, 1]$ of the boundary of \mathcal{B} . In this case, to verify the sliceness of K , we have to go 'deep' into \mathcal{B} .

An easier task might be to find a smooth homology 4-ball X with \mathbb{S}^3 boundary such that there is a knot in the boundary that bounds a smooth properly embedded disk in X but not in \mathbb{D}^4 , however, this is also an open problem. In [Fre+10], the authors investigate the possibility of proving that a homotopy 4-ball \mathcal{B} with \mathbb{S}^3 boundary is exotic by taking a knot in the boundary that bounds a smooth properly embedded disk in \mathcal{B} and computing the Khovanov homology s -invariant [Ras10] of K , in the hopes that $s(K) \neq 0$, whereby they could then conclude that \mathcal{B} is exotic. Unfortunately for this approach as noted in the paper, it turns out that the homotopy 4-ball that they were studying was in fact diffeomorphic to \mathbb{D}^4 , see [Akb10]. It is still open whether the s -invariant can obstruct the sliceness of knots in \mathbb{D}^4 that are slice in some homotopy 4-ball, as is noted in the corrigendum to [KM13].

We call a knot $K \subset \partial X$ *smooth shallow slice* in X if there is a smooth properly embedded disk in a collar $\partial X \times [0, 1]$ with boundary K . If K is smoothly slice in X , but not smooth shallow slice, we will call it *smooth deep slice* in X . We also call a slice disk which is contained in the collar a *shallow disk*. Shallow sliceness implies that the knot is nullhomotopic in the boundary, so we usually only consider

these notions for knots in the trivial homotopy class. Similar definitions can be made in the topological category, where the slice disks are required to be locally flat. A *2-handlebody* is a smooth 4-manifold with a handle decomposition that contains one 0-handle, some non-zero finite number of 2-handles and no handles of any other index.

THEOREM (8.1). *Every 2-handlebody contains a null-homotopic knot in the boundary which bounds a smooth slice disk in the 2-handlebody, but where such a smooth disk cannot exist in a collar of the neighborhood of the boundary. With the above terminology, these are smoothly deep slice knots.*

Depending on whether the boundary of the 2-handlebody X^4 is simply connected or has nontrivial elements in the fundamental group, the construction of the deep slice knots uses different tools. If there is a non-nullhomotopic meridian to a handle in the boundary, its Whitehead double with respect to a specific framing bounds a slice disk in X and is null-homotopic in ∂X . In that case, we can apply Schneiderman's self-intersection invariant μ , a second-order invariant which counts double point loops in the track of a null-homotopy [Sch03]. This intersection count takes values in a specific quotient of the group ring over the fundamental group; if it is non-zero in the quotient, the knot cannot be shallow slice. For simply connected boundaries, we know that the 2-handlebody can be capped off with a 4-handle, and we translate shallow sliceness into the question of representing a specific homology class in the closed 4-manifold by a smoothly embedded sphere. This is again related to the comparison of smooth and topological genus bounds, and, assuming results on the genus function, we can give various examples of deep slice knots in Section 8.2.

Topological and smooth sliceness are already very different notions in the 4-ball. For example, the untwisted positive Whitehead double $\text{Wh}_+(T_{2,3}, 0)$ of the trefoil knot is topologically slice since it has Alexander polynomial one [FQ90, Sec. 11.7], [GT04]. Its smooth sliceness can be obstructed using gauge theory techniques [Akb83], [Akb16, Ex. 11.4, p. 143] that depend on Donaldson's theorem which states that intersection forms of positive definite smooth closed oriented 4-manifolds are diagonalizable [Don83]. The smooth sliceness of this Whitehead double can also be obstructed using the more modern Khovanov homology s -invariant [Ras10] or the Heegaard-Floer homology τ -invariant [OS03]. These are usually easier to compute; for example, for a knot K such that $\tau(K) > 0$, none of the iterated untwisted positive Whitehead doubles are smoothly slice because they have non-zero τ -invariant [Hed07].

Such examples can be placed into a 4-manifold X^4 with 3-sphere boundary and thus, if the knot is smoothly slice in X , it has to be smoothly deep slice in X . For example, $\text{Wh}_+(T_{2,3}, 0)$ is smoothly slice in a punctured $\mathbb{S}^2 \times \mathbb{S}^2$ or in a punctured $\mathbb{C}\mathbb{P}^2$. Therefore, $\text{Wh}_+(T_{2,3}, 0)$ is an example of a knot in the boundary of a 4-manifold which is topologically shallow slice but smoothly deep slice. But this knot $K = \text{Wh}_+(T_{2,3}, 0)$ is *local* in the boundary ∂X , which means that it is contained in an embedded 3-ball $K \subset \mathbb{D}^3 \subset \partial X$. Therefore these old examples are not very interesting in the context of deep sliceness, since they do not say anything new about surfaces in the (4-manifold, 3-manifold) pair, but only about the pair $(\mathbb{D}^4, \mathbb{S}^3)$.

Our new contribution is the construction of non-local examples of knots in 3-manifolds which do bound a topological shallow slice disk in a 4-manifold and are smoothly slice in the 4-manifold, but there cannot exist a smooth shallow disk.

THEOREM (9.1). *The (-1) -trace of the left-handed trefoil knot $X_{-1}(T_{2,-3})$ is a 4-dimensional 2-handlebody X^4 with infinitely many non-local null-homotopic knots in the boundary which are topologically shallow slice, but smoothly deep slice in X^4 .*

The shallow topological slice is constructed using results of Freedman [Fre88], who found topological disks inside the simplest Casson tower of height 3, with boundary the attaching circle of the tower. Here

‘simplest’ means that there is only a single self-plumbing in each stage of the Casson-tower, all of these of the same sign.

The smooth shallow slice obstruction comes from the τ -invariant of Heegaard-Floer theory, which by a result of Hedden-Raoux [HR21b] gives a smooth genus bound on surfaces in certain 4-dimensional cobordisms. The τ -invariant of a knot K in an integral homology 3-sphere L-space admits various equivalent definitions, for example as the Alexander filtration of a distinguished generator in a spectral sequence converging to the Heegaard-Floer homology of the ambient 3-manifold. We restrict to integral homology 3-spheres so that there is a unique Spin^c -structure of the 3-manifold, which streamlines the discussion of Heegaard-Floer invariants. The L-space property says that the Floer homology of the 3-manifold is as simple as possible, which is used in the definition of the aforementioned distinguished generator.

There is a scarcity of computations of τ -invariants in general 3-manifolds in the literature. For this reason, we put a particular focus on applying the techniques in ambient 3-manifolds which are at the same time integral homology 3-spheres and Heegaard-Floer L-spaces. We give a new proof in the 0-twisting case of Hedden’s Whitehead double formula for the τ -invariant [Hed07] which works in integral homology 3-sphere L-spaces. Similarly, we look at special cases of Hom’s cabling formula for τ -invariants [Hom14], and give a new proof for $(p, 1)$ -cables.

Bordered Heegaard-Floer homology [LOT18] is a powerful tool that allows assembling Floer invariants of the pieces of a 3-manifold, which has been cut along embedded surfaces, into invariants of the whole manifold. Unfortunately, the algebraic objects involved, such as type A and type D structures over surface algebras, are complicated and not necessarily user-friendly. In our exposition, we use the language of immersed curves, introduced by Hanselman-Rasmussen-Watson [HRW17]. This way we can represent chain complexes, their maps and even certain spectral sequence computations in a pictorial way via curves in surfaces, which can be easily visualized and manipulated. For example, the τ -invariant of the companion knot in a satellite construction can be read off from a certain slope of the immersed curve in a punctured torus $\mathbb{T}^2 - \{z\}$. Secretly, this immersed curve encodes a type D structure describing the bordered Floer homology of the companion’s complement.

The proofs of the Whitehead and cable formulas are based on Chen’s pairing theorem for satellites of $(1, 1)$ -pattern knots in the solid torus [Che19]. The recipe for representing invariants of the satellite is to superimpose the bordered Heegaard diagram of the pattern knot over the immersed-curve diagram of the knot complement of the companion. Intersection points between the β -curve of the pattern and the immersed α -curve of the companion are in correspondence with generators of the knot Floer homology of the satellite. This leads to a convenient pictorial method for computing the τ -invariant of the satellite knot in the pairing diagram, compare the description in [Che19]. We pass from one page of the Heegaard-Floer spectral sequence to the next by canceling a pair of generators where the difference in Alexander filtration is minimal among the remaining intersection points. Geometrically, this cancellation corresponds to a Whitney move on the β -curve, where we push it across a basepoint z and remove a pair of oppositely signed intersections between the immersed curves of the companion and pattern. At the end of such an iterative procedure, the τ -invariant of the satellite is the Alexander filtration of the remaining intersection point.

In Section 10, we obtain results comparing deep and shallow slice links. The definition of deep sliceness is analogous to the case of knots, where we focus on the notion of strong sliceness, in which there is a collection of disjoint slice disks, one for each link component. Proper sublinks of our examples are shallow slice, so the deep sliceness is really a property of the link as a whole, and does not come from a single component on its own. We generalize the earlier observations on deep slice knots in 2-handlebodies in two directions: For every 2-handlebody X^4 with non-simply connected boundary, there exists a 2-component link with unknotted components which is topologically deep strong slice in X . We also construct link null-homotopic examples in 2-handlebodies with integral homology sphere boundary via Whitehead doubling.

Then we contrast topological shallow strong sliceness with smooth deep strong sliceness, see also the discussion of results in [Section 2](#).

THEOREM (10.8). *There exists a non-local 2-component link J in the boundary $Y = \partial X$ of the 2-handlebody $X = X_{-1}(T_{2,-3})$ which is Brunnian (so every proper sublink of J is smoothly shallow slice), bounds smooth strong slice disks in the 2-handlebody X , is topologically shallow strong slice in $Y \times [0, 1]$, but is **not** smoothly shallow strong slice in $Y \times [0, 1]$. Moreover, J is link homotopic to the split unlink in the boundary and a boundary link.*

In the final [Section 11](#) of this part, we start with the following observation: Given a fixed local knot $K \subset M^3$ in a closed orientable 3-manifold, there is a compact orientable 4-manifold in which K is smoothly H -slice. H -slice means that the knot is slice via a null-homologous disk in the 4-manifold. On the other hand, the Norman-Suzuki trick [[Nor69](#), Cor. 3], [[Suz69](#), Thm. 1] constructs slice disks for every knot in the boundary of a punctured bounded $\mathbb{S}^2 \times \mathbb{S}^2$ (where the slice disk is usually not null-homologous). One might ask whether there is a 4-manifold that combines these two properties: Is there a fixed compact, oriented 4-manifold V^4 with $\partial V = \mathbb{S}^3$ such that every knot $K \subset \mathbb{S}^3$ is slice in V^4 via a null-homologous disk? Such a space would be a *universal slicing manifold*, however we show that it cannot exist, by proving the following.

THEOREM (11.1). *Every compact oriented topological 4-manifold V^4 with $\partial V = \mathbb{S}^3$ contains a knot in its boundary that is not topologically H -slice in V^4 .*

The proof employs a Levine-Tristram inequality which implies that the signature and Euler characteristic of the 4-manifold puts restrictions on the signatures of H -slice knots.

Relaxing the H -slice requirement leads to interesting open questions. The torus knot $T_{2,-15}$ is not slice in $\mathbb{C}\mathbb{P}^2$ [[Yas91](#)], where we do not restrict the homology class of the disk. Manolescu-Marengon-Piccirillo [[MMP20](#), Qn. 6.1] ask whether there is a knot which is not smoothly slice (again no assumption on homology class) in an indefinite 4-manifold, such as the K3 surface. These questions also connect to our first motivation of proving a smooth structure to be exotic by slicing certain knots. Manolescu-Piccirillo [[MP21b](#)] outline variations of this strategy and provide a list of 23 knots in the 3-sphere such that if any of them is smoothly H -slice in a bounded punctured $\#^n \mathbb{C}\mathbb{P}^2$ for some $n \geq 1$, this would prove the existence of an exotic $\#^n \mathbb{C}\mathbb{P}^2$. Recall that there is no known example of an exotic, definite 4-manifold.

An alternative approach to the Smooth 4-Dimensional Poincaré Conjecture (SPC4) is to find a compact 3-manifold M that embeds smoothly in some homotopy 4-sphere Σ^4 , but not in the standard \mathbb{S}^4 . Notice that if a smooth integral homology sphere M smoothly embeds in Σ , then M is the boundary of a smooth homology 4-ball [[AGL17](#), Prop. 2.4]. However, there is no known example of an integral homology sphere M that is the boundary of a smooth homology 4-ball, but that does not smoothly embed into \mathbb{S}^4 . Both this and the approach at the beginning are not able to get beyond the homological level. Further discussion of knots in homology spheres and concordance in homology cylinders can be found in for example [[HLL18](#); [Dav20](#)].

The unsolved smooth Schoenflies conjecture proposes that if $\mathcal{S} \subset \mathbb{S}^4$ is a smoothly embedded submanifold with \mathcal{S} homeomorphic to \mathbb{S}^3 , then \mathcal{S} bounds a submanifold $\mathcal{B} \subset \mathbb{S}^4$ that is diffeomorphic to \mathbb{D}^4 . The SPC4 implies the Schoenflies conjecture.

Question 1.1. Does every smooth homotopy 4-ball \mathcal{B} smoothly embed into \mathbb{S}^4 ?

Note that if the answer to [Question 1.1](#) is yes, then the Schoenflies conjecture implies the SPC4 and hence the two conjectures are equivalent: If every homotopy 4-ball would embed into \mathbb{S}^4 and thus, by

the Schoenflies conjecture, would be diffeomorphic to \mathbb{D}^4 , then all homotopy 4-balls would be standard, so all homotopy 4-spheres would be standard.

In any case, if the answer to [Question 1.1](#) is yes, then no homotopy 4-ball can have deep slice knots. Suppose that X is a closed smooth 4-manifold with universal cover \mathbb{R}^4 or \mathbb{S}^4 , and let X° be X with a smooth open 4-ball removed, $X^\circ = X - \text{int } \mathbb{D}^4$. We observe in [Proposition 7.5](#) that then X° has no deep slice knots. Thus if the answer to [Question 1.1](#) is yes, the approach towards SPC4 mentioned in this section would never succeed. Similarly, there would be no 3-manifold that would smoothly embed into a homotopy 4-sphere but not into \mathbb{S}^4 . This is because any such embedding into a homotopy sphere avoids a standard 4-ball and after removing this ball the complement is a homotopy 4-ball, which we assume embeds into \mathbb{S}^4 , so this approach to SPC4 would also be a dead end.

[Part III](#) starts with a rapid introduction to *bridge trisections* of smoothly knotted surfaces in the 4-sphere [\[MZ17\]](#). In general [\[MZ18\]](#), bridge trisections of smooth surfaces in trisected 4-manifolds are the 4-dimensional analogue of bridge splittings of classical links in Heegaard split 3-manifolds. The genus 0-trisection of the 4-sphere cuts \mathbb{S}^4 into three 4-balls, which have specific pairwise and triple overlaps along common parts of their boundaries: Pairs of these 4-balls meet in 3-balls, and the triple intersection is in an unknotted 2-sphere in \mathbb{S}^4 . A knotted surface in bridge position is required to intersect each of the 4-balls in a trivial collection of disks, whereas in the 3-balls we see trivial tangles; see [Section 13](#). The data of a bridge trisection is determined by this triple of trivial tangles, all meeting at the central 2-sphere in a set of common bridge points.

For smooth closed oriented 4-manifolds, a surprising result of Abrams-Gay-Kirby states that the smooth topology is completely encoded in a *group trisection*, an algebraic analogue of a trisection in which the fundamental group of the 4-manifold is decomposed into three free groups together with ‘algebraic’ gluing data [\[AGK18\]](#). Here we develop a knotted surface analogue of group trisections, which for a smoothly knotted bridge trisected surface $F \subset \mathbb{S}^4$ is a commutative cube of group homomorphisms as shown in the diagram.

$$\begin{array}{ccccc}
 & & \pi_1(\mathbb{D}^3 - T_\alpha) & \xrightarrow{\quad} & \pi_1(\mathbb{S}^3 - U_{\alpha\cup\beta}) \\
 & & & & \cong \pi_1(\mathbb{D}^4 - D_{\alpha\cup\beta}) \\
 & \nearrow & \downarrow & \nearrow & \downarrow \\
 \pi_1(\mathbb{S}^2 - \{2b \text{ pts.}\}) & \xrightarrow{\quad} & \pi_1(\mathbb{D}^3 - T_\beta) & & \\
 & & \downarrow & & \downarrow \\
 & & \pi_1(\mathbb{S}^3 - U_{\alpha\cup\gamma}) & \xrightarrow{\quad} & \pi_1(\mathbb{S}^4 - F) \\
 & & \cong \pi_1(\mathbb{D}^4 - D_{\alpha\cup\gamma}) & & \\
 & \searrow & \downarrow & \searrow & \\
 \pi_1(\mathbb{D}^3 - T_\gamma) & \xrightarrow{\quad} & \pi_1(\mathbb{S}^3 - U_{\beta\cup\gamma}) & & \\
 & & \cong \pi_1(\mathbb{D}^4 - D_{\beta\cup\gamma}) & &
 \end{array}$$

The algebraic pieces of a *group trisection of knotted surface type* consist of the homomorphisms on fundamental groups induced by the inclusions of a punctured sphere $\mathbb{S}^2 - \{2b \text{ points}\}$ into a trivial tangle complement $\mathbb{D}^3 - T_\mu$, where μ is one of $\{\alpha, \beta, \gamma\}$. We call an epimorphism between groups of this form which satisfies an additional natural conjugate condition a *trivial tangle homomorphism*, for details see [Definition 13.1](#). The trivial tangle homomorphisms are colored in red, blue and green in the diagram; b is the *bridge number* of the group trisection of knotted surface type.

Three trivial tangle homomorphism, such that a pairwise compatibility condition holds, determine a parameterized bridge trisection of a knotted surface in the following way; see [Section 14](#): From a trivial tangle homomorphism we obtain a parameterized trivial tangle in the 3-ball, which can be recovered

algorithmically. This trivial tangle is unique, which follows from Dehn's lemma applied to specific disks in the tangle complements. In the definition of a group trisection of knotted surface type we require that the pairwise pushouts of the trivial tangle homomorphisms are free groups. From this it follows that the endpoint-unions of pairs of trivial tangles T_μ, T_ν yield links in the 3-sphere whose fundamental group of the complement is free, which implies that they are unlinks $\mathcal{U}_{\mu \cup \nu} \subset \mathbb{S}^3$. This suffices to build a unique bridge trisected surface in the 4-sphere, by capping each pairwise union unlink off with a trivial disk system $D_{\mu \cup \nu} \subset \mathbb{D}^4$ in each of the 4-ball sectors of the genus 0-trisection of the 4-sphere.

The remaining [Sections 16](#) and [17](#) are computational, where we construct group trisections of knotted surface type of certain twist spun torus knots and of Suciu's ribbon family with the trefoil group. These provide examples of smoothly knotted surfaces in the 4-sphere whose complements have isomorphic fundamental groups, but which are in distinct smooth isotopy classes.

THEOREM (16.1). *There exist at least three non-isomorphic group trisections of knotted surface type with bridge number ≤ 7 of the group $\mathbb{Z} \times \text{Dod}^*$, the product of the integers with the 120 element binary dodecahedral group. Under topological realization these correspond to knotted genus zero surfaces in \mathbb{S}^4 .*

THEOREM (17.2). *There exist infinitely many non-isomorphic 7-bridge group trisections of knotted surface type of the trefoil knot group.*

Bridge trisections of knotted surfaces in the 4-sphere can be encoded in triplane-diagrams, which are triples of projections of trivial tangles whose pairwise endpoint-unions form diagrams of unlinks in the 3-sphere. We discuss how the Wirtinger algorithm applies to these projections, and some subtleties that arise in choosing free generators for trivial tangle complements. Stallings' folding technique encodes subgroups of free groups as immersions of graphs, and we show how this applies to study the trivial tangle homomorphisms which make up a group trisection of knotted surface type.

Another result of [Part III](#) is our computer implementation of group trisections of knotted surface type as a python class in a SageMath-program [[Rup21a](#)], whose main functions are documented in [Section 15.2](#).

2 STATEMENTS OF THE NEW RESULTS

While several of the results in this thesis have been published in [JKRS20], [KR21] and [Rup21b], it contains much that is new, as we now outline.

Part I – Casson-Whitney unknotting:

In this part, we generalize constructions from [JKRS20] to more cases, in particular investigating which results remain true for positive genus knotted surfaces. We also define a notion of *length* between homotopic knotted surfaces, such that the *Casson-Whitney number* is the special case which measures the length to an unknotted surface in the 4-sphere.

- **Theorem 4.2:** We give an explicit construction of regular homotopies between twist rim surgeries which subsumes some of the previous applications to upper bounds on the Casson-Whitney number of twist-spun knots $\tau^m k$.
- **Section 4.1.3:** The Nakanishi index of a classical knot k is a lower bound on the Casson-Whitney numbers of its roll-spins $\rho^n k$. Using Teragaito’s results from [Ter94b], we reformulate the smooth unknotting conjecture for 1-roll m -twist spun knots $\rho^1 \tau^m k: \mathbb{S}^2 \hookrightarrow \mathbb{S}^4$ in terms of certain quotients of the knot group in **Proposition 4.14**.
- **Theorem 6.3:** This is a generalization of the fusion number upper bound for the Casson-Whitney number which now applies to both genus zero and positive genus g orientable ribbon surfaces $K: \Sigma_g \hookrightarrow \mathbb{S}^4$ in the 4-sphere.
- **Proposition 6.10:** We found 2-knots with arbitrarily high Casson-Whitney length to a ribbon 2-knot $K: \mathbb{S}^2 \hookrightarrow \mathbb{S}^4$. This uses Cochran’s result [Coc83, Thm. 2.2] that the abelianization $H_1([\pi_K, \pi_K]; \mathbb{Z})$ of the commutator subgroup of a ribbon 2-knot group $\pi_K := \pi_1(\mathbb{S}^4 - K)$ is \mathbb{Z} -torsion free. Connected sums of 2-twist spins of 2-bridge knots, $\#^N \tau^2 k$, where the double branched cover of $k: \mathbb{S}^1 \hookrightarrow \mathbb{S}^3$ is the lens space $L(p, q)$ with fundamental group of order p , have a commutator subgroup with \mathbb{Z} -torsion isomorphic to $\bigoplus^N \mathbb{Z}/p$. Take p to be prime, then a single finger move is only able to remove a one dimensional subspace of the torsion, so we need at least N finger moves to get to a ribbon 2-knot.

The results on the Casson-Whitney numbers and related invariants for Suciú’s ribbon knots $R_l: \mathbb{S}^2 \hookrightarrow \mathbb{S}^4$ are new, which are supplemented by the SageMath computations in [Rup21a].

- **Theorem 6.11:** The stabilization number for each of Suciú’s ribbon knots is equal to one, $u_{\text{st}}(R_l) = 1$ for all $l \geq 1$. One possible choice of a stabilization tube connects two of the minima in a natural fusion number two ribbon presentation of the knots.
- **Theorem 6.19:** The Casson-Whitney length between the standard unknotted $\mathbb{RP}^2 \subset \mathbb{S}^4$ and Suciú’s associated \mathbb{RP}^2 -knots $R_l \# \mathbb{RP}^2$ is equal to one.
- **Section 6.3.2:** We obtain partial results on the algebraic Casson-Whitney number of Suciú’s knots, for example observing that $\text{alg}_{\text{CW}}(R_2)$ and $\text{alg}_{\text{CW}}(R_3)$ are both equal to one. This is based on computer assisted computations within (quotients of) the knot groups, see our SageMath and GAP implementation and its documentation in [Rup21a].

Part II – Deep and shallow slice knots in 4-manifolds:

[KR21] and [Rup21b] worked purely in the smooth category. Here, we compare with the topological category, and apply new tools like Casson towers, Heegaard-Floer homology and covering links.

- **Section 8.2:** We give an overview of how genus bounds for representing homology classes by locally flat embedded surfaces can be used to obstruct topological shallow sliceness.
- **Section 9.2:** We give a new proof of Hedden’s Whitehead doubling formula [Hed07] for the Heegaard-Floer τ -invariant in the untwisted case using the immersed curves language of Hanselman-Rasmussen-Watson [HRW17]. The argument is based on Chen’s pairing theorem for satellites with $(1, 1)$ -pattern [Che19].
- **Section 9.4.1:** This section contains a new proof of Hom’s cabling formula [Hom14] for the τ -invariant of $(p, 1)$ -cables using immersed curve techniques.
- We observe that both the Whitehead doubling formula (**Theorem 9.8**) and the cabling formula (**Theorem 9.25**) for the τ -invariant are true for knots in ambient 3-manifolds which are integral homology 3-sphere Heegaard-Floer L-spaces.
- **Theorem 9.1:** The (-1) -trace of the left handed trefoil, $X = X_{-1}(T_{2,-3})$, is a 4-dimensional 2-handlebody with infinitely many non-local knots in the boundary $\partial X \cong \mathbb{S}_{-1}^3(T_{2,-3})$ which exhibit the difference between shallow topological sliceness and smooth deep sliceness. Non-localness shows that these examples are not just imported from the difference between the topological and smooth category in the 4-ball. The main steps in the proof proceed as follows:
 - **Theorem 9.23:** We first construct a single example $J = \text{Wh}_+^{(3)}(\text{Wh}_+(\tilde{K}, +1), 0)$, an iterated Whitehead double of the dual knot \tilde{K} in (-1) -surgery on the left handed trefoil in the 3-sphere, $\mathbb{S}_{-1}^3(T_{2,-3})$. The twisting parameters for the Whitehead doubles are carefully chosen to arrange the smooth deep sliceness in the 2-handlebody.
 - Freedman [Fre88] proved the existence of a topological slice disk for 3-fold iterated positively clasped Whitehead doubles.
 - The τ -invariant gives a smooth slice obstruction in the collar $\partial X \times [0, 1]$. The τ -invariant of the dual knot \tilde{K} is computed in **Proposition 9.18** to be $\tau(\mathbb{S}_{-1}^3(T_{2,-3}), \tilde{K}) = +1$. This uses the filtered mapping cone formula for Heegaard-Floer theory, as outlined in [Zho20].
 - **Theorem 9.27:** We further take $(p, 1)$ -cables to obtain an infinite family $J_{p,1}$, where we compute the τ -invariant using Hom’s formula that we generalize to integer homology 3-sphere L-spaces in **Theorem 9.25**.
- **Section 9.3.3:** This section contains computations of the Thurston-Bennequin and rotation number of a Legendrian representative of the dual knot and a certain twisted Whitehead double in the Poincaré sphere Y . It uses a contact surgery description of Y and Kegel’s formulas [Keg16] for converting between classical invariants of front projections in surgery diagrams.
- **Section 10:** This section is dedicated to examples of deep versus shallow sliceness for links.
 - **Proposition 10.1:** We construct deep slice links which have shallow slice components in the non-simply connected boundaries of certain 2-handlebodies X^4 . They appear as Bing doubles $\text{BD}(m, 0)$ of meridians m of 2-handle attaching circles in a handle decomposition of X , where the meridians are required to be nontrivial in homotopy. Here and in the following, all framings are taken with respect to the boundary \mathbb{S}^3 of the 0-handle of the 2-handlebody X .
 - **Proposition 10.6:** If the boundary ∂X of a 4-dimensional 2-handlebody X is an integral homology 3-sphere, the determinant of a link is a shallow slice obstruction for $\text{Wh}_{+,1}(\text{BD}(\alpha, 0), 0) \subset \partial X$. This link is the 0-twisted Whitehead double of the first component of the 0-twisted Bing double of the loop $\alpha \subset \partial X$, with certain conditions on the framing and linking of α with the handle attaching circles in the boundary of the 0-handle of X .

- **Theorem 10.8:** We exhibit the difference between smooth deep strong sliceness and shallow topological strong sliceness for links, by iterated Whitehead doubling one component of the Bing double $BD(\tilde{K}, 0)$ of the dual knot \tilde{K} in the Poincaré sphere, which yields the link $Wh_{+1}^{(3)}(BD(\tilde{K}, 0), 0)$. Topological shallow strong sliceness again follows from Freedman’s construction of topological slices in certain height 3 Casson towers. The smooth shallow slice obstruction comes from a combination of a covering link argument and computations of τ -invariants of Whitehead doubles of certain curves in connected sums of Poincaré spheres.

Part III – Trisecting groups of knotted surface complements:

The results in this part, transferring the notion of a *group trisection* to the case of bridge trisected knotted surfaces in the 4-sphere, have not been published before; the construction will be generalized to arbitrary bridge trisected surfaces in trisected 4-manifolds in [BKKLR22].

- **Section 13:** We define *group trisections of knotted surface type* as an algebraic analogue of bridge trisections of knotted surfaces in the 4-sphere [MZ17]. This is a triple of epimorphisms from the group of a punctured 2-sphere to free groups, with a certain condition on the images of the meridians of the punctures, and a pairwise compatibility condition on the resulting pushout groups.
- **Section 14:** We give a careful exposition on how parameterized bridge trisections induce a ‘Seifert-van Kampen cube’ of group homomorphisms. There is a subtlety in the choice of fundamental group generators on the central punctured 2-sphere, and in **Proposition 15.1** we find an example of a 2-bridge trivial tangle such that the minimal number of meridians on the 2-sphere generating the tangle complement is three. The technique for the proof is Stallings’ folding algorithm, which represents subgroups of free groups as immersions of graphs.
- **Section 15.2** contains documentation of our SageMath program, available from [Rup21a], which assists with bookkeeping in the Wirtinger algorithm applied to triplane diagrams. This SageMath class in particular includes methods for computing group trisections of knotted surface type from a triplane diagram.
- **Section 16** includes computations of group trisections of knotted surface type of twist-spun 2-bridge and 3-bridge torus knots. An interesting family is given by the following:
 - $\tau^3 T_{2,5}$, the 3-twist spin of the $(2, 5)$ -torus knot in **Section 16.1.1**
 - $\tau^5 T_{2,3}$, the 5-twist spin of the $(2, 3)$ -torus knot in **Section 16.1.2**
 - $\tau^2 T_{3,5}$, the 2-twist spin of the $(3, 5)$ -torus knot in **Section 16.2.1**.
 These knotted spheres are pairwise non-isotopic, but all have the same fundamental group of the complement, which is isomorphic to $\mathbb{Z} \times \text{Dod}^*$. In particular, these lead to non-isomorphic group trisections of knotted surface type with the same group.
- **Section 17:** We construct a 7-bridge trisection of Suciú’s ribbon 2-knots from their fusion number two ribbon presentation. Afterwards, we compute the infinite family of group trisections of knotted surface type of the trefoil group corresponding to Suciú’s family.

We briefly mentioned the results of the author’s articles [KPR20; KNR21] towards the beginning of the introduction, however further details are not included in this thesis.

PART I

 CASSON-WHITNEY UNKNOTTING

This part reports on and extends joint work with Jason Joseph, Michael Klug and Hannah Schwartz [JKRS20].

We recall in Section 3 the setup for defining the *Casson-Whitney length* between smoothly embedded surfaces in an ambient 4-manifold in terms of the length of a regular homotopy. The *Casson-Whitney number* u_{CW} is the special case measuring the length to an unknotted surface in the 4-sphere. We also lay the foundation for later arguments involving the fundamental group of the complement of a surface, and discuss lower bounds for Casson-Whitney numbers coming from the Alexander module. This section closely follows the introduction of [JKRS20].

In Section 4 we study Casson-Whitney lengths between rim surgeries on surfaces and generalize certain constructions of regular homotopies from [JKRS20]. We also recall the relationship between the Casson-Whitney number and the stabilization number in Section 5.

Then Section 6 focuses on the class of ribbon surfaces in the 4-sphere. We first point out how the Casson-Whitney unknotting procedure of [JKRS20] generalizes to higher genus ribbon surfaces. Further we investigate an interesting family of ribbon 2-knots, originally constructed by Suciú [Suc85]. The members of this infinite family have surprising behavior under stabilizations and finger moves. We show that all of Suciú's examples have stabilization number equal to one. Then we observe that the associated \mathbb{RP}^2 -knots form an infinite family of distinct knotted projective planes in the 4-sphere all of which yield isotopic immersed surfaces after a single finger move.

Parts of the paper [JKRS20] have appeared in Jason Joseph's PhD thesis submitted to the University of Georgia [Jos20]. The topics included in Joseph's thesis are summarized below.

The *algebraic Casson-Whitney number* alg_{CW} of an embedded knotted surface in \mathbb{S}^4 is the minimal number of meridian-commuting relations that are necessary for abelianizing the fundamental group of the complement (Definition 3.19). It gives a lower bound on u_{CW} , which has applications to the classical unknotting number when it is combined with an upper bound on twist-spun knots (Corollary 4.4). Theorem 2.2 and Proposition 3.24 make use of determinants, and we take this opportunity to introduce their definition now.

The *Alexander module* of an oriented knotted surface in \mathbb{S}^4 is the first homology of the infinite cyclic cover, viewed as a $\mathbb{Z}[t^{\pm 1}]$ -module, where t acts as the generator of the covering transformations. The *determinant* of an oriented knotted surface K in \mathbb{S}^4 is defined in [Jos19] as the positive generator of the evaluation of the Alexander ideal at $t = -1$, i.e. $\Delta(K)|_{t=-1} := n$, where $n > 0$ is the generator of the principal ideal $\{f(-1) \mid f(t) \in \Delta(K)\} \subseteq \mathbb{Z}$. Equivalently, it is the order of the \mathbb{Z} -module induced by setting $t = -1$ in the Alexander module. As with classical knots this is always an odd integer, and in [Jos19, Prop. 5.9] it is shown that even twist-spinning preserves the determinant, while odd twist-spins always have determinant 1. A *Fox p -coloring* of a (classical or 2-) knot is a surjection from its knot group

onto the dihedral group $\text{Dih}_p \cong \mathbb{Z}_p \rtimes \mathbb{Z}_2$, which sends meridians of the knot to reflections. The classical fact that a 1-knot k admits a Fox p -coloring for prime p if and only if p divides the classical determinant $|\Delta_k(-1)|$, where $\Delta_k(t)$ is the Alexander polynomial of k , carries over without change to this definition of determinant for non-principal ideals.

Scharlemann proved that unknotting number one knots are prime, i.e. if k_1 and k_2 are nontrivial classical knots, then the unknotting number of $k_1 \# k_2$ is at least two [Sch85]. We can prove a special case of the analogous statement for u_{CW} , which works whenever the 2-knots in question have nontrivial determinants, or equivalently whenever their knot groups admit nontrivial Fox colorings. This reproves the same special case of Scharlemann's theorem for classical knots, via the bound given by Corollary 4.4. The technical core of the proof (which we do not reproduce here) is a Freiheitssatz for one-relator quotients of free products of cyclic groups due to Fine-Howie-Rosenberger [FHR88]. This can be applied to show that the image of a finger move relation in a quotient of the knot group of certain connected sums cannot abelianize the group.

THEOREM 2.1 ([JKRS20]). *Let K_1 and K_2 be smoothly knotted 2-spheres in \mathbb{S}^4 with determinant $\Delta(K_i)|_{-1} \neq 1$. Then $u_{\text{CW}}(K_1 \# K_2) \geq 2$.*

Thus, Casson-Whitney number one 2-knots cannot be factored into a connected sum of two 2-knots, each with nontrivial determinant.

For odd integers $p, q \in \mathbb{Z}$, let $K_{p,q} = \tau^0(T_{2,p} \# T_{2,q})$ denote the spin of the connected sum of torus knots $T_{2,p} \# T_{2,q}$. Miyazaki proved that $u_{\text{st}}(K_{p,q}) = 1$, whenever $q = p + 2, p + 4$, or $p + 6$, when $\gcd(p, p + 6) = 1$ [Miy86], thus u_{st} fails to be additive in these cases. However, it follows from Theorem 2.1 that u_{CW} is additive for this connected sum, and in particular that $u_{\text{CW}}(K_{p,q}) = 2$.

THEOREM 2.2 ([JKRS20]). *There are infinitely many 2-knots $K: \mathbb{S}^2 \hookrightarrow \mathbb{S}^4$ with $u_{\text{st}}(K) = 1$ and $u_{\text{CW}}(K) = 2$.*

The Casson-Whitney number shows strong non-additivity in certain cases, which we take to mean that the difference $u_{\text{CW}}(K_1) + u_{\text{CW}}(K_2) - u_{\text{CW}}(K_1 \# K_2)$ can become arbitrarily large. An alternative proof of this result is given in [JP21] in the context of meridional ranks of knotted spheres.

Conventions: In this part, all manifolds and maps are smooth unless stated otherwise. All ambient 3- and 4-manifolds are connected and orientable, and both manifolds and immersed surfaces are compact. We allow non-orientable embedded and immersed surfaces in particular. A *2-knot* specifically refers to a knotted genus zero surface, i.e. a knotted 2-sphere $\mathbb{S}^2 \hookrightarrow X$ embedded in an ambient 4-manifold X^4 .

3 REGULAR HOMOTOPIES OF SURFACES AND STABILIZATION

The classical unknotting number of a 1-knot in the 3-sphere records the minimal number of double points which occur during a regular homotopy to the unknot. The analogue we consider in the 4-dimensional setting is the minimal number of Whitney moves needed in a regular homotopy taking a knotted surface K in the 4-sphere to the unknot (double points are introduced/removed by a finger move/Whitney move). We call the minimal number of Whitney moves the *Casson-Whitney number* $u_{CW}(K)$ of the knot K . This notion of an unknotting number of knotted spheres in the 4-sphere in terms of the length of a regular homotopy to the unknot has appeared in [JKRS20]. Here, we generalize the same idea to define a length between regularly homotopic surfaces in an ambient 4-manifold X^4 .

3.1 The Casson-Whitney length

The following paragraphs are taken from the introduction in [JKRS20].

By Smale [Sma58, Thm. D] and Hirsch [Hir59, Thm. 8.3], embedded surfaces in an orientable 4-manifold, with identical Euler number of their normal bundle, are homotopic if and only if they are *regularly homotopic*, i.e. homotopic through immersions. For further discussion of generic immersions and their regular homotopy classes in the smooth setting, see [GG73]. Topological regular homotopies of simply connected surfaces in 4-manifolds are discussed for example in [FQ90, Lem. 1.2, Prop. 1.6] and [PRT21, Thm. 1.2]; more general statements for locally flat surfaces of arbitrary genus can be found in [Kas+22, Thm. 2.27]. Generically, there are only finitely many times during a regular homotopy at which the immersed surface is not self-transverse. At these times, double points of opposite sign are either introduced or canceled.

Definition 3.1. The local model for the regular homotopy removing pairs of double points is called a *Whitney move*. This homotopy is supported in a regular neighborhood of a *Whitney disk* W . The inverse to this homotopy is called a *finger move*, which is supported in a regular neighborhood of an arc α whose endpoints lie on the surface, and whose interior is embedded in the complement. We call the arc α a *guiding arc for the finger move*.²

These two homotopies are depicted in Figure 1. Also labeled in the figure are the *Whitney arcs* ω_1 and ω_2 , whose union is the boundary of the *Whitney disk* W . Each Whitney arc connects a pair of double points along one of the sheets of the immersed surface.

Remark 3.2. To explicitly define a Whitney move in local coordinates, one requires that the normal disk bundle of the Whitney disk be framed ‘compatibly’ with respect to its boundary on the immersed sphere; refer to [FQ90] as well as Casson’s lectures in [Cas86] for more details. Likewise, a framing of the normal \mathbb{D}^3 -bundle of the guiding arc compatible with the surface at its endpoints is needed to explicitly define a finger move. The choice of framing for the guiding arc will be suppressed, however, since (as with stabilizations) the resulting immersed surface, up to ambient isotopy, is independent of this choice of framing and depends only on the homotopy class of the arc itself, rel boundary; see the discussion in [Gab20, Rem. 5.3] for instance.

From now on, we shall always consider *generic* regular homotopies, in the sense that they are compositions of finger moves, Whitney moves, and isotopies as in Definition 3.1. In fact, since the guiding arcs of the finger moves can be isotoped away from the Whitney disks in the ambient 4-manifold, a deformation of the homotopy (without increasing the number of finger and Whitney moves) arranges for all of the finger moves to occur first and simultaneously, followed by all of the Whitney moves. A more detailed discussion of this folklore fact can be found in [Qui86, Sec. 4.1]. We will always assume that our regular homotopies are of this form.

² Compare with the guiding arc for stabilizations in Definition 3.11.

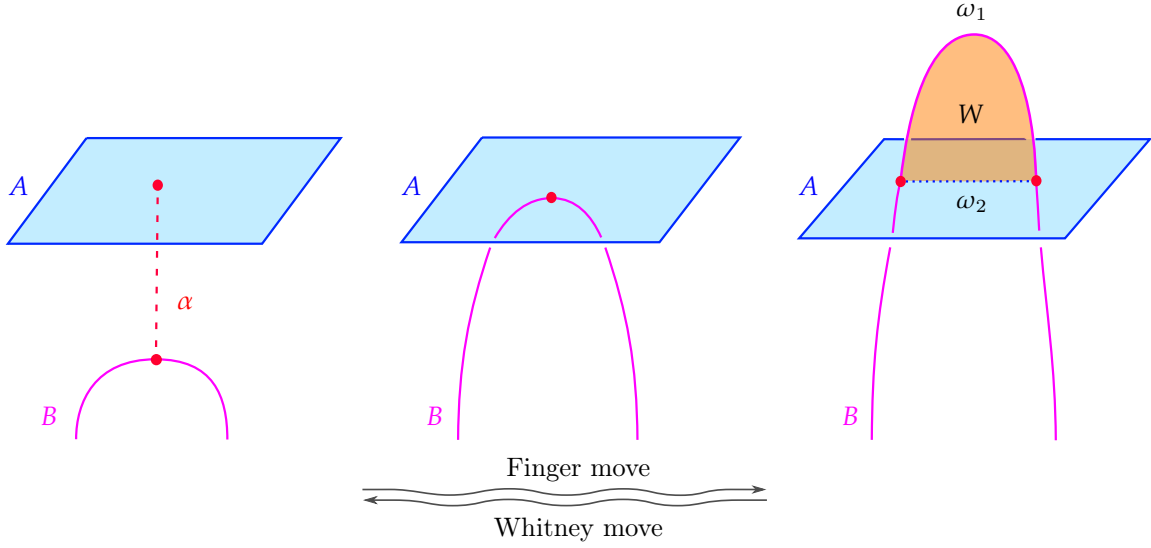


Figure 1. The local model of a finger move between the sheets A and B of a surface along the guiding arc α , and Whitney move along the Whitney disk W with boundary the union of the Whitney arcs ω_1 and ω_2 .

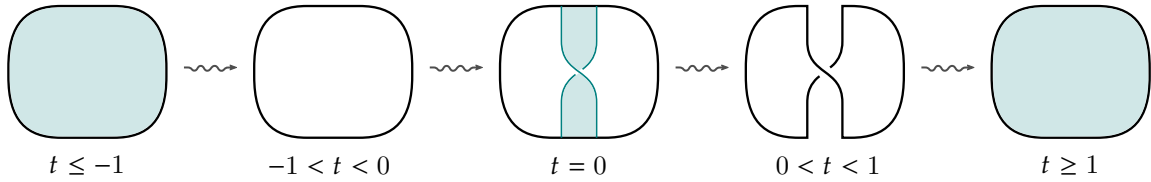


Figure 2. Movie describing the level sets $\mathbb{S}^3 \times \{t\}$ of $\mathbb{S}^3 \times \mathbb{D}^1$ and their intersections with an unknotted projective plane $P_+ \subset \mathbb{S}^3 \times \mathbb{D}^1 \subset \mathbb{S}^4$. At heights $t = -1$ and $t = 1$ a shaded disk bounded by an unknot is shown, corresponding to an index 0 and index 2 handle respectively. At height $t = 0$ we see a shaded band representing a saddle of the surface, i.e. a 1-handle attachment. For a movie of P_- reflect all of the crossings. The Euler number of their normal bundle is $e(P_+) = +2$ and $e(P_-) = -2$.

Definition 3.3. The *length* of a regular homotopy between surfaces is the total number of its constituent finger moves, or equivalently, Whitney moves. The *Casson-Whitney number* $u_{CW}(K)$ of a knotted surface $K \subset \mathbb{S}^4$ is the minimal length of any regular homotopy from K to the unknot.

Definition 3.4. A smoothly *unknotted orientable surface* U_g in \mathbb{S}^4 is a smoothly embedded connected surface of any genus that bounds a smoothly embedded solid 1-handlebody $\natural^g \mathbb{S}^1 \times \mathbb{D}^3 \hookrightarrow \mathbb{S}^4$.

A smoothly *unknotted non-orientable surface of genus 1* in \mathbb{S}^4 is a smoothly embedded projective plane \mathbb{RP}^2 which is isotopic to one of the standard models P_+ , P_- as shown in the movie³ in Figure 2. Let $P_{i,j} = \#^i P_+ \#^j P_-$. A smoothly *unknotted non-orientable surface of genus g* is a smoothly embedded connected non-orientable surface isotopic to $P_{i,j}$ for some choice of $i + j = g$, where $i, j \in \mathbb{N}_0$.

Since \mathbb{S}^4 is simply connected, the cores of the 1-handles of any pair of handlebodies of the same genus are isotopic. This can be used to guide an isotopy to show that there is a unique unknotted orientable surface of each genus.

For non-orientable surfaces of genus one there are precisely two unknotted projective planes P_+ and P_- . There are $g + 1$ many unknotted non-orientable surfaces of genus g which are distinguished by the Euler number of the normal bundle. The possible Euler numbers for non-orientable surfaces in \mathbb{S}^4 are discussed in [Mas69], in particular any projective plane embedded in \mathbb{S}^4 has Euler number ± 2 . By the discussion

³ We further elaborate on the motion picture method for describing knotted surfaces in Section 6.3.

in [HK79, Sec. 3] a connected smoothly embedded non-orientable surface in \mathbb{S}^4 bounds a non-orientable handlebody if and only if it is smoothly unknotted and the embedding has Euler number zero. As noted in [Jos+21, Rem. 2.10], the orientation convention for the ambient 4-sphere in [HK79] and [Kam89] does not agree with the standard choice; in our notation, the Euler numbers of the unknotted projective planes are $e(P_+) = +2$ and $e(P_-) = -2$.

In general, finger moves (and stabilizations) depend on the choice of guiding arc up to homotopy rel boundary. If two guiding arcs are homotopic and (using that the ambient dimension is 4) hence isotopic rel endpoints, then performing finger moves along these arcs results in immersions that are ambiently isotopic in X^4 .

Definition 3.5. Let $K \subset X$ be a knot of codimension 2 in an ambient manifold with closed normal bundle $\bar{\nu}(K)$. Then let $\iota_*: \pi_1(\partial\bar{\nu}(K), *) \rightarrow \pi_1(X - K, *)$ be the map on fundamental groups induced by the inclusion. We call its image $\iota_*(\pi_1(\partial\bar{\nu}(K), *))$ in the knot group $\pi_1(X - K, *)$ the *peripheral subgroup* of K .

For knotted spheres $K: \mathbb{S}^2 \hookrightarrow \mathbb{S}^4$, the peripheral subgroup is the image of the cyclic subgroup generated by a meridian. Boyle [Boy88] gave a classification of guiding arcs for stabilizations (which also applies to guiding arcs of finger moves) in terms of double cosets of the peripheral subgroup.⁴ In particular, it is critical to many of our arguments that all guiding arcs, and hence finger moves, are isotopic in the complement of the unknot U_g in the 4-sphere. Non-orientable analogues of Boyle's results were found by Kamada [Kam14].

Definition 3.6. We call the result of performing n finger moves on the unknot $U_g \subset \mathbb{S}^4$ the *standard immersed sphere* with $2n$ double points. Often, we reserve the use of the letter Σ to denote this immersion.

We later observe that there is indeed a unique standard orientable immersed surface for each genus and number of double points $2n$, up to ambient isotopy in \mathbb{S}^4 . A similar statement holds for standard immersed non-orientable surfaces for each genus, i.e. finger moves on a connected sum of unknotted projective planes, if we restrict the Euler number of the normal bundle.

Definition 3.7. After the finger moves and before the Whitney moves, any regular homotopy from an orientable knotted surface $K \subset \mathbb{S}^4$ to the unknot U_g restricts to the standard immersion Σ .

$$\text{knotted surface } K \begin{array}{c} \xrightarrow{\text{finger moves}} \\ \xleftrightarrow{\text{Whitney moves}} \end{array} \text{standard immersion } \Sigma \begin{array}{c} \xleftarrow{\text{Whitney moves}} \\ \xleftarrow{\text{finger moves}} \end{array} \text{unknot } U_g$$

Therefore, a regular homotopy from a knotted surface K to the unknot U_g is given by two collections of Whitney disks that pair the double points of the standard immersion: a set of *standard* Whitney disks leading to the unknot U , and a set of *knotted* Whitney disks leading to the knot K , as illustrated in Figure 3.

Remark 3.8. For general regular homotopies between knotted objects, i.e. those not necessarily leading to the unknotted 2-sphere, these have been called the *ascending* and *descending* Whitney disks and Whitney arcs [Sch21].

Definition 3.9. Let $K_0, K_1: \Sigma_g \hookrightarrow X^4$ be a pair of regularly homotopic oriented knotted surfaces in a smooth 4-manifold X^4 . The regular homotopy can be decomposed into a sequence of finger moves introducing pairs of double points, followed by a sequence of Whitney moves which remove double points, with isotopies in between. Then the *Casson-Whitney length* (or *relative Casson-Whitney number*)

$$\text{length}_{\text{CW}}(K_0, K_1) \in \mathbb{Z}_{\geq 0}$$

⁴ The second homology of the resulting knot group can be used to distinguish trivial stabilizations from non-trivial stabilizations, see also [Lit81].

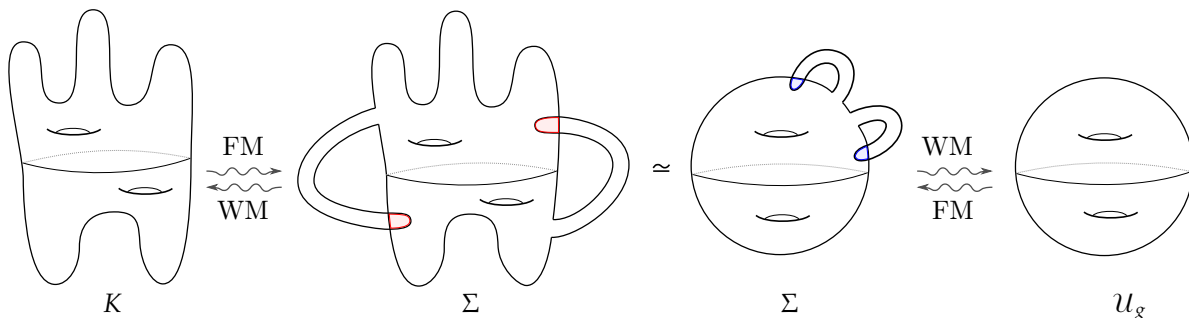


Figure 3. Decomposing a regular homotopy from a knotted surface K to the unknot U_g . The standard immersed surface Σ obtained after the finger moves (FM) and before Whitney moves (WM) on K is drawn from two different perspectives (middle left and middle right) to show the knotted and standard Whitney disks (red and blue respectively).

is the minimal length of such a regular homotopy from K_0 to K_1 , where length is the number of finger moves in the regular homotopy, equivalently the number of Whitney moves.

A similar definition is possible for non-orientable surfaces, where we assume that the normal bundles of the surfaces have the same Euler number to begin with. We are calling this a ‘length’ instead of a ‘distance’ to avoid confusion with a very similarly defined invariant $\text{dist}_{\text{sing}}$ in [Sin20] and [JZ18], which records the minimal ‘width’ of a sequence double points in a regular homotopy instead. In our terminology, the *Casson-Whitney (unknotting) number* of an oriented knotted surface $K: \Sigma_g \hookrightarrow \mathbb{S}^4$ in the 4-sphere is $u_{\text{CW}}(K) = \text{length}_{\text{CW}}(K, U_g)$, where $U_g: \Sigma_g \hookrightarrow \mathbb{S}^4$ is the smoothly unknotted genus g surface in \mathbb{S}^4 .

Remark 3.10 (Comments on the topological category). A topologically embedded sphere $K: \mathbb{S}^2 \hookrightarrow \mathbb{S}^4$ whose complement has infinite cyclic fundamental group $\pi_1(\mathbb{S}^4 - K) \cong \mathbb{Z}$ is topologically unknotted [FQ90, Thm. 11.7A], i.e. it extends to an embedding of a topologically locally flat embedded 3-ball. For topologically locally flat surfaces of genus $g \geq 3$, a similar statement holds [CP20]: They are topologically unknotted⁵ if and only if their complement has infinite cyclic fundamental group. The genus $g = 1$ and $g = 2$ cases appear to be still unknown; observe the correction in [HT97] to [HK95].

3.2 The stabilization number

The following paragraphs are taken from the introduction in [JKRS20]. For all definitions below, let S be a smoothly immersed surface in \mathbb{S}^4 ; in particular, this means that S can be embedded.

Definition 3.11. Suppose α is an arc with interior embedded in $\mathbb{S}^4 - S$ and whose endpoints lie on the oriented immersed surface S . The normal bundle of α in \mathbb{S}^4 contains an embedded copy of $\mathbb{D}^2 \times [0, 1]$ intersecting S in exactly $\mathbb{D}^2 \times \partial[0, 1]$ such that the surface

$$(S - (\mathbb{D}^2 \times \partial[0, 1])) \cup (\partial\mathbb{D}^2 \times [0, 1])$$

(with corners smoothed) is orientable; see Figure 4. This resulting surface is the *stabilization of S along α* , and we call α the *guiding arc for the stabilization*.

Observe that, as suggested by our terminology, in the oriented case the isotopy class of the stabilization depends only on the guiding arc α and not on the choice of sub-bundle $\mathbb{D}^2 \times [0, 1]$; see Remark 3.2 for a similar discussion and [Gab20, Rem. 5.3] for more detail. Since guiding arcs with the same endpoints that are homotopic rel boundary are also isotopic rel boundary in dimension 4, the stabilizations along these

⁵ *Topologically unknotted* means that they bound a topologically locally flat embedded 3-dimensional handlebody; compare with the smooth Definition 3.4.

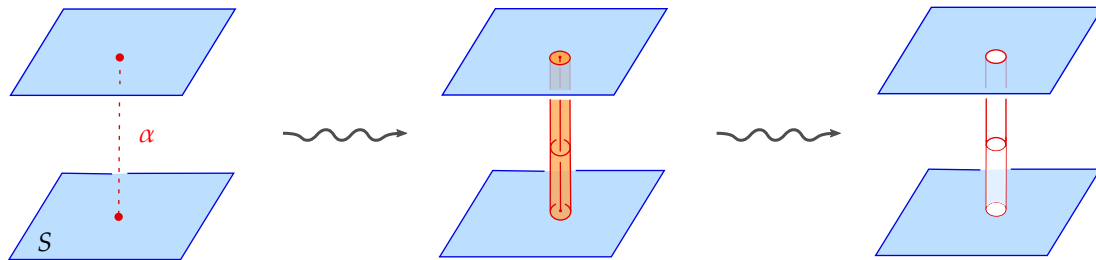


Figure 4. The result of stabilization (**right**) of a surface S along the guiding arc α .

arcs are isotopic. We can similarly stabilize a non-orientable surface, which will produce a non-orientable surface of higher genus [Kam89]. In that case, there are potentially two ways of attaching a handle along a framed guiding arc, distinguished by assigning local orientations. Different choices of framing might lead to isotopic surfaces, compare [BS16, Lem. 4].

Any closed oriented smooth embedded surface K in the 4-sphere is smoothly isotopic to an unknotted oriented surface after a finite number of stabilizations.⁶ To see this, note that such a surface K bounds a smoothly embedded 3-manifold $M^3 \subset \mathbb{S}^4$ called its *Seifert solid* whose relative handle decomposition can be built from $K \times [0, 1]$ by attaching 1-handles to $K \times \{1\}$, followed by 2- and 3-handles. Performing stabilizations to K along the core arcs of the 1-handles of M gives a surface K' that bounds the solid handlebody consisting of the 2- and 3-handles of M , and so by definition is unknotted. This argument in the 4-sphere was already observed by [HK79], and has been generalized to various settings in other 4-manifolds as discussed in Section 5.

Definition 3.12. The *stabilization number* $u_{\text{st}}(K) \in \mathbb{N}_0$ of a smoothly knotted surface K in the 4-sphere is the minimal number of 1-handle stabilizations needed to obtain a smoothly unknotted surface.

In the literature, the stabilization number has traditionally been called an “unknotting number for knotted surfaces” [HMS79]. This is analogous to the minimal number of 1-dimensional stabilizations (i.e. oriented band attachments) of a 1-knot needed to obtain an unknot or unlink. The band unknotting number is bounded above by twice the classical unknotting number, since crossing changes can be realized by two band attachments. But these invariants are **not** in general equal, for example they differ for a fusion number 1 ribbon knot with unknotting number ≥ 2 such as 9_{46} . For lower bounds on the band unlinking number of classical knots see [JMZ20a]. We will generalize the stabilization number to relate pairs of knotted surfaces in terms of the length of a stabilization and destabilization sequence in Definition 5.1.

3.3 Fundamental group calculations

The following paragraphs are taken from the introduction in [JKRS20]. This section will mainly be spent analyzing the algebraic impact of the geometric operations we will be interested in.

Below, we describe the effects of finger moves and stabilizations on the fundamental group of the complement of a (possibly immersed) surface $S = S_1 \cup \dots \cup S_n \subset X^4$ in an ambient oriented 4-manifold. The surface S can be disconnected, and have both orientable and non-orientable components. Each move introduces one relation to the fundamental group as stated in the results below; for detailed proofs, we refer to the original sources [Cas86; Boy88; Kir89].

⁶ For the analogous statement for non-orientable surfaces, see [BS16, Thm. 6]: A non-orientable surface S in the 4-sphere with Euler number $e(S)$ becomes isotopic to an unknotted non-orientable surface with Euler number $e(S)$ after a finite number of stabilizations.

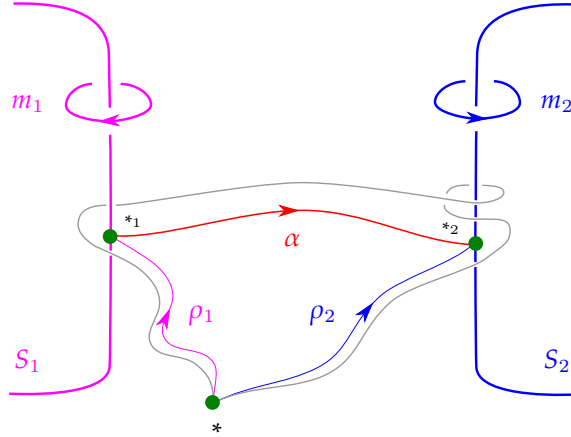


Figure 5. A choice of pushoff in gray, giving an element of $\pi_1(X - S, *)$ corresponding to the red guiding arc α for some knotted surface $S \subset X^4$. Also pictured are unbased meridians m_i for the components S_i .

Begin by picking a basepoint $*$ in the complement of the surface link S and a basepoint $*_i \in S_i$ on each component of S . For each i , fix an arc ρ_i with interior in $X - S$ connecting the basepoint $*$ to the basepoint $*_i$ on the i th component.

Definition 3.13. A *meridian* of S , and more specifically of the component S_i , is an element of $\pi_1(X - S)$ that can be represented by a simple closed curve $\gamma: \mathbb{S}^1 \hookrightarrow X - S$ bounding a disk in the 4-manifold X that transversely intersects S_i in a single point.

For a surface S an orientation of the orientable components of S and the ambient space induces a positive orientation on the meridians of these components. The set of positively oriented meridians of an oriented connected component of an knotted surface forms a conjugacy class of the fundamental group of its complement. That is, x is a meridian of S_i if and only if $x^w := w^{-1}xw$ is as well, for any $w \in \pi_1(X - S)$. If S is connected, this element w may be chosen to lie in the commutator subgroup $[\pi_1(X - S), \pi_1(X - S)]$, by multiplying a power of a meridian to ensure linking number zero of the arc w with the surface S . The same notion of a meridian applies to non-orientable surfaces as well, but observe that these might have finite order in the knot group. For example, the meridian of an unknotted projective plane in the 4-sphere has order 2.

Definition 3.14. Let α be an arc with interior embedded away from S , connecting $*_i$ to $*_j$ for (possibly equal) indices i, j . We call this a *guiding arc* for S . Each push-off of the loop $\rho_i\alpha\rho_j^{-1}$ into the complement of the surface S gives an element $g \in \pi_1(X - S)$ that is said to *correspond* to the arc α ; see Figure 5. Note that the element g is well-defined (i.e. independent of the push-off) up to left multiplication by meridians of S_i and right multiplication by meridians of S_j .

From now on, we will always assume that the guiding arcs used for both stabilizations and finger moves are of this form, i.e. connecting a basepoint $*_i \in S_i$ to a basepoint $*_j \in S_j$ for some (possibly equal) indices i, j . We often refer to arcs corresponding to the identity element, as well as stabilizations and finger moves done along such a guiding arc, as *trivial*.

Remark 3.15. Let α and β be guiding arcs for S with the same endpoints $*_i$ on S_i and $*_j$ on S_j . Suppose that α corresponds to an element $g \in \pi_1(X - S)$ and β corresponds to $m_1^{n_1} g m_2^{n_2}$ for some $n_1, n_2 \in \mathbb{Z}$ and meridians m_i, m_j to S_i, S_j respectively. Then, the guiding arcs α and β are isotopic in the complement of S rel boundary via a sequence of *boundary twists* as pictured in Figure 6. It follows that the surfaces obtained by either stabilizing or performing finger moves along these arcs are ambiently isotopic.

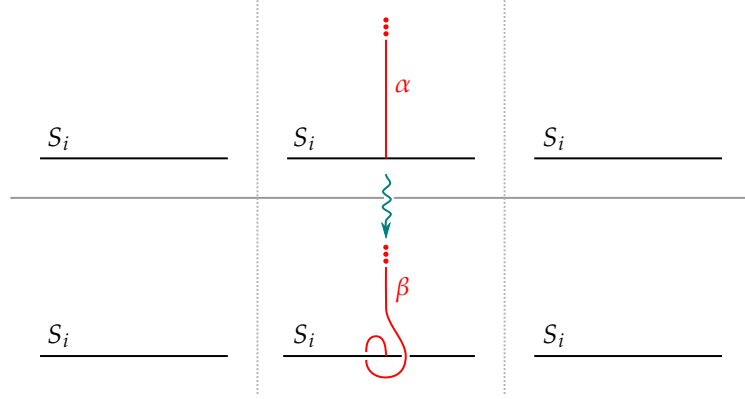


Figure 6. The guiding arcs from Remark 3.15 in red, before (top) and after (bottom) a boundary twist. Here we draw the fourth coordinate as a horizontal time direction, such that the knotted surface component S_i intersects each time slice in a black line.

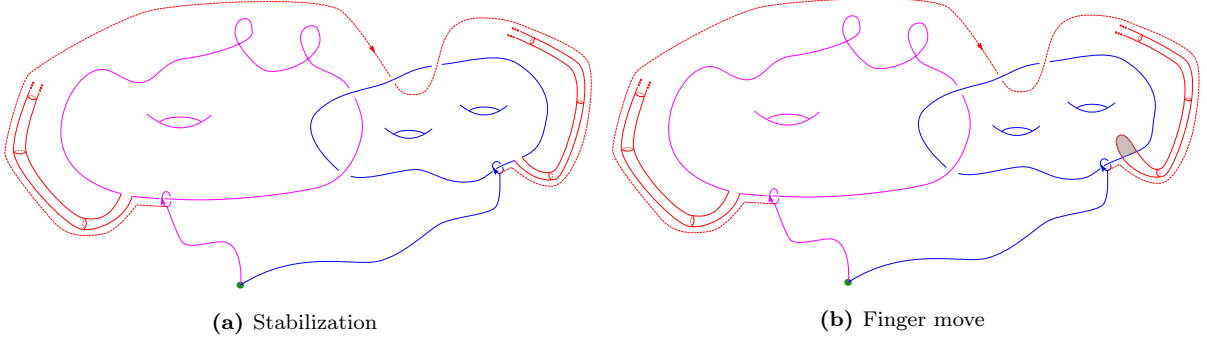


Figure 7. Illustrating Lemmas 3.16 and 3.18, with the meridian a_i in fuchsia, the meridian b_i in blue, and a guiding arc α in red.

In particular, it follows from Remark 3.15 that all guiding arcs for the unknotted orientable surfaces U_g in the 4-sphere are isotopic, since $\pi_1(\mathbb{S}^4 - U_g) \cong \mathbb{Z}$ is cyclic generated by the meridian. This uniqueness of guiding arcs is also true for unknotted non-orientable surfaces in \mathbb{S}^4 , since $\pi_1(\mathbb{S}^4 - P_{i,j}) \cong \mathbb{Z}/2$ is cyclic as well. So for any $n > 0$, there is a unique orientable surface (up to isotopy) resulting from n stabilizations of U_g – namely, the genus $g + n$ unknotted surface, as in Definition 3.4. Similarly, the immersed surface resulting from n finger moves on U_g is ambiently isotopic to the standard immersion with $2n$ double points, as in Definition 3.6. Analogous statements are true for non-orientable surfaces, which follows for example from the guiding arc classification in [BS16, Lem. 4].

LEMMA 3.16 (Stabilization relation). *Let $\alpha_1, \dots, \alpha_k$ be disjointly embedded guiding arcs stabilizing $S \subset X^4$ along which gives the surface S' . Then*

$$\pi_1(X - S') \cong \pi_1(X - S) \Big/ \langle\langle g_i^{-1} a_i g_i b_i^{-1} \rangle\rangle$$

where a_i, b_i are meridians to the components of S containing the endpoints of α_i (as in Definition 3.13), and the element g_i corresponds to α_i (as in Definition 3.14).

Refer to Figure 7a for a schematic of the set-up in Lemma 3.16. Note that each $g_i^{-1} a_i g_i$ is also a meridian, hence the relation introduced by stabilizing can also be thought of as one which simply identifies two meridians.

We make the following definitions of the *algebraic stabilization number* and *algebraic Casson-Whitney number* for (connected) knots of arbitrary dimension, because we will think about them in reference to

classical knot groups as well as knotted surface groups. These invariants are in particular well-defined for n -knots $\mathbb{S}^n \hookrightarrow \mathbb{S}^{n+2}$ for all $n \geq 1$ because they only depend on the knot group and the information of a meridian.

Definition 3.17. Let K be a knot of codimension 2 in an ambient manifold. The minimal number of relations of the form $x = y$, where x, y are meridians of K , which abelianize the knot group is called the *algebraic stabilization number* $\text{alg}_{\text{st}}(K)$ of K .

LEMMA 3.18 (Finger move relation). *Suppose that S' is the result of performing finger moves on $S \subset X^4$ along disjointly embedded guiding arcs $\alpha_1, \dots, \alpha_k$. Then,*

$$\pi_1(X - S') \cong \pi_1(X - S) \Big/ \langle\langle [a_i, g_i^{-1} b_i g_i] \rangle\rangle$$

where a_i, b_i are meridians to the components of S containing the endpoints of α_i (as in [Definition 3.13](#)), and the element g_i corresponds to α_i (as in [Definition 3.14](#)).

[Figure 7b](#) gives a schematic of the set-up in [Lemma 3.18](#). Note that while the stabilization relation identifies two meridians, a finger move relation can only make them commute. This discrepancy leads to our result in [Theorem 2.2](#) that the stabilization and Casson-Whitney numbers are not equal in general.

Definition 3.19. Let K be a knot of codimension 2 in an ambient manifold. The minimal number of relations of the form $xy = yx$ which abelianize the knot group, where x, y are meridians of K , is called the *algebraic Casson-Whitney number* $\text{alg}_{\text{CW}}(K)$ of K .

This minimum gives an algebraic lower bound for $u_{\text{CW}}(K)$ in the 4-sphere, since a regular homotopy from a knotted surface K to the unknot starts with a sequence of finger moves on K to the standard immersion Σ with $\pi_1(\mathbb{S}^4 - \Sigma) \cong \mathbb{Z}$, thus the corresponding finger move relations abelianize $\pi_1(\mathbb{S}^4 - K)$; analogously for non-orientable surfaces in \mathbb{S}^4 . We summarize the results of this section in the following proposition. To our knowledge, these are the sharpest known algebraic lower bounds for the unknotting numbers.

PROPOSITION 3.20. *For any knotted surface K in the 4-sphere, $\text{alg}_{\text{st}}(K) \leq u_{\text{st}}(K)$ and $\text{alg}_{\text{CW}}(K) \leq u_{\text{CW}}(K)$.*

3.4 Algebraic lower bounds

The following is taken from [\[JKRS20\]](#). In this section, we further discuss the *algebraic Casson-Whitney number* $\text{alg}_{\text{CW}}(K)$ of a knotted surface K in the 4-sphere, the minimal number of meridian-commuting relations which abelianize the knot group of K (see [Definition 3.19](#)). This algebraic invariant is the sharpest lower bound we are aware of for the Casson-Whitney number u_{CW} , and in [Proposition 4.9](#) we show that the algebraic Casson-Whitney number is also a lower bound for the classical unknotting number of a 1-knot $k: \mathbb{S}^1 \hookrightarrow \mathbb{S}^3$. It is clear that $\text{alg}_{\text{st}}(K) \leq \text{alg}_{\text{CW}}(K)$, as stabilization relations identify two meridians, while finger move relations merely force them to commute; see [Section 3.3](#) for a thorough description of the effects of the corresponding geometric operations on the knot group. This subtle difference is used to prove [Theorem 2.2](#), which constructs 2-knots $K: \mathbb{S}^2 \hookrightarrow \mathbb{S}^4$ with $\text{alg}_{\text{st}}(K) < \text{alg}_{\text{CW}}(K)$ and where this difference is realized geometrically.

3.4.1 Previously known results. The minimal number of generators of the Alexander module, called the *Nakanishi index* $m(K)$, is a classical lower bound for the unknotting number of 1-knots [\[Nak81\]](#). In [\[Miy86\]](#) and [\[MP19\]](#) it is shown that the Nakanishi index is also a lower bound for the stabilization number $u_{\text{st}}(K)$ of oriented knotted surfaces in the 4-sphere. Indeed, any set of relators which abelianize the group of a knot must normally generate its commutator subgroup. It is an exercise to show that the images of these relators generate the Alexander module; cf. [\[Rol90, Exercise 7.D.5\]](#).

As noted in [Proposition 3.20](#), the algebraic stabilization number, $\text{alg}_{\text{st}}(K)$, is a natural lower bound for the stabilization number $u_{\text{st}}(K)$. This is studied in [\[Kan96\]](#), where it is called the *weak unknotting number*. A subtler but sharper bound for the classical unknotting number is the *Ma-Qiu index* $a(K)$, defined as the minimal number of relations needed to abelianize the knot group [\[MQ06\]](#). In fact, the algebraic stabilization number $\text{alg}_{\text{st}}(k)$ ([Definition 3.17](#)) is also a lower bound for the classical unknotting number of a 1-knot $k: \mathbb{S}^1 \hookrightarrow \mathbb{S}^3$. This is evident from the proof of [\[MQ06\]](#), and also by combining the inequalities from [Proposition 3.20](#) and [Corollary 4.4](#), applied to the spin^7 of a classical knot k :

$$\text{alg}_{\text{st}}(k) = \text{alg}_{\text{st}}(\tau^0 k) \leq \text{alg}_{\text{CW}}(\tau^0 k) \leq u_{\text{CW}}(\tau^0 k) \leq u(k).$$

We summarize the previously known results regarding these invariants in the proposition below.

PROPOSITION 3.21 (Kanenobu, Ma-Qiu, Miyazaki, Nakanishi). *If $k: \mathbb{S}^1 \hookrightarrow \mathbb{S}^4$ is a 1-knot, then*

$$m(k) \leq a(k) \leq \text{alg}_{\text{st}}(k) \leq u(k).$$

If $K: \Sigma_g \hookrightarrow \mathbb{S}^4$ is an oriented knotted surface, then

$$m(K) \leq a(K) \leq \text{alg}_{\text{st}}(K) \leq u_{\text{st}}(K).$$

As pointed out in [\[MQ06\]](#), the first inequality above is often strict: The Ma-Qiu index is positive whenever $\pi_1(\mathbb{S}^4 - K)$ is not abelian, but the Alexander module and hence the Nakanishi index can be zero for nontrivial knots, e.g. Alexander polynomial one knots. While $m(k)$, $a(k)$, and $\text{alg}_{\text{st}}(k)$ are known to be non-additive on certain classical knots (see the end of [Section 3.4.2](#)), we are unaware of any classical knots for which alg_{CW} is non-additive. We show in [\[JKRS20, Sec. 6\]](#) that it is non-additive on certain 2-knots.

3.4.2 The algebraic Casson-Whitney number. Recall from [Section 3.3](#) that each finger move on a knotted surface K in the 4-sphere adds a relation of the form $[x, y] = 1$, where x, y are meridians of K . As noted after [Definition 3.13](#), y is equal to $x^w = w^{-1}xw$ for some $w \in [\pi_1(\mathbb{S}^4 - K), \pi_1(\mathbb{S}^4 - K)]$ in the commutator subgroup. Therefore, the algebraic Casson-Whitney number $\text{alg}_{\text{CW}}(K)$ is equal to the minimal number of elements $w_i \in [\pi_1(\mathbb{S}^4 - K), \pi_1(\mathbb{S}^4 - K)]$ such that the relations $\{[x, x^{w_i}] = 1\}$ abelianize $\pi_1(\mathbb{S}^4 - K)$.

These finger move relations are ‘weaker’ than the relations induced by stabilizations, in that every finger move relation is also a stabilization relation. Recall from [Definition 3.17](#) that $\text{alg}_{\text{st}}(K)$ denotes the minimal number of stabilization relations needed to abelianize the knot group. These relations are of the form $x = y$, where x and y are meridians, or equivalently $[x, w] = 1$, where $w \in [\pi_1(\mathbb{S}^4 - K), \pi_1(\mathbb{S}^4 - K)]$ and $y = x^w$. Thus $\text{alg}_{\text{st}}(K)$ is the minimal number of elements $w_i \in [\pi_1(\mathbb{S}^4 - K), \pi_1(\mathbb{S}^4 - K)]$ such that the relations $\{[x, w_i] = 1\}$ abelianize $\pi_1(\mathbb{S}^4 - K)$. Although x^w is not in the commutator subgroup, $x^w = x[x, w]$, so the finger move relation $[x, x^w] = 1$ is equivalent to the stabilization relation $[x, [x, w]] = 1$, and we see that $\text{alg}_{\text{st}}(K) \leq \text{alg}_{\text{CW}}(K)$.

On the other hand, an obvious upper bound for $\text{alg}_{\text{CW}}(K)$ is $\mu(K) - 1$, where $\mu(K)$ is the *meridional rank* of K , the minimal number of meridians of K needed to generate $\pi_1(\mathbb{S}^4 - K)$. This is because forcing any single meridian to commute with the other elements of a generating set of meridians will force that meridian into the center of the group. Since all knot groups of connected surfaces are normally generated by any meridian, this abelianizes the group. We summarize the relationships between these invariants below.

PROPOSITION 3.22. *For any n -knot $K: \mathbb{S}^n \hookrightarrow \mathbb{S}^{n+2}$,*

$$m(K) \leq a(K) \leq \text{alg}_{\text{st}}(K) \leq \text{alg}_{\text{CW}}(K) \leq \mu(K) - 1.$$

⁷ We introduce twist spun knots in [Definition 4.3](#).

In [Theorem 2.2](#) we show that the inequality $\text{alg}_{\text{st}}(K) \leq \text{alg}_{\text{CW}}(K)$ can be strict. In fact, we find infinitely many 2-knots K with $\text{alg}_{\text{st}}(K) = 1 = \text{u}_{\text{st}}(K)$ and $\text{alg}_{\text{CW}}(K) = 2$, enabling us to prove that $\text{u}_{\text{st}}(K) < \text{u}_{\text{CW}}(K)$ for infinitely many 2-knots K . The last inequality $\text{alg}_{\text{CW}}(K) \leq \mu(K) - 1$ may also be strict, for the same reason pointed out after [Theorem 6.3](#).

PROPOSITION 3.23. *For $\alpha \in \{a, \text{alg}_{\text{st}}, \text{alg}_{\text{CW}}\}$ and for n -knots $K_1, K_2: \mathbb{S}^n \hookrightarrow \mathbb{S}^{n+2}$,*

$$\max\{\alpha(K_1), \alpha(K_2)\} \leq \alpha(K_1 \# K_2) \leq \alpha(K_1) + \alpha(K_2).$$

Proof. The proof is the same in all three cases following Kanenobu in [\[Kan96\]](#) for $\alpha = \text{alg}_{\text{st}}$. Let g_1, \dots, g_n be a minimal set of relators of the required form (depending on α) which abelianize $\pi_1(\mathbb{S}^{n+2} - (K_1 \# K_2))$. Let ϕ be the surjection $\phi: \pi_1(\mathbb{S}^{n+2} - (K_1 \# K_2)) \rightarrow \pi_1(\mathbb{S}^{n+2} - K_1)$ which sends all meridians of K_2 to the meridian of amalgamation. Notice that $\pi_1(\mathbb{S}^{n+2} - K_1) / \langle\langle \phi(g_1), \dots, \phi(g_n) \rangle\rangle \cong \mathbb{Z}$ and that each $\phi(g_i)$ is a relator of the required form for computing $\alpha(K_1)$. Therefore, $\alpha(K_1 \# K_2) \geq \alpha(K_1)$. Repeating the argument for K_2 yields the first inequality.

The second is obtained by imposing relations on the group of $K_1 \# K_2$ which abelianize K_1 and K_2 separately. Since $\pi_1(\mathbb{S}^{n+2} - (K_1 \# K_2)) \cong (\pi_1(\mathbb{S}^{n+2} - K_1) * \pi_1(\mathbb{S}^{n+2} - K_2)) / \langle\langle x_1^{-1} x_2 \rangle\rangle$, where x_i are meridians of K_i , these relations abelianize the group of the connected sum. \square

As a first application of [Proposition 3.22](#), we show that any natural number can occur as the Casson-Whitney number of a 2-knot.

PROPOSITION 3.24. *Let $n \in \mathbb{N}_0$. Then there exists a 2-knot $K: \mathbb{S}^2 \hookrightarrow \mathbb{S}^4$ with $\text{u}_{\text{CW}}(K) = n$.*

Proof. Let J be any 2-knot with $\text{u}_{\text{CW}}(J) = 1$ and Nakanishi index $m(J) = 1$, for instance J could be any even twist-spin of a 2-bridge knot, by [Theorem 3.25](#): 2-bridge knots have nontrivial determinants, which are preserved by even twist-spinning [\[Jos19\]](#). Therefore the Alexander module of J is nontrivial, so it must be cyclic since it is a quotient of the original 2-bridge knot's Alexander module.

Then letting $K = \#^n J$ yields the desired result: the Nakanishi index $m(K) = n$, since the Alexander module of K is generated by n elements and surjects onto a vector space of dimension n , so by [Proposition 3.22](#) we know $\text{u}_{\text{CW}}(K) \geq n$. Conversely, K can be unknotted via n pairs of finger and Whitney moves by performing the optimal length one regular homotopy for J on each summand. \square

Finally we state without proof an upper bound on the Casson-Whitney number of twist spins of classical 2-bridge knots.

THEOREM 3.25 ([\[JKRS20, Thm. 4.7\]](#)). *If $k: \mathbb{S}^1 \hookrightarrow \mathbb{S}^3$ is a classical 2-bridge knot and the n -twist spin $\tau^n k$ is not unknotted, then $\text{u}_{\text{CW}}(\tau^n k) = 1$.*

The proof in [\[JKRS20\]](#) is inspired by the result of Satoh [\[Sat04\]](#) that the stabilization number of a twist spin $\tau^n k$ of a classical b -bridge knot k is bounded from above by the bridge number minus 1, $\text{u}_{\text{st}}(\tau^n k) \leq b - 1$. We were able to imitate this for twist spins of classical knots of bridge number $b = 2$, but could not extend the argument to higher bridge number because in contrast to 1-handles, finger moves cannot be slid over each other.

Remark 3.26. Singular banded unlink diagrams, together with a calculus of singular band moves relating different diagrams of smoothly isotopic immersions, are introduced in [\[HKM21\]](#). Additional representations of finger and Whitney moves allow diagrammatic descriptions of regular homotopies as well. This leads to an alternative banded unlink diagram proof [\[HKM21, Thm. 4.5\]](#) of the bridge number bound on Casson-Whitney numbers in [Theorem 3.25](#).

4 RIM SURGERY AND CASSON-WHITNEY LENGTH

In this section we construct a regular homotopy between certain rim surgeries on surfaces, which is related to constructions that have appeared in the literature before [BS16; JZ18; JKRS20; NS20]. For a classical based knot $J \subset \mathbb{S}^3$, let J_+ be the knotted arc in the 3-ball obtained by removing a small open standard 3-ball containing the arc segment J_- around the basepoint. We assume that the feet of the arc J_+ have been placed at the north and south poles N, S of the 3-ball \mathbb{D}^3 ; see the right hand side of [Figure 8](#). An open tubular neighborhood of J_+ has complement in \mathbb{D}^3 diffeomorphic to the exterior X_J of J in the 3-sphere.

4.1 Twist rim surgery and the accordion homotopy

We construct a *twisting map* $\tau: \mathbb{D}^3 \rightarrow \mathbb{D}^3$ as follows. Parameterize the knot J with a coordinate $x \in [0, 1]/(0 \sim 1)$. Identify a closed tubular neighborhood $\bar{\nu}(J \subset \mathbb{S}^3) \cong J \times \mathbb{D}^2$ of the knot J in the 3-sphere in such a way that for $\theta \in \partial\mathbb{D}^2 = \mathbb{S}^1 \cong [0, 2\pi]/(0 \sim 2\pi)$ the section $J \times \{\theta\}$ is null-homologous in the exterior X_J , i.e. corresponds to a Seifert longitude. Identify $\partial X_J \times [0, 1]$ with a collar of the peripheral torus $\partial X_J \times \{0\} \cong J \times \partial\mathbb{D}^2 \times \{0\}$ in the exterior X_J . The twisting map on the 3-sphere is defined as

$$\begin{aligned} \tau: \mathbb{S}^3 &\rightarrow \mathbb{S}^3 \\ (x, \theta, \varphi) &\mapsto (x, \theta + 2\pi\varphi, \varphi) && \text{for } (x, \theta, \varphi) \in J \times \partial\mathbb{D}^2 \times [0, 1] \\ y &\mapsto y && \text{for } y \notin J \times \partial\mathbb{D}^2 \times [0, 1] \end{aligned}$$

The map τ is the identity on the closed tubular neighborhood $\bar{\nu}(J \subset \mathbb{S}^3) \cong J \times \mathbb{D}^2$, and thus restricts to a map of the pair $\tau: (\mathbb{D}^3, J_+) \rightarrow (\mathbb{D}^3, J_+)$.

We write $\mathbb{S}^1 \times_{\tau^m} (\mathbb{D}^3, J_+)$ for the image of the product $\mathbb{S}^1 \times (\mathbb{D}^3, J_+)$ under the m -fold iterated twist map $\mathbb{S}^1 \times \mathbb{D}^3 \rightarrow \mathbb{S}^1 \times \mathbb{D}^3$, which rotates the 3-ball located at $\{z\} \times \mathbb{D}^3$ by $n \cdot z$ radians around a vertical axis through the poles of the 3-ball \mathbb{D}^3 . This can also be identified with the mapping cylinder of τ^m , given as a quotient

$$(\mathbb{D}^3, J_+) \times [0, 1] \Big/ (x, 0) \sim (\tau^m(x), 1) \text{ for } x \in \mathbb{D}^3.$$

Definition 4.1. *Rim surgery* on a locally flat embedded surface $F^2 \subset X^4$ is the following construction, schematically illustrated in [Figure 8](#). Given an embedded closed curve $\alpha \subset F$ and a classical knot $J \subset \mathbb{S}^3$ in the 3-sphere, the m -*twist rim surgery* is a new locally flat embedded surface denoted by $F_{\tau^m}(\alpha, J) \subset X$. Here the knot $J \subset \mathbb{S}^3$ and its associated knotted arc $J_+ \subset \mathbb{D}^3$ are called the *pattern*. Let $\bar{\nu}(\alpha \subset X)$ be a closed tubular neighborhood of the curve α in the ambient 4-manifold such that $\bar{\nu}(\alpha \subset X) \cap F$ is an annulus. Choose a trivialization of the normal bundle $\bar{\nu}(\alpha \subset X) \rightarrow \alpha \times \mathbb{D}^3 \cong \alpha \times [0, 1] \times \mathbb{D}^2$ which agrees on $\alpha \times [0, 1]$ with the normal bundle $\bar{\nu}(\alpha \subset F)$ of α in the surface F . Then to construct the rim surgery, remove the annulus $\bar{\nu}(\alpha \subset F)$ given by the closed normal neighborhood of the curve $\alpha \subset F$ in the surface, and put back a knotted twisted annulus:

$$(X, F_{\tau^m}(\alpha, J)) := (X, F) - (\mathbb{S}^1 \times (\mathbb{D}^3, [0, 1])) \cup_{\partial=\mathbb{S}^1 \times (\mathbb{S}^2, \{N, S\})} \mathbb{S}^1 \times_{\tau^m} (\mathbb{D}^3, J_+).$$

Here we needed to identify a closed neighborhood of α in X with $\alpha \times \mathbb{D}^3$ in such a way so that $\alpha \times [0, 1]$ lies in the surface F . This still leaves a choice of trivialization of the 2-dimensional bundle $\bar{\nu}(\alpha \times [0, 1] \subset X)$. Usually we take the convention that for some point $p \in \partial\mathbb{D}^2$, the section given by the image of the vector $\{0\} \times p$ under translation around the circle \mathbb{S}^1 is required to be trivial in the first homology $H_1(X - F; \mathbb{Z})$ of the complement of F . In other words, we want this section to have linking number zero with the surface $F \subset X$.

An alternative perspective on the rim surgery construction is replacing $\mathbb{S}^1 \times (\mathbb{D}^3, [0, 1])$ with the untwisted product $\mathbb{S}^1 \times (\mathbb{D}^3, J_+)$, but putting the twisting into the gluing map. The version of rim surgery with

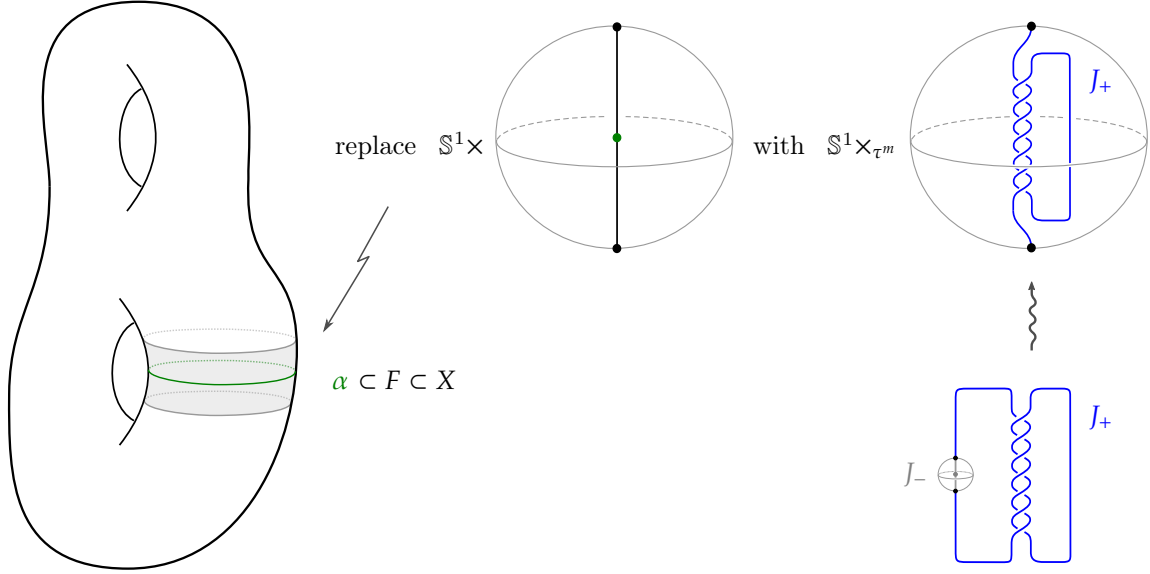


Figure 8. Schematic illustration of m -twist rim surgery on a curve $\alpha \subset F^2$ on a surface embedded in an ambient 4-manifold X^4 .

additional twisting was originally introduced by Kim [Kim06]; see that reference for the equivalence with the alternative definitions. Twist rim surgery is a special case of concordance rim surgery [JMZ20b].

THEOREM 4.2. Fix $m \in \mathbb{Z}$ and an embedded smoothly knotted surface $F^2 \subset X^4$. Let J_1 and J_2 be classical knots which differ by c crossing changes. Then there is a regular homotopy of length c between the m -twist rim surgeries $F_{\tau^m}(\alpha, J_1)$ and $F_{\tau^m}(\alpha, J_2)$. In other words, the Casson-Whitney length between twist rim surgeries is bounded above by the Gordian distance between the pattern knots,

$$\text{length}_{\text{CW}}(F_{\tau^m}(\alpha, J_1), F_{\tau^m}(\alpha, J_2)) \leq \text{dist}_{\text{Gord}}(J_1, J_2).$$

The regular homotopy is supported in a neighborhood of the surgery curve $\alpha \subset F$.

Proof. We will show that there is an immersed surface $F'_{\tau^m}(\alpha, J)$ with $2c$ double points that can be obtained as the result of c finger moves on both $F_{\tau^m}(\alpha, J_1)$ and $F_{\tau^m}(\alpha, J_2)$.

$$\begin{array}{ccc} F_{\tau^m}(\alpha, J_1) & & F_{\tau^m}(\alpha, J_2) \\ & \swarrow \text{c finger moves} & \nwarrow \text{c finger moves} \\ & F'_{\tau^m}(\alpha, J) & \end{array}$$

The local situation in a neighborhood of the curve α before and after the rim surgery is illustrated in Figure 9. The surface F intersects the closed neighborhood $\bar{\nu}(\alpha) \cong \alpha \times \mathbb{D}^3$ in an annulus, where for $x \in \alpha$ the intersection with the 3-ball $\{x\} \times \mathbb{D}^3$ is depicted as a straight arc segment. Going around the circle α , this line segment might rotate in the ambient 4-manifold depending on the framing of the curve α on F . We will parameterize the circle α with a coordinate $[-\pi, \pi]/(-\pi \sim \pi) \rightarrow F$.

Focus on the neighborhood of the circle α in the range $[-\varepsilon, \varepsilon]$. We can place the track of a homotopy, reading from left to right, of a crossing change followed by its reverse in this range of arc values, which corresponds exactly to a finger move in the surface, as shown in Figure 10. In particular, we can realize the c crossing changes on J_1 simultaneously to obtain an immersion which contains the pattern knot J_2 in the range $[-\frac{\varepsilon}{2}, \frac{\varepsilon}{2}]$ as in the third row of Figure 10.

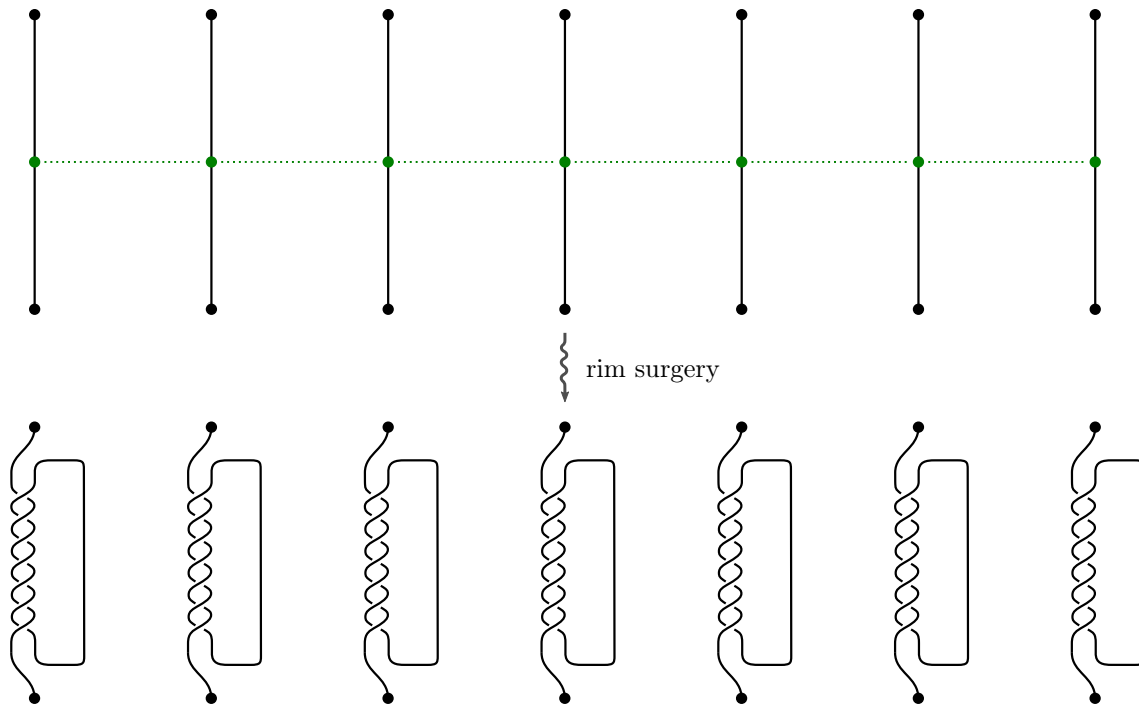


Figure 9. Local situation close to the curve $\alpha \subset F$, whose circle coordinate is drawn horizontally, before and after the rim surgery. Each frame is showing a 3-ball containing a properly embedded arc, which is the intersection of the neighborhood of $\alpha \subset X$ with the surface F (**top**) and with $F_{\tau^m}(\alpha, J_1)$ (**bottom**).

Now we will describe the eponymous construction: The *accordion homotopy* (or rather isotopy) of the immersion stretches the small segment $[-\frac{\epsilon}{2}, \frac{\epsilon}{2}]$ containing the pattern J_2 around the length of the circle parameter of α , while compressing the complement containing the pattern J_1 into the remaining segment $[\pi - \frac{\epsilon}{2}, \pi + \frac{\epsilon}{2}]$. The $2c$ double points, in terms of their α -coordinate, will be relocated from the $\pm \frac{\epsilon}{2}$ position to $\pi \pm \frac{\epsilon}{2}$. If the number of twists m in the rim surgery is nontrivial, think of the twisting as happening in a small sub-interval of α away from a neighborhood of 0 and π , and the accordion isotopy pushes the double points through the twisting. The bottom row of [Figure 10](#) illustrates the initial motion of the immersion under the accordion homotopy, in particular, take note of the red double points.

In the interior of the interval $[\pi - \frac{\epsilon}{2}, \pi + \frac{\epsilon}{2}]$, the pattern knot is still given by J_1 . This is illustrated in the second row of [Figure 11](#), where the π -coordinate value of α is now placed at the center of the figure. The last step is reinterpreting this immersion as the result of c finger moves performed on $F_{\tau^m}(\alpha, J_2)$, whose guiding arcs are located at the circle parameter π ; see the bottom two rows of [Figure 11](#). \square

4.1.1 Special cases of the accordion homotopy. Twist rim surgeries on the unknotted 2-sphere in \mathbb{S}^4 yield Zeeman's *twist spun knots* [[Zee65](#)]. More generally, twist rim surgery on a curve on a surface F which cuts off a disk contained in F has the same effect as connect summing with a twist spun knot [[Kim06](#), Lem. 2.2]. We will insert an alternative definition of twist spun knots here, where they are constructed by spinning 3-balls containing properly embedded knotted arcs through an open book decomposition of \mathbb{S}^4 with binding an unknotted $\mathbb{S}^2 \subset \mathbb{S}^4$.

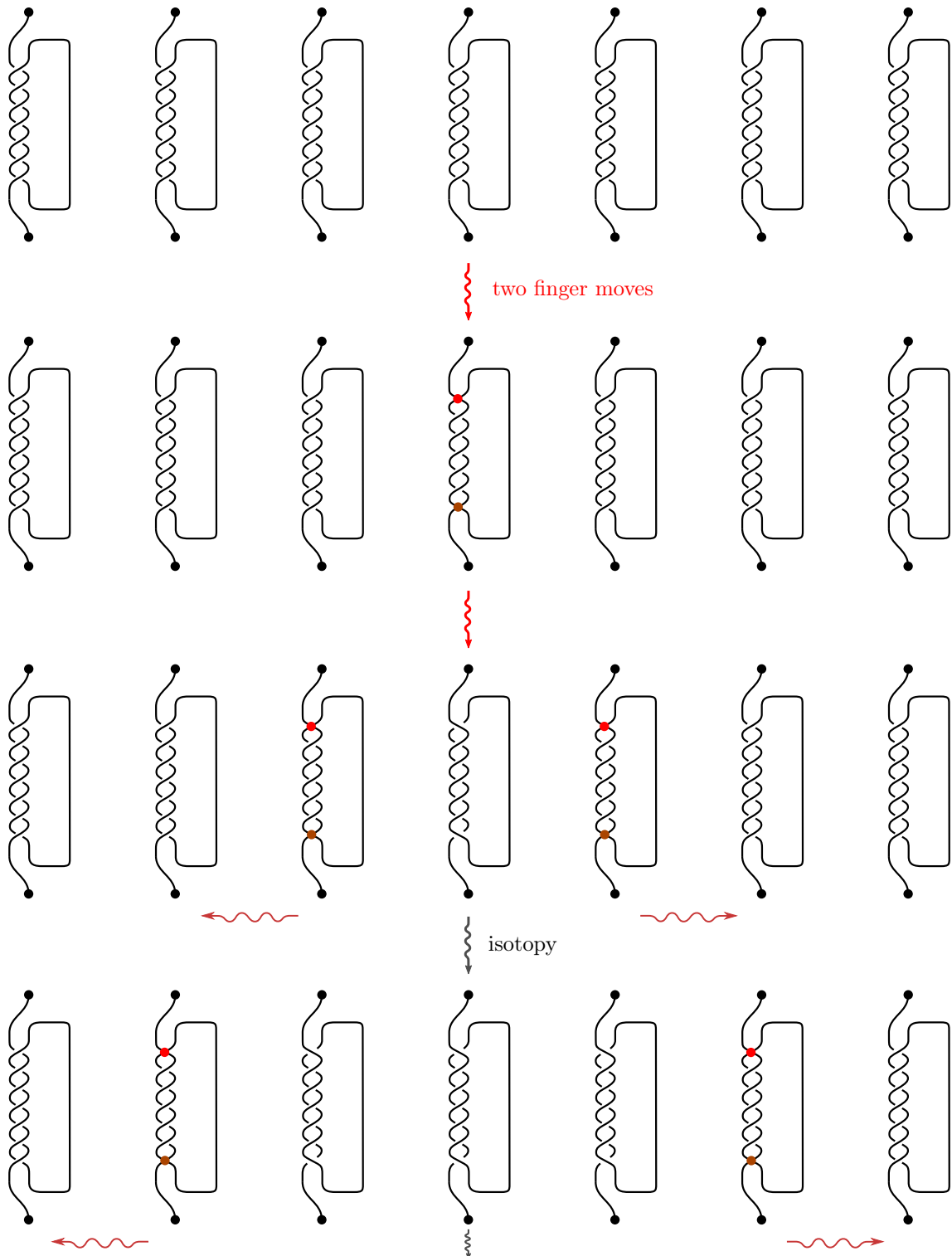


Figure 10. **Top row:** Initial position of $F_{\tau^m}(\alpha, J_1)$ before the finger moves. **Second row:** The singular point during a pair of finger moves, in the moment where the tips of the fingers on one of the sheets are touching the other sheet of the surface. **Third row:** After two finger moves, which introduce four red double points in total. **Bottom row:** Isotopy which makes the double points travel along the circle coordinate.

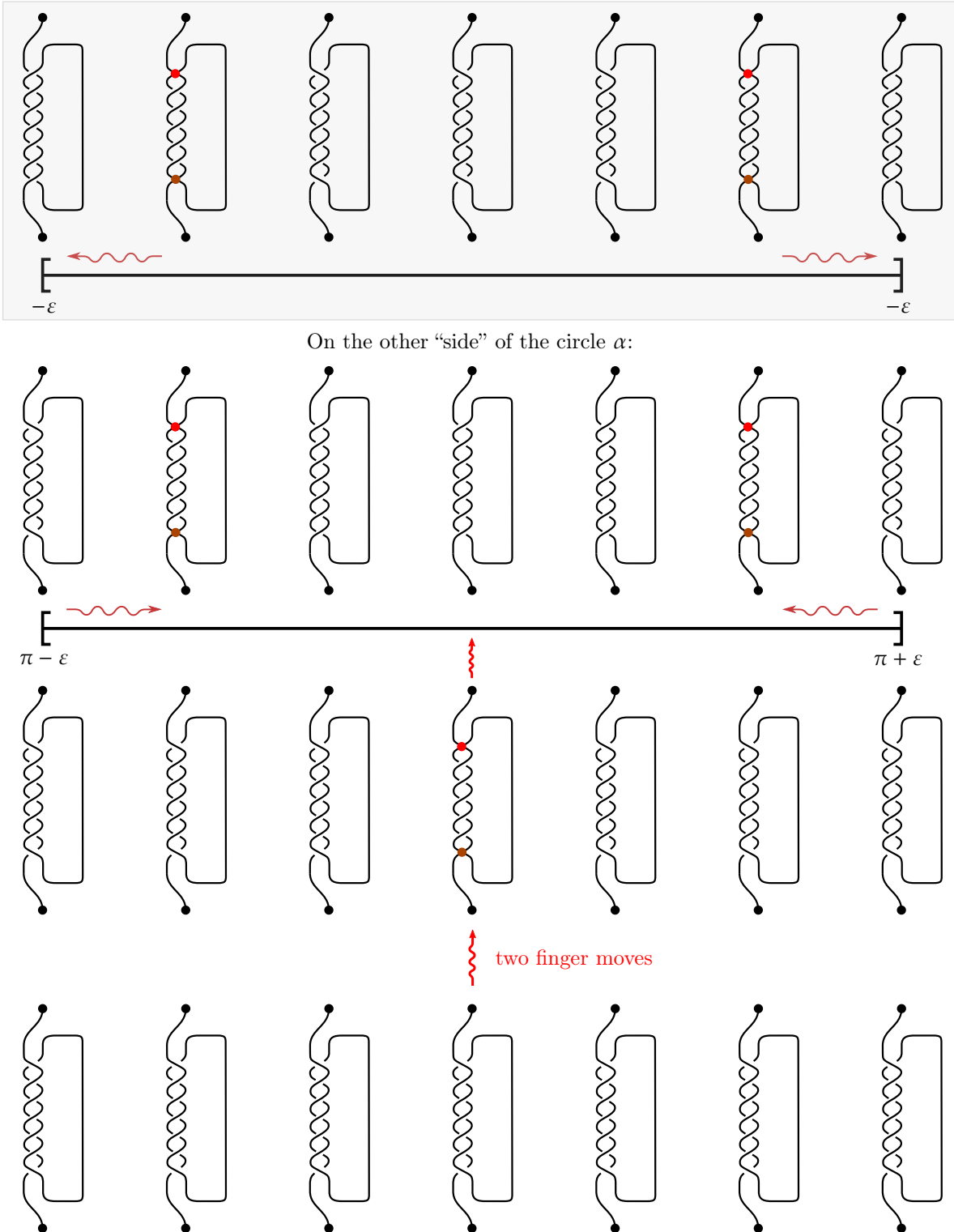


Figure 11. **Top row:** Reproduction of the final row of Figure 10, with the double points moving towards the π -coordinate value of α . **Second row:** Focusing on the π -coordinate value of α , with the double points moving towards it. **Bottom rows:** Reinterpreting the immersion as the result of c finger moves on $F_{\tau^m}(\alpha, J_2)$.

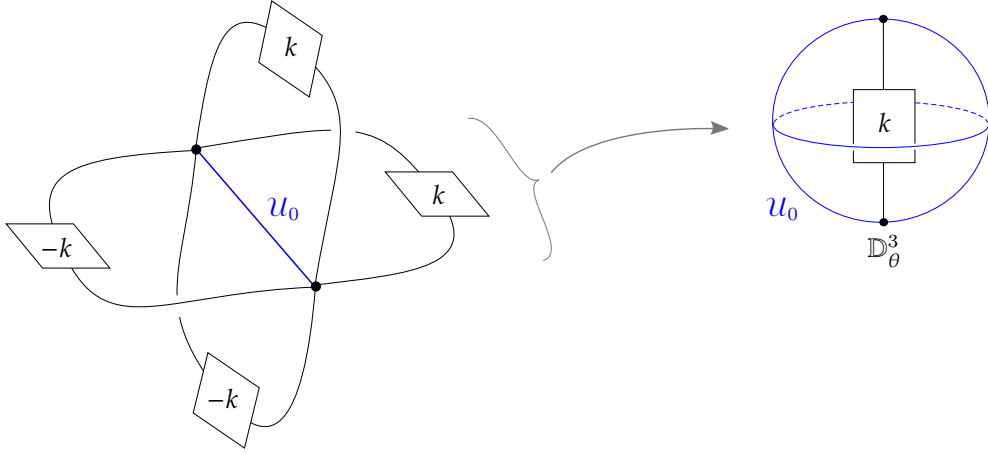


Figure 12. A schematic for the spin $\tau^0 k$ and the twist spins $\tau^n k$ of a 1-knot $k: \mathbb{S}^1 \hookrightarrow \mathbb{S}^3$. The open book decomposition of \mathbb{S}^4 from [Definition 4.3](#) is depicted schematically reduced by one dimension on the left, and so the blue 2-sphere \mathcal{U}_0 around which the knotted arc is spun is depicted as a blue circle (only an arc of which is drawn). Note that viewing a page \mathbb{D}_θ^3 from the ‘opposite side’ reverses its orientation, and therefore also the orientation of k .

Definition 4.3 (Twist spun knots). Given a 1-knot $k: \mathbb{S}^1 \hookrightarrow \mathbb{S}^3$, let k_+ be its associated properly embedded knotted arc in the 3-ball. For $n \in \mathbb{Z}$, consider the quotient

$$(\mathbb{D}^3, k_+) \times \mathbb{S}^1 \Big/ (\tau_\theta^n(x), \theta) \sim (x, 0) \text{ for } x \in \partial\mathbb{D}^3, \theta \in [0, 2\pi] / 0 \sim 2\pi$$

where $\tau_\theta^n: \mathbb{D}^3 \rightarrow \mathbb{D}^3$ denotes the ambient isotopy rotating \mathbb{D}^3 by an angle of $n \cdot \theta$ radians about an axis with endpoints $\partial k_+ = \{N, S\} \subset \partial\mathbb{D}^3$. For each n , this quotient space is diffeomorphic to \mathbb{S}^4 , and gives an open book decomposition with binding an unknotted 2-sphere \mathcal{U}_0 and 3-ball pages \mathbb{D}_θ^3 for all $\theta \in \mathbb{S}^1$. The quotient of $k_+ \times \mathbb{S}^1$ is a 2-sphere $\tau^n k: \mathbb{S}^2 \hookrightarrow \mathbb{S}^4$ called the n -twist spin of k . This is schematically illustrated in [Figure 12](#).

Due to Artin [[Art25](#)], the collection of 0-twist spun knots, often simply called *spun knots*, were the first examples of non-trivially knotted spheres in \mathbb{S}^4 . Artin proved that the group of the spun knot $\tau^0 k$ is isomorphic to the group of the classical knot k , showing that every 1-knot group is also a 2-knot group. For twist-spun knots in the 4-sphere, the construction of the regular homotopy in [Theorem 4.2](#) leads to the following corollary.

COROLLARY 4.4 ([[JKRS20](#)]). *Let $k: \mathbb{S}^1 \hookrightarrow \mathbb{S}^3$ be a classical knot. For any twist spin $\tau^n k$, the Casson-Whitney number $u_{\text{CW}}(\tau^n k) \leq u(k)$ is bounded by the classical unknotting number $u(k)$ of k .*

We are not aware of another instance of [Corollary 4.4](#) in the literature. The analogous result for u_{st} was proved by Satoh [[Sat04](#)], and also follows from [[BS16](#), Prop. 9]. Compare with the construction of the regular homotopy in [[JZ18](#), Prop. 2.21], but observe that their double point width μ_{Sing} measures the maximal number of simultaneous pairs of double points, as opposed to our Casson-Whitney length recording the total number.

Remark 4.5. The quantities in the inequality of [Corollary 4.4](#) can be arbitrarily far apart. For instance, each nontrivial 2-bridge $(2, p)$ -torus knot $T_{2,p}$ has unknotting number $\frac{1}{2}|p-1|$ by [[KM93](#)]. Therefore, by [Theorem 3.25](#), $u_{\text{CW}}(\tau^n T_{2,p}) = 1 < u(T_{2,p})$ for any nontrivial twist spin of $T_{2,p}$, whenever $p \geq 5$.

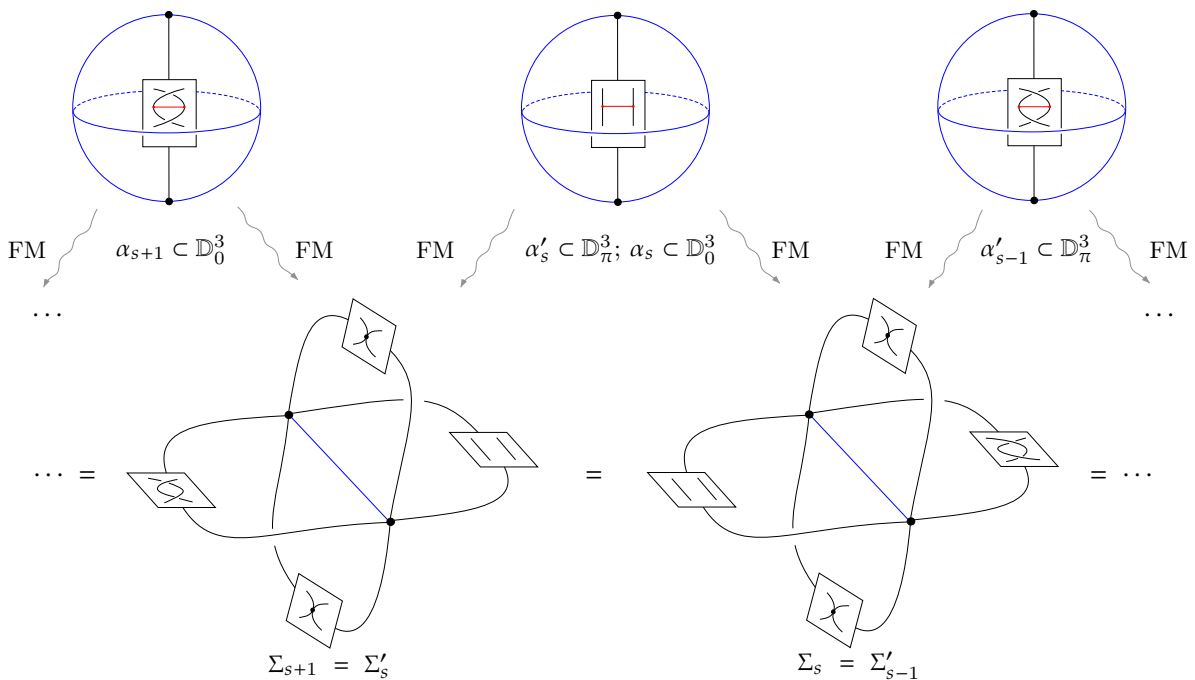


Figure 13. Top row: The intersections of the twist spins $\tau^n(k_{s+1})$, $\tau^n(k_s)$ and $\tau^n(k_{s-1})$ with \mathbb{D}_0^3 and \mathbb{D}_π^3 , as in Definition 4.3. Only the relevant crossing of each cross section is drawn. **Bottom row:** Schematics of the immersed spheres (compare to the embedded spheres in Figure 12) obtained by doing finger moves along the red guiding arcs in each diagram of the top row. Again, only the relevant crossing of the cross section in each page \mathbb{D}_θ^3 is shown. The isotopy between the two immersions Σ'_s and Σ_s is via a rotation by π (and potentially isotoping the twisting region around the circle).

We will now discuss how Theorem 4.2 relates to other constructions of regular homotopies. In [JKRS20] we observed that for twist-spun knots, introducing a finger move allows inserting any number of full-twists into adjacent strands of the knot being spun.

LEMMA 4.6 ([JKRS20]). *Let $k: \mathbb{S}^1 \hookrightarrow \mathbb{S}^3$ be a classical knot on which two parallel strands have been fixed. Let k_s for $s \in \mathbb{Z}$ be obtained by inserting $|s|$ positive or negative full-twists into these strands. Then for any number of twists in the spinning construction $n \in \mathbb{Z}$ and full-twists $s, t \in \mathbb{Z}$ in the strands, there is a length 1 regular homotopy from $\tau^n(k_s)$ to $\tau^n(k_t)$.*

The argument presented in the paper [JKRS20] constructs an immersion with two double points which can be obtained from any of the 2-knots k_s . We include the proof here to point out that this argument uses the rotational symmetry of the twist spin around the axis of rotation, and thus cannot be applied to rim surgeries on the nose, since this symmetry is not ‘localized’ to the surgery annulus. In the rim surgery, the endpoints of the pattern arcs being inserted into the rim annulus are ‘spread around’ the pair of boundary circles of the annulus, where they are attached to the part of the surface which remains unchanged. For twist spun knots, we can think of all of the 1-dimensional arcs as coming together at the poles (the pair of thick black dots on the spheres in the bottom row of Figure 13), through which an axis of rotational symmetry is placed.

Proof. This proof is taken from [JKRS20]. Remember the use of subscripts \mathbb{D}_θ^3 for $\theta \in \mathbb{S}^1$ to denote the 3-ball pages of the open book decomposition of \mathbb{S}^4 .

By performing a finger move on $\tau^n(k_{s+1})$ along the arc $\alpha_{s+1} \subset \mathbb{D}_0^3$ as in Figure 13, we obtain an immersed surface Σ_{s+1} . This immersion is also obtained by a finger move to $\tau^n(k_s)$ along $\alpha'_s \subset \mathbb{D}_\pi^3$ which we will

denote Σ'_s , so that $\Sigma'_s = \Sigma_{s+1}$. These finger moves differ in the ‘side’ of the circle coordinate in which they are located. Note that the twist spin parameter n is unchanged since the twisting can be assumed to occur in a small interval in \mathbb{S}^1 away from the double points of the immersion, and the knotted arc k_s twists n times in both Σ'_s and Σ_{s+1} .

By instead performing a finger move on $\tau^n(k_s)$ along the arc $\alpha_s \subset \mathbb{D}_0^3$, we obtain a surface Σ_s where $\Sigma_s = \Sigma'_s$ by rotation. Similarly, by performing a finger move to $\tau^n(k_{s-1})$ along the arc $\alpha'_{s-1} \subset \mathbb{D}_\pi^3$, we obtain a surface Σ'_{s-1} with $\Sigma'_{s-1} = \Sigma_s$.

Thus, we have equivalent immersed surfaces

$$\dots = \Sigma_{s+1} = \Sigma'_s = \Sigma_s = \Sigma'_{s-1} = \dots$$

so that for any $s, t \in \mathbb{Z}$, the two knots $\tau^n(k_s)$, $\tau^n(k_t)$ are related by a single finger and Whitney move. \square

Observe that the key insight to using a single finger-Whitney move pair for undoing multiple full-twists in the strands was in identifying the different immersions with each other.

Remark 4.7. Based on Zeeman’s result that 1-twist spins are smoothly unknotted 2-spheres, Kim [Kim06] explored techniques of constructing topologically isotopic surfaces via 1-twist rim surgery.⁸ In particular, as explained in [JMZ20b, Thm. 2.5], if we start with a curve α on $F^2 \subset X^4$ such that α bounds a topologically locally flat disk avoiding F except on the disk’s boundary, then the 1-twist rim surgery $F_{\tau^1}(\alpha, k)$ is topologically isotopic to the original F .⁹ In this setting, for any choice of patterns k, l , the knotted surfaces $F_{\tau^1}(\alpha, k)$, F and $F_{\tau^1}(\alpha, l)$ cannot be distinguished just by looking at the fundamental group of their complement or their Alexander module. Given such an *exotic pair of knotted surfaces*, which are topologically but not smoothly isotopic, we know that their Casson-Whitney length is at least equal to 1.

Question 4.8. Do there exist topologically isotopic surfaces with Casson-Whitney length ≥ 2 between them?

4.1.2 Application to classical unknotting number. As noted at the start of Section 3.4.1, the Nakanishi index, Ma-Qiu index, and algebraic stabilization number are all previously established lower bounds for the classical unknotting number. In this section we point out that the algebraic Casson-Whitney number is also a lower bound for the classical unknotting number, which is sharper than the aforementioned invariants in many cases.

One reason to study alg_{CW} as a lower bound for the unknotting number is that the above three invariants all fail to be additive in many simple cases, such as $T_{2,p} \# T_{2,q}$ when p, q are coprime [KY10]. By Theorem 2.2, $\text{alg}_{\text{CW}}(T_{2,p} \# T_{2,q}) = 2$ for all (odd) p, q . We do not know any cases where alg_{CW} fails to be additive on classical knots, although it seems difficult to prove this is always the case. Still, this poses a potentially interesting avenue to study the classical unknotting number, via a lower bound which comes from four dimensional techniques.

Let k be a 1-knot. Remembering that spinning preserves the knot group and its meridians, $\text{alg}_{\text{CW}}(k) = \text{alg}_{\text{CW}}(\tau^0 k)$. By Proposition 3.20, $\text{alg}_{\text{CW}}(\tau^0 k) \leq u_{\text{CW}}(\tau^0 k)$, and by Corollary 4.4, $u_{\text{CW}}(\tau^0 k) \leq u(k)$. Putting these facts together, we have:

PROPOSITION 4.9 ([JKRS20]). *For any 1-knot $k: \mathbb{S}^1 \hookrightarrow \mathbb{S}^3$, $\text{alg}_{\text{CW}}(k) \leq u(k)$.*

⁸ These can sometimes be obstructed from being smoothly equivalent using Seiberg-Witten invariants [Kim06, Thm. 3.4].

⁹ Juhász-Miller-Zemke [JMZ20b] use maps induced on perturbed sutured Floer homology to obstruct ambient diffeomorphism for rim surgeries on properly embedded surfaces $F \subset \mathbb{D}^4$ with non-empty boundary in $\partial\mathbb{D}^4$.

As noted in the introduction to this part, together with the additivity in [Theorem 2.1](#) this reproves a special case of Scharlemann's theorem that unknotting number one knots are prime [[Sch85](#)]. Namely, if k_1 and k_2 are classical knots with nontrivial determinants, then $u(k_1 \# k_2) \geq 2$.

4.1.3 Fundamental groups of complements of rim surgeries. *Roll-twist rim surgery* is a generalization of twist rim surgery where the annulus replacing the neighborhood of the simple closed curve $\alpha^1 \subset F^2 \subset X^4$ is obtained by simultaneously twisting and rolling the pattern knot J while it moves along the circle coordinate parameterizing α . We define the rolling map $\rho: \mathbb{D}^3 \rightarrow \mathbb{D}^3$ as follows; see also [[Ter93](#)] and the references in [Section 4.1.4](#). Recall the setup at the beginning of [Section 4.1](#) where we parameterize the knot J with a coordinate $x \in [0, 1]/(0 \sim 1)$. The knot $J \subset \mathbb{S}^3$ has a closed tubular neighborhood $\bar{v}(J \subset \mathbb{S}^3) \cong J \times \mathbb{D}^2$ such that for $\theta \in \partial\mathbb{D}^2 = \mathbb{S}^1 \cong [0, 2\pi]/(0 \sim 2\pi)$ the section $J \times \{\theta\}$ is null-homologous in the exterior X_J . Identify $\partial X_J \times [0, 1]$ with a collar of the peripheral torus $\partial X_J \times \{0\} \cong J \times \partial\mathbb{D}^2 \times \{0\}$ in the exterior X_J . The longitudinal rolling map on the 3-sphere is defined as

$$\begin{aligned} \rho: \mathbb{S}^3 &\rightarrow \mathbb{S}^3 \\ (x, \theta, \varphi) &\mapsto (x + \varphi, \theta, \varphi) && \text{for } (x, \theta, \varphi) \in J \times \partial\mathbb{D}^2 \times [0, 1] \\ y &\mapsto y && \text{for } y \notin J \times \partial\mathbb{D}^2 \times [0, 1] \end{aligned}$$

This is the identity on the closed tubular neighborhood of the knot J , therefore it restricts to a map $\rho^n: (\mathbb{D}^3, J_+) \rightarrow (\mathbb{D}^3, J_+)$. The mapping cylinder of the n th power of ρ ,

$$(\mathbb{D}^3, J_+) \times_{\rho^n} \mathbb{S}^1 = (\mathbb{D}^3, J_+) \times [0, 1] \Big/ (x, 0) \sim (\rho^n(x), 1) \text{ for } x \in \mathbb{D}^3,$$

contains the roll-spun annulus of the pattern knot J .

Combinations of twist- and roll-spin rim surgery are possible by composing powers of the twist map τ and the roll map ρ . As in [Definition 4.1](#), this can be used to define the *m -twist n -roll rim surgeries*

$$(X, F_{\tau^m \rho^n}(\alpha, J)) := (X, F) - (\mathbb{S}^1 \times (\mathbb{D}^3, [0, 1])) \cup_{\partial = \mathbb{S}^1 \times (\mathbb{S}^2, \{N, S\})} \mathbb{S}^1 \times_{\tau^m \rho^n} (\mathbb{D}^3, J_+)$$

Roll-twist spun knots $\tau^m \rho^n(J): \mathbb{S}^2 \hookrightarrow \mathbb{S}^4$ are the special case of roll-twist rim surgery on the equator α of an unknotted 2-sphere in \mathbb{S}^4 .

Remark 4.10. Naylor and Schwartz [[NS20](#)], in their investigation of Gluck twists on roll-spun knots, observe that an argument similar to the proof of [Lemma 4.6](#) applies to certain roll-twist spun knots if the regular homotopy is going to the unknot. They showed that there is a regular homotopy of length c from any m -twist n -roll spin of a classical unknotting number c knot to the unknot. However, their argument uses the following fact in an essential way: After the finger moves, rolling the unknot summand in $K\#U$ is isotopic to not doing any rolling at all. Thus it is not obvious how this statement could be generalized to apply to regular homotopies between arbitrary roll-twist spins.

Kim [[Kim06](#)] defined m -twist rim surgery and studied its effect on the fundamental group of the knotted surface, by decomposing the complement of the rim surgery $F_{\tau^m \rho^n}(\alpha, J)$ into a neighborhood of the surgery curve $\alpha \subset F$ on the surface, and the complement of the piece of F which remains unchanged. The resulting Seifert-van Kampen pushout for roll-twist rim surgery can be written as the following diagram of group homomorphisms:

$$\begin{array}{ccc} \pi_1(\mathbb{S}^1 \times (\mathbb{S}^2 - \{N, S\})) & \longrightarrow & \pi_1(X - F) \\ \downarrow & & \downarrow \\ \pi_1(\mathbb{S}^1 \times_{\tau^m \rho^n} (\mathbb{D}^3 - J_+)) & \longrightarrow & \pi_1(X - F_{\tau^m \rho^n}(\alpha, J)) \end{array}$$

Here $\pi_1(\mathbb{S}^1 \times_{\tau^m \rho^n} (\mathbb{D}^3 - J_+))$ is an HNN extension of the classical knot group $\pi_1(\mathbb{D}^3 - J_+) \cong \pi_1(\mathbb{S}^3 - J)$ where the action of the generator $\langle t \rangle$ of the circle factor \mathbb{S}^1 is conjugation with $\mu^m \lambda^n$, with μ an oriented meridian of J_+ and λ a zero-framed longitude. Observe that the order in which we perform the twisting

and rolling does not matter, as a meridian will always commute with a (zero-framed) longitude in the knot group, $\lambda\mu = \mu\lambda$.

If we assume that the ambient 4-manifold is simply connected and that the fundamental group of the complement $\pi_1(X - F, *)$ of the surface F is a cyclic group generated by a meridian μ of F , we can write down an explicit presentation of the group of the 0-roll rim surgery. Kim [Kim06, Lem. 3.1] states this as follows: Suppose that F^2 is a surface in the simply connected 4-manifold X^4 such that $\pi_1(X - F, *) \cong \mathbb{Z}/d$. Let μ be a meridian of the knotted arc $J_+ \subset \mathbb{D}^3$, and take $*$ to be a basepoint on the tubular neighborhood of J_+ throughout. Then

$$\pi_1(X - F_{\tau^m \rho^0}(\alpha, J)) \cong \pi_1(\mathbb{D}^3 - J_+, *) \Big/ \mu^d = 1, \beta = \tau_*^m(\beta) \text{ for } \beta \in \pi_1(\mathbb{D}^3 - J_+, *)$$

where $\tau: (\mathbb{D}^3, J_+) \rightarrow (\mathbb{D}^3, J_+)$ is the twist map which has been used for the gluing in the twisted product.

We can obtain a similar result from the Seifert-van Kampen decomposition of the complement of m -twist n -roll spun knots in the 4-sphere.

$$\begin{array}{ccc} \pi_1(\mathbb{S}^1 \times (\mathbb{S}^2 - \{N, S\})) & \longrightarrow & \pi_1(\mathbb{D}^2 \times (\mathbb{S}^2 - \{N, S\})) \\ \downarrow & & \downarrow \\ \pi_1(\mathbb{S}^1 \times_{\tau^m \rho^n} (\mathbb{D}^3 - J_+)) & \longrightarrow & \pi_1(\mathbb{S}^4 - \tau^m \rho^n(J)) \end{array}$$

Here the action of the roll-twist map $\tau^m \rho^n: (\mathbb{D}^3, J_+) \rightarrow (\mathbb{D}^3, J_+)$ on the fundamental group is $(\tau^m \rho^n)_*(\beta) = \mu^m \lambda^n \beta (\mu^m \lambda^n)^{-1}$ for $\beta \in \pi_1(\mathbb{D}^3 - J_+, *)$. This leads to the presentation

$$\pi_1(\mathbb{S}^4 - \tau^m \rho^n(J)) \cong \pi_1(\mathbb{D}^3 - J_+, *) \Big/ \beta = \mu^m \lambda^n \beta (\mu^m \lambda^n)^{-1} \text{ for } \beta \in \pi_1(\mathbb{D}^3 - J_+, *).$$

The discussion justifies the following slogans for the groups of spun and rolled knots in the 4-sphere: For an m -twist spun knot $\tau^m(k)$ its group is the quotient of the original classical knot group where the m th power of a meridian is forced into the center of the group. For an n -roll spin $\rho^n(k)$, the n th power of a zero-framed longitude is centralized. Combining twisting and spinning makes the corresponding product $\lambda^n \mu^m$ of meridians and longitudes central. Observe that the meridian and longitude of a knot commute in its group because they live on the peripheral torus, so for the group it does not matter in which order we write the powers of longitudes and meridians.

Teragaito [Ter93, Thm. 1] observed that since a zero-framed longitude lies in the second commutator subgroup of the knot group, the Alexander module of every n -roll spin $\rho^n k$ agrees with that of the classical knot k (and thus also with its 0-twist spin $\tau^0 k$). In particular, the lower bound from Proposition 3.22 on the algebraic Casson-Whitney number coming from the Nakanishi index $m(k)$ is the same for all roll-spins.

PROPOSITION 4.11. *For every n -roll spin $\rho^n k$ of a classical knot k , the Nakanishi index $m(k)$ gives a lower bound*

$$m(k) = m(\rho^n k) \leq \text{alg}_{\text{st}}(\rho^n k) \leq \text{alg}_{\text{CW}}(\rho^n k)$$

4.1.4 Aside: Roll-twist spinning yielding trivial knots and the unknotting conjecture. In some instances, 4-dimensional techniques can give interesting perspectives on problems with classical 3-dimensional objects. For example we saw in Proposition 4.9 that the (algebraic) Casson-Whitney number is a lower bound on the classical unknotting number, and alluded to our reproof (in special cases) of Scharleman's theorem that unknotting number 1 classical knots are prime. This short section presents as a small curiosity a 4-dimensional characterization of the classical problem of finding knots which admit lens space surgeries.

Twist spinning a non-trivial classical knot with twisting parameter $\neq \pm 1$ always yields a non-trivial knotted sphere; this follows from the generalized Smith conjecture [Mor84] and Zeeman's fibration result that $\tau^m(k)$ is fibered by a punctured bounded $\Sigma_m(k)$. See [GK78; FO15] for expositions of Zeeman's fibration theorem. An alternative argument using the group of the complement can be made as follows: For 0-twists, the spun knot has the same group as the classical knot being spun, which is non-cyclic for non-trivial knots. For a number of twists $\neq 0, \pm 1$ the resulting sphere is never a ribbon knot [Coc83] which can be detected from the knot group. We will discuss Cochran's argument further in [Theorem 6.8](#).

Let us give a short overview on the literature of groups of twist-roll spun knots, where we will not define all the terms and constructions. Fox [Fox66] computed the group of what is now called the *symmetry spun* figure eight knot, and showed that it is not isotopic to any twist spin of the figure eight knot. Litherland introduced *deform-spinning* [Lit79] and extended Zeeman's fibration theorem to a large class of deformations in the case that there is non-trivial twisting. Teragaito [Ter93] (observe the corrigendum [Ter94a]) states the presentation for the fundamental group of a roll spin as a quotient of the classical knot group where a power of a longitude is centralized. He introduces a combination of twist- and roll-spinning as well [Ter94b]. Related to this, see Plotnick's overview [Plo84] over fibered knots coming from spinning and twisting constructions. Generalizing further, [Fuk17] give presentations for groups of *branched twist spins*.

Taking notation from [Ter94b], for $m \neq 0$,¹⁰ the m -twist n -roll $\tau^m \rho^n$ is fibered by $(\mathbb{S}^3 - \nu(k))^m (\frac{1}{n})$, where $(\mathbb{S}^3 - \nu(k))^m$ denotes the m -fold cyclic cover of the knot exterior and the $(\frac{1}{n})$ describes a Dehn filling. By our convention $\frac{a}{b}$ -filling, where a and b are coprime integers, is the process of sewing in a solid torus $k \times \mathbb{D}^2$ via a homeomorphism $k \times \partial \mathbb{D}^2 \rightarrow k \times \mathbb{D}^2$ which sends a meridian of k to $a \cdot \text{meridian}_k + b \cdot \text{longitude}_k$. Litherland [Lit79] observes that by interchanging the order of the surgery and taking the branched cover, the fiber is the same as $\Sigma_m(\mathbb{S}^3(\frac{m}{n}, k), k)$, the m -fold cyclic branched cover of the $(\frac{m}{n})$ -surgery on k , where we branch over the surgery core k .

This fibration leads to an alternative presentation of the fundamental group of the complement of a twist-roll spin: It is the semi-direct product of the group of the fiber with an infinite cyclic group generated by the meridian μ , which acts via the induced map of the monodromy φ of the fibration,

$$\pi_1(\mathbb{S}^4 - \tau^m \rho^n) \cong \pi_1((\mathbb{S}^3 - \nu(k))^m (\frac{1}{n})) \rtimes_{\varphi} \langle \mu \rangle.$$

Compare this with the discussion in [Section 4.1.3](#), where we obtained the quotient of the classical knot group by centralizing the element $\mu^m \lambda^n$, with λ a zero-framed longitude and μ a meridian of the knot group.

Using Perelman's solution of the Geometrization Conjecture [Per03], the proof of [Ter94b, Thm. 4] shows the following: The m -twist 1-roll spin $\tau^m \rho^1(k)$ of a classical knot $k: \mathbb{S}^1 \hookrightarrow \mathbb{S}^3$ is a smoothly unknotted 2-sphere in \mathbb{S}^4 if and only if the m -Dehn surgery $\mathbb{S}_m^3(k) = (\mathbb{S}^3 - \nu(k))(\frac{m}{1})$ on k is a lens space. Also from Geometrization we know that a closed 3-manifold Y^3 is a lens space if and only if its group $\pi_1(Y)$ is finite cyclic. The group of the m -Dehn surgery can be computed from $\pi_1(\mathbb{S}^3 - k)$ by killing the word $\mu^m \lambda$, along which the 2-handle of the surgery solid torus is attached.

Example 4.12. Concrete examples mentioned in [Ter94b] are twist-roll spins of the pretzel knots $k = P(-2, 3, 7)$, for these $\tau^{18} \rho^1(k)$ and $\tau^{19} \rho^1(k)$ are unknotted 2-spheres. \triangle

For classical knots in the 3-sphere, it is a consequence of Dehn's lemma that $k: \mathbb{S}^1 \hookrightarrow \mathbb{S}^3$ is unknotted if and only if $\pi_1(\mathbb{S}^3 - k) \cong \mathbb{Z}$. The same statement up one dimension in the smooth category has not

¹⁰ The condition that the number of twists is non-zero is essential: A 0-twist spun knot is fibered if and only if the classical knot is fibered. One way to see this is Stallings' fibration theorem [stallings1962fiberings] which states that a classical knot is fibered if and only if its commutator subgroup is finitely generated; recall that the classical knot and its 0-twist spin have isomorphic commutator subgroups.

been answered, and might very well turn out to be false. In the literature, it is known as the smooth unknotting conjecture.

CONJECTURE 4.13 (Smooth unknotting conjecture). *A smoothly embedded 2-sphere $S: \mathbb{S}^2 \hookrightarrow \mathbb{S}^4$ is smoothly unknotted if and only if the group of its complement is infinite cyclic, $\pi_1(\mathbb{S}^4 - S) \cong \mathbb{Z}$.*

As mentioned earlier, in the topological category it is known that a topologically flat 2-sphere in the 4-sphere bounds a topologically flat 3-ball if and only if its group is infinite cyclic [FQ90, Thm. 11.7A].

For example, the smooth unknotting conjecture is known to be true for twist-spun knots. This follows from a case by case analysis just like in the first paragraph of this section: The 0-twist spin $\tau^0 k$ shares its group with k , which is infinite cyclic if and only if k is unknotted in \mathbb{S}^3 , whose spin is the smoothly unknotted 2-sphere in \mathbb{S}^4 . Any (± 1) -twist spin is smoothly unknotted which can be seen from Zeeman's fibration theorem, so the equivalence is trivial for these. Additionally, as we will elaborate on in Section 6.2, Cochran [Coc83] showed that for $m \neq 0, \pm 1$ and k non-trivial, the m -twist spin $\tau^m k$ is never a ribbon 2-knot, and thus always non-trivial. In particular, this non-triviality can be detected from their groups.

We will now state what the Geometrization extension of Teragaito's observation says about the smooth unknotting conjecture for 1-roll twist spins.

PROPOSITION 4.14. *The smooth unknotting conjecture for 1-roll m -twist spun knots is equivalent to the following. For all classical knots $k: \mathbb{S}^1 \hookrightarrow \mathbb{S}^3$ the 'Dehn surgery quotient'*

$$\pi_1(\mathbb{S}^3 - k) \Big/ \langle\langle \mu^m \lambda = 1 \rangle\rangle \cong \mathbb{Z}/m$$

is finite cyclic if and only if the 'roll-twist quotient'

$$\pi_1(\mathbb{S}^3 - k) \Big/ \langle\langle \mu^m \lambda \text{ central} \rangle\rangle \cong \mathbb{Z}$$

is infinite cyclic.

Proof. The quotient

$$\pi_1(\mathbb{S}^4 - \rho^1 \tau^m(k)) \cong \pi_1(\mathbb{S}^3 - k) \Big/ \langle\langle \mu^m \lambda \text{ central} \rangle\rangle$$

is the group of the 1-roll spin and

$$\pi_1(\mathbb{S}_m^3(k)) \cong \pi_1(\mathbb{S}^3 - k) \Big/ \langle\langle \mu^m \lambda = 1 \rangle\rangle$$

is the group of m -Dehn surgery on k . The latter group is finite cyclic if and only if $\mathbb{S}_m^3(k)$ is a lens space if and only if $\rho^1 \tau^m(k)$ is smoothly unknotted by Teragaito. \square

Remark 4.15. It is still an open question to characterize the classical knots $k: \mathbb{S}^1 \hookrightarrow \mathbb{S}^3$ with lens space surgeries. The (unresolved) Berge conjecture posits that the only knots in the 3-sphere which admit a lens space surgery are the *doubly primitive knots*. Those are knots k which can be placed on a genus 2 Heegaard surface of \mathbb{S}^3 so that in each of the handlebodies of the splitting, k intersects some meridian disk geometrically once. The Dehn surgery coefficient yielding the lens space is then induced from the surface framing on the knot.

5 STABILIZATION LENGTH VERSUS CASSON-WHITNEY LENGTH

Definition 5.1. The *stabilization length* $\text{length}_{\text{st}}(K, J)$ between two knotted surfaces K and J in an ambient 4-manifold which become isotopic after a sequence of stabilizations and destabilizations is defined to be the minimal length of such a sequence relating K and J , where each stabilization or destabilization adds 1 to the count. If the surfaces are not related by stabilizations and destabilizations we define the length to be infinite.

In particular, for an orientable knotted surface K in the 4-sphere the stabilization length between K and the orientable unknotted surface U_g is the *stabilization number* $u_{\text{st}}(K) = \text{length}_{\text{st}}(K, U_g)$ from Definition 3.12. Baykur-Sunukjian [BS16, Thm. 1] observe that $\text{length}_{\text{st}}(K, J)$ is a well-defined finite number for any pair of homologous smoothly embedded surfaces K, J in a compact orientable smooth 4-manifold, since they show that these become smoothly isotopic after stabilizing both enough times.

In this section, based on our [JKRS20], we want to investigate the relation between the Casson-Whitney $\text{length}_{\text{CW}}$ and stabilization $\text{length}_{\text{st}}$. Recently, the relationship between two similar invariants dist_{st} and $\text{dist}_{\text{sing}}$ was studied by Singh [Sin20]. The invariant $\text{dist}_{\text{sing}}$ already appeared (with the notation μ_{sing}) in the article [JZ18]. Singh's invariants record the minimal 'width' of a sequence of stabilizations and destabilizations or the 'width' of the double points in a regular homotopy, meaning the maximum number of additional stabilizations or double points that occur **simultaneously**. The invariants we consider, on the other hand, record the minimal 'length' of a sequence of stabilizations and destabilizations or the 'length' of the double points in a regular homotopy, meaning the total number of stabilizations or double points that occur **overall**. Many of the geometric techniques used in our arguments are inspired by those of Singh, as well as both Gabai [Gab20] and Schneiderman-Teichner [ST19]. A recent paper of Miller-Powell [MP19] also studies a version of the stabilization length between arbitrary surfaces in \mathbb{S}^4 , as well as the related relative setting of properly embedded surfaces in \mathbb{D}^4 .

Definition 5.2. Given an oriented immersed surface Σ in an oriented 4-manifold X^4 with algebraically zero double points, and any choice of disjointly embedded arcs on Σ pairing double points of opposite sign, there is an *associated tubed surface* obtained by tubing the double points along these arcs as in Figure 14. Note that this surface is oriented, since the endpoints of each arc are double points of opposite local orientation. A priori the smooth (and even topological) isotopy class of the resulting surface depends on the arcs along which the tubing is done.

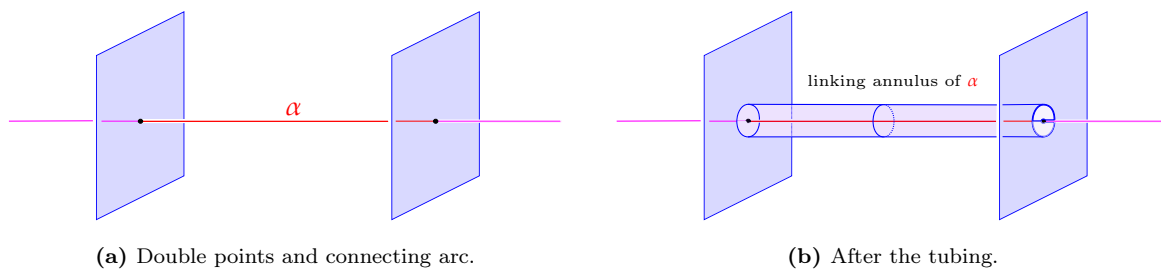


Figure 14. Tubing an immersed surface along a red arc α that connects oppositely signed double points. Sheets of the surface are drawn in pink and blue; the pink sheet is an arc persisting into the past and future. To tube the double points together, remove a disk in the blue sheet around each double point and add the linking annulus of the guiding arc α as shown on the right.

Although we choose not to define it rigorously here, the procedure of 'tubing' employed in the definition above is described in [Gab20, Rem. 5.3], as well as in [Sin20, Def. 2.6]. Indeed, isotopies between associated tubed surfaces are the focus of both papers. To ensure that the associated tubed surfaces that arise in our discussions are isotopic, we will be especially interested in regular homotopies of the following type.

Definition 5.3. A regular homotopy of length n from K to \mathcal{U}_g in \mathbb{S}^4 is called *arc-standard* if its standard Whitney disks W_1, \dots, W_n and knotted Whitney disks V_1, \dots, V_n have at least one Whitney arc in common for each $i = 1, \dots, n$.

Remark 5.4. It is unknown whether or not every orientable knotted surface, or even 2-knot, in \mathbb{S}^4 admits an arc-standard regular homotopy to the unknot, let alone one of minimal length. There are many *non-simply connected* 4-manifolds containing pairs of 2-spheres between which there is no analogue of an arc-standard homotopy. For instance, any pair of spheres related by such a homotopy must have vanishing Freedman-Quinn invariant¹¹ since in this case all double curves of the trace of the homotopy are trivially double covered. However, there are many instances where this does not hold; see [ST19; Gab20; Sch19] for example.

With this terminology in place, we state our first result. Although this fact is implied by Singh’s proof of [Sin20, Thm. 1.4], we state and prove it here in our setting.

PROPOSITION 5.5. *If there is a length n arc-standard homotopy from $K: \Sigma_g \hookrightarrow \mathbb{S}^4$ to \mathcal{U}_g , then K can be unknotted with n stabilizations.*

Proof. Such a regular homotopy is given by a set of standard Whitney disks W_1, \dots, W_n and knotted Whitney disks V_1, \dots, V_n for the standard immersion Σ with $2n$ double points, as in Definition 3.6 and Definition 3.7. Since the regular homotopy is arc-standard, by definition for each i the standard and knotted Whitney disks have at least one common Whitney arc α_i .

The end of the Whitney homotopy for each Whitney disk W_i and V_i gives a local model of the resulting embedded surface, as illustrated in the top left and right of Figure 15. Stabilizing K along guiding arcs connecting the sheets of K parallel to each knotted Whitney disk gives an embedded genus $g + n$ surface F_K shown on the bottom left of Figure 15. Likewise, stabilizing the unknot \mathcal{U}_g along guiding arcs connecting the sheets of \mathcal{U}_g parallel to each standard Whitney disk gives a genus $g + n$ standard surface $F_{\mathcal{U}_g}$ shown on the bottom right of Figure 15. Both F_K and $F_{\mathcal{U}_g}$ are isotopic to the associated tubed surface Σ stabilized along the common Whitney arcs $\alpha_1, \dots, \alpha_n$ depicted on the bottom center of Figure 15 (the tube along the Whitney arc α_i is shown in green). Since the surface $F_{\mathcal{U}_g}$ is a stabilization of the unknot, it follows that $F_{\mathcal{U}_g}$ and hence F_K is unknotted. \square

We know of the following inequality between stabilization number and Casson-Whitney number (where we unfortunately could not get rid of the ‘+1’):

THEOREM 5.6 (Generalization of [JKRS20, Thm. 1.1]). *For a smoothly knotted orientable surface $K: \Sigma_g \hookrightarrow \mathbb{S}^4$,*

$$u_{\text{st}}(K) \leq u_{\text{CW}}(K) + 1.$$

The proof here depended on Singh’s arguments in [Sin20], the ‘+1’ comes from adding an extra stabilization tube so that we could apply Singh’s moves, and the main new idea was that this extra tube could be ‘reused’ to construct all the necessary isotopies one after another. We reproduce the proof below to observe that it also works in the case of a positive genus surface.

Proof. Take a length $u_{\text{CW}}(K)$ regular homotopy from K to \mathcal{U}_g , with associated tubed surfaces $F_{\mathcal{U}_g}$ and F_K constructed as before. Note that since the homotopy is not necessarily arc-standard, the double points of Σ are tubed together along different arcs, thus it a priori unclear whether or not $F_{\mathcal{U}_g}$ and F_K are isotopic. In his proof of [Sin20, Thm. 1.4], Singh produces a sequence of tubed surfaces T_1, \dots, T_m for the standard

¹¹ This concordance invariant was defined by Freedman and Quinn [FQ90] in the ‘90s, and later corrected by Stong [Sto94]. Schneiderman and Teichner give a new exposition in [ST19].

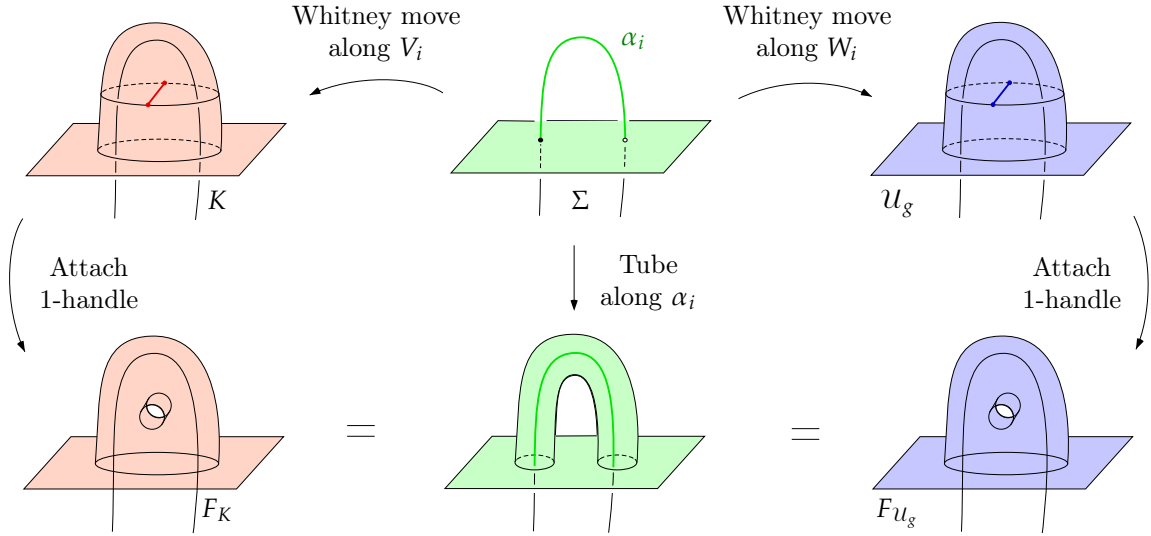


Figure 15. Local pictures of the surfaces U_g and K (top right and left) given by Whitney moves on the immersion Σ , and their isotopic stabilizations F_{U_g} and F_K along the red or blue guiding arcs (lower right and left). Note that although the local models of U_g and K after the Whitney moves look identical, the interiors of the Whitney disks W_i and V_i , and hence these portions of U_g and K , may be embedded very differently in the ambient 4-manifold X^4 .

immersed surface Σ such that at the start $T_1 = F_{U_g}$, at the end $T_m = F_K$, and such that each consecutive pair T_i and T_{i+1} becomes isotopic after a single stabilization.

Note that $\pi_1(\mathbb{S}^4 - T_i) \cong \mathbb{Z}$ for each i . This follows from the computation of the fundamental group after a finger move, since each T_i is an associated tubed surface for the standard immersion Σ with $\pi_1(\mathbb{S}^4 - \Sigma) \cong \mathbb{Z}$. Thus, any stabilization of T_i is isotopic to the stabilization done along the trivial guiding arc. This, combined with the fact that T_i and T_{i+1} become isotopic after a single stabilization, implies that the trivial stabilizations of the tubed surfaces T_1, \dots, T_m are all pairwise isotopic. In particular, F_{U_g} and F_K become isotopic after a single stabilization because we can re-use this trivial stabilization tube in each step of the construction. \square

In the 4-sphere and regular homotopies of knotted 2-spheres going to the unknot, we can show that Casson-Whitney number equal to 1 implies that the stabilization number is equal to 1 as well.

THEOREM 5.7 ([JKRS20]). *For a smoothly knotted 2-sphere $K: \mathbb{S}^2 \hookrightarrow \mathbb{S}^4$,*

$$u_{\text{CW}}(K) = 1 \implies u_{\text{st}}(K) = 1.$$

The argument in our paper depends on the assumption that the length 1 regular homotopy is leading to the unknotted 2-sphere, so that we can apply a result of Schneiderman-Teichner [ST19] on normal forms of the immersed genus 0 unknot. Furthermore, the Schneiderman-Teichner normal form is only stated for the case of knotted spheres, and so we cannot immediately generalize the theorem to higher genus surfaces.

Question 5.8. Does $\text{length}_{\text{CW}}(K, K') = 1$ imply $\text{length}_{\text{st}}(K, K') = 1$ for $K, K': \mathbb{S}^2 \hookrightarrow \mathbb{S}^4$ arbitrary knotted 2-spheres (i.e. not assuming one of them is the unknot)? Is this also true if K and K' have positive genus?

Proof sketch for Theorem 5.7. This is a short sketch of the main proof idea from [JKRS20].

We argue that for K with $u_{\text{CW}}(K) = 1$, there is an arc-standard length one regular homotopy from K

to the unknot \mathcal{U}_0 . It then follows from [Proposition 5.5](#) that $u_{\text{st}}(K) = 1$. Start by letting Σ denote the standard immersion with two oppositely signed double points.

Fix a parametrization $f: \mathbb{S}^2 \looparrowright \mathbb{S}^4$ of Σ with double point pre-images $\mathbf{p} = \{p, p^*\}$ and $\mathbf{n} = \{n, n^*\}$. By definition of the Casson-Whitney number, there is a regular homotopy from Σ to K consisting of a single Whitney move along a knotted Whitney disk V with pre-image $f^{-1}(\partial V)$ equal to a pair of ‘knotted’ arcs $v, v^* \subset \mathbb{S}^2$ with $\partial v = \{p, n\}$ and $\partial v^* = \{p^*, n^*\}$.

We claim that there is a standard Whitney disk W one of whose boundary arcs has pre-image equal to v . To see this, let W be any standard Whitney disk with $f^{-1}(\partial W)$ equal to the ‘standard’ arcs $w, w^* \subset \mathbb{S}^2$.

We then proceed to construct a sequence of moves which arranges this equality of one pair of arcs. One of the moves is a *braid twist* about the points $p \cup p^*$ that fixes the arc γ connecting p to p^* setwise. Since Σ is a standard immersion, the loop $f(\gamma)$ bounds an embedded disk (usually referred to in the literature as an *accessory disk*) in \mathbb{S}^4 away from Σ . It therefore follows from the normal form [[ST19](#), Lem. 3.9]¹² that there is an ambient isotopy $\rho: \mathbb{S}^4 \times [0, 1] \rightarrow \mathbb{S}^4$ with $\rho_1(\Sigma) = \Sigma$ carrying the standard Whitney disk W to one whose boundary arcs are the image under the braid twist of those for W , as illustrated in [[ST19](#), Fig. 18]. We retain the labels w, w^* , and W even after such an isotopy occurs.

We can then find another isotopy of the arcs so that $\partial w = \{p, n\} = \partial v$ for some choice of labeling of the standard arcs. Note that w and v are now isotopic rel the points in $\mathbf{p} \cup \mathbf{n}$ if and only if the loop $w \cup v$ (with either orientation) is null homologous in the annulus $\mathbb{S}^2 - \bar{v}\{p^*, n^*\}$. This can be arranged by another isotopy to insert full-twists of w around p^* .

For the standard Whitney disk W with $w = v$, the regular homotopy from K to \mathcal{U}_0 consisting of the finger move that is inverse to the Whitney move along the knotted Whitney disk V , followed by the Whitney move along W , is now arc-standard, which completes the proof. \square

Baykur-Sunukjian [[BS16](#)] use a ‘tube version’ analogue of the accordion homotopy to construct stabilization sequences between rim surgeries of surfaces. Observe that their arguments in [[BS16](#), Sec. 3] depend on the complement of the surface being simply connected, so that they can appeal to Boyle’s classification of 1-handles [[Boy88](#)] and conclude that the handles are trivial in this case. We are able to make an analogous argument for rim surgeries in the case that the Gordian distance of the surgery pattern knots to the unknot is known.

PROPOSITION 5.9. *Let $k, l: \mathbb{S}^1 \hookrightarrow \mathbb{S}^3$ be classical knots with Gordian distances to the unknot $u: \mathbb{S}^1 \hookrightarrow \mathbb{S}^3$, i.e. their classical unknotting numbers, given as $\text{dist}_{\text{Gord}}(k, u)$ and $\text{dist}_{\text{Gord}}(l, u)$. Let $F^2 \subset X^4$ be smoothly knotted surface, with rim surgery curve $\alpha \subset F$. Then the Casson-Whitney length between the twist rim surgeries, with twisting parameters $n_1, n_2 \in \mathbb{Z}$, is bounded above by the maximum,*

$$\text{length}_{\text{CW}}(F_{\tau^{n_1}}(\alpha, k), F_{\tau^{n_2}}(\alpha, l)) \leq \max\{\text{dist}_{\text{Gord}}(k, u), \text{dist}_{\text{Gord}}(l, u)\}.$$

Proof. Without loss of generality assume k takes the value of the maximum

$$M = \max\{\text{dist}_{\text{Gord}}(k, u), \text{dist}_{\text{Gord}}(l, u)\}$$

of the Gordian distances of the classical knots to the unknot. Perform M finger moves on $F_{\tau^{n_1}}(\alpha, k)$ which realize these crossing changes on the surgery pattern knot k , which leads to the unknot u . After the accordion homotopy, we see that the resulting immersion F' is isotopic to M finger moves on the original surface F . The guiding arcs of the finger moves are localized in a neighborhood of the rim surgery curve α . In particular, since the homotopy leads to the surface where the surgery arc is the unknot in the 3-ball, there is a unique choice for each finger move in $\mathbb{S}^1 \times (\mathbb{D}^3 - u^\circ)$. Moreover, M finger

¹² Although Schneiderman and Teichner are working in a different context, their Lemma 3.9 applies in our case since as they note in the discussion in Section 3.G their isotopy is supported locally, in the neighborhood of an accessory disk.

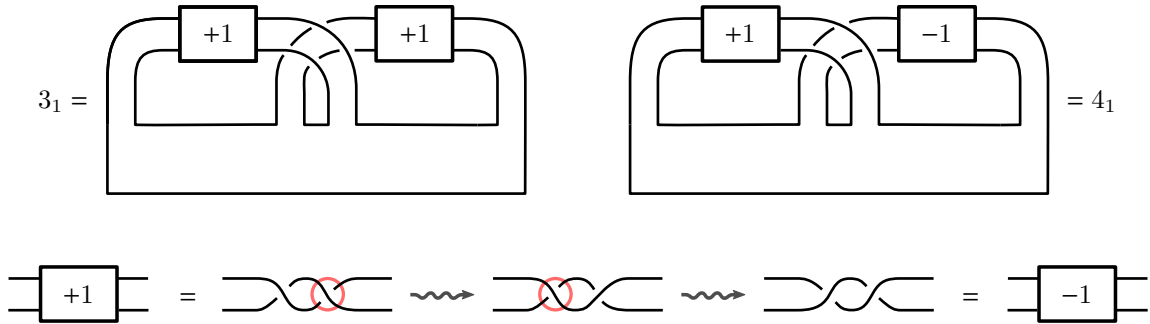


Figure 16. The trefoil 3_1 and figure eight 4_1 knot constructed as plumbings of Hopf bands, where for the trefoil we take two bands with positive twists, while for the figure eight, one band is positive and the other negative. At the bottom we show two crossing changes in one of the twist regions taking 3_1 to 4_1 .

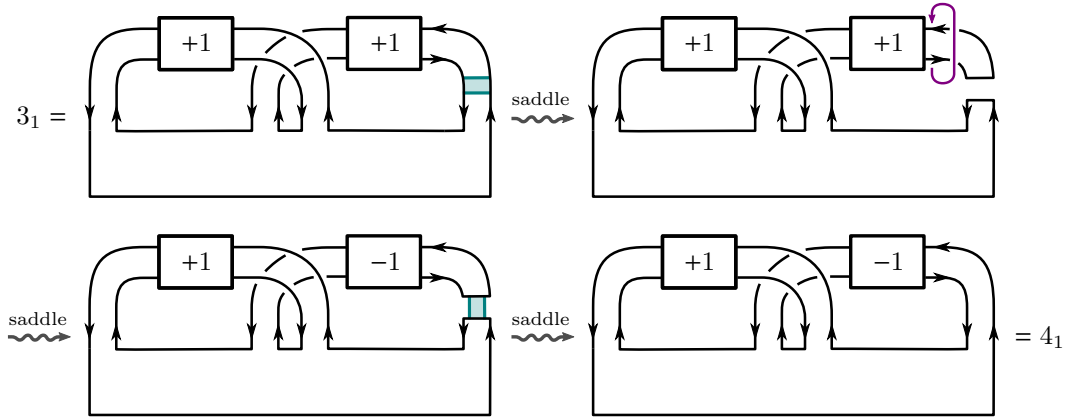


Figure 17. Genus 1 cobordism between the trefoil 3_1 and figure eight 4_1 .

moves on $F_{\tau^{n_2}}(\alpha, l)$ suffice to arrive at the same immersion F' . Here a modification between the twisting parameters n_1, n_2 is possible, because at the intermediate step we are looking at a rim surgery with pattern the unknot, where any amount of twisting can be added without changing the result. \square

Example 5.10. The Gordian distance between the trefoil 3_1 and the figure eight 4_1 is 2, where the lower bound comes from the Alexander module [Kaw12]. Two crossing changes suffice to change the sign of the twisting of a band in the diagram as shown in Figure 16. The Gordian distance from 3_1 and 4_1 to the unknot u is equal to 1. Thus there is no crossing change taking 3_1 to 4_1 , but according to Proposition 5.9 there is a single finger-Whitney move pair between the twist spins $\tau^n 3_1$ and $\tau^n 4_1$. A similar argument shows that both $\tau^n 3_1$ and $\tau^n 4_1$ are a single stabilization away from the unknotted torus, so the stabilization length between them is 1. Also compare this to the genus 1 cobordism between the classical knots 3_1 and 4_1 , which is show in Figure 17.

In particular, even though the knots $u, 3_1$ and 4_1 do not form a clique in the classical Gordian graph, the twist spinning operation sends them to a clique in the ‘Gordian graph for knotted surfaces in the 4-sphere’, where edges correspond to one of the unknotting operations discussed (stabilization or a finger-Whitney move pair). \triangle

6 RIBBON KNOTS AND CASSON-WHITNEY LENGTH

Definition 6.1. A connected orientable *ribbon surface* $K: \Sigma_g \hookrightarrow \mathbb{S}^4$ is the result of the following procedure: Start with an unlink of 2-spheres with $n + 1$ components in \mathbb{S}^4 , which we will call the *minima*. Then stabilize this unlink at least n times to obtain a connected surface.

The minimal number of stabilization tubes needed to put K into this position is called the *fusion number* of K and is denoted $\text{fus}(K) \in \mathbb{N}_0$.

The stabilization tubes in the construction are allowed to link the minima in any sequence, and as usual determined by the isotopy class of their guiding arc. Moreover, since the ambient space is 4-dimensional, the isotopy class of a guiding arc only depends on its homotopy class relative to the endpoints.

Remark 6.2. There exist various different perspectives on ribbon surfaces which we want to mention now. A *ribbon disk* is a properly embedded \mathbb{D}^2 in the 4-ball such that there are no local maxima with respect to the radial Morse function of \mathbb{D}^4 . Ribbon 2-knots appear precisely as the *doubles* of ribbon disks $\Delta: \mathbb{D}^2 \hookrightarrow \mathbb{D}^4$, where the double of Δ is the 2-sphere $\Delta \cup_{\partial\Delta} \Delta \subset \mathbb{D}^4 \cup_{\mathbb{S}^3} \mathbb{D}^4 \cong \mathbb{S}^4$. In a banded unlink diagram, it encodes such a double if the members of the two sets of bands are parallel. We will recall *banded unlink diagrams* for knotted surfaces in [Section 6.3](#). Given a ribbon presentation with minima and saddles, there is a straightforward procedure to construct a banded unlink diagram in which each saddle is represented by a pair of dual bands.

Alternatively, ribbon 2-knots are precisely those smooth 2-spheres where the embedding $K: \mathbb{S}^2 \hookrightarrow \mathbb{S}^4$ extends to an immersion of a 3-ball $\mathbb{D}^3 \looparrowright \mathbb{S}^4$ with only ribbon intersections.¹³ Here the ribbon singularities are self-intersections in 2-dimensional disks, such that the preimage in the 3-ball consists of two components, one of which is properly embedded in \mathbb{D}^3 while the other lies completely in the interior. Thinking 5-dimensionally, where we can push the intersections into the \mathbb{D}^5 bounding \mathbb{S}^4 , we see that ribbon 2-knots bound properly embedded 3-balls $\mathbb{D}^3 \hookrightarrow \mathbb{D}^5$ where the radial Morse function of \mathbb{D}^5 restricted to the embedded ribbon 3-ball does not have local maxima.

In [Definition 6.7](#) we will recall the definition of the potentially weaker notion of handle ribbon 2-knots. In [Section 6.1.1](#) we will discuss Satoh's tube map, which is a shorthand description of ribbon 2-knots resulting from welded arcs.

6.1 Fusion number upper bound on Casson-Whitney length

The following paragraphs generalize upper bound for ribbon knots from [\[JKRS20, Sec. 4\]](#).

Miyazaki proved in [\[Miy86\]](#) that for a ribbon 2-knot K in the 4-sphere, the fusion number gives an upper bound on the stabilization number. In the case of an orientable knotted genus g surface, the upper bound is the fusion number minus the genus of the knotted surface. Observe that the quantity $\text{fus}(K) - g$ agrees with the number of minima minus 1 in the most efficient ribbon presentation of K . We prove the corresponding statement for the Casson-Whitney number in [Theorem 6.3](#) below. The proof is inspired by Miyazaki's, however the argument is subtler and requires an inductive step, so we first sketch Miyazaki's argument.

Let K be a genus g ribbon surface in the 4-sphere, formed by stabilizing the unlink $U_1 \sqcup \cdots \sqcup U_{n+1}$ of 2-spheres along guiding arcs connecting consecutive components U_i and U_{i+1} , possibly together with additional stabilizations which each increase the genus by one, as in [Definition 6.1](#). The 'obvious' stabilizations of K which fuse the minima U_i to U_{i+1} as in [Figure 18](#) result in an unknotted surface K' : Think of K' as first formed by attaching this second set of tubes, and then the original tubes defining K , which produces the same surface K' . This is clearly unknotted, since the 'obvious' tubes result in an

¹³ A similar characterization holds for ribbon surfaces, which extend to immersions of a solid handlebody in the 4-sphere.

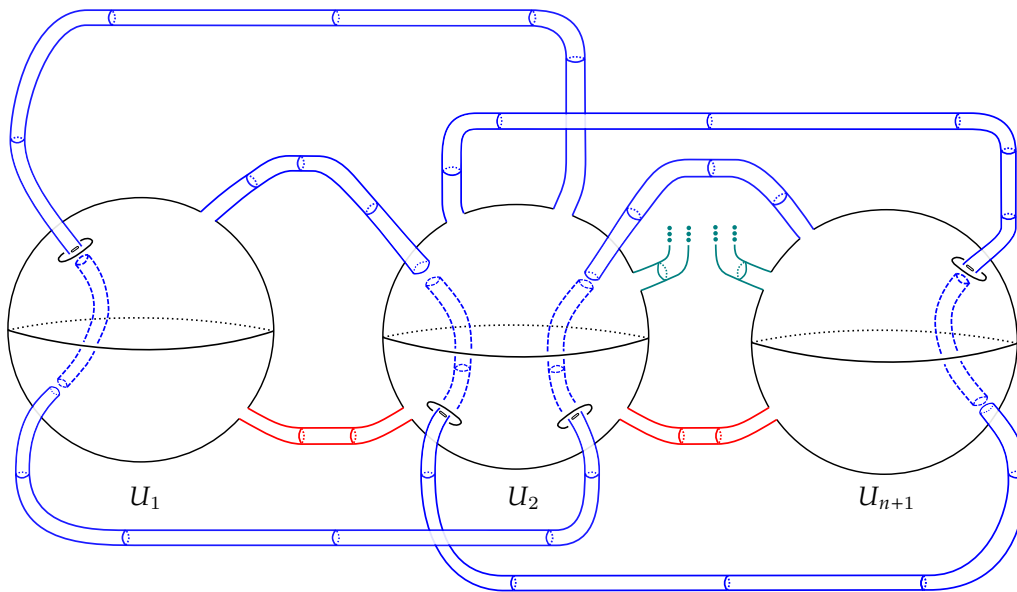


Figure 18. Miyazaki's proof that $u_{\text{st}}(K) \leq \text{fus}(K) - g$ for a genus g ribbon surface K in the 4-sphere: The red stabilization of the black unlink is the unknot U . Hence, the guiding arcs for the blue stabilizations are isotopic rel boundary to trivial arcs in the complement of U . Analogously the additional genus increasing stabilizations (where we only show the feet of a stabilization tube in teal) are trivial. In this and the following figures of ribbon knots, we represent the knotted surfaces via broken surface diagrams; for these diagrams see also Section 6.1.1.

unknotted sphere, and so the original tubes are (trivial) stabilizations of an unknotted surface, which must be unknotted. This finishes Miyazaki's argument.

One could perform $\text{fus}(K) - g$ finger moves from the last minimum to all the others to abelianize the group of K . In the resulting group this last meridian becomes central in the group, and since all the other meridians around the minima are conjugates of the last one they are all equal. But the rest of Miyazaki's argument breaks down in our case: If one thinks of the finger moves as performed just on the $n + 1$ component unlink without any fusion tubes, then the group of the complement is not abelian since it takes $\binom{n+1}{2}$ finger moves to abelianize the free group of the complement of this unlink. To remedy this, we think of all but one of the tubes as already attached and proceed by induction, allowing us to work with two components instead of $n + 1$. This leads to the following generalization of [JKRS20, Thm. 1.4], which was only stated for genus $g = 0$, to the case of potentially higher genus ribbon surfaces in the 4-sphere.

THEOREM 6.3. *In the 4-sphere, the Casson-Whitney length of an orientable ribbon surface $K: \Sigma_g \hookrightarrow \mathbb{S}^4$ to the unknotted surface U_g is bounded above by the fusion number minus the genus g of the surface,*

$$\text{length}_{\text{CW}}(K, U_g) \leq \text{fus}(K) - g.$$

Proof. This proof idea is very similar to [JKRS20, Thm. 1.4], with a minor modification to take care of the extra fusion tubes that are present in the higher genus case.

Let $n = \text{fus}(K)$. Then the ribbon knot K can be obtained from the unlink $U = U_1 \sqcup \cdots \sqcup U_{n+1-g}$ by n stabilizations along guiding arcs $\alpha_1, \dots, \alpha_n$. We will divide these stabilizations into the collection of *connecting fusions* which decrease the number of components of the link, and the *genus increasing fusions* which join a connected component to itself. After a possible reordering of the order in which the fusions occur, we can assume that all connecting fusions happen before all genus increasing fusions. Additionally with an isotopy consisting of slides of the fusion tubes over each other, we may assume that each of the

connecting fusions α_i connects U_i to U_{i+1} as in [Figure 19a](#).

In the following, we set aside the genus increasing fusion tubes, and think of them as being added back in after we constructed the regular homotopy. The regular homotopy will not interfere with these tubes, as it consists only of finger moves and isotopies of guiding arcs, which by general position can be made disjoint from these additional fusions.

Let L be the 2-component link obtained by stabilizing the unlink U only along the guiding arcs $\alpha_2, \dots, \alpha_{n-g}$. Remember that the guiding arcs $\alpha_2, \dots, \alpha_{n-g}$ were allowed to interact and link with the first minimum U_1 , so in general the resulting link will not be a split union. Recall from the behavior of the fundamental group under stabilization that

$$\pi_1(\mathbb{S}^4 - L) \cong \langle m_1, m_2, \dots, m_{n+1} \mid m_j^{g_j} = m_{j+1} \text{ for } 1 < j < n + 1 \rangle$$

where the group elements g_j correspond to the guiding arcs α_i as in [Definition 3.14](#), and $m_1, \dots, m_{n+1} \in \pi_1(\mathbb{S}^4 - U)$ are meridians of each component U_1, \dots, U_{n+1} . We use the exponent notation $m^g = g^{-1}m$ for conjugation.

Perform $n - g$ finger moves to L along trivial guiding arcs from U_{n+1-g} to $U_i, i \leq n - g$ as in [Figure 19b](#) and call the resulting immersed 2-component link S . By the behavior of the fundamental group under finger moves, we have made the last meridian m_{n+1-g} commute with m_i for all $i < n + 1 - g$, therefore by considering the previous stabilization relations we see that $\pi_1(\mathbb{S}^4 - S) \cong \mathbb{Z} \oplus \mathbb{Z}$ generated by m_1 and m_2 . Now consider the element g_1 corresponding to the guiding arc α_1 as in [Figure 19b](#). Since $\pi_1(\mathbb{S}^4 - S)$ is abelian and generated by m_1 and m_2 , by boundary twisting, α_1 is isotopic to a trivial arc between U_1 and U_2 as shown in [Figure 19c](#).

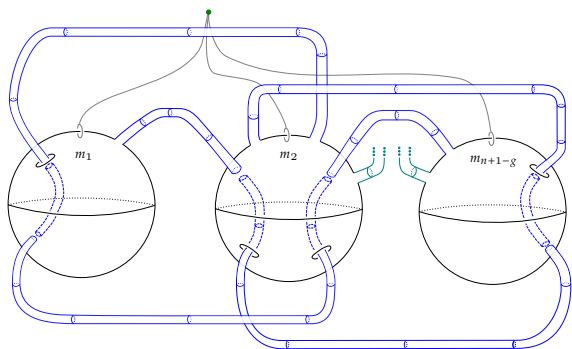
We can now undo the finger move that intersects U_1 (i.e. do the Whitney move) and proceed, by the same reasoning, to straighten out all of the other arcs α_i to be trivial arcs as in [Figure 19d](#). Continuing in this way unknots K without the genus increasing tubes (by trivializing the guiding arcs $\alpha_1, \dots, \alpha_{n-g}$) with $n - g$ finger moves and $n - g$ Whitney moves.

Now re-adding the genus-increasing tubes is a necessarily trivial stabilization of an unknot, and this yields the unknotted genus g surface. \square

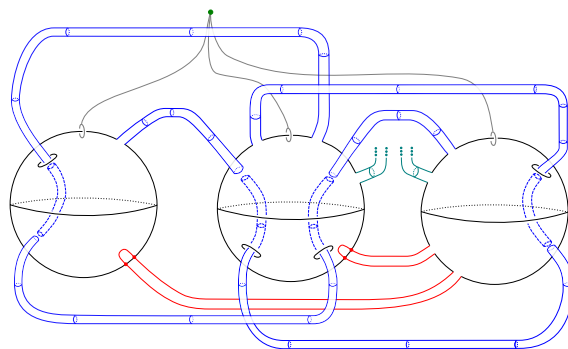
The inequality for ribbon surfaces $K: \Sigma_g \hookrightarrow \mathbb{S}^4$ from [Theorem 6.3](#) can be strict, already for the genus 0 case where it specializes to $u_{CW}(K) \leq \text{fus}(K)$. For instance, let k be a 1-knot with unknotting number $u(k) = 1$ and meridional rank $\mu(k) > 2$ (in fact, it is shown in [\[BK20\]](#) that there exist unknotting number one knots with arbitrarily large meridional rank). Then, we saw in [Corollary 4.4](#) that the spun knot $K = \tau^0(k)$ has $u_{CW}(K) = 1$. Moreover, the isomorphism between $\pi_1(\mathbb{S}^4 - K)$ and $\pi_1(\mathbb{S}^3 - k)$ preserves the meridians, and so the meridional ranks of K and k are equal. This gives $u_{CW}(K) < \text{fus}(K)$, since spun knots are ribbon and the meridional rank of any ribbon 2-knot is less than or equal to one more than its fusion number.

Remark 6.4. The regular homotopy in the proof of [Theorem 6.3](#) above has standard and knotted Whitney disks whose entire boundaries agree (so, they are ‘doubly’ arc-standard). However, since the homotopy of the tubes in the proof interacts with the standard Whitney disks, the interiors of the standard and knotted Whitney disks are necessarily distinct.

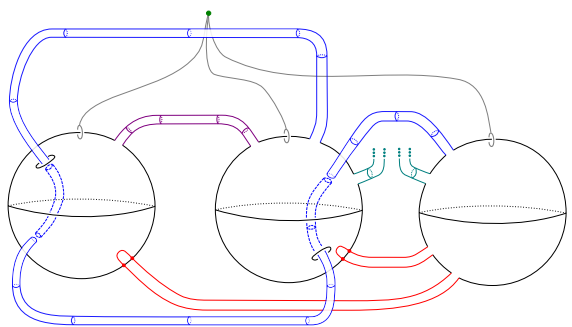
6.1.1 Satoh’s tube map and Casson-Whitney lengths. The construction in the proof of [Theorem 6.3](#) does not easily generalize to fusion number bounds for regular homotopies between arbitrary knotted ribbon surfaces, i.e. for regular homotopies which lead to non-trivially knotted surfaces as opposed to the unknot. We now elaborate on why the proof technique does not appear to work. For simplicity, let $K: \mathbb{S}^2 \hookrightarrow \mathbb{S}^4$ be a ribbon sphere of n -fusion in normal form as in the beginning of the proof, and perform n many finger moves from the last minimum to all the others. Again forgetting the



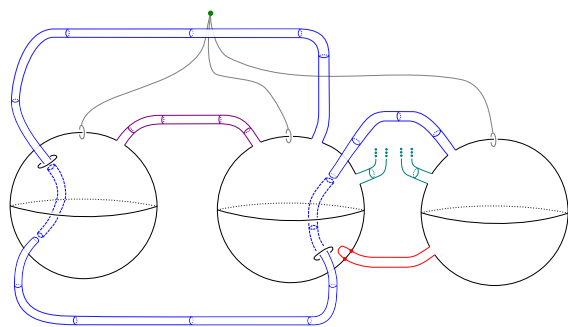
(a) Ribbon presentation of K with the first and second stabilization along the guiding arcs a_1 and a_2 respectively drawn as blue tubes. Additional genus increasing tubes in teal can be ignored for the inductive argument.



(b) Finger moves (red) along trivial arcs.



(c) The guiding arc of the first stabilization is isotopic to a trivial arc in the complement of the immersion.



(d) Undo the first finger move in order to proceed inductively and trivialize the remaining stabilizations.

Figure 19. Illustrating the proof of the fusion number upper bound in [Theorem 6.3](#).

first stabilization, we see that the group of the 2-component link consisting of U_1 and a stabilization of $U_2 \sqcup \dots \sqcup U_{n+1}$ is $\mathbb{Z} \oplus \mathbb{Z}$. We can homotope (and thus isotope) the guiding arc of the first stabilization in the immersion complement to follow any word in the meridians of our choosing. But if we do not make this first stabilization into a trivial arc connecting the minima straight across, the inductive step appears to break down. We do not know whether the group of the link consisting of an arbitrary stabilization of $U_1 \cup U_2$ and a stabilization of $U_3 \cup \dots \cup U_{n+1}$, where the stabilization tubes are allowed to link any of the U_i , is necessarily abelian, even after forcing the last generator m_{n+1} into the center of the group.

We now introduce a convenient shorthand notation of ribbon surfaces, and explain how it can be used to construct regular homotopies. Satoh proved in [Sat00] that every ribbon 2-knot in \mathbb{S}^4 is the *tube* of a virtual arc in the 3-sphere. Earlier, Yajima [Yaj62] already defined the tube of a classical arc, and Satoh extended this language to be compatible with virtual crossings. Essentially, one can use virtual diagrams¹⁴ to make a shorthand picture for a broken surface diagram of a ribbon 2-knot. A *broken surface diagram* is a generic projection of a smoothly embedded surface in \mathbb{S}^4 to 3-space, where the self-intersections are arcs of double points, branch points or triple points. In the diagrams, we delete a neighborhood of the intersection around the double points on the sheet of the surface that had a lower fourth coordinate before projecting. In other words, we break parts of the surface in the 3-dimensional diagram, and the resulting over/under information encodes the smooth isotopy class of the embedding in

¹⁴ In this context sometimes also called *welded diagrams*.

4-space. For a detailed definition of broken surface diagrams for knotted surfaces see for example [CS98].
broken surface diagram

Under the tube map, the strands of the virtual arc or knot k are inflated into tubes in 4-space. Classical crossings ‘tube’ to a linking, where one tube crosses from above and then below the other tube. Virtual crossings ‘tube’ to not actually cross in \mathbb{R}^3 , these crossings are only an artifact of the further projection to \mathbb{R}^2 when we draw the broken surface diagram flat. In particular, [Sat00] showed that welded moves of k correspond to isotopies of the surface $\text{Tube}(k)$. By joining the ends of a welded arc, similarly every ribbon torus is the tube of a welded knot. Further extensions to higher genus ribbon surfaces corresponding to welded graphs are also possible [KF08]. The singularities in a broken surface diagram of such a ribbon presentation only consist of double point circles between the minima 2-spheres and fusion tubes.

The 0-twist spin of a classical knot $k: \mathbb{S}^1 \hookrightarrow \mathbb{S}^3$ is the result of applying the tube map to k° , the arc which comes from removing a small segment of k , in other words $\text{Tube}(k^\circ) = \tau^0(k)$; this observation is attributed to Roseman [roseman1998surfaces] and Satoh.

In this language, changing a virtual crossing to a positive or a negative classical crossing is achieved by a finger move and then a Whitney move on its tube, the analogue in this setting of the homotopy in Figure 20. Concatenating two of these operations, i.e. changing a positive to a negative crossing in the virtual arc, corresponds to a length two regular homotopy between the associated surfaces.

For stating a proposition which summarizes the above discussion, we generalize the definition of *Gordian distance* to virtual arcs as follows: For virtual arcs k and j , the distance $\text{dist}_{\text{Gord}}(k, j) \in \frac{1}{2}\mathbb{N}_0$ is the minimal number of virtual crossing changes required to turn a diagram of j into a diagram of k , where we minimize over all possible diagrams of k respectively j . A virtual crossing change can be of two types: Converting a classical crossing into a virtual crossing or vice versa, which contributes $\frac{1}{2}$ to the distance, or a classical crossing change (changing a positive crossing into a negative crossing or vice versa) which contributes 1 to the distance. The above discussion proves the following, which gives an upper bound on the Casson-Whitney length between ribbon 2-knots:

PROPOSITION 6.5. *Let $K, J: \mathbb{S}^2 \hookrightarrow \mathbb{S}^4$ be ribbon 2-knots in the 4-sphere. For every pair of virtual arcs k and j such that $\text{Tube}(k) = K$ and $\text{Tube}(j) = J$, the Casson-Whitney length between K and J is bounded above by twice the virtual Gordian distance between k and j ,*

$$\text{length}_{\text{CW}}(K, J) \leq 2 \text{dist}_{\text{Gord}}(k, j).$$

Remark 6.6 (HC-unknotted). In [Kan00], Kanenobu introduces the *HC-unknotted number* u_{HC} of ribbon 2-knots $K: \mathbb{S}^2 \hookrightarrow \mathbb{S}^4$, where the ‘‘HC’’ stands for *handle change*. This is a local move which allows interchanging a pair of neighboring letters in the sequence describing the linking of a fusion tube with the minima 2-spheres of the ribbon knot. He observes the lower bound $u_{\text{st}}(K) \leq u_{\text{HC}}(K)$, but also that for any pair of integers satisfying the constraints $1 \leq q \leq p + q$, and $q \geq 1$, $p \geq 1$ the connected sum $K_{p,q} = R(p, -1, -1, 1, -p, 1, p, -1) \#^{q-1} R(-1, 1)$ satisfies $u_{\text{st}}(K_{p,q}) = q$ and $u_{\text{HC}}(K_{p,q}) = p + q$. Here $R(a_1, b_1, a_2, b_2, \dots, a_n, b_n)$ is a ribbon 2-knot of 1-fusion, where the sequence of integers a_i, b_i describes in what manner the fusion tube links with the two minima. As the knot $K_{p,q}$ has fusion number $\text{fus}(K_{p,q}) = q$, we know from Theorem 6.3 that $u_{\text{CW}}(K_{p,q}) \leq q$, while Kanenobu also computes the Nakanishi index to be $m(K_{p,q}) = q$. Thus from the Alexander module lower bound we conclude $u_{\text{CW}}(K_{p,q}) = q$. This proves that arbitrary gaps between Kanenobu’s u_{HC} and our u_{CW} are possible, even for ribbon 2-knots of 1-fusion.

6.2 Handle ribbon 2-knots and Casson-Whitney length

This section is not part of [JKRS20].

Any 0-twist spin of a classical knot is a ribbon 2-knot. As discussed in Section 6.1.1, the spin of a classical knot agrees with the result of Satoh’s tube map applied to the virtual arc obtained by removing a small

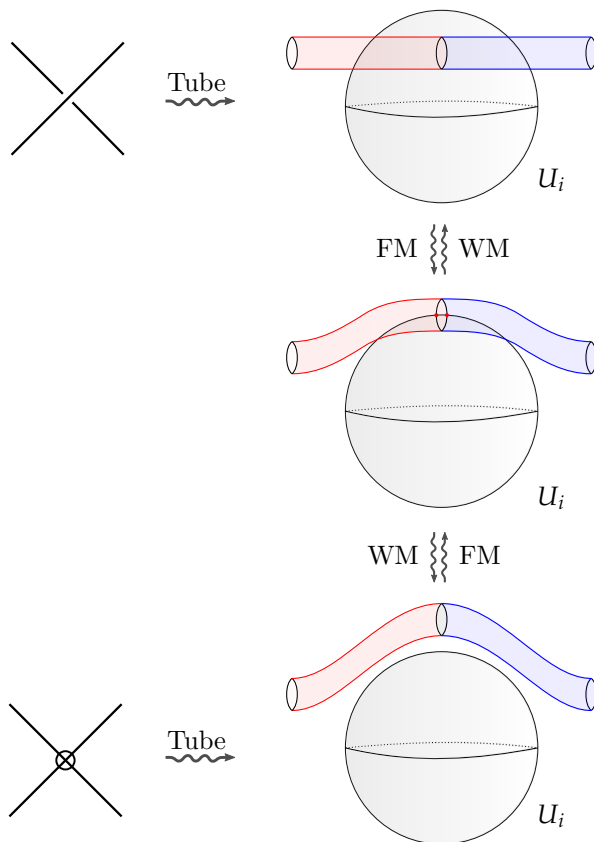


Figure 20. On the right, a regular homotopy of a ribbon 2-knot K , as in Definition 6.1, supported near one component U_i of the unlink and one guiding arc of a stabilization. The various shadings of K suggest its fourth coordinates – so, the red and blue portions of the surface are disjoint from the black ones. The homotopy consists of one finger move (FM) followed by one Whitney move (WM), and (thought of from top to bottom) has the effect of removing a meridian of U_i from the word in $\pi_1(\mathbb{S}^4 - U_1 \sqcup \cdots \sqcup U_{n+1})$ giving the homotopy class of the guiding arc of the stabilization. On the left we see local pieces of a welded diagram. Under the tube map, the classical crossing at the top corresponds to the linking of the guiding arc with U_i , which has been removed in the virtual crossing at the bottom.

piece from the classical knot, which leads to upper bounds on the Casson-Whitney length between ribbon knots. In this section, we want to recall various ribbon obstructions for 2-knots in the 4-sphere, and finally put this into context of the Casson-Whitney length.

The double of the ‘standard’ 2-minima ribbon disk of the stevedore knot 6_2 is a ribbon knot which is not a spun knot since its Alexander polynomial $2t - 1$ is not symmetric under the involution $t \mapsto t^{-1}$. Thus the group of the double of the stevedore, which is also known as the Baumslag-Solitar group $B(1, 2) \cong \mathbb{Z} \rtimes \mathbb{Z}[\frac{1}{2}]$, is not a classical knot group. Further discussion of the difference between classical and higher dimensional knot groups can be found in [Kaw96, Ch. 14].

A potentially weaker notion of ‘ribbonness’ can be defined by requiring the handle decomposition of the exterior of a 3-ball in the 5-ball bounding a 2-knot in the 4-sphere to be of a simple form.

Definition 6.7 (Handle-ribbon 2-knot). A 2-knot $K: \mathbb{S}^2 \hookrightarrow \mathbb{S}^4 = \partial\mathbb{D}^5$ is *handle ribbon* if it bounds a properly embedded 3-disk $D_K: \mathbb{D}^3 \hookrightarrow \mathbb{D}^5$ such that the exterior $\mathbb{D}^5 - \nu(D_K)$ has a handlebody decomposition consisting of only 0-, 1- and 2-handles.

Ribbon 2-knots are handle-ribbon, which follows from the rising-water principle: A ribbon 2-knot bounds a properly embedded 3-disk in the 5-ball whose restriction of the radial Morse function of the 5-ball

contains only index 0 (minima) and index 1 (saddles) critical points. For the handle-decomposition of the exterior each index 0-critical point leads to a 1-handle and each index 1-critical point to a 2-handle.

Let $\text{Rib}^{(2,4)} \subseteq \text{HanRib}^{(2,4)} \subsetneq \text{Slice}^{(2,4)} = \text{Knots}^{(2,4)}$ denote the collection of ribbon 2-knots, handle ribbon 2-knots, slice 2-knots and all 2-knots $K: \mathbb{S}^2 \hookrightarrow \mathbb{S}^4$ respectively. Whether the first inclusion in this chain is strict, i.e. whether there exist handle ribbon knots which are not ribbon, is still unknown. For the classical case of 1-knots in the 3-sphere, it is a major open question whether every slice knot is a ribbon knot. In higher dimensions of knotted $(n-2)$ -spheres in the n -sphere for $n \geq 4$, examples are known which show that the concept of slice and (handle) ribbon differ [Hit79]. For $n = 4$, Kervaire observed that every 2-knot is slice [Ker65].

Ribbon groups have deficiency 1 and admit a Wirtinger presentation with respect to a meridian. Cochran [Coc83] studied the commutator subgroup of the knot group of ribbon 2-knots, which lead to a ribbon obstruction, as we now explain. Since the handle decomposition of the complement of a handle ribbon knot is the reason for the special form of the group presentations, this is actually a handle ribbon obstruction.

THEOREM 6.8 ([Coc83, Thm. 2.2]). *Let $K: \mathbb{S}^2 \hookrightarrow \mathbb{S}^4$ be a handle ribbon 2-knot with group $\pi_K := \pi_1(\mathbb{S}^4 - K)$. Then the commutator subgroup $[\pi_K, \pi_K]$ is an E -group, which are by definition the fundamental groups of connected 2-complexes Y (not assumed to be finite) such that $H_1(Y; \mathbb{Z})$ is torsion-free and $H_2(Y; \mathbb{Z}) = 0$. In particular, the group homology of the commutator subgroup satisfies that $H_1([\pi_K, \pi_K]; \mathbb{Z})$ is \mathbb{Z} -torsion free and $H_2([\pi_K, \pi_K]; \mathbb{Z}) = 0$.*

Let X be the result of surgery on the sphere K , observe that $\pi_1(X) \cong \pi_K$. Let $\widehat{X}_{\mathbb{Z}} \rightarrow X$ be the regular \mathbb{Z} -cover of X and $i: \widehat{X}_{\mathbb{Z}} \rightarrow K([\pi_K, \pi_K], 1)$ a classifying map for its fundamental group (we can build an Eilenberg-MacLane space $K([\pi_K, \pi_K], 1)$ by attaching 3-cells and higher to $\widehat{X}_{\mathbb{Z}}$). Then the classifying map induces the zero map on third homology with arbitrary coefficients in an abelian group C , that is $0 = i_: H_3(\widehat{X}_{\mathbb{Z}}; C) \rightarrow H_3([\pi_K, \pi_K]; C)$.*

Proof ideas. The ribbon knot group π_K is an E -group because π_K is isomorphic to the fundamental group of the complement of the handle-ribbon disk $\mathbb{D}^5 - \nu(D_K)$, homotopy equivalent to a 2-complex which is a homology circle by Alexander duality. Now theorems of Adams and Strebel imply that any term in the derived series of an E -group is an E -group itself. The second item follows because the map on homology factors through a 2-complex which has trivial homology in degree 3. \square

For fibered 2-knots, Cochran obtained additional handle ribbon obstructions. The following is a simplification of his statement using that the 3-dimensional Poincaré conjecture has been solved.

THEOREM 6.9 ([Coc83, Thm. 3.0]). *Let $K: \mathbb{S}^2 \hookrightarrow \mathbb{S}^4$ be a fibered 2-knot with fiber 3-manifold M° . The 2-knot K is handle ribbon if and only if the closed fiber M is a connected sum $\#^r \mathbb{S}^1 \times \mathbb{S}^2$.*

As a corollary, Cochran observed that a non-trivial twist-spun knot $\tau^m k$, which by Zeeman is fibered by the punctured m -fold cyclic branched cover $\Sigma_m(k)$, cannot be a handle ribbon knot. This follows because the branched cover does not have $\mathbb{S}^1 \times \mathbb{S}^2$ summands in its prime decomposition. We will apply these ideas to show that handle-ribbon 2-knots do not approximate the collection of all 2-knots well with respect to the Casson-Whitney length.

PROPOSITION 6.10. *There exists a family of 2-knots whose Casson-Whitney length to the collection of handle ribbon 2-knots $\text{HanRib}^{(2,4)}$ grows arbitrarily large.*

Proof. Recall that the 2-fold branched cover over a 2-bridge knot k is a lens space. By Zeeman's fibration theorem [Zee65], the 2-twist spin over a 2-bridge knot $\tau^2 k$ is fibered by a punctured bounded lens space

$L(p, q)$. These examples were already given by Hitt [Hit79] as slice 2-knots which are not ribbon. Let k be a chosen 2-bridge knot such that the parameter p in the lens space is prime. Then the commutator subgroup $[\pi_1(\mathbb{S}^4 - \tau^2 k), \pi_1(\mathbb{S}^4 - \tau^2 k)] \cong \pi_1(L(p, q)) \cong \mathbb{Z}/p$ is equal to its abelianization $H_1([\pi_1(\mathbb{S}^4 - \tau^2 k), \pi_1(\mathbb{S}^4 - \tau^2 k)]; \mathbb{Z})$, and in particular p -torsion.

The commutator subgroup of a connected sum is the free product of the commutator subgroups of the summands. Therefore by taking connected sums $\#^N \tau^2 k$, we can build examples of 2-knots with torsion in the abelianization of the commutator subgroup

$$H_1([\pi_1(\mathbb{S}^4 - \#^N \tau^2 k), \pi_1(\mathbb{S}^4 - \#^N \tau^2 k)]; \mathbb{Z}) \cong \bigoplus^N \mathbb{Z}/p$$

a vector space of dimension N . By looking at the dimension of this torsion group, we observe that the Casson-Whitney length from $\#^N \tau^2 k$ to any handle-ribbon 2-knot is at least N . This follows because every finger move relation is only able to kill at most a rank one \mathbb{Z} -submodule in the Alexander module as in Proposition 3.22. Additionally, the length to the unknot $\text{length}_{\text{CW}}(\#^N \tau^2 k, \mathcal{U})$, which is handle ribbon, is precisely N from the upper bound on the Casson-Whitney number for twist-spins of 2-bridge knots in Theorem 3.25. \square

6.3 Suciú's family of ribbon 2-knots and Casson-Whitney length

This section consists of new material, which has not been previously published.

Suciú [Suc85] constructs an infinite family of ribbon 2-knots $R_k: \mathbb{S}^2 \hookrightarrow \mathbb{S}^4$ in the 4-sphere (indexed by the natural numbers $k \in \mathbb{N}_{\geq 1}$), each of which with $\pi_1(\mathbb{S}^4 - R_k)$ isomorphic to the group of the trefoil knot $T_{2,3}: \mathbb{S}^1 \hookrightarrow \mathbb{S}^3$. The fibration of the trefoil complement by punctured tori induces the following presentation of $\pi_1(\mathbb{S}^3 - T_{2,3})$ as an HNN-extension of the free group $\langle u, v \rangle$ of rank 2 of the fiber by the cyclic group $\langle t \rangle$ whose generator is a meridian to the knot.

$$\langle t, u, v \mid tut^{-1} = v, tvt^{-1} = u^{-1}v \rangle$$

In particular, R_1 is the spun trefoil knot with meridian t . The other knots appear via modifications of the monodromy, and they have different meridians $t_k = u^k t$. Suciú's family of knots is studied via their 2-fold branched cover in [KS20].

A ribbon presentation with three minima t_k, c, d and of fusion number 2 (with fusion bands homotopic to $w_1 = t_k(dc^{-1})^{-k+1}$ and $w_2 = t_k cd^{-1} t_k^{-1}$) is given as

$$\begin{aligned} \langle t_k, c, d \mid d = \underbrace{t_k(dc^{-1})^{-k+1}}_{w_1} \cdot t_k \cdot \underbrace{(t_k(dc^{-1})^{-k+1})^{-1}}_{w_1^{-1}}, c = \underbrace{t_k cd^{-1} t_k^{-1}}_{w_2} \cdot d \cdot \underbrace{(t_k cd^{-1} t_k^{-1})^{-1}}_{w_2^{-1}} \rangle \\ \cong \langle t_k, c, d \mid d = w_1 \cdot t_k \cdot w_1^{-1}, c = w_2 \cdot d \cdot w_2^{-1} \rangle \end{aligned}$$

In Suciú's original paper, the fusion number 2 ribbon presentation is drawn in [Suc85, Fig. 6], which we reproduce in Figure 22a. We will now explain how to interpret this diagram as describing a ribbon disk, and how its double yields a ribbon 2-knot. The diagram is a shorthand for a level picture in 4-space, where we think of the last coordinate as time and watch a movie of consecutive 3-dimensional slices of the space. The Figure 22a is looked at from above, where the knot $J \subset \partial \mathbb{D}^4$ lives in the boundary of a 4-ball, and the time coordinate will take us deeper towards the center of the ball. In the picture, we encoded a collection of *ribbon moves*, each of which attaches a 1-handle $\mathbb{D}^1 \times \mathbb{D}^1$ along $\partial \mathbb{D}^1 \times \mathbb{D}^1$ to the current link. Such a saddle point changes the link by a surgery. After all the ribbon moves, we are left with an unlink, which determines a unique collection of trivial 2-disks capping off the minima. Note that for describing a general slice disk, we would additionally need to allow the birth of 2-handles corresponding to maxima at the beginning of the process. Also compare this with the discussion of level pictures in [GS99, Sec. 6.2].

Let $\Delta: \mathbb{D}^2 \hookrightarrow \mathbb{D}^4$ be such a ribbon disk encoded via a diagram of the equatorial knot $J \subset \mathbb{S}^3$ together with a system of bands which surger J into an unlink. The *double* of Δ is a ribbon 2-sphere $\Delta \cup_J \Delta \subset \mathbb{D}^4 \cup_{\mathbb{S}^3} \mathbb{D}^4 \cong \mathbb{S}^4$ in the 4-sphere. In the movie perspective this corresponds to reading the same collection of ribbon bands both going upwards and downwards in the height/time coordinate. Diagrammatically, this double can be encoded as the knot J together with the collection of parallel ribbon bands.

For describing general knotted surfaces, which are not necessarily ribbon, the collection of downwards-bands can differ from the collection of upwards-bands. Usually in these descriptions, instead of starting with the equatorial level, one draws an unlink representing the minima, together with a collection of fusion bands which connect the components together, and a separate collection of fission bands, which surger the middle level into an unlink. This final unlink can then be capped off with maxima disks, and a picture of this form is called a *banded unlink diagram*. An example of a banded unlink diagram for Suciú's knot R_2 is shown in [Figure 21](#) and for R_3 in [Figure 22b](#). The general pattern for the knot R_k for arbitrary $k \in \mathbb{N}_{\geq 1}$ amounts to adding additional alternating linking of the orange band with the minima corresponding to d and c so that its guiding arc follows $w_1 = t_k(dc^{-1})^{-k+1}$.

Yoshikawa [[Yos94](#)] collected a list of knotted surfaces in the 4-sphere with lowest ‘complexity’ in terms of their banded unlink diagrams. Furthermore, Yoshikawa’s proposed set of moves on banded unlink diagrams representing smooth isotopy is known to be complete [[Swe01](#)] (with an alternative proof in [[KK08](#)]). A generalization of banded unlink diagrams to smoothly knotted surfaces embedded in arbitrary 4-manifolds appeared in [[HKM20](#)], together with a complete set of moves relating banded unlink diagrams of smoothly isotopic surfaces.

Upcoming work of Harvey-Joseph-Jung-Kim [[Har+22](#)] shows that Suciú’s knots R_k have fusion number equal to 2, except the spun trefoil R_1 which is the spin of a 2-bridge knot and thus has fusion number equal to 1.¹⁵

Since Suciú’s ribbon 2-knots are of fusion number $\text{fus}(R_k) \leq 2$, we can conclude from Miyazaki’s upper bound [[Miy86](#)] that their stabilization number $u_{\text{st}}(R_k) \leq 2$ is bounded by 2, and similarly for the Casson-Whitney number from [Theorem 6.3](#), we know $u_{\text{CW}}(R_k) \leq 2$. As a special case, the spun trefoil $R_1 = \tau^0 T_{2,3}$ is non-trivial and of fusion number $\text{fus}(R_1) = 1$ and therefore $u_{\text{st}}(R_1) = 1 = u_{\text{CW}}(R_1)$.

In [Section 6.3.1](#) we compute the stabilization number of each of Suciú’s knots to be equal to one. Then in [Section 6.3.3](#) we investigate the behavior of the connected sums $R_k \# \mathbb{R}\mathbb{P}^2$ with an unknotted projective plane. Lastly, we present some partial result on the algebraic Casson-Whitney number of Suciú’s trefoil group in [Section 6.3.2](#). The results of this section are based on initial exploration utilizing the computer algebra systems SageMath [[Sag21](#)] and GAP [[GAP21](#)]; our code related to Casson-Whitney numbers and Suciú’s examples can be found at [[Rup21a](#)].

6.3.1 Stabilization of Suciú’s knots. Even though the knots in Suciú’s family share the group of their complements, they have interesting behavior under stabilization and Casson-Whitney unknotting. According to [[Suc85](#)] a group isomorphism between the groups $\pi_1(\mathbb{S}^4 - R_i)$ and $\pi_1(\mathbb{S}^4 - R_j)$ for $i \neq j$ cannot preserve the (conjugacy class of a) meridian. Thus a priori, the algebraic lower bounds on u_{st} , u_{CW} by looking at the minimal number of stabilization relations (setting a pair of meridians to be equal) or finger move relations (making a pair of meridians commute) that force the group of the complement to be abelian, could give different results for $i \neq j$.

THEOREM 6.11. *The stabilization number for each of Suciú’s ribbon knots is equal to one, $u_{\text{st}}(R_k) = 1$ for all $k \geq 1$.*

¹⁵ Their proof of the fusion number lower bound is a combination of two observations: For K, J ribbon 2-knots of 1-fusion (or the unknot), the corresponding $\mathbb{R}\mathbb{P}^2$ -knots $K \# \mathbb{R}\mathbb{P}^2 \cong J \# \mathbb{R}\mathbb{P}^2$ are isotopic if and only if their determinants agree. But for Suciú’s family, $R_i \# \mathbb{R}\mathbb{P}^2 \cong R_j \# \mathbb{R}\mathbb{P}^2$ if and only if $i = j$; so they cannot be 1-fusions.

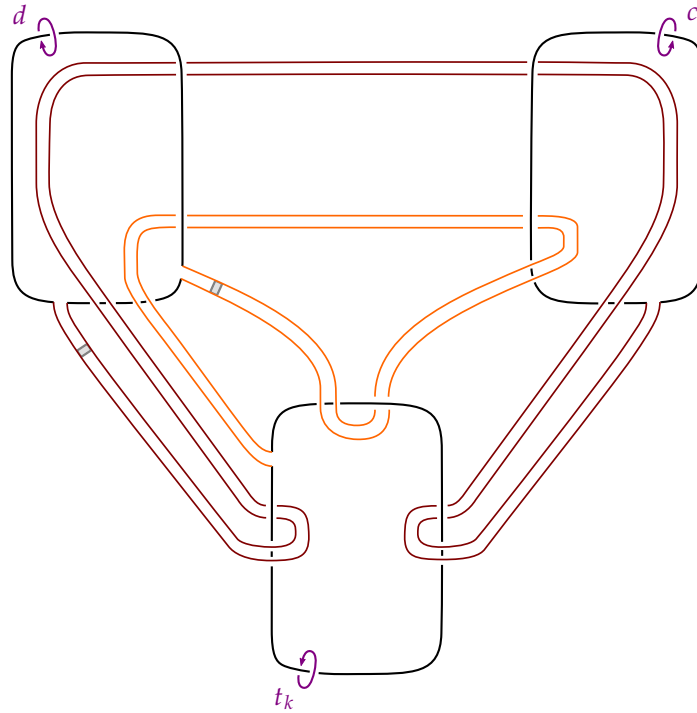
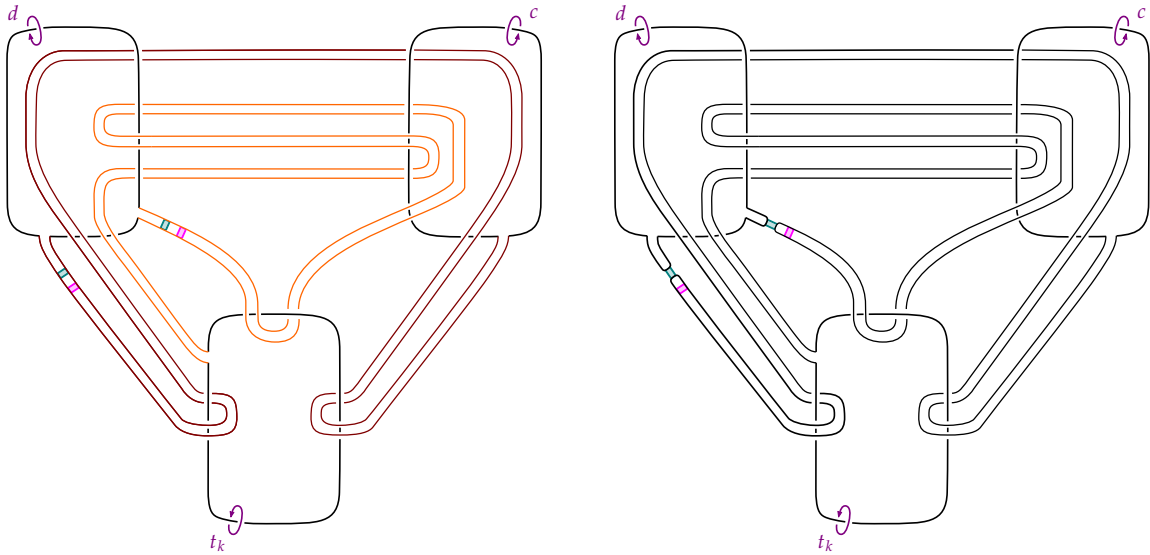


Figure 21. Equatorial cross-section of Suci's knot R_2 with two saddle moves describing a ribbon disk in the 4-ball. There are two ribbon bands, drawn in brown for the guiding arc $w_2 = t_k c d^{-1} t_k^{-1}$ and in orange for the guiding arc $w_1 = t_k (d c^{-1})^{-k+1}$, where here $k = 2$.



(a) R_3 as double of a ribbon disk.

(b) Banded unlink diagram for R_3 .

Figure 22. Left: Equatorial cross-section of Suci's knot R_3 with two pairs of parallel saddle moves describing the double of a ribbon disk. Compare the cores of the ribbon bands with the ribbon group presentation $\langle t_3, c, d \mid d = t_3 (d c^{-1})^{-2} \cdot t_3 \cdot (d c^{-1})^2 t_3^{-1}, c = t_3 c d^{-1} t_3^{-1} \cdot d \cdot (t_3 c d^{-1} t_3^{-1})^{-1} \rangle$. The ribbon disks for the other R_k are constructed by taking the same brown ribbon band, and making the orange band with guiding arc $w_1 = t_k (d c^{-1})^{-k+1}$ alternate $k - 2$ times between the d and c minimum.

Right: Banded unlink diagram of Suci's knot R_3 obtained by resolving the teal collection of ribbon bands.

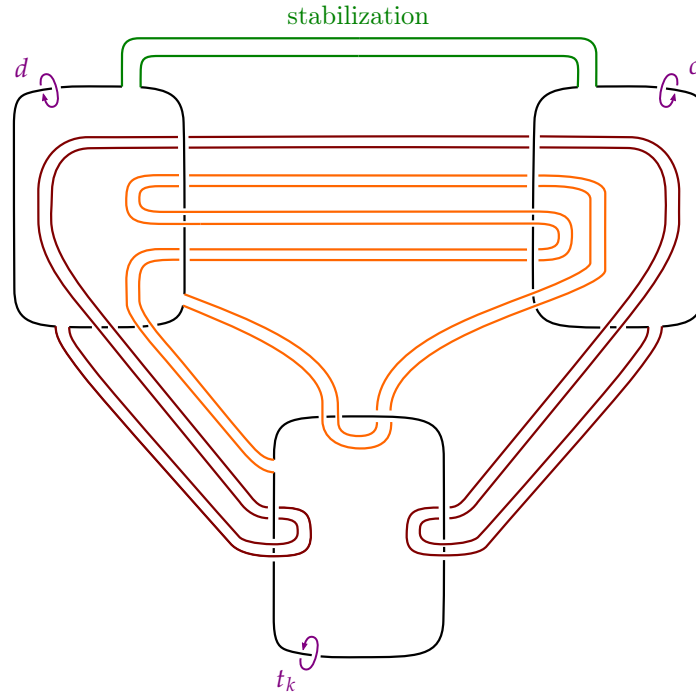


Figure 23. Suci's knot R_3 with a stabilization tube between the minima corresponding to c and d .

Proof. The spun trefoil R_1 is fusion number one and nontrivial, thus from Miyazaki's upper bound we get $u_{\text{st}}(R_1) = 1$.

For $k \geq 2$, attach a tube between the minima corresponding to the meridians c and d , as in [Figure 23](#). In the banded unlink diagram, the cross-section of this tube appears as a band which fuses together the unlink components labeled with c and d . Algebraically, this corresponds to introducing the relation $c = d$ into the knot group. The second relation $c = t_k c d^{-1} t_k^{-1} \cdot d \cdot (t_k c d^{-1} t_k^{-1})^{-1}$ simplifies to $c = d$, while the first relation $d = t_k (d c^{-1})^{-k+1} \cdot t_k \cdot (t_k (d c^{-1})^{-k+1})^{-1}$ cancels down to $d = t_k$. Therefore the stabilization relation $c = d$ abelianizes the group $\pi_1(\mathbb{S}^4 - R_k)$, and moreover we can see geometrically that all the fusion bands simplify as in [Figure 24](#).

We now describe the isotopy in words, which is guided by the algebra simplifying the ribbon relations in the fundamental group. We first *swim* the brown band through the green stabilization, which corresponds to canceling the phrase $c d^{-1}$ from the word of the guiding arc of the brown band. Then we observe that the brown band is actually trivial and parallel to the stabilization. Remember that a *band pass* on a pair of ribbon bands does not change the isotopy class of the surface encoded in the diagram. Similarly, we can swim the orange band $(k - 1)$ times through the stabilization band, where each of these operations removes one copy of $d c^{-1}$ from the ribbon word. Finally, the knot can be recognized as the fusion of the split component belonging to t_k with an unknotted torus. \square

We could also have argued in the following way: Observe that the 2-sphere formed by the orange fusion and the green stabilization has infinite cyclic complement. Thus the guiding arc of the brown fusion is homotopic, and thus isotopic, relative to the endpoints to the trivial stabilization between c and d . Then a similar argument trivializes the orange fusion.

6.3.2 Partial results on the algebraic Casson-Whitney number of Suci's knots. Here we summarize some partial results towards determining the Casson-Whitney number of the knots in Suci's family. For this it is convenient to convert between different presentations of the groups, see also [\[Suc85\]](#).

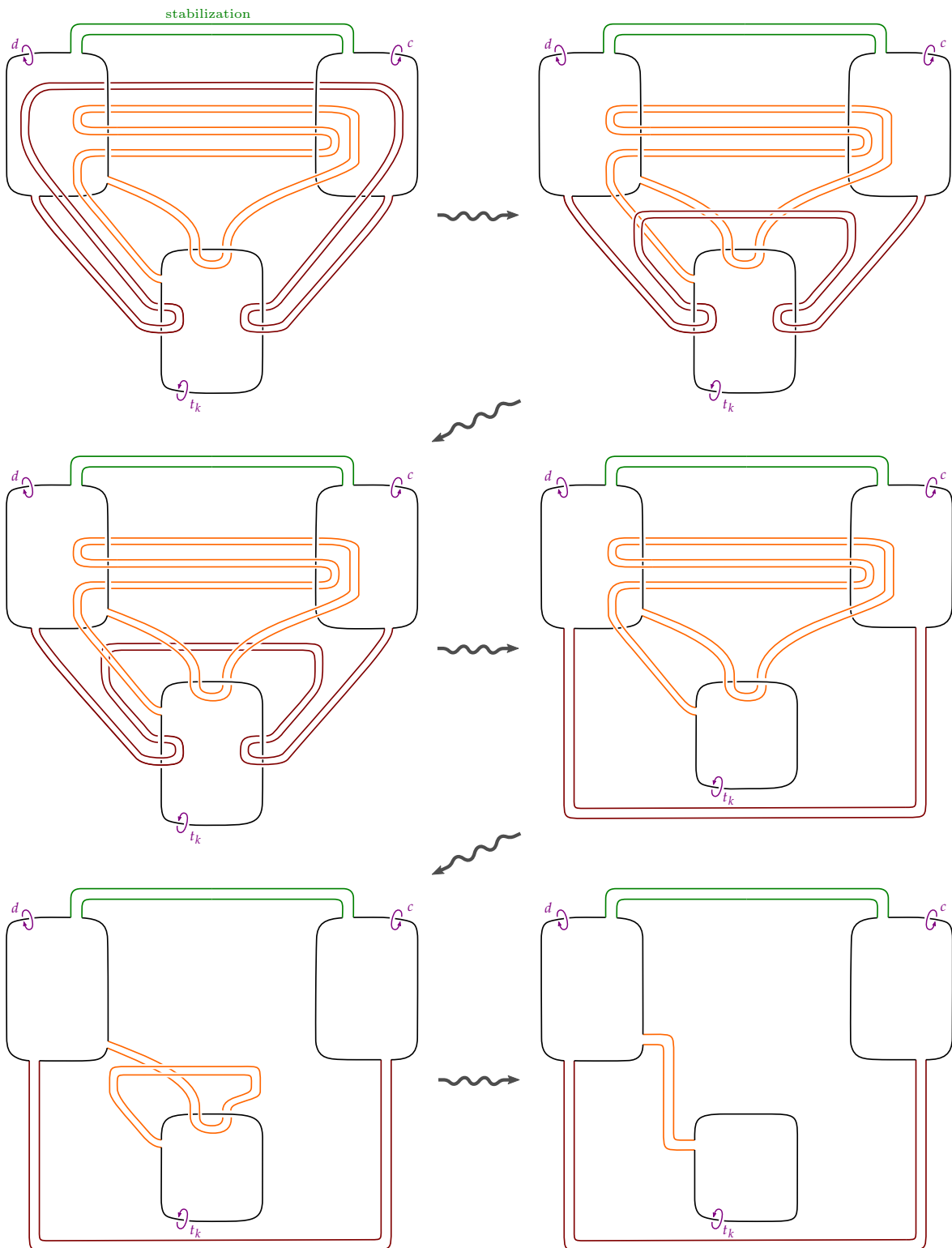


Figure 24. Isotopy from Suci's knot R_3 stabilized between c and d to the unknotted torus.

LEMMA 6.12. *Let $k \in \mathbb{N}$. Under the isomorphisms*

$$\begin{aligned}
& \langle t_k, c, d \mid d = t_k(dc^{-1})^{-k+1} \cdot t_k \cdot (t_k(dc^{-1})^{-k+1})^{-1}, c = t_kcd^{-1}t_k^{-1} \cdot d \cdot (t_kcd^{-1}t_k^{-1})^{-1} \rangle \\
& \quad \downarrow t_k \mapsto u^k t, c \mapsto tu^k, d \mapsto utu^{k-1} \\
& \langle t, u, v \mid tut^{-1} = v, tvt^{-1} = u^{-1}v \rangle \\
& \quad \downarrow t \mapsto t, u \mapsto t^{-1}x, v \mapsto xt^{-1} \\
& \langle t, x \mid txt = xtx \rangle \\
& \quad \downarrow t \mapsto b^{-1}a, x \mapsto ab^{-1} \\
& \langle a, b \mid a^2 = b^3 \rangle
\end{aligned}$$

the image of the finger move relation $[c, d]$ is

$$[c, d] \mapsto b^{-1}a(a^{-1}bab^{-1})^{k+1}b^{-1}aba^{-1}(a^{-1}bab^{-1})^{-k+1}a^{-1}b(a^{-1}bab^{-1})^{-1}.$$

We will denote the composition of these maps as

$$\varphi_k: \langle t_k, c, d \mid d = t_k(dc^{-1})^{-k+1} \cdot t_k \cdot (t_k(dc^{-1})^{-k+1})^{-1}, c = t_kcd^{-1}t_k^{-1} \cdot d \cdot (t_kcd^{-1}t_k^{-1})^{-1} \rangle \rightarrow \langle a, b \mid a^2 = b^3 \rangle.$$

PROPOSITION 6.13. *The algebraic Casson-Whitney number of R_1 , R_2 and R_3 is one,*

$$\text{alg}_{\text{CW}}(R_1) = 1$$

$$\text{alg}_{\text{CW}}(R_2) = 1$$

$$\text{alg}_{\text{CW}}(R_3) = 1$$

and the finger move relation $[c, d]$ abelianizes the groups $\pi_1(\mathbb{S}^4 - R_k)$ for $k = 1, 2, 3$.

Proof. From the fusion number bound for the spun trefoil R_1 , we already know the stronger statement that $u_{\text{CW}}(R_1) = 1$. For $k = 2$ and $k = 3$ the statement was verified by computer using GAP and the presentation $\langle a, b \mid a^2 = b^3 \rangle$ of the knot group. The cases $k = 2$ and $k = 3$ differ in the relation which is killed in the quotient, since the expression of the elements c, d as words in a, b depends on the number $k \in \mathbb{N}_{\geq 1}$. By Lemma 6.12, for $k = 2$ killing the finger move relation $[c, d]$ corresponds to killing

$$(ab^{-1}a^{-1}b)^2ab^{-2}a(ba^{-1})^3b^{-1}a$$

while for $k = 3$, it corresponds to

$$(ab^{-1}a^{-1}b)^3ab^{-1}(b^{-1}a(ba^{-1})^2)b^{-1}a.$$

Auxiliary files for the computation can be found in [Rup21a]. □

Question 6.14. Are the geometric Casson-Whitney numbers $u_{\text{CW}}(R_2)$, $u_{\text{CW}}(R_3)$ equal to 1 as well?

For $k \geq 4$, the computer search was inconclusive, and I was not able to determine whether the algebraic Casson-Whitney number is one or two for these knots. Trying a brute-force search through the available finger moves showed that the majority does not trivialize the Alexander module, but for those which do, we unfortunately do not have a good tool for obstructing the quotient from being abelian.

Question 6.15. For $k \geq 4$, is the algebraic Casson-Whitney number $\text{alg}_{\text{CW}}(R_k)$ of Suciú's ribbon knots R_k equal to 1 or 2?

It is possible that a single finger move is not enough to abelianize their groups. In our proof for Theorem 2.1 of the lower bound on connected sums of knots with non-trivial determinants, we proceeded via the following strategy: Let x be a meridian of R_k for $k \geq 4$. The claim to be proved is that for any $w \in [\pi_1(\mathbb{S}^4 - R_k), \pi_1(\mathbb{S}^4 - R_k)]$ in the commutator subgroup, the relation $[x, x^w] = 1$ does not abelianize

$\pi_1(\mathbb{S}^4 - R_k)$. If this was true, then also $u_{\text{CW}}(R_k) \geq \text{alg}_{\text{CW}}(R_k) \geq 2$. We can make a fixed choice for the meridian x since any other choice will only differ by conjugation, say in this case $x = t_k$, and now need to check that relations of the form $[t_k, t_k^w] = [t_k, w^{-1}t_k w]$ do not abelianize the group. A sufficient criterion for this would be if it, or rather its image, did not abelianize a quotient of the knot group.

Unfortunately, it turns out that the finger move relation $[c, d]$ does indeed abelianize certain natural quotients of the knot group. For example we can work in $\text{PSL}(2, \mathbb{Z}) \cong \langle A, B \mid A^2, B^3 \rangle$, which is the further quotient of $\langle a, b \mid a^2 = b^3 \rangle$ by the relation $a^2 = 1$ (equivalent to $b^3 = 1$), and we use capital letters A, B for the images of a, b in the quotient. GAP confirms that for $k = 1, \dots, 10$ the quotient

$$\text{PSL}(2, \mathbb{Z}) \Big/ \varphi_k([c, d]) \cong \mathbb{Z}/6$$

is abelian, see [Rup21a] for additional documentation. We can also try to trivialize n th powers of a meridian,

$$\pi_1(\mathbb{S}^4 - R_k) \Big/ \langle\langle t_k^n \rangle\rangle.$$

but again (with GAP confirmation for $k = 1, \dots, 10$, and $n = 1, \dots, 10$) this quotient after the finger move is abelian, more precisely

$$\pi_1(\mathbb{S}^4 - R_k) \Big/ \langle\langle t_k^n, [c, d] \rangle\rangle \cong \mathbb{Z}/n.$$

6.3.3 Knotted real projective planes. Recall Definition 3.4 of the standard unknotted projective plane in the 4-sphere $\mathbb{RP}^2 \hookrightarrow \mathbb{S}^4$, which can be described by the explicit banded unlink diagram as in [Jos+21, Fig. 2], compare our Figure 2. Here we will write \mathbb{RP}^2 to denote this standard embedding in the 4-sphere, and we will study the effect that it has on Suciú's ribbon knots under connected sum.

Remark 6.16. Let $S \subset \mathbb{S}^4$ be a smoothly knotted surface. The effect of connect summing with an unknotted projective plane on the group $\pi_1(\mathbb{S}^4 - S)$ is making a meridian have order 2. This is because the group of an unknotted projective plane in the 4-sphere is $\pi_1(\mathbb{S}^4 - \mathbb{RP}^2) \cong \mathbb{Z}/2$, and the connected sum corresponds to an amalgamated free product which identifies the order 2 meridian of the projective plane with a meridian of the knotted surface S .

Remark 6.17. The group of the quotient of $\pi_1(\mathbb{S}^4 - R_k)$ after killing a square of a meridian, and the group of the double branched cover $\pi_1(\Sigma_2(R_k))$ are related in the following manner, see [Har+22]:

$$\pi_1(\mathbb{S}^4 - R_k) \Big/ \langle\langle t_k^2 \rangle\rangle \cong \pi_1(\mathbb{S}^4 - R_k \# \mathbb{RP}^2) \cong \pi_1(\Sigma_2(R_k)) \rtimes \mathbb{Z}/2.$$

By counting conjugacy classes of non-abelian $\text{SL}(2, \mathbb{C})$ -representations of the groups of the double branched cover, Kanenobu-Sumi [KS20] show that for $k \in \mathbb{N}_{\geq 1}$ the groups $\pi_1(\Sigma_2(R_k))$ are mutually non-isomorphic. With the above chain of isomorphisms and restricting to the commutator subgroup $\pi_1(\Sigma_2(R_k))$ of $\pi_1(\mathbb{S}^4 - R_k \# \mathbb{RP}^2)$, this implies that for $k \in \mathbb{N}_{\geq 1}$ the knotted projective planes $R_k \# \mathbb{RP}^2$ are pairwise not smoothly isotopic.

Example 6.18. Supplementing the examples in Section 6.3.2, further finite quotients of Suciú's trefoil knot group can be explicitly determined. Kanenobu-Sumi [KS20] observe that for $k = 1, 2, 3$ the groups $\pi_1(\Sigma_2(R_k))$ are finite: $\pi_1(\Sigma_2(R_1)) \cong \mathbb{Z}/3$ is cyclic of order 3, $\pi_1(\Sigma_2(R_2))$ is the binary tetrahedral group of order 24 and $\pi_1(\Sigma_2(R_3))$ is the direct product $\mathbb{Z}/3 \times \text{Ico}^*$ of a cyclic group with the binary icosahedral group Ico^* which has order 120.

We do not know whether $\pi_1(\Sigma_2(R_k))$ is finite or infinite for $k \geq 4$. Using GAP we can describe the finite extensions in the semidirect product: $\pi_1(\mathbb{S}^4 - R_1 \# \mathbb{RP}^2) \cong S_3$ is the symmetric group on 3 letters, while $\pi_1(\mathbb{S}^4 - R_2 \# \mathbb{RP}^2) \cong \text{GL}(2, \mathbb{Z}/3)$.

Finally we want to mention another finite quotient whose structure can be determined by GAP, see also the documentation in [Rup21a]. For $k = 2$, killing a third power of a meridian results in a direct product

of finite groups,

$$\pi_1(\mathbb{S}^4 - R_2) \Big/ \langle\langle t_2^3 \rangle\rangle \cong \mathrm{SL}(2, \mathbb{Z}/5) \times \mathrm{SL}(2, \mathbb{Z}/3).$$

This finite group has order 2880. △

As discussed in [Remark 6.17](#), if we take connected sums of Suciu's knots with an unknotted projective plane we obtain an infinite family of non-isotopic non-orientable surfaces. But it turns out that there is a single finger move between the minima c and d which leads to a trivial immersion.

THEOREM 6.19. *The Casson-Whitney length between any of Suciu's associated \mathbb{RP}^2 -knots $R_k \# \mathbb{RP}^2$ and the standard unknotted projective plane $\mathbb{RP}^2 \subset \mathbb{S}^4$ is*

$$\mathrm{length}_{\mathrm{CW}}(R_k \# \mathbb{RP}^2, \mathbb{RP}^2) = 1.$$

More precisely, the finger move relation $[c, d]$ abelianizes any of the groups $\pi_1(\mathbb{S}^4 - R_k \# \mathbb{RP}^2)$, and the immersion resulting from a finger move between the minima c and d is isotopic to a finger move on the standard projective plane.

Proof. By [Remark 6.16](#), the connected sum with the unknotted projective plane has the following effect on the group: Taking the meridian $t_k \in \pi_1(\mathbb{S}^4 - R_k)$ for the amalgamated free product leads to the quotient

$$\pi_1(\mathbb{S}^4 - R_k \# \mathbb{RP}^2) \cong \pi_1(\mathbb{S}^4 - R_k) \Big/ \langle\langle t_k^2 \rangle\rangle.$$

If we additionally make the meridians c and d commute with a finger move, we observe that the group

$$\pi_1(\mathbb{S}^4 - R_k \# \mathbb{RP}^2) \cong \pi_1(\mathbb{S}^4 - R_k) \Big/ \langle\langle t_k^2, [c, d] \rangle\rangle$$

is abelian, and thus isomorphic to $H_1(\mathbb{S}^4 - R_k \# \mathbb{RP}^2) \cong \mathbb{Z}/2$. Now the algebra will guide the topology in untangling the ribbon bands. In the figures, we do not explicitly draw the \mathbb{RP}^2 -summands, and in fact only use its effect on the fundamental group to guide the isotopies of the fusion bands. For concreteness, we can think of the projective plane summand as being contained in a local ball connected to the minimum labeled by the generator c .

We will consider the 2-component link formed by the minima with the brown fusion band, after the finger move, and rearrange the word describing the guiding arc of the orange fusion. Again, what is a priori a homotopy of the orange fusion can be realized by an isotopy. Use the commutativity of c and d in the guiding arc $t_k(dc^{-1})^{-k+1}$ of the orange fusion to rewrite it as $t_k c^{k-1} d^{-k+1}$. Now the proof splits up into two cases depending on whether k is even or odd.

- **k odd (see [Figure 25](#)):** For k odd, both c^{k-1} and d^{-k+1} are even powers of a meridian, and thus trivial in the fundamental group because of the \mathbb{RP}^2 -connected summand. Thus the orange band is isotopic to the band which attaches to the minimum t_k , twists around t_k and then connects to d on the other end. As usual, we can undo the twisting around the feet of the tube, and see that it is a trivial tube fusing the d and t_k minima, which corresponds to the relation $t_k = d$ in the group. Now, focus on the guiding arc of the brown band which we can simplify to $t_k c d^{-1} t_k^{-1} = t_k c$. Using the commutativity and twisting around the feet again, the brown band is trivially connecting d to c . Thus this immersion can be recognized as a (necessarily trivial) finger move on an unknotted \mathbb{RP}^2 .
- **k even (see [Figure 26](#)):** For k even, the c^{k-1} and d^{-k+1} occurring in the word of the orange fusion bands are odd powers, and thus the guiding arc of orange can be reduced to $t_k c d^{-1}$ by canceling all powers of two. Now we use that the finger move makes c and d commute, to isotope the orange fusion to follow the word $t_k d^{-1} c$, which can be changed to $t_k d c^{-1}$ since the meridians are of order 2. Sliding the brown band following $t_k c d^{-1} t_k^{-1}$ over orange results in a trivial fusion joining the minima t_k and

c. Now the orange band can be simplified to a trivial fusion as well, similar to the previous isotopies, recognizing this as a finger move on an unknotted $\mathbb{R}\mathbb{P}^2$.

Now in both cases, retracting the finger corresponds to a Whitney move leading to an embedded, unknotted $\mathbb{R}\mathbb{P}^2 \subset \mathbb{S}^4$. \square

6.3.4 Further directions. Connected sums of different members of Suciú's family would be an interesting object of further study. Observe that when computing the group of a connected sum

$$\pi_1(R_k \# R_l) \cong \pi_1(R_k) *_{\langle t_k=t_l \rangle} \pi_1(R_l)$$

this yields a free product amalgamated over the corresponding meridians of the summands. A possible choice for amalgamating meridian can be to take t_k and t_l respectively, and we want to emphasize here that a 'connected sum of knot groups' is only well defined after fixing these classes of meridians. One could also compare this to Maeda's investigations of the algebraic bridge index in [Mae77].

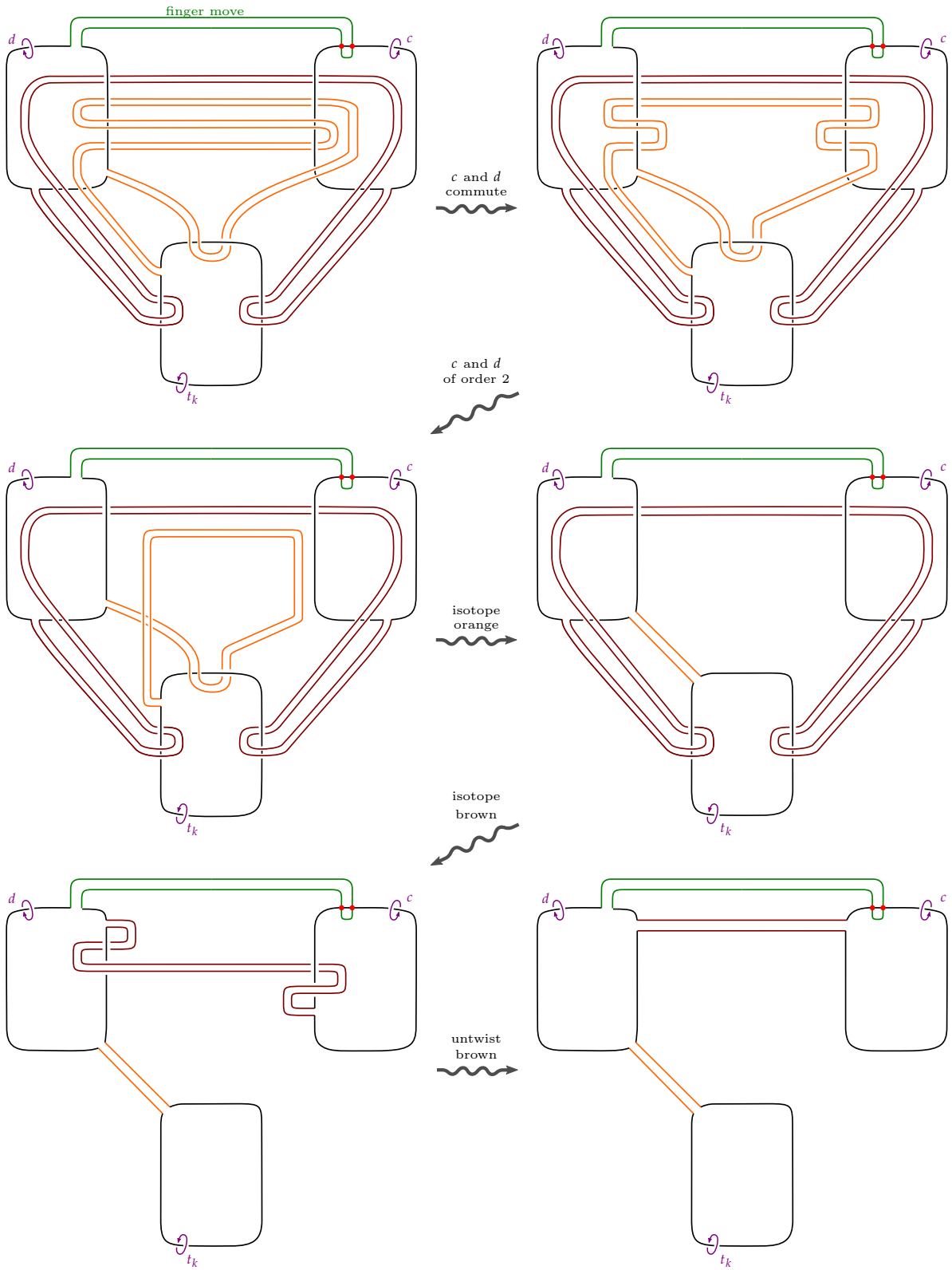


Figure 25. Isotopy of the immersion after a finger move with relation $[c, d]$ on $R_k \# \mathbb{R}P^2$ for k odd.

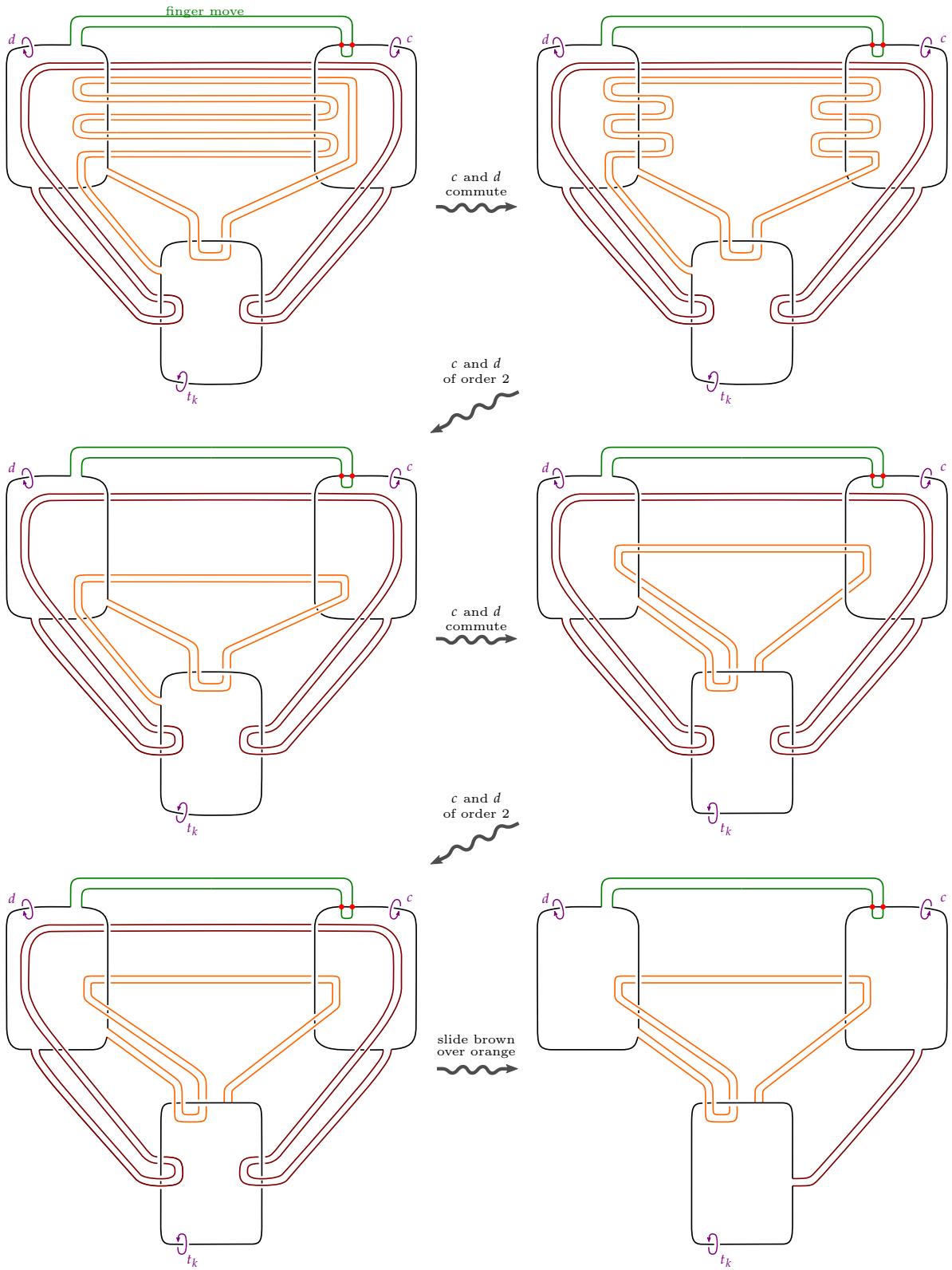


Figure 26. Isotopy of the immersion after a finger move with relation $[c, d]$ on $R_k \# \mathbb{R}P^2$ for k even.

PART II

DEEP AND SHALLOW SLICE KNOTS IN 4-MANIFOLDS

In this part [Sections 7, 8](#) and [11](#) contain joint work with Michael Klug [\[KR21\]](#). [Sections 9](#) and [10](#) consist of new results of the author which appear here for the first time.

We study slice disks in general 4-manifolds, setting up terminology in [Section 7](#). In particular, we establish a difference between ‘shallow slice disks’ which live in collars of the boundary of 4-manifolds, compared to ‘deep slice disks’ that have to use the nontrivial topology of the interior of a 4-manifold in an essential way.

The proof of the main existence result from [\[KR21\]](#) of deep slice knots in the boundary of every 2-handlebody is reproduced in [Section 8](#), with an emphasis on the difference between the smooth and topological category.

In [Section 9](#), exhibiting the difference between smooth and locally flat surfaces in 2-handlebodies, we construct non-local knots which are topologically shallow slice, but smoothly deep slice. The shallow topological slices are constructed by applying results of Freedman on iterated Whitehead doubles. As the smooth shallow slicing obstruction, we use an adjunction inequality of Hedden-Raoux [\[HR21b\]](#), and compute Heegaard-Floer τ -invariants in integral homology 3-sphere L-spaces. For this we will need a generalization of Hedden’s Whitehead double formula for the τ -invariant [\[Hed07\]](#) which works in integral homology 3-sphere L-spaces. We will give a new proof of the formula in the 0-twisting case using Chen’s immersed curve techniques for bordered Floer homology [\[Che19\]](#), which in turn are based on Hanselman-Rasmussen-Watson [\[HRW17\]](#). Similarly, we give a new proof of Hom’s τ -invariant cabling formula [\[Hom14\]](#) for $(p, 1)$ -cables.

Then [Section 10](#) is an excursion to discuss the notion of deep sliceness for links. As is customary for generalizations to multi-component links, we want to avoid trivial examples in which individual components of the link are responsible for the properties under investigation. Rather, we would like to construct examples where every proper sublink is ‘trivial’ in an appropriate sense, and the interesting behavior only appears when the link is viewed as a whole. Our main results are the following: For every 2-handlebody X^4 with non-simply connected boundary, there exists a 2-component link with unknotted component which is topologically deep strong slice in X . Here the obstruction to topological shallow strong sliceness is Schneiderman’s μ -invariant [\[Sch03\]](#). Alas, these examples coming from Bing doubling are often not link homotopic to the unlink, which immediately gives another topological shallow strong sliceness obstruction. We construct link null-homotopic examples in 2-handlebodies with integral homology sphere boundary via Whitehead doubling, and using the determinant as a shallow sliceness obstruction. Finally, we employ a covering link argument combined with our computations of the τ -invariant of iterated Whitehead doubles in connected sums of the Poincaré sphere to construct links which are topologically shallow strong slice, but smoothly deep strong slice.

[Section 11](#) closely follows [\[KR21, Sec. 4\]](#), in which we show that for every oriented compact 4-manifold X^4 with boundary $\partial X = \mathbb{S}^3$, there exists a knot in ∂X which is not H -slice in X .

7 DEFINITION OF DEEP SLICE KNOTS

In the study of concordance, interesting phenomena occur when comparing the smooth with the topological category. We will set up our definitions to distinguish between the two categories, where CAT is either TOP or SM.

In the smooth category $\text{CAT} = \text{SM}$, embeddings of slice disks or surfaces $\Sigma \hookrightarrow X^4$ into an ambient smooth manifold are required to be smooth maps.

In the TOP category, topological slice disks or more generally surfaces in an ambient topological manifold X are assumed to be locally flat. Here a 2-dimensional properly embedded submanifold $N \subset X$ in a 4-manifold is *locally flat* if the following conditions hold: For every point x in the interior of N , there exists an open set $U \subseteq X$ containing x such that the pair $(U, U \cap N)$ is homeomorphic to $(\mathbb{R}^4, \mathbb{R}^2)$. For every point x in the boundary $\partial N \subset \partial X$, there exists an open set $U \subseteq X$ containing x such that the pair $(U, U \cap N)$ is homeomorphic to $(\mathbb{R}_+^4, \mathbb{R}_+^2)$. That is, locally the embedding of the surface looks like the standard linear real plane (or half-plane) in an ambient 4-dimensional vector (half-) space. We include the locally flat requirement to exclude singular points in the submanifold such as cones on knots. In fact, locally flat submanifolds of topological 4-manifolds have normal bundles [FQ90, Sec. 9.3], therefore locally flat surfaces in 4-manifolds are automatically globally flat. Smooth embeddings have smooth tubular neighborhoods, and thus are locally flat.

Starting from an n -manifold M^n without boundary, we obtain a *bounded punctured* M by removing a small open n -ball $M^\circ := M \setminus \text{int } \mathbb{D}^n$, which yields a manifold with boundary $\partial M^\circ = \mathbb{S}^{n-1}$. Observe that a bounded punctured M is the same as an interior connected sum $M^\circ \cong M \# \mathbb{D}^n$ with a closed n -ball.

Definition 7.1. A knot $K \subset M^3$ in the boundary 3-manifold $M^3 = \partial X^4$ of a CAT 4-manifold X^4 is called CAT *slice in* X if it bounds a properly embedded CAT disk $\Delta: \mathbb{D}^2 \hookrightarrow X$.

The knot K is CAT *H-slice in* X (or CAT *null-homologous slice in* X) if it bounds a properly embedded CAT disk $\Delta: \mathbb{D}^2 \hookrightarrow X$ which is null-homologous. Here we say that a properly embedded disk Δ in a manifold X is *null-homologous* if its relative fundamental class $[\Delta, \partial\Delta] \in H_2(X, \partial X; \mathbb{Z})$ is trivial.

Since by Poincaré-Lefschetz duality the intersection pairing $H_2(X; \mathbb{Z}) \otimes_{\mathbb{Z}} H_2(X, \partial X; \mathbb{Z}) \rightarrow \mathbb{Z}$ of a compact oriented 4-manifold X is non-degenerate, a null-homologous disk is characterized by the property that it intersects all closed second homology classes algebraically zero times. The terminology ‘*H-slice*’ was coined in the paper [MMP20].

We illustrate the setting in the ‘half-dimensional’ schematics Figures 27 and 28. Here the 4-manifold X^4 is represented as a 2-dimensional surface, to indicate that it might have non-trivial topology, and we see various properly embedded intervals representing disks in X^4 . These slice disks have boundary a knot $K \subset \partial X$, which is drawn as two points.

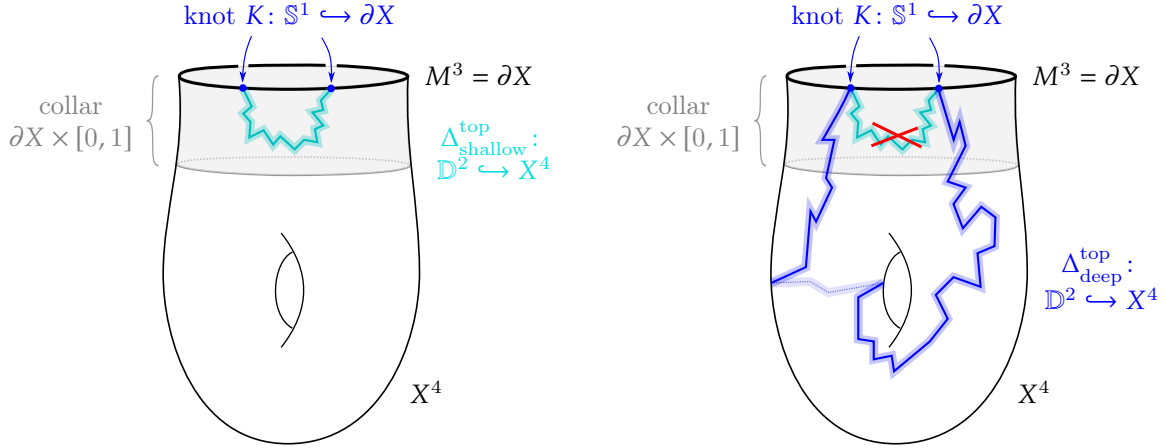
Definition 7.2 (Shallow slice and deep slice knots). A knot $K \subset M^3$ in the boundary 3-manifold $M^3 = \partial X^4$ of a CAT 4-manifold X^4 is called CAT *shallow slice in* X if it bounds a properly embedded CAT-disk $\Delta: \mathbb{D}^2 \hookrightarrow \partial X \times [0, 1] \subset X$ in a collar of the boundary of X .

If the knot K is CAT slice in X , but not CAT shallow slice it is called CAT *deep slice in* X .

We use the phrase *shallow disk* to refer to a slice disk $\Delta \subset X$ such that there exists a collar $C \cong \partial X \times [0, 1]$ of the boundary in X with $\Delta \subset C$. A slice disk which is not a shallow disk is referred to as a *deep disk*. Note that the existence of a single deep slice disk for K does not imply that the knot is deep slice, which means that K is slice in X and **every** slice disk for K is deep.

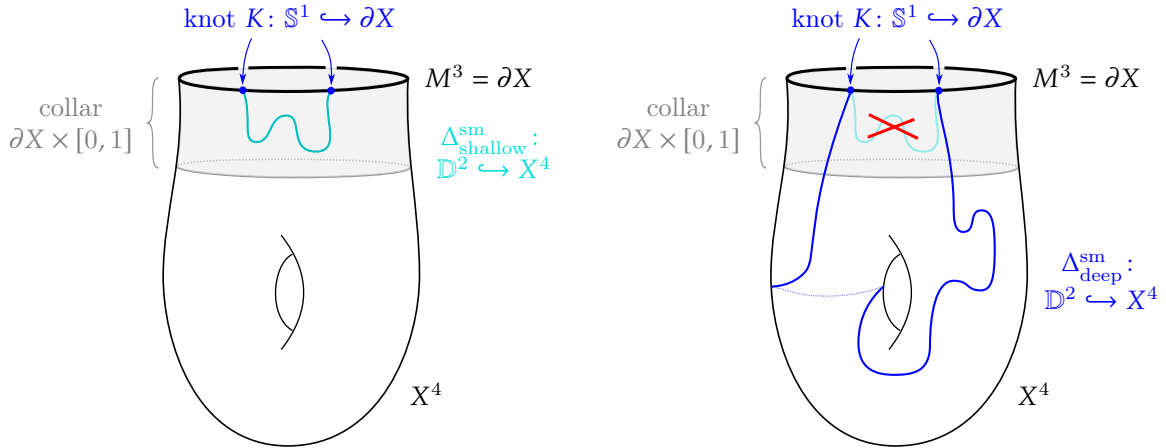
We illustrate the difference between deep and shallow sliceness in various schematic pictures, in particular to give a pictorial guide to the difference between the topological and smooth notions. We draw a

topological shallow slice disk in Figure 27a as a jagged line that does not leave the collar neighborhood of the boundary. A smooth shallow slice contained in the collar is pictured in Figure 28a. Deep disks as in Figures 27b and 28b make use of the entirety of the 4-manifold X^4 . The knot is called smoothly deep slice if there is such a smooth disk, but no smooth shallow disk in the collar.



(a) Schematic of a topologically shallow slice knot. (b) Schematic of a topologically deep slice knot.

Figure 27. Schematic illustration of the difference between topological shallow and deep sliceness. We consider a 4-manifold X^4 , with a knot $K \subset \partial X$ living in the boundary. We study properly embedded locally flat disks $\Delta: \mathbb{D}^2 \hookrightarrow X$ with boundary the knot K . Shaded in gray is a collar $\partial X \times [0, 1]$ of the boundary.



(a) Schematic of a smoothly shallow slice knot. (b) Schematic of a smoothly deep slice knot.

Figure 28. Schematic illustration of the difference between smooth shallow and deep sliceness.

In this language, Problem 1.95 on Kirby’s list [Kir95] (attributed to Akbulut) can be reformulated as follows: Are there contractible smooth 4-manifolds with boundary an integral homology 3-sphere which contain deep slice knots that are null-homotopic in the boundary?

Let us also introduce terminology for concordances in general 3-manifolds. For a 3-manifold M^3 containing a knots $K, J: \mathbb{S}^1 \hookrightarrow M$, we say that K is CAT concordant to J in $M \times [0, 1]$ if there is a properly embedded CAT annulus $\mathbb{S}^1 \times [0, 1] \hookrightarrow M \times [0, 1]$ cobounded by $K \subset M \times \{0\}$ on one end and $J \subset M \times \{1\}$ on the other. As a special case, K is CAT null-concordant in $M \times [0, 1]$ or CAT slice in $M \times [0, 1]$ if there is a properly embedded CAT annulus $\mathbb{S}^1 \times [0, 1] \hookrightarrow M \times [0, 1]$ cobounded by $K \subset M \times \{0\}$ on one end and

an unknot U contained in a 3-ball $U \subset \mathbb{D}^3 \subset M \times \{1\}$ on the other. Equivalently, $K \subset M \times \{0\}$ bounds a CAT properly embedded disk in $M \times [0, 1]$.

Definition 7.3. A knot $K \subset M^3$ in a 3-manifold is called *local* if it is contained in an embedded 3-ball $K \subset \mathbb{D}^3 \subset M^3$.

For a local knot we can consider them in the boundary of any 4-manifold and discuss if they are slice there. To avoid confusion when we say that a (local) knot in a 3-manifold M^3 is null-concordant we will usually qualify it with ‘in X^4 ’.

By projecting a concordance annulus in the product through the map $Y \times [0, 1] \rightarrow Y$, we obtain a free homotopy between the knots on its ends. In particular, a topologically shallow slice knot is automatically freely null-homotopic in the boundary, since it bounds an immersed disk obtained by projecting a shallow slice disk from the collar into the boundary via $\partial X \times [0, 1] \rightarrow \partial X$. Thus any knot that is not null-homotopic in the boundary ∂X of a 4-manifold will not be shallow slice and thus if it is slice in X , it will be deep slice. For this reason we will be looking for deep slice knots that are null-homotopic in the boundary ∂X . Local knots are automatically null-homotopic in the boundary.

7.1 First examples

The following paragraphs are taken from [KR21].

PROPOSITION 7.4. *There are no deep slice knots in a 4-dimensional 1-handlebody $\natural^k \mathbb{S}^1 \times \mathbb{D}^3$, $k \geq 0$.*

Proof. Let $K \subset \#^k \mathbb{S}^1 \times \mathbb{S}^2 = \partial(\natural^k \mathbb{S}^1 \times \mathbb{D}^3)$ be a knot such that K is slice in $\natural^k \mathbb{S}^1 \times \mathbb{D}^3$. Then, thinking of $\natural^k \mathbb{S}^1 \times \mathbb{D}^3$ as a wedge of k copies of \mathbb{S}^1 thickened to be 4-dimensional, if Δ is any slice disk for K we can isotope Δ such that it does not intersect a one-dimensional wedge of circles that $\natural^k \mathbb{S}^1 \times \mathbb{D}^3$ deformation retracts onto.¹⁶ Therefore, Δ can be perturbed to be contained in a collar neighborhood of the boundary $\#^k \mathbb{S}^1 \times \mathbb{S}^2$ and thus K is shallow slice. \square

We now give a criterion that shows that certain 4-manifolds have no local deep slice knots in the boundary. This idea is also contained in [Suz69, Thm. 0] and its variants.

PROPOSITION 7.5. *Let X^4 be a CAT compact 4-manifold with a local knot $\gamma \subset \mathbb{D}^3 \subset \partial X$ that is CAT slice in X . If there is a cover of X which can be CAT embedded into \mathbb{S}^4 , then $\gamma \subset \mathbb{D}^3 \hookrightarrow \mathbb{S}^3 = \partial \mathbb{D}^4$ is CAT slice in \mathbb{D}^4 . Hence, γ is CAT shallow slice in X .*

Proof. Fix the smooth or topological category for the manifolds. Let \tilde{X} be a cover of X with a CAT embedding $\tilde{X} \subset \mathbb{S}^4$ into \mathbb{S}^4 and let $\tilde{\Delta}$ be a lift of a slice disk for γ to \tilde{X} with $\tilde{\gamma} = \partial \tilde{\Delta}$. Note that the knot $\tilde{\gamma}$ is the same as γ , since γ is contained in a 3-ball and the only covers of a 3-ball are disjoint unions of 3-balls. Puncture \mathbb{S}^4 by removing a small ball B close to $\tilde{\gamma}$ and such that $\tilde{\gamma}$ can be connected by an annulus disjoint from \tilde{X} to ∂B and such that the other end of the annulus is (the mirror image of) $K \subset \partial B$. Then since $\mathbb{S}^4 - \text{int } B \cong \mathbb{D}^4$, the annulus together with $\tilde{\Delta}$ show that K is slice in the \mathbb{D}^4 which is the complement of the small ball. Therefore γ is shallow slice in X . \square

As an example, Proposition 7.5 implies that $\natural^k \mathbb{S}^2 \times \mathbb{D}^2$, $k \geq 1$ contains no deep slice local knots, since these manifolds can all be embedded in \mathbb{S}^4 . However, these manifolds all contain deep slice knots, necessarily non-local, as will be seen shortly in Section 8. Additionally, we have:

¹⁶ This is sometimes called a *spine* of the 1-handlebody.

COROLLARY 7.6. *Suppose that X is a closed smooth 4-manifold with universal cover \mathbb{R}^4 or \mathbb{S}^4 , and let X° denote the bounded punctured version. Then X° has no deep slice knots.*

7.2 Concordances in non-orientable 3-manifolds

To conclude this section, we want to mention a surprising result of Boden-Nagel [BN17, Lem. 2.11], which relies on the fact that every punctured compact 3-manifold smoothly embeds into \mathbb{S}^3 , a consequence of Perelman's solution [Per03] of the Geometrization conjecture. Boden-Nagel used a lifting argument to the universal cover of the punctured 3-manifold M^3 to show that any slice disk for a local knot which exists in the product $M^3 \times [0, 1]$ has to come from a slice disk in $\mathbb{S}^3 \times [0, 1]$. That is, the additional topology of M^3 does not create more room for concordances between local knots.

PROPOSITION 7.7 (Special case of [Nag+19, Prop. 2.9]). *If a local knot $K \subset \mathbb{D}^3 \subset M^3$ is smoothly null-concordant in $M^3 \times [0, 1]$, then K is smoothly null-concordant in $\mathbb{S}^3 \times [0, 1]$.*

In [KR21] we observe that an analogous conclusion does not hold for non-orientable 3-manifolds. As an explicit example, we can take the connected sum of a left-handed trefoil $T_{2,-3}$ with itself, $K = T_{2,-3} \# T_{2,-3}$. The Levine-Tristram signature as a lower bound on the topological 4-genus witnesses that every properly embedded surface in $\mathbb{S}^3 \times [0, 1]$ with boundary $T_{2,-3} \# T_{2,-3} \subset \mathbb{S}^3 \times \{0\}$ needs to be of genus at least 2. We define the CAT $(M^3 \times [0, 1])$ -4-genus of a knot $J \subset M^3$ as

$$g_{M \times [0,1]}^{\text{CAT}}(J) := \min\{g \mid \exists \text{ CAT proper embedding } \Sigma_{g,1} \hookrightarrow M \times [0, 1] \text{ with } \partial \Sigma_{g,1} = J \subset M \times \{0\}\}.$$

Here $\Sigma_{g,1}$ is an orientable genus g surface with one boundary component. Observe that in this notation the usual CAT 4-ball genus is $g_4 = g_{\mathbb{S}^3 \times [0,1]}$ and we can rephrase Proposition 7.7 as $g_{M \times [0,1]}^{\text{sm}}(K) = 0$ implies $g_4^{\text{sm}}(K) = 0$ for local knots K . Similar notions of 4-genera were introduced in Celoria's investigation of almost-concordance [Cel18, Def. 12]. By the above discussion the topological $(\mathbb{S}^3 \times [0, 1])$ -4-genus of the connected sum of a left-handed trefoil with itself is

$$g_{\mathbb{S}^3 \times [0,1]}^{\text{top}}(T_{2,-3} \# T_{2,-3}) = 2.$$

By splitting the sum with a saddle and making one of the summands travel around an orientation-reversing loop in N^3 , we can construct a more efficient surface of genus 1. This surface appears by fusing the summands back together, which yields the ribbon knot $T_{2,-3} \# -T_{2,-3}$ that can be capped off with a ribbon disk, see Figure 29. In terms of the smooth $(N \times [0, 1])$ -4-genus this shows

$$g_{N^3 \times [0,1]}^{\text{sm}}(T_{2,-3} \# T_{2,-3}) \leq 1.$$

We summarize the result of this construction in the following theorem:

THEOREM 7.8 ([Rup21b]). *For any **non-orientable** 3-manifold N^3 , there is an example of a local knot $K \subset \mathbb{D}^3 \subset N^3$ for which the smooth $(N^3 \times [0, 1])$ -4-genus is strictly less than the topological $(\mathbb{S}^3 \times [0, 1])$ -4-genus.*

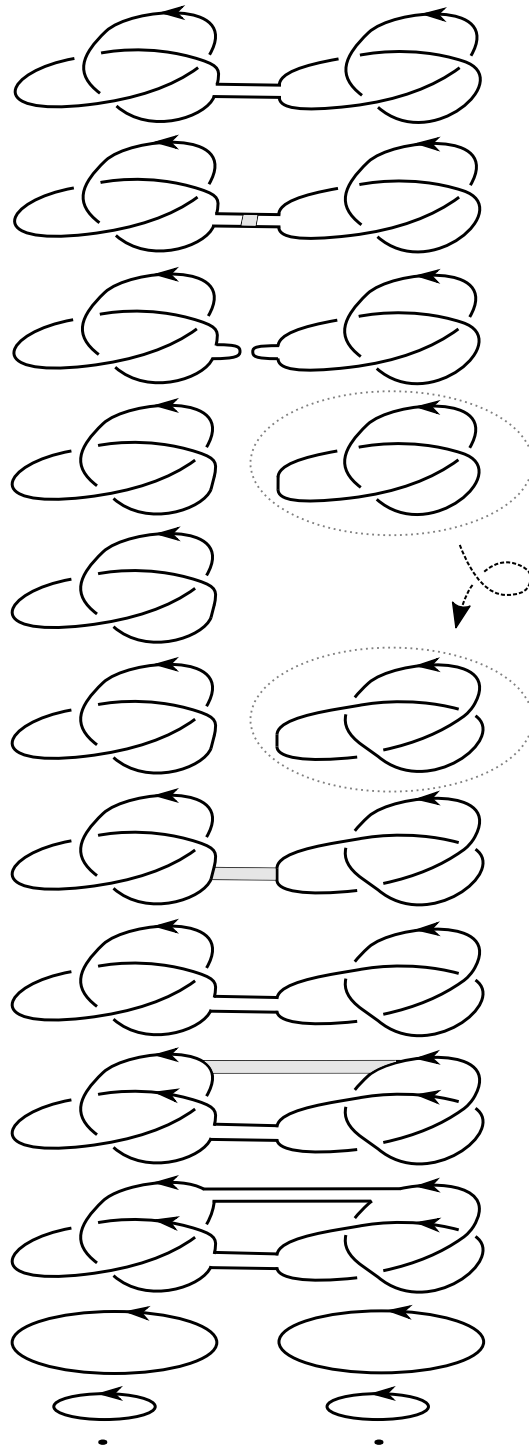


Figure 29. Punctured genus 1 surface with boundary $T_{2,-3} \# T_{2,-3}$ properly embedded in $N^3 \times [0, 1]$, where N^3 is a non-orientable 3-manifold. The dashed arrow indicates that one of the trefoil summands travels around an orientation reversing loop in N^3 .

8 DEEP SLICE KNOTS IN 2-HANDLEBODIES

A 4-manifold with a handle decomposition that contains one 0-handle, some non-zero finite number of 2-handles and no handles of any other index will be called a *2-handlebody*.¹⁷ Examples of this are *knot traces*, where a single 2-handle is attached to the 4-ball along a framed knot.

This section contains the proof of the main existence result in [KR21]. Additionally, we will in put a particular emphasis on the difference between smooth and topological arguments.

THEOREM 8.1 ([KR21, Thm. 3.1]). *Every 2-handlebody X^4 contains a null-homotopic smoothly deep slice knot in its boundary.*

Remark 8.2. For the special case of the 2-handlebody $\mathbb{D}^2 \times \mathbb{S}^2$ the existence of smoothly deep slice knots was already observed in [Dav+18, Thm. B]. There only the winding number $w = 0$ examples give null-homotopic knots. Furthermore the authors construct an infinite family of slice knots which are pairwise different in topological concordance in a collar of the boundary. Also see the discussion of related work in Section 9.1.

Proof of Theorem 8.1. The proof breaks up into two cases depending on whether the boundary has nontrivial π_1 or not (i.e. if it is or is not the 3-sphere).

In the case where $\pi_1(\partial X) \neq \{1\}$, see Proposition 8.11. There is a concordance invariant for knots in arbitrary 3-manifolds, closely related to the Wall self-intersection number (see [Wal99], [FQ90], and [Sch03]), that will allow us to show that some Whitehead double of a meridian of a 2-handle attaching curve is not topologically shallow slice.

In the case where $\pi_1(\partial X)$ is trivial, and therefore by the 3-dimensional Poincaré conjecture [Per03] $\partial X \cong \mathbb{S}^3$, the Wall self-intersection number is of no use. However, in this case see Proposition 8.3 The consideration of whether a knot that is slice in X is deep slice in X is related to the existence of smooth spheres representing various homology classes in the manifold obtained by closing X off with a 4-handle. \square

8.1 Deep slice knots in 2-handlebodies with simply connected boundary

We first construct null-homotopic deep slice knots in 2-handlebodies whose boundary is simply connected, so by the 3-dimensional Poincaré conjecture has to be a 3-sphere. The argument in this case depends on a theorem of Rohlin [Roh71] on the minimal genus of a closed smooth surface representing a second homology class. Rohlin's result is in the smooth category, thus in this case we only obtain an obstruction to smooth shallow sliceness. Let us state a proposition summarizing the situation first:

PROPOSITION 8.3 ([KR21, Sec. 3]). *Let X^4 be a 2-handlebody with simply connected boundary $\partial X \cong \mathbb{S}^3$. Then there is a null-homotopic knot in ∂X , smoothly slice in X , but not smoothly shallow slice in the collar $\partial X \times [0, 1]$. So in our terminology, this knot is smoothly deep slice in X .*

The following paragraphs are taken from [KR21]. Let $\widehat{X} = X \cup_{\partial X} \mathbb{D}^4$ denote the closed 4-manifold obtained by capping off X with a 4-handle. We will discuss a normal form of surfaces in 2-handlebodies, whose statement is standard and could alternatively be concluded from the KSS-normal form for surfaces as in [Kam17, Thm. 3.2.7] and [KSS82].

LEMMA 8.4. *Let X be a closed smooth 4-manifold with a handle decomposition consisting of only 0-, 2-, and 4-handles, with exactly one 0-handle and one 4-handle. Every element of $H_2(X; \mathbb{Z})$ can be represented*

¹⁷ Since by convention we require a non-zero number of 2-handles, the 4-ball itself is not a 2-handlebody.

by a smooth closed oriented surface whose intersection with the union of the 0- and 2-handles of X is a single disk.

Proof. Let $X_{\leq 2}$ denote the union of the 0- and 2-handles of X , so that $X = X_{\leq 2} \cup \mathbb{D}^4$. For every 2-handle h_i , there is an element $H_2(X; \mathbb{Z})$ obtained by taking the co-core disk D_i for h_i and capping it off with an oriented surface in the 4-handle. Let $\{F_i\}$ denote a choice of these surfaces, one for each 2-handle. These surfaces form a basis for $H_2(X; \mathbb{Z})$ and note that each has the desired property that $F_i \cap X_{\leq 2} = D_i$ is a disk.

Given an arbitrary element $x \in H_2(X; \mathbb{Z})$, we have $x = a_1[F_1] + \cdots + a_n[F_n]$ for some integral coefficients $a_i \in \mathbb{Z}$. Therefore, by taking parallel copies of the F_i for each summand, we can find an immersed (possibly disconnected) oriented surface F' representing x , with $F' \cap X_{\leq 2}$ a union of $\sum |a_i|$ disjoint disks. By taking arcs in $\partial X_{\leq 2}$ that connect the different boundaries of the disks all together, and attaching tubes to F' along these arcs, we obtain a connected oriented immersed surface F'' representing x whose intersection with $X_{\leq 2}$ is now a disk. In particular, the tubing is done so that half of the tube is contained in $X_{\leq 2}$ and the other half is in the 4-handle, and therefore $F'' \cap X_{\leq 2}$ is the result of boundary summing together the disks in $F' \cap X_{\leq 2}$.

To make F'' into an embedded surface, we can resolve the double points in the 4-handle by increasing the genus, and arrive at a surface representing x with the desired property. \square

The main ingredient for the proof of the simply connected boundary case of the existence theorem is the following genus bound of Rohlin, and in particular the corollary that follows. Rohlin's theorem has been used in a similar way to study slice knots in punctured connected sums of projective spaces, for example in [Yas91] and [Yas92].

THEOREM 8.5 (Rohlin, [Roh71]). *Let X^4 be an oriented closed smooth 4-manifold with $H_1(X; \mathbb{Z}) = 0$. Let $\psi \in H_2(X; \mathbb{Z})$ be a second homology class that is divisible by 2, and let F be a closed oriented surface of genus g smoothly embedded in X that represents ψ . Then*

$$4g \geq |\psi \cdot \psi - 2\sigma(X)| - 2b_2(X)$$

where $\psi \cdot \psi$ is the self-intersection number of ψ and $b_2(X)$ the second Betti number and $\sigma(X)$ the signature of X .

Rohlin's proof is based on computing signatures of a cyclic branched cover over F in terms of the signature of X , the self-intersection number $\psi \cdot \psi$ and the number of sheets of the cover.

COROLLARY 8.6. *Let X^4 be a closed smooth 4-manifold with $H_1(X; \mathbb{Z}) = 0$, and $H_2(X; \mathbb{Z}) \neq 0$. Then there exists a homology class $\psi \in H_2(X; \mathbb{Z})$ that cannot be represented by a smoothly embedded sphere.*

Proof of Corollary 8.6. To apply Theorem 8.5, we must find a homology class ψ that is divisible by 2 where the right hand side $|\psi \cdot \psi - 2\sigma(X)| - 2b_2(X) > 0$. Since the intersection form on X is unimodular, there exists some element α which pairs non-trivially with itself $\alpha \cdot \alpha \neq 0$. From Poincaré duality together with the universal coefficient theorem and our hypothesis that $H_1(X; \mathbb{Z}) = 0$, we know that $H_2(X; \mathbb{Z})$ is torsion free. Then by taking k to be a sufficiently large integer, we can make $|(2k\alpha) \cdot (2k\alpha) - 2\sigma(X)|$ arbitrarily large. By taking $\psi = 2k\alpha$, the result follows. \square

Proof of Proposition 8.3. By Corollary 8.6, let $\psi \in H_2(\widehat{X}; \mathbb{Z})$ be a homology class that cannot be represented by a smoothly embedded sphere. Using Lemma 8.4, let F be a smooth closed oriented surface representing ψ whose intersection with $X = \widehat{X}_{\leq 2}$ is a disk D , as illustrated schematically in Figure 30.

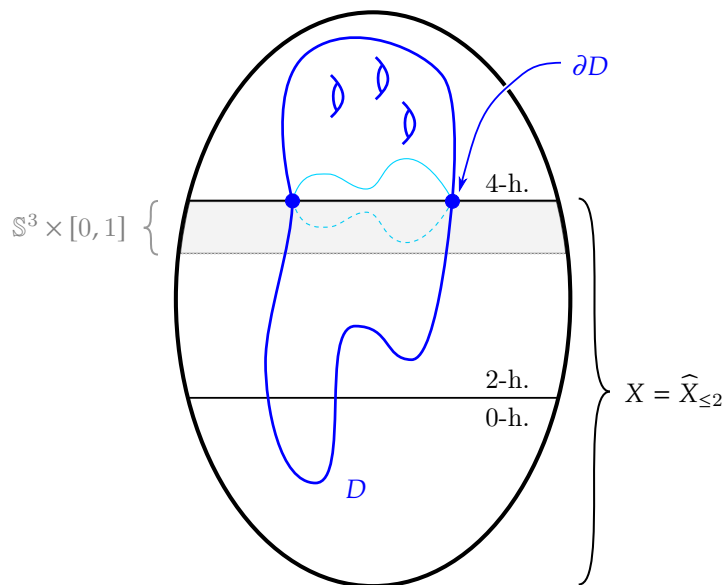


Figure 30. Schematic of the blue surface F in the 2-handlebody, intersecting $X =$ the union of the 0- and 2-handles in a disk D . If ∂D was shallow slice (dashed light blue) in X , disk D union the shallow slice disk flipped into the 4-handle (solid light blue) would be an impossible sphere representative of the homology class of F .

Then $\partial D \subset \partial X$ bounds the smooth slice disk D in X . But ∂D is not smoothly shallow slice, since otherwise the positive genus surface obtained by intersecting F with the 4-handle could be replaced with a disk without altering the homology class, violating the assumption that ψ cannot be represented by a smoothly embedded sphere. To see that the homology class is not altered, observe that in any 2-handlebody the homology class of a surface is determined by how it intersects the 0- and 2-handles. Also observe that in this case the deep slice knot $\partial D \subset \partial X = \mathbb{S}^3$ is local. \square

Remark 8.7. Since the trivial second homology class is always represented by a smooth local unknotted sphere, we know that the slice disk appearing in the proof of [Proposition 8.3](#) is not an H -slice disk. There are cases, for example a knot with nontrivial Arf-invariant in a bounded punctured $\mathbb{S}^2 \times \mathbb{S}^2$, where there does not exist any H -slice disk in the 2-handlebody.

8.2 Obstructing topological shallow sliceness with genus bounds

This section was not part of [\[KR21\]](#).

As we discussed earlier, Rohlin's theorem ([Theorem 8.5](#)) can be used to rule out smooth sphere representatives for a fixed given homology class, which leads to smooth shallow slice obstructions. A similar strategy can be employed to construct topologically deep slice knots whenever we have an obstruction for a homology class being represented by a topologically embedded sphere. We next collect some such genus function results from the literature.

Tristram [[Tri69](#), Thm. 4.5] used signatures of knots to show that in $X^4 = \mathbb{S}^2 \times \mathbb{S}^2$, if the homology class $q \cdot [\mathbb{S}^2 \times \{\text{pt}\}] + r \cdot [\{\text{pt}\} \times \mathbb{S}^2] \in H_2(\mathbb{S}^2 \times \mathbb{S}^2; \mathbb{Z})$ is represented by a locally flat embedded sphere, then $\gcd(q, r) = 1$. We assume $q, r \neq 0, 1$ here, because in these cases the homology class can be represented smoothly. In the other direction, by Freedman [[Fre82](#), Cor. 1.1], if q, r are coprime then $q \cdot [\mathbb{S}^2 \times \{\text{pt}\}] + r \cdot [\{\text{pt}\} \times \mathbb{S}^2] \in H_2(\mathbb{S}^2 \times \mathbb{S}^2; \mathbb{Z})$ is representable by a locally flat embedded sphere.

For comparison, in the smooth setting the following is known: Kervaire-Milnor [KM61, Cor. 1] observed that $2 \cdot [\mathbb{S}^2 \times \{\text{pt}\}] + 2 \cdot [\{\text{pt}\} \times \mathbb{S}^2] \in H_2(\mathbb{S}^2 \times \mathbb{S}^2; \mathbb{Z})$ cannot be represented by a smoothly embedded sphere. The minimal genus of smooth representative of $q \cdot [\mathbb{S}^2 \times \{\text{pt}\}] + r \cdot [\{\text{pt}\} \times \mathbb{S}^2] \in H_2(\mathbb{S}^2 \times \mathbb{S}^2; \mathbb{Z})$ is now known to be $(|q| - 1)(|r| - 1)$. See the references given in [GS99, Thm. 2.1.8].

In $\mathbb{C}\mathbb{P}^2$, again by Tristram [Tri69] the homology class $r \cdot [\mathbb{C}\mathbb{P}^1] \in H_2(\mathbb{C}\mathbb{P}^2; \mathbb{Z})$ can be represented by a locally flat embedded sphere if and only if $|r| \leq 2$. Lee-Wilczyński [LW97] used Freedman's results to show that $r \cdot [\mathbb{C}\mathbb{P}^1] \in H_2(\mathbb{C}\mathbb{P}^2; \mathbb{Z})$ can be represented by a locally flat embedded surface of genus $\lceil \frac{1}{4}d^2 - 1 \rceil$. Further Lee-Wilczyński and Hambleton-Kreck [HK93] found lower bounds for locally flat embedded surfaces in simply connected closed 4-manifolds assuming the fundamental group of the complement of the surface is abelian. This assumption is necessary for their application of surgery techniques.

The smooth problem in $\mathbb{C}\mathbb{P}^2$ (also known as the Thom conjecture) was solved by Kronheimer-Mrowka [KM93] who showed that the minimal genus of a smooth embedded representative of $r \cdot [\mathbb{C}\mathbb{P}^1] \in H_2(\mathbb{C}\mathbb{P}^2; \mathbb{Z})$ is $\frac{1}{2}(r-1)(r-2)$ for $r \neq 0$. Recently, a new gauge-theory free proof using the language of bridge trisected surfaces was given in [Lam20].

We now apply Tristram's obstruction to topological embeddings of spheres for finding topologically deep slice knots in a punctured bounded $\mathbb{S}^2 \times \mathbb{S}^2$. For this, we will think of the 2-skeleton X^4 of $\mathbb{S}^2 \times \mathbb{S}^2$ as a pair of 2-handles attached to the Hopf link in the boundary of the 4-ball, each with the 0-framing.

Definition 8.8 (Satellite knot). Let $P \subset \mathbb{S}^1 \times \mathbb{D}^2$ be a *pattern link* in the solid torus, and $C \subset Y^3$ a framed knot in a 3-manifold Y , which we will call the *companion*. Here a framing of the companion is an identification of the closed tubular neighborhood $h: \mathbb{S}^1 \times \mathbb{D}^2 \xrightarrow{\cong} \bar{\nu}(C)$ with a solid torus. The *satellite link* $P(C) := h(P) \subset Y$ is the image of the pattern under this identification.

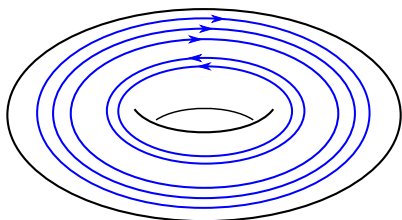


Figure 31. Pattern of the (a, b) -shake satellite, here for $(a, b) = (2, 3)$.

Such satellite operations, which map the preferred longitude of $\mathbb{S}^1 \times \mathbb{D}^2$ under the identification to the longitude of the companion determined by the framing, are sometimes called *faithful*. An (a, b) -shake satellite, $a, b \in \mathbb{N}_0$ of a framed knot $K \subset M^3$ in a 3-manifold is the resulting link of the satellite with pattern shown in Figure 31. This is a collection of $a + b$ many parallels of K taken with respect to the framing, with a components oriented in the same direction as K and b in the opposite direction. In particular, the homology class of the satellite is $(a - b)[K] \in H_1(M; \mathbb{Z})$. As a special case the homology class of the result of taking an $(n + 1, n)$ -satellite for $n \in \mathbb{N}_0$ agrees with $[K]$.

THEOREM 8.9. Let q, r be integers neither 0 nor ± 1 with $\gcd(q, r) > 1$, and choose any numbers $a_1, b_1, a_2, b_2 \in \mathbb{N}_0$ with $a_1 - b_1 = p$, $a_2 - b_2 = q$. Let L be any link that appears as an (a_1, b_1) and (a_2, b_2) -satellite of the components of the 0-framed Hopf link. We write X for the 2-handlebody that is the result of attaching 4-dimensional 2-handles to the 4-ball along the 0-framed Hopf link; this 4-manifold is a bounded punctured $\mathbb{S}^2 \times \mathbb{S}^2$. Then for every band fusion of L yielding a knot, the result $K \subset \partial(\mathbb{S}^2 \times \mathbb{S}^2)^\circ \cong \mathbb{S}^3$ is topologically deep slice in X .

Proof. The satellite L bounds a collection of disks in X , which is an appropriate push-off of the core disks of the 2-handles of X . Now the fusion bands as in Figure 32 join these disks together, each decreasing the number of link components and disks, and exhibiting a smooth slice disk for K . By construction, the knot K lies in the complement of the attaching link of the 2-handles in the boundary of the 0-handle of X . This is also contained in the boundary 3-sphere $\partial X \cong \mathbb{S}^3$ of the bounded punctured $\mathbb{S}^2 \times \mathbb{S}^2$. If

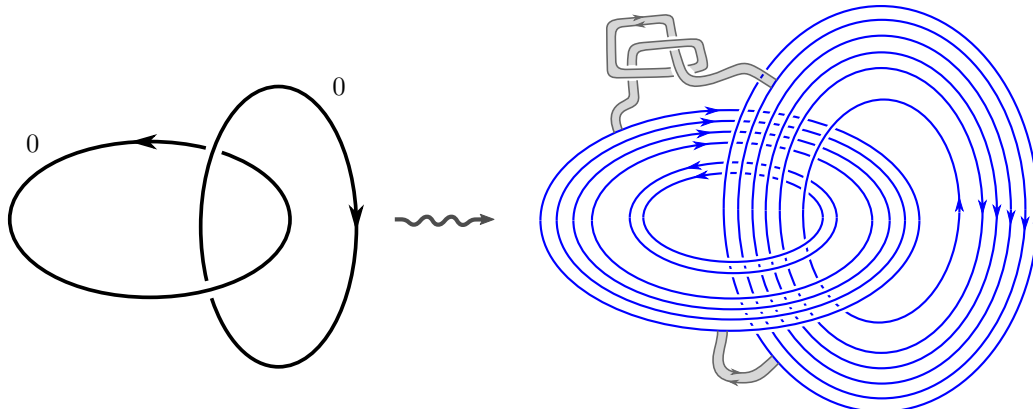


Figure 32. The link on the right hand side in blue is an $(a_1, b_1) = (2, 4)$ and $(a_2, b_2) = (5, 1)$ -satellite of the components of the black 0-framed Hopf link on the left. We also illustrate two gray oriented fusion bands which connect pairs of link components. Any such fusion resulting in a knot is topologically deep slice in the 2-handlebody X , since the homology class $(2 - 4) \cdot [\mathbb{S}^2 \times \{\text{pt}\}] + (5 - 1) \cdot [\{\text{pt}\} \times \mathbb{S}^2] \in H_2(\mathbb{S}^2 \times \mathbb{S}^2; \mathbb{Z})$ cannot be represented by a topological embedded sphere.

K were topologically shallow slice, we could place a topological slice disk into the 4-handle of the closed up manifold $\widehat{X} = \mathbb{S}^2 \times \mathbb{S}^2$. This would construct a topological sphere representing the homology class $q \cdot [\mathbb{S}^2 \times \{\text{pt}\}] + r \cdot [\{\text{pt}\} \times \mathbb{S}^2] \in H_2(\mathbb{S}^2 \times \mathbb{S}^2; \mathbb{Z})$, which is impossible from Tristram's signature obstruction [Tri69, Thm. 4.5]. \square

8.3 Overview: The Schneiderman-Wall μ -invariant

This exposition is taken from [KR21]. Following [Yil18] and [Sch03], we briefly introduce the Wall self-intersection number in the setting that we will be working in, and state some of its basic properties. Let Y^3 be a closed oriented 3-manifold and let $\gamma: \mathbb{S}^1 \hookrightarrow Y$ be an oriented knot in Y . Let $\mathcal{C}_\gamma^{\text{CAT}}(Y)$ denote the set of CAT concordance classes of oriented knots in Y that are freely-homotopic to γ . In particular $\mathcal{C}_U^{\text{CAT}}(Y)$ denotes the set of CAT concordance classes of oriented null-homotopic knots in Y , where we write U for the unknot in Y . Given an oriented null-homotopic knot $K \subset Y$, by (topological) transversality [FQ90] there exists an oriented immersed disk D in $Y \times [0, 1]$ with boundary $K \subset Y \times \{0\} = Y$ that has only double points of self-intersection. Let $*$ $\in Y$ denote a basepoint which we implicitly use for $\pi_1(Y) = \pi_1(Y \times [0, 1])$ throughout. Choose an arc, which we will call a whisker, from $*$ to D . For each double point of self-intersection $p \in D$ choose a numbering of the two sheets of D that intersect at p . Then let $g_p \in \pi_1(Y)$ be the homotopy class of the loop in $Y \times [0, 1]$ obtained by starting at $*$, taking the whisker to D , taking a path to p going in on the first sheet, then taking a path back to where the whisker meets D that leaves p on the second sheet, and finally returning to $*$ using the whisker. Note that changing the order of the two sheets would transform the double point loop g_p to g_p^{-1} . Also, since K and Y are oriented, the disk D and $Y \times [0, 1]$ inherit orientations with the convention that $K \subset Y \times \{0\} = Y$, and therefore, for every self-intersection point $p \in D$, there is an associated sign which we will denote by $\text{sign}(p)$.

Define the quotient of abelian groups

$$\widetilde{\Lambda} := \frac{\mathbb{Z}[\pi_1(Y)]}{\langle \{g - g^{-1} \mid g \in \pi_1(Y)\} \oplus \mathbb{Z}[1] \rangle}.$$

In particular, we want to emphasize that even though the group ring $\mathbb{Z}[\pi_1(Y)]$ carries a multiplication, this is not supposed to be a quotient of rings. The *Schneiderman-Wall self-intersection number* of K is

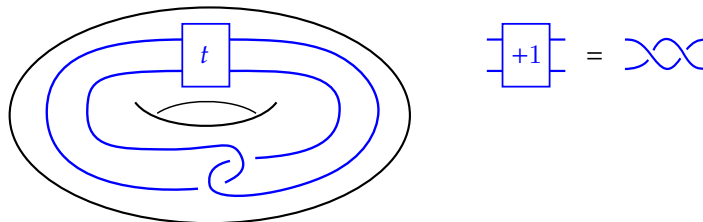


Figure 33. The t -twisted positively clasped Whitehead pattern $\text{Wh}_+(U, t)$ in the solid torus, where the integer $t \in \mathbb{Z}$ indicates the number of full-twists. For the negatively clasped version, change the two crossings at the bottom.

defined to be the signed sum of double point loops for D considered in this quotient,

$$\mu(K) = \sum_{p \in D \cap D} \text{sign}(p) \cdot g_p \in \tilde{\Lambda}.$$

See [Sch03] for a proof that in $\tilde{\Lambda}$ the value of μ is independent of the choice of nullhomotopy D , the choice of whisker, and the choice of orderings of the sheets of D around the double points. Further, μ is a topological concordance invariant in $Y \times [0, 1]$, and therefore defines a map

$$\mu: C_U^{\text{top}}(Y) \rightarrow \tilde{\Lambda}.$$

Notice that if $g \in \pi_1(Y)$ and $g \neq 1$ then g is non-zero in $\tilde{\Lambda}$. To see this, we can consider the map

$$\frac{\mathbb{Z}[\pi_1(Y)]}{\langle \{g - g^{-1} \mid g \in \pi_1(Y)\} \rangle \oplus \mathbb{Z}[1]} \rightarrow \frac{\mathbb{Z}[\pi_1(Y)]}{\mathbb{Z}[1]} \\ a \mapsto a + \bar{a}$$

The map is well-defined, because $(a - \bar{a}) + \overline{(a - \bar{a})} = 0$. Additionally, this map sends $\mu(\Delta) \mapsto \lambda(\Delta, \Delta^\uparrow) = \mu(\Delta) + \overline{\mu(\Delta)}$ where the usual Euler number term at the trivial group element does not appear since we are modding out by the effect of the cusp homotopy. Here the involution of the group ring is defined on group elements $g \in \pi_1(Y)$ as $\bar{g} = w_1(g) \cdot g^{-1}$, with $w_1: \pi_1(Y) \rightarrow \{\pm 1\}$ the orientation character which assigns -1 to orientation-reversing loops. In particular, the orientation character is constant $+1$ for Y an oriented manifold, which we are also using for this argument.

8.4 Deep slice knots in 2-handlebodies with non-simply connected boundary

The examples constructed in this section are Whitehead doubles of certain curves in a 3-manifold. Since they will be featured again in Section 9.2 we want to set up a general definition which includes the sign of the clasp and twisting.

Definition 8.10 (Whitehead double). The t -twisted positively clasped *Whitehead double* $\text{Wh}_+(C, t)$ of a framed knot $C \subset M^3$ in a 3-manifold M^3 is the satellite with pattern shown in Figure 33. Alternatively, this is the satellite of the 0-twisted pattern, i.e. $t = 0$, but where the gluing map identifies a longitude of the solid torus with a t -framed curve on the neighborhood of the companion.

PROPOSITION 8.11 ([KR21, Sec. 3]). Let X^4 be a 2-handlebody with non-simply connected boundary ∂X , i.e. X^4 is built from a 4-ball by attaching a non-zero finite number of 2-handles. Let $m \subset \partial X$ be a (based) meridian of one of the 2-handle attaching circles which is non-trivial in $\pi_1(\partial X, *)$. We take the blackboard framing of m as in Figure 34, which agrees with the 0-framing in the boundary of the

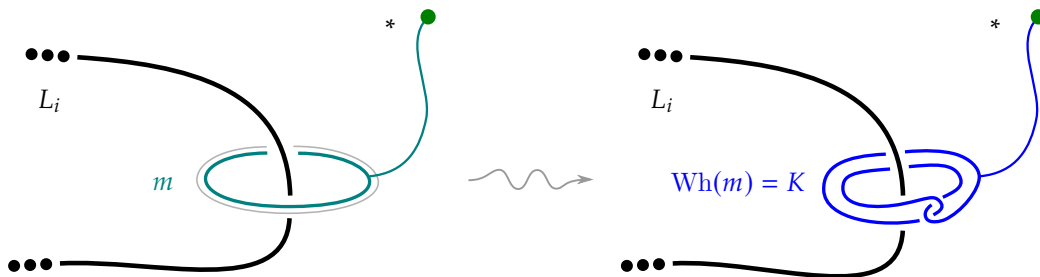


Figure 34. The Whitehead double of a nontrivial framed meridian m (with framing given as a parallel in gray) to one of the surgery link components is deep slice in X .

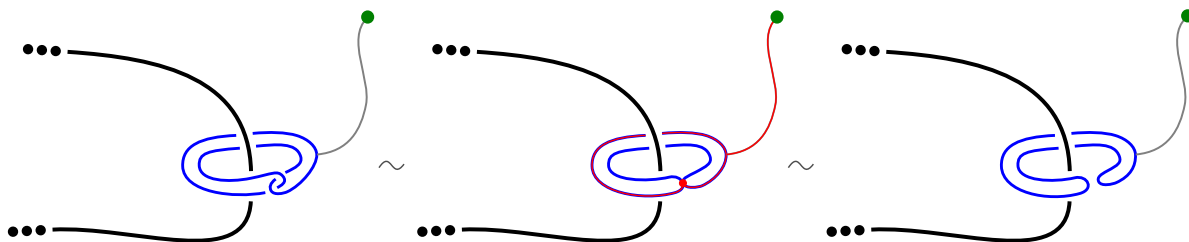


Figure 35. Track of a homotopy from the Whitehead double $Wh_+(m, 0)$ to the unknot giving an immersed disk with a single double point (red in the middle frame). The red double point loop based at the green basepoint calculates that $Wh_+(m, 0) = m$.

0-handle. Then the 0 -twisted Whitehead double $Wh_{\pm}(m, 0)$ is null-homotopic in ∂X , smoothly H -slice in X , but not even topologically shallow slice in the collar $\partial X \times [0, 1]$.

Proof of non-simply connected existence Proposition 8.11. This proof is taken from [KR21, Sec. 3], except there all was stated in the smooth category.

Let $L \subset \partial\mathbb{D}^4$ be a framed link describing the attaching curves of the 2-handles to the 0-handle \mathbb{D}^4 . Since $\pi_1(\partial X)$ is (normally) generated by the meridians of L and $\pi_1(\partial X) \neq 1$, there is some meridian m of L that is nontrivial in $\pi_1(\partial X)$ as in the statement of the proposition.

Notice that if we are given a 2-handlebody described by a framed link L and K is a knot in the boundary of the 2-handlebody that is shown in the framed link diagram as an unknot (possibly linked with L), then K is smoothly slice in the 2-handlebody – just forget all of the other 2-handles and take an unknotting disk whose interior has been pushed into the 0-handle.

Now, take K in ∂X to be the Whitehead double of m as in Figure 34, which is a null-homotopic knot in the boundary. By the previous observation, since K is unknotted in the boundary of the 0-handle, K is slice in X . This actually constructs an H -slice since the Whitehead double links the components of L algebraically zero times. Additionally, one computes that $\mu(K) = m \neq 1 \in \tilde{\Lambda}$, for example using the null-homotopy in Figure 35. Therefore, K is not topologically null-concordant in ∂X , so K is deep slice in X . □

9 COMPARING SMOOTH AND TOPOLOGICAL DEEP AND SHALLOW SLICENESS

In this section, we discuss the difference between the smooth and topological category in the context of deep and shallow slice disks. We will construct knots which exhibit the difference between smooth and topological shallow sliceness, while being smoothly slice in the 4-manifold X^4 .

THEOREM 9.1. *There exist 2-handlebodies X^4 with infinitely many non-local null-homotopic knots in the boundary which are topologically shallow slice, but smoothly deep slice in X^4 .*

Proof outline. In [Lemma 9.16](#) we give a recipe for how the examples of topologically shallow slice and smoothly deep slice knots arise by iterated Whitehead doubling curves with certain properties. Then in [Proposition 9.18](#) we compute the τ -invariant of the dual curve $\tilde{K} \subset \mathbb{S}_{-1}^3(T_{2,-3}) = Y$ in the Poincaré sphere, observing that it satisfies the assumptions of the lemma. Using the results on the dual curve, in [Theorem 9.23](#) we construct the topologically shallow slice but smoothly deep slice knot $J = \text{Wh}_+^{(3)}(\text{Wh}_+(\tilde{K}, +1), 0) \subset \mathbb{S}_{-1}^3(T_{2,-3}) = Y$ in the boundary of the (-1) -trace $X = X_{-1}(T_{2,-3})$ of the left-handed trefoil $T_{2,-3}$. An infinite family of examples is given by the $(p, 1)$ -cables $J_{p,1}$ discussed in [Theorem 9.27](#). \square

The non-local property of the examples [Theorem 9.1](#) shows that they really make use of the non-triviality of the 3-manifold, and do not just appear from the difference between the topological and smooth category for concordances in $\mathbb{S}^3 \times [0, 1]$. For example, we can import local examples into our setting as follows. The positive Whitehead double of the trefoil knot, $\text{Wh}_+(T_{2,3}, 0)$ is topologically slice in $\mathbb{S}^3 \times [0, 1]$ from Freedman-Quinn's result on Alexander polynomial one knots [[FQ90](#), Sec. 11.7], [[GT04](#)], and thus $\text{Wh}_+(T_{2,3}, 0)$ is topologically shallow H -slice in every 4-manifold with boundary \mathbb{S}^3 . This Whitehead double is not smoothly slice in $\mathbb{S}^3 \times [0, 1]$ which can for example be detected with the τ - or s -invariant, and thus if it is smoothly slice in a 4-manifold X^4 it has to be smoothly deep slice in X^4 . We will see in the following paragraphs that $\text{Wh}_+(T_{2,3}, 0)$ is smoothly slice in a punctured bounded $\mathbb{S}^2 \times \mathbb{S}^2$ or alternatively in a punctured bounded $\mathbb{C}\mathbb{P}^2$. Therefore, $\text{Wh}_+(T_{2,3}, 0) \subset \mathbb{D}^3 \subset \partial X$ is an example of a local knot in the boundary of a 4-manifold which is topologically shallow slice but smoothly deep slice. The explicit examples we will construct for [Theorem 9.1](#) are Whitehead doubles as well, but we will show that they are non-local.

We now want to elaborate on some of the standard constructions of slice disks in 4-manifolds. The Norman-Suzuki trick [[Nor69](#), Cor. 3], [[Suz69](#), Thm. 1] shows that every knot $K \subset \mathbb{S}^3$ bounds a smooth slice disk in a punctured $\mathbb{S}^2 \times \mathbb{S}^2$ as follows. The track of a null-homotopy of K in \mathbb{D}^4 placed in a collar of the punctured $\mathbb{S}^2 \times \mathbb{S}^2$ gives a disk that we can assume to be a generic immersion, missing the coordinate spheres $\mathbb{S}^2 \vee \mathbb{S}^2 \cong \mathbb{S}^2 \times \{\text{pt}\} \cup \{\text{pt}\} \times \mathbb{S}^2 \subset (\mathbb{S}^2 \times \mathbb{S}^2)^\circ$, and with a finite number of double points. By tubing into the spheres $\mathbb{S}^2 \times \{\text{pt}\}$, $\{\text{pt}\} \times \mathbb{S}^2$ we can remove all the intersections, but observe that each tubing changes the homology class of the disk by adding the generator of the coordinate sphere. Thus this disk is not necessarily an H -slice disk.

A knot is topologically H -slice in a connected sum $\#^N \mathbb{S}^2 \times \mathbb{S}^2$ for some $N \in \mathbb{N}_0$ if and only if its Arf invariant is zero, see for example [[FK78](#); [Mat86](#); [COT03](#)]. For one direction, $\text{Arf } K = 0$ implies that the knot is band-pass equivalent to the unknot. Such a band pass can be realized by sliding the oppositely oriented strands of a pair of bands over the coordinate spheres in a $\mathbb{S}^2 \times \mathbb{S}^2$ factor, thus adding this sphere algebraically zero times to the second homology class of the slice disk that can be constructed from the track of this isotopy. Conway-Nagel [[CN20](#)] define and study the *stabilizing number*, the minimal number of summands N needed to find an H -slice disk in a punctured $\#^N \mathbb{S}^2 \times \mathbb{S}^2$.

For every local knot $K \subset M^3$ in a closed orientable 3-manifold, there is a compact smooth orientable 4-manifold in which K is smoothly H -slice, as follows. Norman [[Nor69](#), Thm. 4] already observes that for

a knot in the 3-sphere it is possible to take as the 4-manifold a punctured connected sum of the twisted 2-sphere bundles $\mathbb{S}^2 \widetilde{\times} \mathbb{S}^2 \cong \mathbb{C}\mathbb{P}^2 \# \overline{\mathbb{C}\mathbb{P}^2}$. In the same vein, [CL86, Lem. 3.4] discuss that for any knot $K \subset \mathbb{S}^3$ there are numbers $p, q \in \mathbb{N}$ such that K is H -slice in the punctured connected sum $\#^p \mathbb{C}\mathbb{P}^2 \#^q \overline{\mathbb{C}\mathbb{P}^2}$ of complex projective planes. The argument starts with a sequence of positive and negative crossing changes leading from K to the unknot, and then realizes say a positive crossing change by sliding a pair of oppositely oriented strands over the $\mathbb{C}\mathbb{P}^1$ in a projective plane summand. The track of this isotopy, together with a disk bounding the final unknot gives a motion picture of a null-homologous slice disk. Since both positive and negative crossing changes might be necessary, it is important that both orientations $\mathbb{C}\mathbb{P}^2, \overline{\mathbb{C}\mathbb{P}^2}$ are allowed to appear in the connected sum. The $\mathbb{C}\mathbb{P}^2$ -slicing number, measuring the minimal number of summands, is defined in [Kju+21].

For local knots in an oriented 3-manifold M^3 start by taking any compact 4-manifold X' with only 0-, 2-handles and boundary M and let $X = X' \#^N (\mathbb{S}^2 \widetilde{\times} \mathbb{S}^2)$, then run Norman-Suzuki's argument again. Since X' and X are simply connected, the same argument applies to non-local knots, since they bound immersed disks in the 4-manifolds X' and X . Specifically, the knot K bounds an immersed disk which we can assume lives completely in the X' -summand of the connected sum. Then tube into the embedded spheres of the $\mathbb{S}^2 \widetilde{\times} \mathbb{S}^2$ -summand. For non-local knots, the relative homology class of the resulting disk depends on the class of the disk in X' . For example, the knot $K = \{\text{pt}\} \times \mathbb{S}^1 \subset \mathbb{S}^2 \times \mathbb{S}^1 = \partial(\mathbb{S}^2 \times \mathbb{D}^2)$ bounds the disk $\Delta = \{\text{pt}\} \times \mathbb{D}^2$, which generates $H_2(\mathbb{S}^2 \times \mathbb{D}^2, \mathbb{S}^2 \times \mathbb{S}^1)$.

9.1 Relation to previous work

In this section, we want to compare and contrast our result in [Theorem 9.1](#) with the previous literature on concordances in 3-manifolds.

Concordance classes in a 3-manifold are naturally separated by the free homotopy class of any of its representatives, since concordance implies free homotopy. Fixing a free homotopy class in the 3-manifold Y , there is an action of classical knots in the 3-sphere on the CAT-concordance group in the 3-manifold, by tying in an additional local knot.¹⁸ The action is well-defined on concordance classes, because we can similarly tie in the local knot along an arc of the concordance. Two knots which are related by this action are called CAT *almost concordant*.

Celoria [Cel18] constructed distinct smooth almost concordance classes in lens spaces using a version of the τ -invariant, while [Fri+19] investigated similar almost concordance questions in the topological category. For every 3-manifold Y which is not the 3-sphere, [Nag+19] find an infinite family of null-homotopic knots in the 3-manifold which are topologically concordant to each other in $Y \times [0, 1]$, but mutually distinct in smooth almost concordance. This means that even if we allow tying in local knots, no pair of them will be smoothly concordant in $Y \times [0, 1]$. Their result cannot be immediately used to prove our [Theorem 9.1](#), which claims that the notion of smooth deep sliceness and topological shallow sliceness differ for knots in the boundary $Y = \partial X$ of a 2-handlebody. This is because there does not exist a general recipe to construct slice disks in $Y \times [0, 1]$ from concordances in $Y \times [0, 1]$, as we elaborate on below.

Two knots $K_1, K_2 \subset \mathbb{S}^3$ in the 3-sphere are concordant if and only if the connected sum $K_1 \# -K_2$ is slice in \mathbb{D}^4 . Such a reformulation is not obviously true for concordances in general 3-manifolds. Let us describe the situation in more detail. Suppose that a concordance in $Y \times [0, 1]$ is straight on an arc $a = \{\text{pt}\} \times [0, 1]$. A sufficient condition for this is that there exists an arc in the concordance homotopic rel boundary to a straight arc, since homotopy rel boundary implies isotopy rel boundary for 1-manifolds in 4-manifolds. Then let us drill out an open tubular neighborhood $\nu(a)$ of this arc in $Y \times [0, 1]$, which

¹⁸ Formally, this is defined as the connected sum of pairs $(Y, J) \# (\mathbb{S}^3, K)$, where J is the knot in the 3-manifold Y and K coming from the 3-sphere takes the role of the local knot. This uses an identification $Y \# \mathbb{S}^3 \cong Y$.

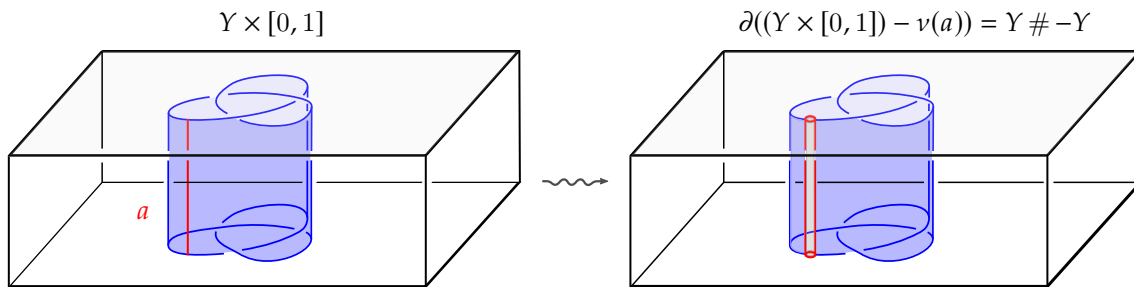


Figure 36. Schematic of the 4-manifold $(Y \times [0, 1]) - \nu(a)$ after drilling out an open tubular neighborhood of an arc a on a concordance.

results in the 4-manifold $(Y \times [0, 1]) - \nu(a)$ with boundary $Y \# -Y$, containing the remaining part of the annulus which is now a disk bounding the connected sum $(Y, K_1) \# (-Y, -K_2)$ of the knots in the boundary. For a schematic illustration see [Figure 36](#). In the other direction, every disk in the 4-manifold $(Y \times [0, 1]) - \nu(a)$ with boundary a connected sum of knots $K_1 \# -K_2$, where the knots each came from one of the summands in the boundary $Y \# -Y$, can be filled in to yield a concordance between K_1 and K_2 in $Y \times [0, 1]$. In particular, observe that for $Y = \mathbb{S}^3$, the 4-manifold $(\mathbb{S}^3 \times [0, 1]) - \nu(a)$ is just a 4-ball, which gives a proof for the equivalence between the notions of concordance in the 3-sphere mentioned at the beginning of this paragraph. But in general, for knots $K \subset Y$ that are slice in $Y \times [0, 1]$, there is no obvious way to translate this into a concordance between two objects (Y, K_1) and (Y, K_2) .¹⁹

Yildiz [[Yil18](#)] used Schneiderman’s μ -invariant to construct, for every 3-manifold Y not the 3-sphere and for any nontrivial element $g \in \pi_1(Y)$, infinitely many distinct smooth almost-concordance classes in the free homotopy class of the unknot. Her argument is actually topological, so it constructs infinitely many distinct topological almost-concordance classes. Additionally, she finds an infinite family of knots in the boundary of the (smooth) Mazur manifold W^4 which are topologically slice in W^4 by Freedman-Quinn [[FQ90](#), Sec. 11.7], [[GT04](#)] since they have Alexander polynomial one but which do not bound piecewise linear disks in W^4 . The PL-obstruction uses a slice-Bennequin inequality, for similar methods see our [Section 9.3.3](#). In contrast, the topological slice disks of our examples in [Theorem 9.1](#) are contained in a collar of the boundary, compare also our discussion in [Remark 9.17](#).

9.2 Knot Floer homology in integral homology 3-sphere L-spaces

We start by setting up some of the Heegaard Floer technology that will be used to obstruct smooth shallow sliceness.

An *integral homology 3-sphere*, or \mathbb{ZHS}^3 , is a closed 3-manifold Y^3 with $H_*(Y; \mathbb{Z}) \cong H_*(\mathbb{S}^3; \mathbb{Z})$. By Poincaré duality a closed 3-manifold is an \mathbb{ZHS}^3 if and only if its first integral homology group $H_1(Y; \mathbb{Z}) = 0$ is trivial. Similarly, a *rational homology 3-sphere*, or \mathbb{QHS}^3 , is a closed 3-manifold Y^3 with $H_*(Y; \mathbb{Q}) \cong H_*(\mathbb{S}^3; \mathbb{Q})$. A closed 3-manifold is an \mathbb{QHS}^3 if and only if its first integral homology group $H_1(Y; \mathbb{Z})$ is finite.

Hedden [[Hed07](#)] studied the filtered knot chain homotopy type of the Knot Floer complex of t -twisted Whitehead doubles $\overline{\text{HF}}\mathbb{K}(\text{Wh}_\pm(K, t))$ and found a formula relating the τ -invariant of the Whitehead double to the τ -invariant of the companion K . In [[Hed07](#), Thm. 1.4] this formula is stated for knots $K \subset \mathbb{S}^3$. We will need a version of this which holds more generally for knots, automatically null-homologous, in integral homology spheres Y^3 which are also Heegaard Floer L-spaces. The slogan is that L-spaces look exactly

¹⁹ There is no notion of connected sums of submanifolds in a fixed 3-manifold. In particular, it is usually not clear why the “obvious” definition is “well-defined”. The well-definedness in the 3-sphere depends on the identification $\mathbb{S}^3 \# \mathbb{S}^3 \cong \mathbb{S}^3$.

like \mathbb{S}^3 to the eye of Heegaard Floer homology, modulo the absolute Maslov grading which is irrelevant to the τ -invariant. In particular, if we are only interested in the τ -invariant we can forget about the Maslov grading when working in an integral homology 3-sphere L-space. At the time of this writing, the only known examples of irreducible²⁰ $\mathbb{Z}HS^3$ which are also an L-space are the Poincaré homology sphere and \mathbb{S}^3 , and it is an open question whether those are the only ones [OS06, Sec. 1.5], [Rus05, Conj. 1.5]. After recalling the relevant definitions, we will state the more general version of Hedden’s formula below.

More details can for example be found in Manolescu’s survey [Man16] and the original sources [OS04c]. Coefficients will be taken in the finite field with 2 elements, usually written as $\mathbb{F} = \mathbb{F}_2$. In our setup we will avoid discussing Spin^c structures in detail. In general Heegaard Floer homology splits as a direct sum over the Spin^c structures of the 3-manifold, which are parameterized non-canonically by elements of $H^2(Y; \mathbb{Z}) \cong H_1(Y; \mathbb{Z})$. Similarly for relative Spin^c structures on 3-manifolds with torus boundary, such as exteriors of knots $Y - \nu(K)$, there is a correspondence with $H^2(Y - \nu(K), \partial\bar{\nu}(K); \mathbb{Z}) \cong H^2(Y, K; \mathbb{Z})$. In particular, integral homology 3-spheres have a unique Spin^c structure, which we will hide in our notation.

An oriented knot $K \subset Y^3$ in a 3-manifold is encoded as a *doubly pointed Heegaard diagram* $(\Sigma, \vec{\alpha}, \vec{\beta}, w, z)$, where Σ is a genus g Heegaard surface with two cut systems $\vec{\alpha}$ and $\vec{\beta}$ describing a Heegaard splitting of the 3-manifold Y . That is, each curve of the *cut system* bounds a properly embedded 2-disk in the handlebody to one side of the central surface Σ , and the exterior of the disks in such a handlebody is a union of 3-balls. By our convention, the α -curves in a Heegaard diagram are drawn in **red** and the β -curves in **blue**. The handlebodies can be recovered by thickening the Heegaard surface to $\Sigma \times [0, 1]$, attaching 2-handles to one side $\Sigma \times \{1\}$ along the curves of the corresponding cut system $\vec{\alpha}$ or $\vec{\beta}$, and filling the resulting 2-sphere boundary components with 3-balls. The points $w \neq z \in \Sigma - \vec{\alpha} - \vec{\beta}$ lie at where the knot K intersects the surface, positively oriented at w and negatively oriented at z . From the doubly pointed diagram we can recover the knot by connecting w to z on Σ in the complement of the α -curves, thus obtaining a trivial arc which can be pushed into the α -handlebody, and similarly connecting z to w in the complement of the β -curves giving an arc in the β -handlebody. In particular, the data $(\Sigma, \vec{\alpha}, \vec{\beta}, w)$ is enough to describe a pointed 3-manifold Y and the extra info z describes a knot in Y .

Remark 9.2. In multi-pointed Heegaard diagrams the knot is allowed to have $2k$ intersections with the central surface, and the intersection of the knot with each of the handlebodies consists of k many trivial arcs.

Up one dimension, *doubly pointed trisection diagrams* [GM18] can be used to describe 1-bridge trisections of smoothly knotted 2-spheres in smooth connected compact orientable 4-manifolds. The theory of bridge trisected surfaces in 4-manifolds is recalled in [Section 13](#).

For describing oriented knots in a 3-manifold with parameterized torus boundary, we use a *doubly pointed bordered Heegaard diagram* as illustrated in [Figure 37](#), see [LOT18, Ch. 4]. In the case of genus 1 this is $(\Sigma, \vec{\alpha}^a, \beta, w, z)$ where Σ is a compact oriented genus 1 surface with a single boundary component, and $\vec{\alpha}^a = (\alpha_1^a, \alpha_2^a)$ a pair of properly embedded, disjoint arcs in Σ such that there is a specific alternating order in which the endpoints of the arcs appear on the oriented boundary $\partial\Sigma$. Additionally, there is a basepoint w on the boundary $\partial\Sigma - \partial\vec{\alpha}^a$ in the complement of the endpoints, and the pieces of the resulting subdivision of $\partial\Sigma$ are labeled in a specific way as a *pointed matched circle*. The β -curve is an embedded, closed loop in the interior of Σ , transverse to the arcs $\vec{\alpha}^a$ and such that the complement $\Sigma - \beta$ is connected. Lastly, there is a basepoint z in the interior of Σ minus all the α -arcs and the β -loop. Again the 3-manifold can be recovered by gluing a 2-handle to the thickening $\Sigma \times [0, 1]$ along $\beta \times \{1\}$, and the knot appears by connecting z to w in the complement of β in Σ pushed into the β -side together with an arc connecting w to z in the complement of $\vec{\alpha}^a$ in Σ . The arcs α_1^a and α_2^a can be thought of as cores of 1-handles of the boundary torus, whose feet are labeled on the boundary of a disk giving the pointed

²⁰ A 3-manifold is *irreducible* if every smoothly embedded 2-sphere bounds a 3-ball.

matched circle. These cores correspond to a meridian and longitude in our parameterization of the torus boundary.

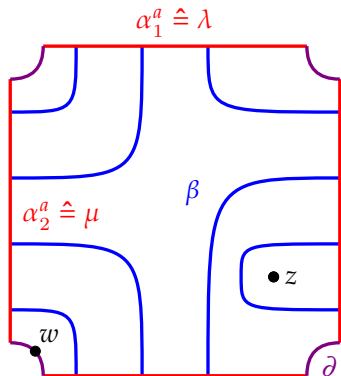


Figure 37. Example of a doubly pointed bordered genus one Heegaard diagram of the Whitehead pattern in the solid torus, with blue β -curve, a pair of red α -arcs and the single boundary component of the genus 1 surface in dark purple.

points $x \in \mathbb{T}_\alpha \cap \mathbb{T}_\beta \subset \text{Sym}^g(\Sigma)$. Its chain homotopy type does not depend on the splitting, thus the homology is an invariant $\widehat{\text{HF}}(Y)$ of the 3-manifold. For manifolds with first Betti number zero, such as \mathbb{Q} -homology spheres, $\widehat{\text{HF}}(Y)$ is also \mathbb{Z} -graded. This *Heegaard Floer homology* $\widehat{\text{HF}}(Y)$ splits as a direct sum over the Spin^c structures of Y .

Recall that a rational homology 3-sphere Y^3 is a *Heegaard Floer L-space* if its Heegaard Floer homology has the simplest form, that is if $\widehat{\text{HF}}(Y; \mathfrak{s}) \cong \mathbb{F}$ for each Spin^c -structure \mathfrak{s} in $\text{Spin}^c(Y)$. Connected sums of L-spaces with either orientation are again L-spaces [OS04b, Sec. 6], see [Pet09] for further discussion and more examples. Our main example of an $\mathbb{Z}H\mathbb{S}^3$ L-space will be the Poincaré homology sphere $Y = \mathbb{S}_{-1}^3(T_{2,-3})$, constructed as (-1) -surgery on the left-handed trefoil knot, and connected sums $\#^k Y \#^l -Y$ thereof.

9.2.1 The τ -invariant. For a filtered chain complex $\dots \subseteq \mathcal{F}_m \subseteq \mathcal{F}_{m+1} \subseteq \dots \subseteq C$ the *associated graded object* is the graded chain complex where the degree m part consists of the quotient $\mathcal{F}_m/\mathcal{F}_{m-1}$. Observe that in the case of modules over a field, the direct sum over the associated graded pieces will be isomorphic to the underlying vector space of the chain complex, but might have other differentials, since the associated graded object only remembers the differentials which map to lower filtration index. Under specific assumptions on the filtration, the spectral sequence of a filtered complex relates the associated graded to the homology of the total complex.

Now re-introducing the null-homologous knot $K \subset Y^3$ in the 3-manifold we obtain the $(\mathbb{Z} \oplus \mathbb{Z})$ -filtered knot Floer complex $\widehat{\text{CF}}(Y, K)$ of K which is invariant up to filtered chain homotopy [OS04a], [Ras03]. Its associated graded complex is $\widehat{\text{CFK}}(Y, K)$, and taking homology yields the knot Floer homology $\widehat{\text{HFK}}(Y, K)$, a bigraded, finitely generated abelian group.

The Alexander filtration $\mathcal{F}_m(Y, K)$ of $\widehat{\text{CF}}(Y)$,

$$0 \subseteq \dots \subseteq \mathcal{F}_m(Y, K) \subseteq \mathcal{F}_{m+1}(Y, K) \subseteq \dots \subseteq \widehat{\text{CF}}(Y)$$

For closed 3-manifolds, using a complex structure on the surface Σ and considering the tori $\mathbb{T}_\alpha = \alpha_1 \times \dots \times \alpha_g$ and $\mathbb{T}_\beta = \beta_1 \times \dots \times \beta_g$ in the g -fold symmetric product of the surface with itself, one can define the *Lagrangian Floer homology* of the pair $(\mathbb{T}_\alpha, \mathbb{T}_\beta)$, see [Flo88] and the references in [Man16]. This is the homology of the Lagrangian chain complex which has generators for each intersection point $x \in \mathbb{T}_\alpha \cap \mathbb{T}_\beta$ and differentials corresponding to pseudo-holomorphic disks in the surface Σ . There are different flavors of this *knot Floer complex*, depending on how we keep track of the interaction of the pseudo-holomorphic disks with the basepoints w and z . We will talk about these variations in the next section. Additionally, the generators corresponding to the intersection points $x \in \mathbb{T}_\alpha \cap \mathbb{T}_\beta$ admit a bigrading (M, A) , which are called the *Maslov or homological grading* $M(x) \in \mathbb{Z}$ and *Alexander grading* $A(x) \in \mathbb{Z}$.

Forgetting the knot for a moment, a pointed Heegaard diagram $(\Sigma, \vec{\alpha}, \vec{\beta}, w)$ for a closed 3-manifold Y^3 also has an associated chain complex $\widehat{\text{CF}}(Y)$, again generated by intersection

induces a spectral sequence converging [OS04a, Lem. 3.6] to the Heegaard Floer homology of the 3-manifold,

$$E^1 = \widehat{\text{HF}}\widehat{\text{K}}(Y, K) \Rightarrow \widehat{\text{HF}}(Y).$$

The whole sequence is an invariant of K , and it is possible to extract concordance invariants out of gradings of specific elements. The τ -invariant is such a homomorphism from the smooth concordance group to the integers, and we will give multiple equivalent definitions now.

Definition 9.3 (τ -invariant via the spectral sequence, [OS04a]). For a knot in Y^3 in an L-space, the spectral sequence converges to $\widehat{\text{HF}}(Y) \cong \mathbb{F}$. The minimal Alexander filtration of the element of $\widehat{\text{HF}}\widehat{\text{K}}(Y, K)$ which survives to the E^∞ page is the τ -invariant $\tau(Y, K) \in \mathbb{Z}$.

Definition 9.4 (τ -invariant via the filtration on the knot Floer complex, [OS03]). We will again only define this for knots in an L-space Y^3 . The τ -invariant is the minimum filtration index n so that the image of $\mathcal{F}_n(Y, K)$ generates the Floer homology of the 3-manifold.

$$\tau(Y, K) = \min\{n \mid H_*(\mathcal{F}_n(Y, K)) \rightarrow \widehat{\text{HF}}(Y)\}$$

This map from the homology of the filtration to the homology of the L-space Y is surjective if and only if the map is non-trivial. For general non L-space 3-manifolds which may have $\widehat{\text{HF}}(Y)$ a vector space of dimension greater than one, this does not need to be true. A definition along these lines of a version of the τ -invariant for knots in rational homology spheres appears in [Rao20, Sec. 2.3], where it can take rational values.

Remark 9.5. The *minus knot Floer chain complex* $\text{CFK}^-(Y, K)$, a free \mathbb{Z} -graded chain complex over $\mathbb{F}[U]$, where U is a formal variable which has Maslov grading -2 . Its homology is the $\mathbb{F}[U]$ -module $\text{HFK}^-(Y, K)$. The minus version of knot Floer homology is also endowed with an Alexander filtration, which in conjunction with the action of the variable U gives yet another definition of the τ -invariant, see also [OST08], [Man16]. Here and in the infinity version below U has bifiltration $(-1, -1)$. We can recover $\widehat{\text{CFK}}$ from CFK^- by setting $U = 0$ (but this does not work for the infinity version as U needs to have a multiplicative inverse in that case).

Definition 9.6 (τ -invariant via minus knot Floer complex, [OST08, App. A]). For a knot in Y^3 an L-space, and using the $\mathbb{F}[U]$ -module structure on $\text{HFK}_{i,s}^-(Y, K)$, where i is the Maslov (or homological) grading and s the Alexander grading, we define

$$\tau(Y, K) = -\max\{s \mid \exists x \in \text{HFK}_{*,s}^-(K, Y) \text{ with } U^j x \neq 0 \text{ for all } j \geq 0\}.$$

For later, we want to mention the infinity version of the knot Floer chain complex. The *full knot Floer chain complex* $\text{CFK}^\infty(Y, K)$ is a $(\mathbb{Z} \oplus \mathbb{Z})$ -filtered chain complex over \mathbb{F} , well defined up to doubly filtered chain homotopy equivalence. Alternatively, CFK^∞ is a \mathbb{Z} -filtered chain complex over the ring $\mathbb{F}[U, U^{-1}]$ with the formal variable U and its inverse U^{-1} . We can recover the \mathbb{Z} -filtered chain complex $\widehat{\text{CFK}}(Y, K)$ by looking at just one of the filtrations or in other words, taking the associated graded object with respect to the filtration that we want to ignore, and forgetting everything except the degree zero part.

As the name suggests, from the full knot Floer complex we can recover the other flavors: $\text{CFK}^-(Y, K)$ is the subcomplex of $\text{CFK}^\infty(Y, K)$ where the first filtration is restricted to $i \leq 0$; $\widehat{\text{CF}}(Y)$ is the subcomplex with $i = 0$, and the knot filtration is given by the other coordinate; $\widehat{\text{CFK}}(Y, K)$ is the subcomplex with $i = 0$ and where we only allow those differentials which preserve the (i, j) -grading.

9.2.2 Bordered Floer homology. We now start to introduce the language of bordered Floer homology, which will be used to study the effect of satellite operations on knot Floer homology. This is a cut-and-paste technique, where we start with a decomposition of a 3-manifold along an embedded essential surfaces, here specifically a torus. The slogan is that the Floer invariants of the entire manifold can be

recovered by suitably putting together the relative Floer invariants of the pieces of the decomposition. For example we can quote such a pairing theorem of Lipshitz-Ozsváth-Thurston:

THEOREM 9.7 ([LOT18, Thm. 11.19]). *Let Y be a closed 3-manifold decomposed as $Y^3 = Y_1 \cup Y_2$, with $\mathbb{T}^2 \rightarrow \partial Y_1$ and $-\mathbb{T} \rightarrow \partial Y_2$ parameterizing the boundaries. Let $K \subset Y_1$ be a knot which is required to be null-homologous in the glued up manifold Y . Then up to homotopy equivalence of chain complexes the knot Floer complex $\widehat{\text{CFK}}(Y, K)$ can be decomposed as a box tensor product*

$$\widehat{\text{CFK}}(Y, K) \simeq \widehat{\text{CFA}}(Y_1, K) \boxtimes \widehat{\text{CFD}}(Y_2)$$

of a filtered type A structure $\widehat{\text{CFA}}(Y_1, K)$ and a type D structure $\widehat{\text{CFD}}(Y_2)$ of the pieces.²¹

We now give some (incomplete) definitions of the algebraic objects involved in this statement. Let \mathcal{A} be a unital algebra over \mathbb{F} , with $\mathcal{G} \subset \mathcal{A}$ the subalgebra of idempotents, and $\{\iota_i\}$ an orthonormal basis for \mathcal{G} which sum to the unit, $\sum \iota_i = 1 \in \mathcal{A}$. A *type D structure* over \mathcal{A} is an \mathbb{F} -vector space N with a left action of the idempotents \mathcal{G} such that there is a direct sum decomposition $N \cong \oplus_i \iota_i N$. Additionally there is a map $\delta: N \rightarrow \mathcal{A} \otimes_{\mathcal{G}} N$ satisfying the type D condition, which is a compatibility between δ and the multiplication $\mu: \mathcal{A} \otimes \mathcal{A} \rightarrow \mathcal{A}$. Another way of stating this condition is requiring $\partial(a \otimes x) = a \cdot \delta(x)$ to be a differential $\partial: \mathcal{A} \otimes_{\mathcal{G}} N \rightarrow \mathcal{A} \otimes_{\mathcal{G}} N$ on the \mathcal{A} -module $\mathcal{A} \otimes_{\mathcal{G}} N$.

For example the type D structure in [Theorem 9.7](#) is defined over the torus algebra $\mathcal{A}(\mathbb{T}^2)$. This torus algebra is generated over \mathbb{F} by two idempotents ι_0, ι_1 and six ‘Reeb elements’ $\rho_1, \rho_2, \rho_3, \rho_{12}, \rho_{23}, \rho_{123}$, where the multiplication rules can be given via explicit relations in the algebra. One usually specifies the parametrization of the boundary torus $\partial Y_i = \pm \mathbb{T}^2$ as a pointed matched circle²² $(\Sigma, z, \partial\alpha_1^a, \partial\alpha_2^a)$.

Let us specialize to the situation we will be interested in, namely the knot Floer homology of the pair (Y^3, K) where the knot $P(C)$ is the satellite of a companion knot $C \subset Y^3$. The first piece $Y_1 \cong \mathbb{S}^1 \times \mathbb{D}^2$ is the solid torus containing the pattern $P \subset Y_1$ and the second piece $Y_2 \cong Y - \nu(C)$ is the companion knot exterior. Then Lipshitz-Ozsváth-Thurston’s theorem gives the decomposition

$$\widehat{\text{CFK}}(Y, P(C)) \simeq \widehat{\text{CFA}}(\mathbb{S}^1 \times \mathbb{D}^2, P) \boxtimes \widehat{\text{CFD}}(Y - \nu(C))$$

We will use Whitehead doubling to construct the examples of smoothly deep slice knots needed for [Theorem 8.1](#). Hedden [Hed07] investigated the behavior of the τ -invariant under Whitehead doubling, with an explicit formula given for doubles of knots in the 3-sphere. As was already observed in [HKL16, Sec. 4.4], the main ingredient, the refiltering theorem, holds more generally knots in 3-manifolds. Therefore Hedden’s arguments transfer to the case of knots in integral homology 3-sphere L-spaces. The slogan here is that L-spaces look exactly like \mathbb{S}^3 to the eyes of Heegaard-Floer homology, modulo the absolute Maslov grading which is irrelevant to the τ -invariant. Let us now restate Hedden’s theorem in the general form needed later.

THEOREM 9.8 (Generalization of [Hed07]). *For a companion knot $C \subset Y^3$ in an integral homology 3-sphere L-space the τ -invariant of the t -twisted positively clasped Whitehead double is determined as*

$$\tau(Y, \text{Wh}_+(C, t)) = \begin{cases} 0 & \text{for } t \geq 2\tau(Y, C) \\ 1 & \text{for } t < 2\tau(Y, C) \end{cases}$$

Here the t -twisting of C comes from comparing with a *Seifert longitude*, by definition the intersection $F \cap \partial \bar{\nu}(C)$ of a Seifert surface F of C with the boundary of a closed tubular neighborhood of C , where the Seifert surface exists since the knot C is automatically null-homologous in an $\mathbb{Z}H\mathbb{S}^3$.

²¹ This also works for decompositions along higher genus surfaces, but we will restrict to the torus case here since the algebraic objects in that case are easier to handle.

²² For higher genus surfaces F , $\mathcal{A}(F)$ is a differential graded algebra. Also, for a torus there is a unique pointed matched circle, but for higher genus surfaces we can obtain different algebras.

In particular for zero-twisted doubles $t = 0$ this says the following, which we will apply in the proof of [Lemma 9.16](#).

$$\tau(Y, \text{Wh}_+(C, 0)) = \begin{cases} 0 & \text{for } \tau(Y, C) \leq 0 \\ 1 & \text{for } \tau(Y, C) > 0 \end{cases}$$

As a consequence, when starting with a companion with $\tau(C) > 0$ every iterated positive zero-twisted Whitehead double is not smoothly slice.

Instead of going through Hedden’s original proof of [Theorem 9.8](#), in this thesis we want to give an alternative argument in the case of zero twisting using the immersed curve pairing theorem of [\[Che19\]](#). To that end, we now recall Chen’s setup, indicating at the appropriate points where the arguments generalize to integral homology 3-sphere L-spaces. For further exposition of the immersed curve techniques, we point to the original sources [\[HRW17\]](#), [\[HRW18\]](#). Another application to the study of Dehn surgeries appears in [\[Var21\]](#). These immersed curves are a pictorial reformulation of the bordered invariants for 3-manifold with boundary, where this boundary in our case is a torus. For a 3-manifold M with boundary a parameterized torus a collection of immersed curves on the punctured torus encodes the bordered invariant $\widehat{\text{CFD}}(M)$. In particular, the immersed curve invariant of a knot exterior of $K \subset M$ encodes the knot Floer homology of K . Pairing results from the bordered theory such as [Theorem 9.7](#) have a reformulation in the language of immersed curves. Given two 3-manifolds M, N with parameterized torus boundary whose Floer invariants are encoded by immersed curves γ_M and γ_N , the Heegaard Floer homology of the closed manifold obtained by gluing via $\varphi: \partial M_2 \rightarrow \partial M_1$ can be computed from the *Lagrangian intersection Floer homology* of the superimposed curves on the punctured torus, $\widehat{\text{HF}}(M \cup_\varphi N) \cong \text{HF}(\gamma_M, \overline{\varphi}(\gamma_N))$. Here $\overline{\varphi}$ is the boundary identification composed with the elliptic involution of the torus. The Lagrangian intersection Floer term $\text{HF}(\gamma_M, \overline{\varphi}(\gamma_N))$ is the homology of a chain complex defined combinatorially from the diagram, where intersection point provide generators and differentials appear from immersed bigons. It is often convenient to move the curves into minimal intersection position, so that there are no differential producing bigons and the rank of the homology is given by the number of intersection points. For the precise statement, see [\[HRW17, Thm. 2\]](#).

We will follow some notation conventions: The letter Y^3 denotes a closed 3-manifold (assumed to be an integral homology 3-sphere L-space), while M^3 is reserved for 3-manifolds with torus boundary. Usually for us, $C \subset Y$ is a companion knot of a satellite construction using a pattern P , where the 3-manifold with torus boundary appears as the exterior $M = Y - \nu(C)$. The β -curve in the genus 1 doubly pointed bordered Heegaard diagram has intersection data $\beta \cdot \mu = 0$ with the meridian and $\beta \cdot \lambda = 1$ with the longitude of the torus.

For the satellite construction, $P \subset \mathbb{S}^1 \times \mathbb{D}^2$ is a $(1, 1)$ -pattern knot in the solid torus, and $P(C) \subset Y$ denotes the result of the untwisted satellite operation. By definition, $(1, 1)$ -patterns are precisely these knots or links in the solid torus which admit a genus 1 doubly pointed bordered Heegaard diagram.²³

Chen’s proof of [\[Che19, Thm. 1.2\]](#) generalizes to \mathbb{ZHS}^3 L-space Y . In particular, the pairing diagram complex is isomorphic to the box tensor product

$$\widehat{\text{CFK}}(\mathbb{T}^2, \alpha, \beta, w, z) \cong \widehat{\text{CFA}}(\mathbb{S}^1 \times \mathbb{D}^2, P, w, z) \boxtimes \widehat{\text{CFD}}(Y - \nu(C), \mu_C, \lambda_C)$$

and this chain complex is isomorphic to the Floer complex of the satellite knot $\widehat{\text{CFK}}(Y, P(C))$. We have augmented the notation to include the basepoints w, z of the pattern in $\mathbb{S}^1 \times \mathbb{D}^2$ and the meridian μ_C and longitude λ_C of the companion C . Chen states that if the α -curve is connected, the isomorphism preserves the Maslov grading and the Alexander filtration. As we will only be interested in the τ -invariant

²³ In general, in the definition of an (b, g) -link the second argument g refers to the canonical genus g Heegaard splitting of \mathbb{S}^3 , and then b refers to the bridge number with respect to this splitting. A 2-bridge knot in \mathbb{S}^3 would be a $(2, 0)$ link, which means it can be constructed by gluing a pair of 2-component unknotted tangles in \mathbb{D}^3 together. For example $(p, 1)$ cable patterns are $(1, 1)$ links, since we consider them as mostly lying on the surface of a torus, with one bridge on the “inside” and another bridge on the “outside”.

of the satellite $\tau(Y, P(C))$, solely the Alexander filtration will be of relevance. We recall in [Definition 9.10](#) below that for computing the τ -invariant, it is enough to restrict to a certain distinguished component of the α -curve.

For computations, it is often convenient to work in a cover of the torus and compute intersections between lifts of curves, most importantly in the universal cover $\pi: \mathbb{R}^2 \rightarrow \mathbb{T}^2$. Take $\tilde{\beta}$, a connected cover of the preimage $\pi^{-1}(\beta)$, and if α is connected,²⁴ let $\tilde{\alpha}$ be a connected component of $\pi^{-1}(\alpha)$. Then the Lagrangian Floer complexes satisfy

$$\widehat{\text{CFK}}(\tilde{\alpha}, \tilde{\beta}, \pi^{-1}(w), \pi^{-1}(z)) \cong \widehat{\text{CFK}}(\alpha, \beta, w, z).$$

9.2.3 Constructing the immersed curves. Chen's proof strategy in [\[Che19\]](#) starts with immersed curves representing the companion complement's type- D structure $\widehat{\text{CFD}}(Y - \nu(C), \lambda_C, \mu_C)$. In general Hanselman-Rasmussen-Watson [\[HRW17\]](#) explain how in a 3-manifold M with torus boundary ∂M , the type D structure $\widehat{\text{CFD}}(M)$ is determined as a set of immersed curves (decorated with local systems) in the punctured torus $\partial M - \{z\}$. This collection of decorated curves $\gamma^i: \mathbb{S}^1 \looparrowright \partial M - \{z\}$ is well-defined up to regular homotopy of the curves and isomorphisms of the local systems. Above a *local system* is a finite dimensional vector space over \mathbb{F} together with an automorphism of that vector space.

As usual let M^3 be a compact 3-manifold with torus boundary. Fixing a base point $z \in \partial M$, the invariant $\widehat{\text{HF}}(M)$ is this data of a collection of immersed curves in $\partial M - \{z\}$ decorated with local systems. Then $\widehat{\text{HF}}(M)$ is determined by $\widehat{\text{CFD}}(M, \alpha, \beta)$, and for every choice of parameterization (α, β) of the boundary, the type D structure $\widehat{\text{CFD}}(M, \alpha, \beta)$ can be recovered from $\widehat{\text{HF}}(M)$. In particular, for our concrete computation we will need to obtain immersed curves for $\widehat{\text{CFD}}(Y - \nu(C))$, where Y^3 is the Poincaré homology sphere and C the companion knot (which in the iterated Whitehead doubling process could be the dual curve, a Whitehead double of the dual curve, and a Whitehead double of a Whitehead double of the dual curve). As these diagrams grow to considerable size, instead of constructing them explicitly we apply Hedden's formula for 0 twisting iteratively to the steps of the process.

In [\[HRW18, Thm. 11, Sec. 4\]](#) Hanselman-Rasmussen-Watson explain how to obtain $\widehat{\text{CFD}}(\mathbb{S}^3 - \nu(C))$ from the knot Floer chain complex of $C \subset \mathbb{S}^3$. We quote their theorem now and comment that this procedure also works for complements of knots in integral homology L -spaces (with exactly the same proof).

THEOREM 9.9 (Generalization of [\[HRW18, Thm. 11 & Prop. 47\]](#)). *Let C be a framed knot in a closed 3-manifold Y which is an integral homology 3-sphere L -space. Let $M_C = Y - \nu(C)$ be the exterior of C in Y . Then $\widehat{\text{HF}}(M_C)$ is determined by the minus knot Floer chain complex $\text{CFK}^-(K)$.*

This theorem is a consequence of [\[LOT18, Sec. 11.5\]](#) who show that $\widehat{\text{CFD}}(M_C)$ is determined by $\text{CFK}^-(K)$, and [\[HRW18\]](#) additionally use an arrow calculus to give an algorithm for the procedure. Here the knot exterior $Y - \nu(C)$ is framed by letting the first arc α_1^q encode the longitude and α_2^q the meridian.

This process is easier to explain if we start with bases of the chain complexes of a particularly simple form, for which we introduce the terminology now. Recall the Alexander filtration and the filtration by negative U -powers on $\text{CFK}^\infty(Y, K)$. We can choose a basis so that the differential strictly drops one of the filtration levels, and call such a filtered complex *reduced*. Given a filtered, reduced chain complex $A_{*,*}$ over $\mathbb{F}[U, U^{-1}]$ with a $\mathbb{F}[U, U^{-1}]$ -basis $\{x_k\}$, this is called a *filtered basis* if the U^\pm -translates give an \mathbb{F} -basis for all the subcomplexes $A_{i \leq a, j \leq b}$. That is, for $a, b \in \mathbb{Z}$ the subcomplex $A_{i \leq a, j \leq b}$ has \mathbb{F} -basis $\{U^n x_k \mid U^n x_k \in C_{i \leq a, j \leq b}, n \in \mathbb{Z}\}$. The analogous condition is required for filtered bases of chain complexes over $\mathbb{F}[U]$.

²⁴ If α is not connected, we need to take all horizontal covering translates of a connected component of the preimage. For computing the τ -invariant, it is enough to look at a single preimage of the distinguished component.

Then a filtered basis $\{x_i\}$ for the $\mathbb{F}[U]$ chain complex $\text{CFK}^\infty(Y, K)$ is *vertically simplified* if for each basis element x_i exactly one of the following conditions on the differentials holds:

- There is a unique incoming vertical arrow, and no outgoing vertical arrow, or
- there is a unique outgoing vertical arrow, and no incoming vertical arrow, or
- there are no vertical arrows.

A *horizontally* simplified basis is defined by replacing each occurrence of ‘vertical’ with ‘horizontal’. In the original work on bordered Heegaard Floer theory, [LOT18, Prop. 11.57] observe that every $(\mathbb{Z} \oplus \mathbb{Z})$ -filtered chain complex has a vertically simplified basis, and a horizontally simplified basis (but maybe not simultaneously).

For a knot K in an integral homology 3-sphere L-space, there is always a *vertically distinguished* element for $\text{CFK}^\infty(Y, K)$, which is an element of a vertically simplified basis with no incoming or outgoing vertical arrows. By [Hom14], it is always possible to find a horizontally simplified basis for $\text{CFK}^\infty(Y, K)$ in which one of the horizontal basis elements x_0 is the vertically distinguished element of some vertically simplified basis. Given this x_0 , Hom’s ε concordance invariant $\varepsilon(Y, K) \in \{-1, 0, +1\}$ associated to $\text{CFK}^\infty(Y, K)$ is defined by the behavior of the horizontal arrows on this element: This is $\varepsilon(Y, K) = +1$ if there is a unique incoming horizontal arrow, $\varepsilon(Y, K) = -1$ if there is a unique outgoing horizontal arrow and $\varepsilon(Y, K) = 0$ if there are no horizontal arrows.

We now return to the translation into immersed curves. The first step of this process is converting $\text{CFK}^-(K)$ of the knot K into the type D structure $\widehat{\text{CFD}}$ of the exterior. This works in ambient homology 3-sphere L-spaces because the only property of the 3-sphere which went into the proof was that there exists a single choice of nontrivial map D_{23} between the $\widehat{\text{HF}}$ -modules corresponding to the Reeb element ρ_{23} , since source and target of D_{23} are 1-dimensional over \mathbb{F} . For more details, compare with the set-up in [LOT18, Thm. 11.36]. In an L-space, this remains true because the $\widehat{\text{HF}}$ -modules are 1-dimensional over \mathbb{F} as well. We do not have to worry about the modules for different Spin^c structures interacting in unpredictable ways, as we are assuming that the 3-manifold is also an integral homology 3-sphere.

In [Proposition 9.18](#) (as a special case of Zhou’s results in [Zho20, Thm. 3.2]) we obtain the full knot Floer complex and the minus version for the dual knot in the Poincaré sphere, with the caveat that this is the result of quotienting by acyclic $\mathbb{F}[U, U^{-1}]$ subcomplexes. These acyclic summands do not play a role in the subsequent application of [Theorem 9.9](#), as the construction splits over direct sums. Moreover, up to homotopy equivalence the resulting type D-structure only depends on the $(\mathbb{Z} \oplus \mathbb{Z})$ -filtered chain homotopy type of the $\mathbb{F}[U]$ -complex $\text{CFK}^-(K)$, see [LOT18, Prop. 11.38].

9.2.4 Concordance invariants from immersed curves. The immersed curves in $\widehat{\text{HF}}(M_C)$ encode the concordance invariants $\tau(Y, C)$ and $\varepsilon(Y, C)$ when they are pulled tight in a peg-board diagram [HRW18, Sec. 4.2]. Here a curve in a *peg-board diagram* is a lift to the covering space which is a (punctured) cylinder where a meridian μ of the torus has been unrolled in the vertical direction. The cover is represented by an infinite strip $[-\frac{1}{2}, \frac{1}{2}] \times \mathbb{R}$ where the edges are identified, and the *pegs* are the lifts of the basepoint $\pi^{-1}(\{z\})$ placed at half-integer heights $(0, n + \frac{1}{2})$ for $n \in \mathbb{Z}$. The grading data in $\widehat{\text{HF}}(M_C)$ allows the specification of this lift of the curve to the infinitely punctured cylinder. When pulled tight, the immersed curves in $\widehat{\text{HF}}(M_C)$ are supported in a neighborhood of the vertical strip of pegs $\{\frac{1}{2}\} \times \mathbb{R}$ except at a segment where the curves wrap around the cylinder horizontally. We illustrate an example of an immersed curve corresponding to a knot like complex in [Figure 38](#).

In the special case where $\text{CFK}^-(Y, K)$ has a basis that is simultaneously horizontally and vertically simplified, the algorithm in [HRW18, Prop. 47] generating a peg-board diagram takes a particularly simple form: For each basis element of $\text{CFK}^-(Y, K)$ place a short horizontal segment between the pegs

with height the Alexander filtration, and then for each vertical differential connect the corresponding left endpoints of the generators with an arc. Similarly for horizontal differentials, connect the right endpoints with arcs. This leaves exactly one left and one right endpoint unconnected, join these to height 0 on the left and right edge of the strip respectively.

Definition 9.10. Often, the immersed curve consists of multiple components, and is not connected. There is always a single *distinguished component* γ_0 which is nontrivial in the homology group $H_1(\partial M_C)$, which means that it wraps around the cylinder. For computing the τ and ε invariant we can restrict to this distinguished component [HRW18].²⁵ As usual, it can be convenient to pass to yet another cover, which is the infinitely punctured plane lying over the punctured cylinder. Here γ_0 lifts to a single curve periodic under the horizontal translation induced by the longitude λ .

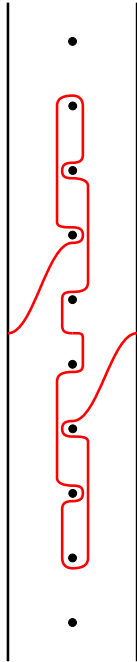


Figure 38. Example of an immersed curve for the exterior $\mathbb{S}^3 - \nu(K)$ of the cable $K = (T_{2,-3})_{2,5}$, computed using the recipe in [HW19]. We see that this knot has $\tau = 2$ and $\varepsilon = -1$.

With this setup $\tau(Y, C)$ is the height (rounded to the nearest integer) where, following the curve rightwards, it first hits the vertical line through the pegs. Remember that the τ -invariant measures the Alexander filtration of the distinguished generator of vertical homology, which is encoded by this right-end of the non-vertical generator. Similarly, $\varepsilon(Y, C)$ can be read off from the behavior of the distinguished curve right after this first intersection point with the vertical axis of meridians of the torus placed at $\{x = 0\}$. If the curve turns downwards²⁶ $\varepsilon(Y, C) = +1$, if it turns upwards then $\varepsilon(Y, C) = -1$, and if it goes straight (which is only possible if it wraps around the cylinder precisely at that height) then $\varepsilon(Y, C) = 0$. In this last case, observe that $\varepsilon(Y, C) = 0$ implies $\tau(Y, C) = 0$ for knots in integral homology 3-sphere L-spaces, recovering a result of Hom [Hom14, Prop. 2.3]. There exist 3-manifolds where this implication is not true, as observed in [HLL18]. In summary, the slope of the non-vertical segment of the pulled-tight distinguished component is determined by the difference $2\tau(Y, K) - \varepsilon(Y, K)$.

Let us summarize the recipe in [Che19, Sec. 4] for computing the τ -invariant of a satellite knot from the pairing diagram for $\overline{\text{CFK}}(Y, P(C))$. For this, we use the definition of the invariant $\tau(Y, P(C))$ as the minimal Alexander grading of the element which survives to the infinity page of the spectral sequence in Definition 9.3 and generates the group $E^\infty \cong \widehat{\text{HF}}(Y) \cong \mathbb{F}$. Recall that E^∞ is one-dimensional since Y is an L-space. We pass from one page of the spectral sequence to the next by canceling a pair of generators where the difference in Alexander gradings is minimal among the remaining intersection points. Geometrically, this cancellation corresponds to a Whitney move on the β -curve, pushing it across a basepoint z and removing a pair of oppositely signed intersections between α and β . We do not allow isotopies of the β -curve over

the w -basepoint. Observe that whenever the β -curve is isotoped across the basepoint z , the intersections with the straight segments are changed and so we need to be careful keeping track of the gradings. Chen introduced a formalism with small arrows added to the curves to record the extra filtration information. Cancel until there is a single intersection point left, this is a generator which generates the E^∞ -page and

²⁵ This distinguished component always carries the trivial one-dimensional local system, because otherwise the rank of the meridional filling of the knot would be greater than one, but we assumed this to be the L-space Y . For *loop type* manifolds the associated local systems are all trivial, see [HW15].

²⁶ Observe that [HRW18, Sec. 4.2] appear to have a typo in the sign for the ε invariant.

its filtration is by definition the τ -invariant of the satellite knot. Thus we can read off this τ -invariant by looking at the grading of that generator in the original pairing diagram.

The distinguished component of the immersed curve for $\widehat{\text{CFD}}(Y-\nu(C))$, originally a curve in the punctured torus, admits a lift to the cover $\mathbb{S}^1 \times \mathbb{R} \rightarrow \mathbb{T}^2$ with the following two properties: As discussed above, it intersects the vertical line $\{\frac{1}{2}\} \times \mathbb{R}$ geometrically in one point. From the symmetries of knot Floer homology we know that after a suitable homotopy it is symmetric under a half-rotation about a center, which we can take to lie at the origin at height 0.

From the intersections of the diagrams, we can usually only deduce the Alexander grading difference between pairs of generators. This is explained in [Che19, Lem. 4.1]: Connect the intersection points $x, y \in \alpha \cap \beta$ with an arc from x to y following β . Then count the signed intersections with the (lifts of) a straight arc $\delta_{w,z}$ connecting the basepoints w to z . The arc $\delta_{w,z}$ is assumed to lie in a single fundamental domain of the torus. This intersection count computes the Alexander filtration difference, $A(y) - A(x) = l \cdot \delta_{w,z}$. To determine the absolute Alexander grading, we require that the maximum Alexander grading appearing overall is the negative of the minimum Alexander grading. In a sense, this is a symmetry condition, similarly to how we normalize Alexander polynomials of knots to be symmetric. In [Che19, p. 31] the absolute Alexander grading of the central intersection point c in the symmetric minimal intersection diagram is determined to be $A(c) = 0$.

9.2.5 Example: Computing $\tau(\mathbb{S}^3, \text{Wh}_+(T_{2,3}, 0))$ via immersed curves. It is instructive to look at a concrete example of this procedure, where we will explain the computation of $\tau(\mathbb{S}^3, \text{Wh}_+(T_{2,3}, 0))$. Then, in the upcoming proof of the Whitehead double formula we sketch the general argument for an arbitrary companion C .

First we discuss the bordered Heegaard diagram for the Whitehead pattern. The Whitehead link is 2-bridge, in Schubert's normal form denoted as $b(8,3)$, and as the Conway rational tangle $C(2,1,2)$. Furthermore the Whitehead link is a $(1,1)$ -link, i.e. it has bridge number one with respect to the (canonical) genus one Heegaard splitting of \mathbb{S}^3 . Taking the complement of the first component, we obtain the Whitehead pattern in the solid torus. In fact the Whitehead link is symmetric, so either component would work here. Further discussion of $(1,1)$ -links and their doubly pointed Heegaard diagrams can be found in [GMM05; Ord06; Ord13].

To convert between the various normal forms which appear in the literature, we can use [Che19, Thm. 5.4]. Given a genus 1 bordered Heegaard diagram, let L be the two-component $(1,1)$ -link in \mathbb{S}^3 built from the meridian and the component determined by a β -curve with r loops and s stripes. Then L is the 2-bridge link with Schubert normal form $b(2|s|+4|r|, \text{sign}(r)(2|r|-1))$. Using the reverse direction of this statement, the Whitehead link $b(8,3)$ has a bordered Heegaard diagram whose β -curve consists of $r = 2$ loops and $s = 0$ stripes. Such a bordered Heegaard diagram for the Whitehead pattern is shown in Figure 39.

The pairing diagram with an immersed α -curve for the companion $T_{2,3}$ is in Figure 40. Lifts of the curve to the universal cover $\mathbb{R}^2 \rightarrow \mathbb{T}^2$ are given in Figure 41. Restricting to a single lift of the α and β -curve yields Figure 42. In general, to simplify the picture we would also single out the distinguished component of the α -curve, which is not necessary in this case because there is only one component.

We now compute the differences between Alexander filtrations of intersection points in Figure 43 by counting intersections with the line segments $\delta_{w,z}$. For this we draw arrows on the segments $\delta_{w,z}$ orienting them, and use this to determine whether the intersections with oriented segments of the blue pattern curve are positive or negative. Note the periodic pattern in the vertical direction of the intersections, where we see a repeating sequence of $\dots, 0, 1, 0, -1, 0, \dots$. As mentioned above, the intersections with $\delta_{w,z}$ provide us with the **differences** between filtrations, but we can normalize the values by either

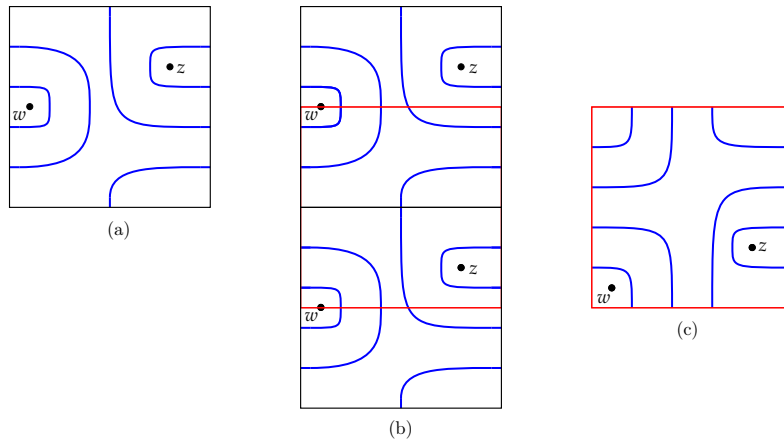


Figure 39. Bordered Heegaard diagram with β -curve for the positively clasped 0-twisted Whitehead pattern. (a) is the normal form with $r = 2$ loops and $s = 0$ stripes. (b) shows two fundamental domains stacked on top of each other. (c) is the result of shifting the fundamental domain vertically to move the w -basepoint into the bottom left corner.

making sure that the minimum and maximum have the same absolute value, or looking for the central point of symmetry which has Alexander filtration 0.

According to the procedure in [Che19, Sec. 4], in each subsequent step we cancel intersection points via Whitney moves between intersections of the lowest Alexander filtration difference in the picture. We start in Figure 43 with Whitney disks disjoint from the z basepoints which remove intersections with filtration difference zero. In the next step in Figure 44 we begin to retract the two blue ‘ β -fingers’ interacting with the red immersed curve of $T_{2,3}$. These are cancellations of pairs which have filtration difference one. This process continues in Figure 45. Finally, in Figure 46 there remains a single intersection point with Alexander filtration $\tau(\mathbb{S}^3, \text{Wh}_+(T_{2,3})) = +1$. This gives us the τ -invariant of the positively clasped, 0-twisted Whitehead double of $T_{2,3}$, confirming the result of Hedden’s formula Theorem 9.8 in this case.

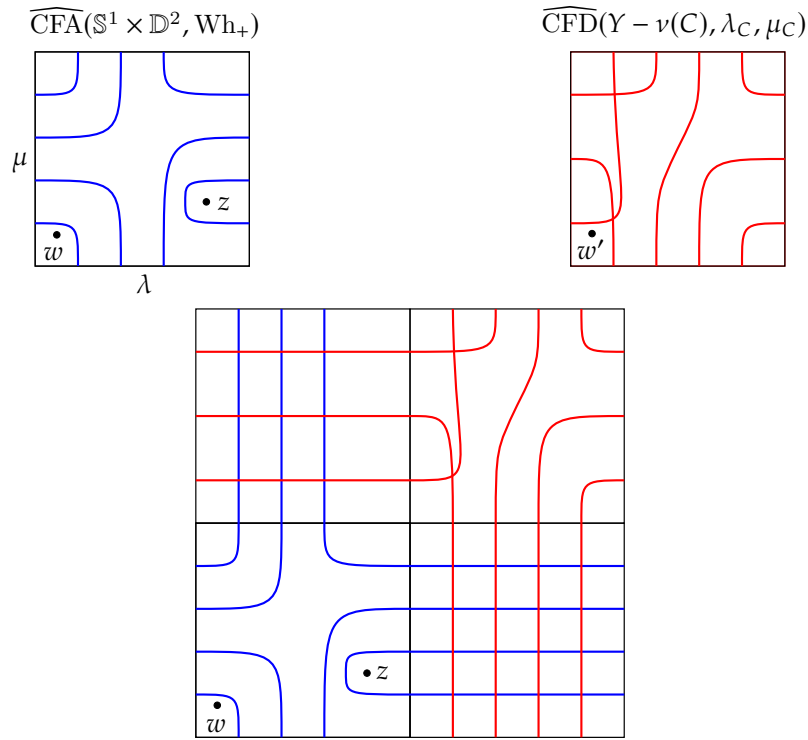


Figure 40. Pairing diagram from [Che19, Fig. 1] adapted to the case of the Whitehead double pattern. The recipe is to superimpose the bordered Heegaard diagram of the Whitehead pattern from Figure 39 (c) over the red immersed-curve diagram of the knot complement of the companion, which in our case is the right-handed trefoil knot $T_{2,3}$ in the 3-sphere.

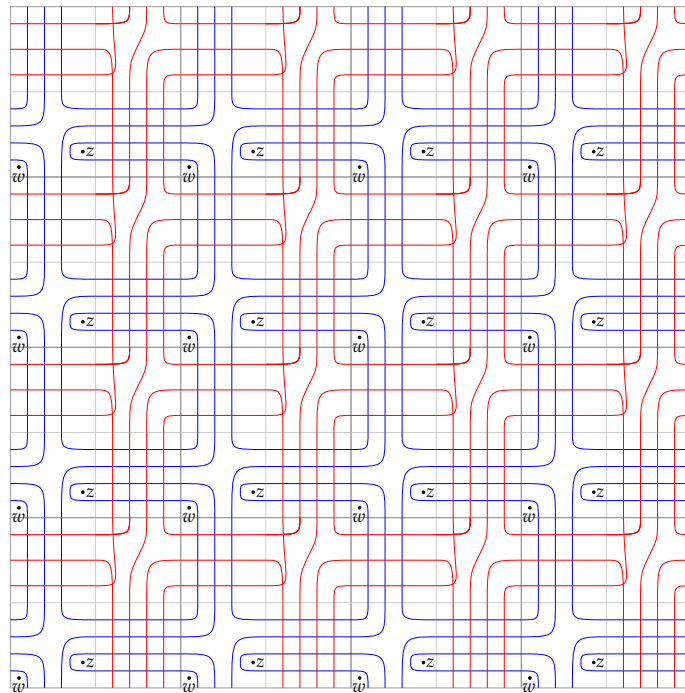


Figure 41. Pairing diagram from Figure 40 of the β -curves of the Whitehead pattern (blue) with the immersed α curves for $T_{2,3}$ (red) lifted to the universal cover of a punctured torus.

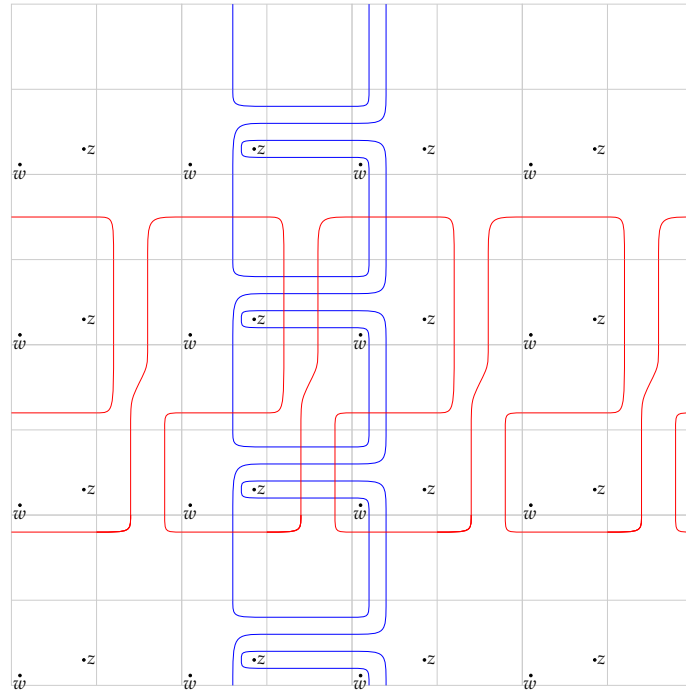


Figure 42. Pairing diagram from Figure 41 of the Whitehead pattern with the immersed curves of the companion in the universal cover with a single lift of α and β .

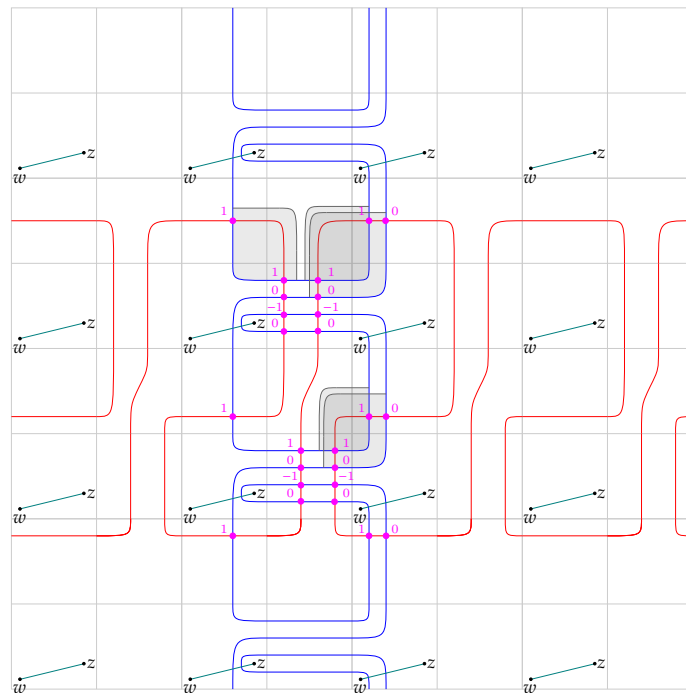


Figure 43. Drawing line segments $\delta_{w,z}$ (teal) between the basepoints in Figure 42, and calculating (differences between) Alexander filtrations (fuchsia) of the intersection points between the red α and blue β -curve. Note the periodic pattern of the Alexander filtration in the vertical direction of the blue pattern. In gray we see the first collection of Whitney moves on the blue curve which removes pairs of intersections with lowest Alexander filtration difference, in this case the filtration difference is $A(y_i) - A(x_i) = 0$.

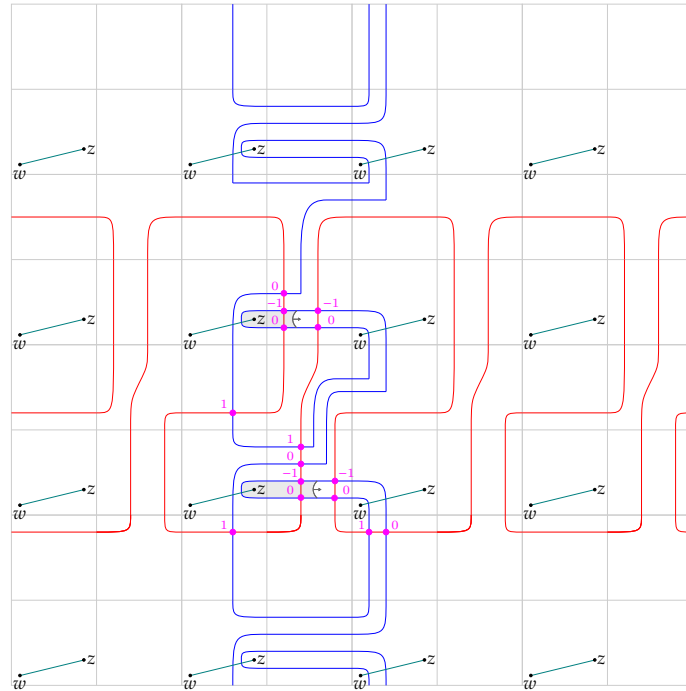


Figure 44. After the Whitney moves in Figure 43. Shaded in gray is a further collection of Whitney moves, each removing pairs of intersections of filtration difference 1. When isotoping β over the z -basepoint, we add small arrows (called *A-buoys* in [Che19]) keeping track of the filtration differences.

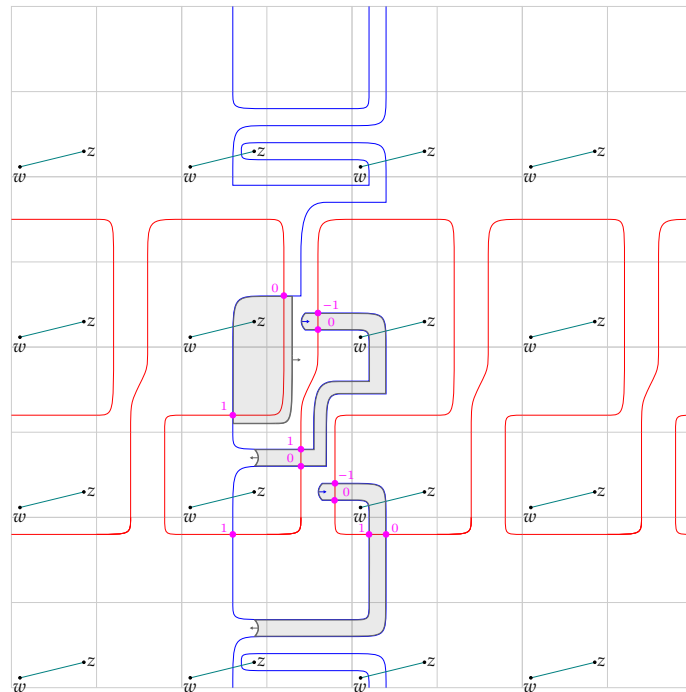


Figure 45. After the moves in Figure 44 eleven intersection points are left, and we choose to match the five pairs in the picture, each with filtration difference one.

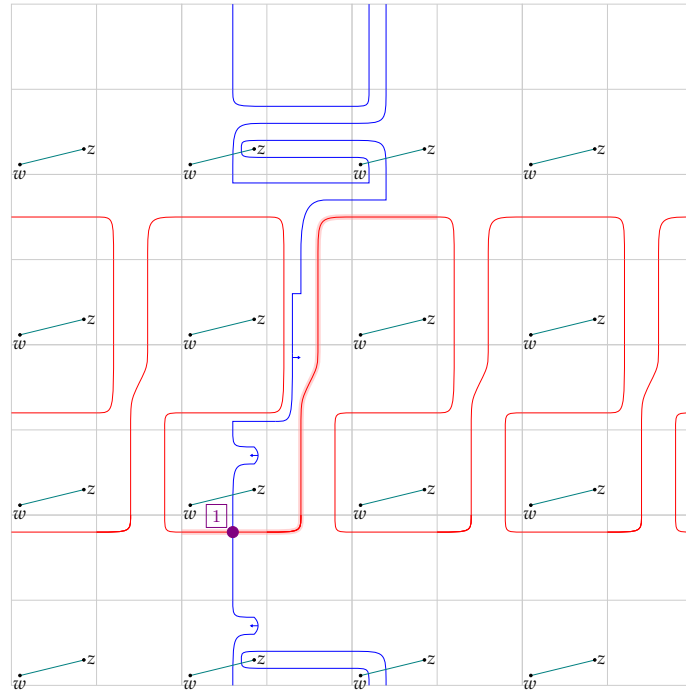


Figure 46. After the moves in Figure 45 the last remaining intersection point is indicated in purple at the bottom, and its Alexander filtration (in this case $+1$) is the final answer $\tau(Y, \text{Wh}_+(C, 0))$. Highlighted in light red is the piece of the immersed curve of the companion which connects adjacent columns of pegs and whose height encodes $\tau(Y, C)$.

9.2.6 Proof of the Whitehead double formula. After this example, we can provide the general proof of the untwisted Whitehead double formula, which states that $\tau(Y, \text{Wh}_+(C, 0)) = 1$ in the case $\tau(Y, C) > 0$, and $\tau(Y, \text{Wh}_+(C, 0)) = 0$ for $\tau(Y, C) \leq 0$. The main idea is contained in the example in [Section 9.2.5](#), and what is left for us is arguing that similar cancellations work for general red immersed curves α .

Proof of [Theorem 9.8](#) for twisting $t = 0$. We will give a proof of the Whitehead double formula in $\mathbb{Z}H\mathbb{S}^3$ L-spaces using immersed curve techniques, following Chen's results on $(1, 1)$ -patterns in [\[Che19\]](#).

We start with the case that the τ -invariant of the companion knot is positive, i.e. $\tau(Y, C) > 0$. Since the first intersection with the central axis $\{x = 0\}$ is at a positive height, the slope of the lift curve is positive, as in [Figure 47](#). The behavior of the remaining part of the curve, which is winding in the neighborhood of the vertical w -line, will not matter. Remembering that the absolute grading of the central intersection point is 0, we can deduce the Alexander gradings of the other intersections. Due to the shape of the blue β -curve of the Whitehead pattern, there is a periodicity, and the Alexander gradings appear in a repeating $-1, 0, 1$ -pattern. We can now remove these intersections with difference 1 using the Whitney disks as indicated on the left of [Figure 47](#). After this, we can pull the blue β -curve away from the z -basepoints in the left hand strip, again only using Whitney disks between filtrations of difference one. It is not necessary to cancel points whose difference in Alexander grading is bigger than one in this process. The intersection point at the very bottom remains, and its original Alexander grading is 1 which follows from the periodicity. The placement of the last intersection required the relevant part of the α -curve to have positive slope. Thus $\tau(Y, \text{Wh}_+(C, 0)) = 1$ if we started with a companion of $\tau(Y, C) > 0$.

We now deal with the case $\tau(Y, C) \leq 0$. For the schematic picture in [Figure 48](#), we assume $\tau(Y, C) < 0$ first, and add a comment at the end that the same strategy works for $\tau(Y, C) = 0$. We can use the same sequence of cancellations as in the positive case. This time, the remaining intersection point is at the top, the reason being the negative slope of the segment of the red α -curve determining the τ -invariant. In this case from the periodicity of the filtrations, the remaining point is in filtration zero. Thus $\tau(Y, \text{Wh}_+(C, 0)) = 0$ if we started with a companion of $\tau(Y, C) < 0$.

If $\tau(Y, C) = 0$ of the companion is zero, the distinguished curve is horizontally constant at height 0 until it intersects the vertical axis. (It might still curve upwards or downwards at this point depending on the ε -invariant.) But schematically the same finger moves on the β -curve apply to remove the intersections, and so in that case $\tau(Y, \text{Wh}_+(C, 0)) = 0$ as well. \square

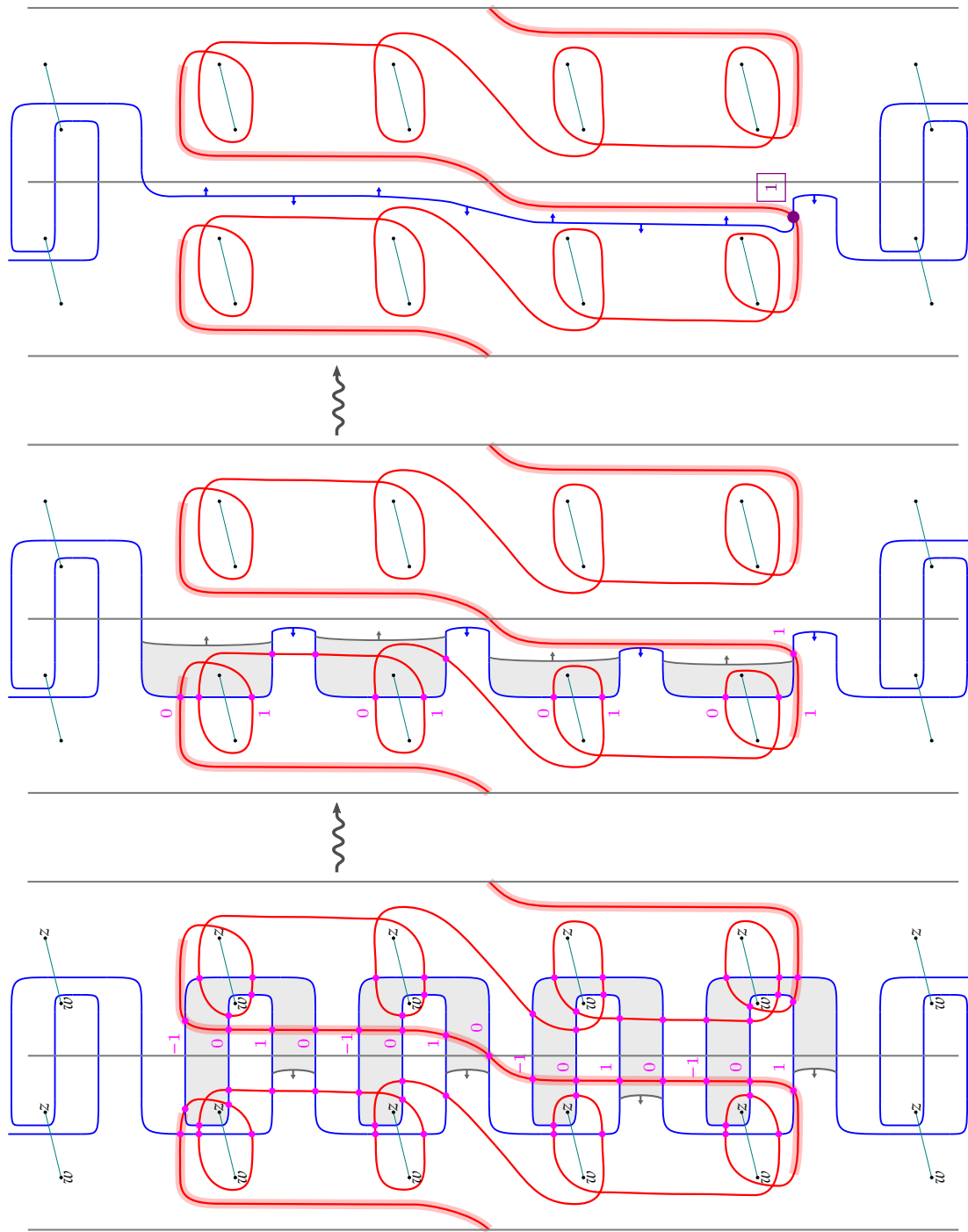


Figure 47. Cancellations of intersections in the case where the companion has $\tau(Y, C) > 0$ (which can be read off from the positive slope of the red immersed curve). We show three steps in the cancellation process, with selected relevant Alexander filtrations labeled in each. The Alexander filtration of the last remaining intersection point in the final step is equal to 1.

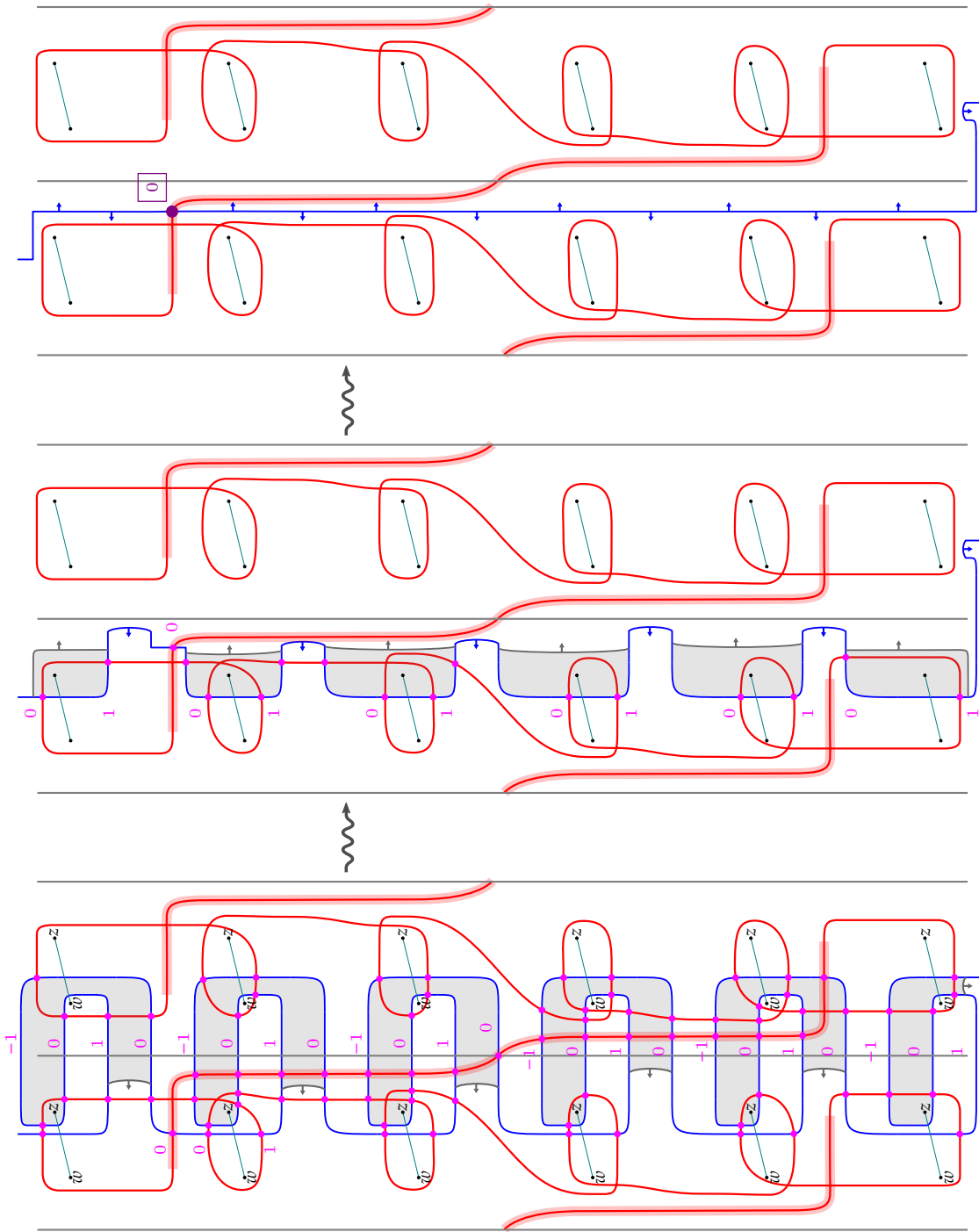


Figure 48. Cancellations of intersections in the case where the companion has $\tau(Y, C) < 0$ (which can be read off from the negative slope of the red immersed curve). The Alexander filtration of the remaining intersection point on the right is equal to 0.

9.3 Construction of topological shallow and smooth deep slice knots

In this section we continue towards a proof of [Theorem 9.1](#) and give a recipe for constructing examples of topologically shallow slice and smoothly deep slice knots by iterated Whitehead doubling.

Convention. In figures of surgery descriptions of 3-manifolds, strands passing through a box labeled with a knot are tied into that knot type, and if there are multiple strands passing through they are 0-framed parallels. Boxes labeled by numbers in a diagram denote full-twists with the corresponding sign.

9.3.1 General construction of topological shallow and smooth deep slice knots. The *linking number*, denoted $\text{lky}(k_1, k_2)$, of oriented integrally null-homologous knots k_1, k_2 in an oriented 3-manifold Y is defined by counting signed intersections of one link component, say k_1 , with an oriented Seifert surface for the other, say k_2 . If an integrally null-homologous knot K is drawn in the complement of the framed surgery link $L \subset \mathbb{S}^3$, we can forget L and consider the picture as a description of a knot in the 3-sphere (represented as the empty surgery diagram). In that case, the blackboard framing of K may neither agree with the 0-framing of the knot in \mathbb{S}^3 nor with the 0-framing in the 3-manifold resulting from surgery on L . We discuss this further in [Remark 9.11](#).

Let Y^3 be a 3-manifold given as Dehn surgery on a link L in the 3-sphere with rational coefficients. Then we can obtain the manifold with opposite (or reverse) orientation, $-Y$, as surgery on the mirror image of L with the negatives of the surgery coefficients. Orientation conventions for Dehn surgeries are discussed in [[Sav12](#), Sec. 2.2, Sec. 3.4].

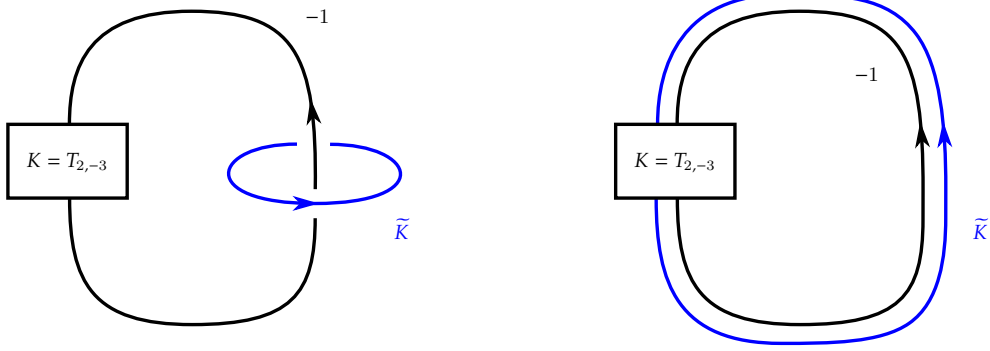
The general lemma explaining the construction of topologically shallow slice and smoothly deep slice knots by iterated Whitehead doubling is [Lemma 9.16](#). It is helpful to have an explicit example in mind, which we introduce now. The companion knots live in the boundary of the 4-dimensional 2-handlebody $X^4 = \mathbb{D}^4 \cup_{T_{2,-3}} (\mathbb{D}^2 \times \mathbb{D}^2)$ which is constructed by attaching a (-1) -framed 2-handle along the left-handed trefoil $K = T_{2,-3} \subset \mathbb{S}^3 = \partial\mathbb{D}^4$. This 4-manifold $X = X_{-1}(K)$ is a *knot trace* of the left-handed trefoil knot. In this case the boundary $\partial X \cong \mathbb{S}_{-1}^3(K)$ is (-1) surgery on $K = T_{2,-3}$ (the Poincaré homology sphere) which is both an integral homology 3-sphere and a Heegaard Floer L-space. For more discussion of the usual choice of orientation of the Poincaré sphere see [Section 9.3.3](#). Promising candidates for the companion knot are loops $\mathbb{S}^1 \hookrightarrow \mathbb{S}^3 - K \subset \mathbb{S}^3 = \partial(0\text{-handle})$ disjoint from the surgery curve K which (after forgetting the surgery curve) are smoothly slice in the 0-handle \mathbb{D}^4 .

For our example, as the companion knot we will take the core of the surgery solid torus \tilde{K} . This is also called the *dual curve* of the surgery, because performing a Dehn surgery the dual curve with 0-framing undoes the original surgery. As usual the 0-framing of the dual curve in $\mathbb{S}_{-1}^3(K)$ is determined by a push-off which has linking number 0 with \tilde{K} . Diagrammatically, for the dual curve we can draw the meridian of the knot K and then think of it placed in the surgered manifold. By sliding this meridian over the surgery curve K , the dual curve can be drawn in a variety of ways in the surgery diagram, for example as a longitudinal parallel to the surgery curve. We illustrate this in [Figure 49](#).

Remark 9.11. Since we are planning to construct various twisted satellites with companion the dual curve \tilde{K} , we discuss in some detail its 0-framed longitude $\lambda_{\tilde{K}}$. First we recall Hoste's formula for computing linking numbers of null-homologous curves in a 3-manifold represented by a Dehn surgery diagram [[Hos86](#), Lem. 1.1]. See [[RR17](#), Sec. 3] for another application of Hoste's linking formula.

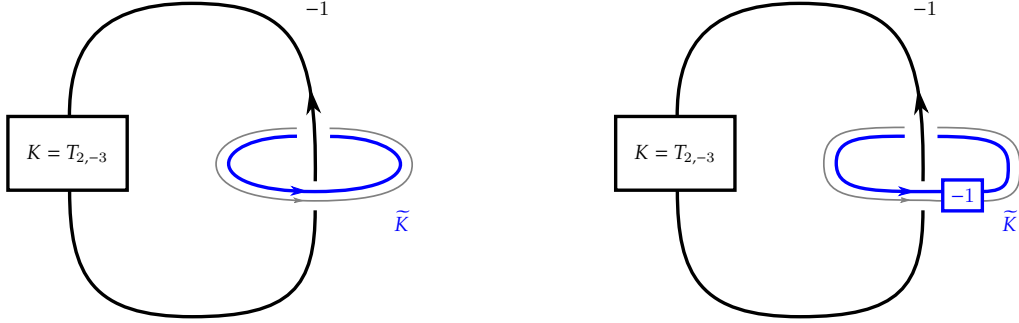
Let Y^3 be an ZHS^3 given by surgery on the rationally framed ordered link²⁷ $L \subset \mathbb{S}^3$ with rational linking-framing matrix B . Knots $k_1, k_2 \subset \mathbb{S}^3 - L$ in the complement of the surgery link can be considered both in the 3-sphere and in the result of the surgery Y^3 . The linking numbers in the respective manifolds are

²⁷ This recipe works more generally for surgeries on links $L \subset M^3$ in an ZHS^3 3-manifold M^3 .



(a) Dual surgery curve \tilde{K} drawn as a meridian in blue. (b) Dual surgery curve after sliding over the black (-1) -framed 2-handle.

Figure 49. Different ways of drawing the dual curve in the Poincaré homology sphere in a surgery diagram of $\mathbb{S}^3_{-1}(T_{2,-3})$.



(a) Gray blackboard framing of the dual surgery curve \tilde{K} . (b) Gray 0-framed longitude $\lambda_{\tilde{K}}$ of the dual surgery curve \tilde{K} .

Figure 50. Longitudes of the dual curve in the surgery diagram $\mathbb{S}^3_{-1}(T_{2,-3})$.

related by Hoste’s formula

$$\text{lk}_Y(k_1, k_2) = \text{lk}_{\mathbb{S}^3}(k_1, k_2) - \text{lk}_{\mathbb{S}^3}(k_1, L) \cdot B^{-1} \cdot \text{lk}_{\mathbb{S}^3}(k_2, L)^T$$

where $\text{lk}_{\mathbb{S}^3}(k_i, L)$ is the vector given by the linking number of k_i with the j -th component L_j of the surgery link in \mathbb{S}^3 . Since the result of the surgery is an integral homology sphere, the inverse B^{-1} which appears in the formula has integral entries.

Example 9.12. In our case the framed surgery link is $L = T_{2,-3} \subset \mathbb{S}^3$ with the (1×1) -matrix $B = (-1)$. For example, to compute the linking number of the blackboard framing curve \tilde{K}^{bb} of the dual \tilde{K} in the surgery diagram **Figure 50a**, we observe the linking numbers in the 3-sphere to be $\text{lk}_{\mathbb{S}^3}(\tilde{K}, \tilde{K}^{\text{bb}}) = 0$ and both $\text{lk}_{\mathbb{S}^3}(\tilde{K}, L) = (+1) = \text{lk}_{\mathbb{S}^3}(\tilde{K}^{\text{bb}}, L)$. Here we have oriented the surgery curve arbitrarily, which does not affect Hoste’s formula as the signs of linking numbers with L appear twice. The choice of orientation for the dual curve, as long as its push-off is oriented compatibly, is irrelevant as well, because a positive twisting is still positive after orientation reversal of the companion. Then by Hoste’s formula, $\text{lk}_Y(\tilde{K}, \tilde{K}^{\text{bb}}) = 0 - 1 \cdot (-1) \cdot 1 = +1$. To correct for this linking number, for the 0-framed longitude $\lambda_{\tilde{K}}$ we have to add twists as in **Figure 50b**. \triangle

Remark 9.13. Let k_1, k_2 be curves for which at least one of them has zero linking number with all of the surgery curves $L \subset \mathbb{S}^3$ with respect to the 3-sphere, say $\text{lk}_{\mathbb{S}^3}(k_1, L) = 0$ is the zero vector. Then Hoste’s

formula implies that the linking number of k_1 and k_2 in the surgery agrees with the linking number in the 3-sphere, i.e. $\text{lk}_Y(k_1, _) = \text{lk}_{\mathbb{S}^3}(k_1, _)$.

To find lower bounds on the genus of a smooth cobordism in a product of a 3-manifold with an interval, we use a special case of the slice genus bound from the τ -invariant in [HR21b]. The statement features a generalization of rational valued τ -invariants for $k \subset Y^3$ a rationally null-homologous knot in a 3-manifold and $\alpha \in \widehat{\text{HF}}(Y)$ a non-zero Floer class. This $\tau_\alpha(Y, k)$ is defined along the lines of Definition 9.4 by asking for the minimum Alexander grading of a cycle homologous to the chosen non-zero Floer class $\alpha \in \widehat{\text{HF}}(Y)$. In particular, for L-spaces Y we take α to be the unique non-zero generator of $\widehat{\text{HF}}(Y)$ and recover the old definition, and will usually suppress α from the notation. The following is a statement of the Hedden-Raoux genus bound in products of 3-manifolds with an interval. After this we will continue the construction of our examples which will make use of this in collars of boundaries of 4-manifolds.

PROPOSITION 9.14 (Special case of [HR21b, Prop. 5.14]). *If $k \subset Y \times \{1\}$ bounds a smoothly embedded surface $\Sigma \subset Y \times [0, 1]$, the τ -invariant gives a bound on its Euler characteristic as $2|\tau_\alpha(Y, k)| \leq 1 - \chi(\Sigma)$. Then if k is smoothly slice in the product $Y \times [0, 1]$, this implies $\tau_\alpha(Y, k) = 0$.*

Example 9.15. There are two natural choices for a 4-manifold bounding the product $\mathbb{S}^2 \times \mathbb{S}^1$. In terms of a Kirby diagram a 0-framed unknot describes the 2-handlebody $\mathbb{S}^2 \times \mathbb{D}^2$ while a dotted unknot represents $\mathbb{D}^3 \times \mathbb{S}^1$. As observed in Proposition 7.4, there are no deep slice knots in $\mathbb{D}^3 \times \mathbb{S}^1$, but in Section 8 we prove that there are non-local deep slice knots in $\mathbb{S}^2 \times \mathbb{D}^2$. The boundary 3-manifold has $\widehat{\text{HF}}(\mathbb{S}^2 \times \mathbb{S}^1)$ two-dimensional over \mathbb{F} . Associated to the two generators, called $t, b \in \widehat{\text{HF}}(\mathbb{S}^2 \times \mathbb{S}^1)$, there are two τ -invariants which can be used in a generalization of the statement of Proposition 9.14 for general 4-manifold bounding the given 3-manifold. In this general statement, the genus inequality depends on the images of Floer classes defining τ under the induced map on Floer homology of the boundary inclusion. The generator $t \in \widehat{\text{HF}}(\mathbb{S}^2 \times \mathbb{S}^1)$ gives a lower bound on the smooth $(\mathbb{D}^3 \times \mathbb{S}^1)$ -genus, $\tau_t(\mathbb{S}^2 \times \mathbb{S}^1, k) \leq g_{\mathbb{D}^3 \times \mathbb{S}^1}^{\text{sm}}(k)$. On the other hand, the generator b leads to the lower bound $\tau_b(\mathbb{S}^2 \times \mathbb{S}^1, k) \leq g_{\mathbb{S}^2 \times \mathbb{D}^2}^{\text{sm}}(k)$. See [HR21b] for further discussion of this.

For example, the Whitehead double $\text{Wh}_+(m)$ of the meridian of the handle (either thought of as a dotted 1-handle or a 0-framed 2-handle) has

$$\begin{aligned} 1 &= \tau_t(\mathbb{S}^2 \times \mathbb{S}^1, \text{Wh}_+(m)) \leq g_{\mathbb{D}^3 \times \mathbb{S}^1}^{\text{sm}}(\text{Wh}_+(m)) \\ 0 &= \tau_b(\mathbb{S}^2 \times \mathbb{S}^1, \text{Wh}_+(m)) \leq g_{\mathbb{S}^2 \times \mathbb{D}^2}^{\text{sm}}(\text{Wh}_+(m)). \end{aligned}$$

Thus it does not bound any smooth slice disk in $\mathbb{D}^3 \times \mathbb{S}^1$ (where every disk would have been shallow). But the τ_b -bound is inconclusive, and $\text{Wh}_+(m)$ does indeed bound a smooth disk in $\mathbb{S}^2 \times \mathbb{D}^2$, which we know from Schneiderman's μ -invariant is a deep disk. \triangle

We are now ready to state the general construction lemma for topologically shallow and smoothly deep slice knots in 2-handlebodies. In Section 9.3.2 this will be applied to $k = \text{Wh}_+(\widetilde{K}, +1)$, the positively clasped 1-twisted Whitehead double of the dual curve \widetilde{K} in the boundary of the (-1) -trace of the left handed trefoil $K = T_{2,-3}$. The dual curve \widetilde{K} itself satisfies most of the assumptions of the lemma except the framing condition, as explained in Example 9.12. Thus we later take an additional twisted Whitehead double in the beginning, and the final examples are 4-fold iterated Whitehead doubles.

LEMMA 9.16. *Let X^4 be a 2-handlebody with boundary ∂X both an integral homology 3-sphere and a Heegaard Floer L -space, which is described as integral surgery on a link $L \subset \mathbb{S}^3$. Let $k: \mathbb{S}^1 \hookrightarrow \mathbb{S}^3 - L$ be any knot in the complement of the surgery link, which is automatically integrally null-homologous in ∂X . Require that k is smoothly slice in the 0-handle of X^4 , but has positive τ -invariant $\tau(\partial X, k) > 0$.*

Assume that the 0-framing of k in \mathbb{S}^3 agrees with the 0-framing of k considered in ∂X . Then the 3-fold iterated positively clasped 0-twisted Whitehead double of k ,

$$\text{Wh}_+^{(3)}(k, \vec{0}) = \text{Wh}_+(\text{Wh}_+(\text{Wh}_+(k, 0), 0), 0)$$

is a knot in ∂X with the following properties:

- null-homotopic in ∂X ,
- smoothly H -slice in X^4 ,
- topologically shallow slice in $\partial X \times [0, 1]$ but
- **not** smoothly shallow slice in $\partial X \times [0, 1]$.

In other words, $\text{Wh}_+^{(3)}(k, \vec{0})$ is topologically shallow slice but smoothly deep slice in X .

Proof. By [Remark 9.13](#) on the framing of knots which have linking number zero with the surgery link L , the twisting of the iterated Whitehead doubles is both zero in the 3-sphere and in ∂X .

Constructing the deep smooth slice disk in X^4 : Let $\Delta: \mathbb{D}^2 \hookrightarrow \mathbb{D}^4$ be the smooth slice disk in the zero-handle of X^4 for $\partial\Delta = k$ which exists by assumption. The *positive Whitehead double of a slice disk* results from taking two parallels of the slice disk and fusing them along a band with positive half twist in the boundary. This disk has as boundary knot the 0-twisted Whitehead double in the 3-sphere, where the framing is inherited as the boundary of the slice disk in the 0-handle. By assumption on the framings, this agrees with $\text{Wh}_+(k, 0)$, where the 0-framing here refers to the boundary ∂X , and the Whitehead double itself has 0-framing agreeing in the 3-sphere and ∂X . We can iterate this process, and so the 3-fold iterated Whitehead double of the disk Δ is a smooth slice disk for $\text{Wh}_+(\text{Wh}_+(\text{Wh}_+(k, 0), 0), 0)$ in X^4 . Since the Whitehead doubles of k have linking number zero with the surgery link L and thus intersect generators for $H_2(X; \mathbb{Z})$ algebraically zero times, we can additionally conclude that the Whitehead doubles of Δ are H -slice disks.

Constructing the shallow topological slice disk in $\partial X \times [0, 1]$: For any curve l in the boundary ∂X , its Whitehead double $\text{Wh}_+(l, 0)$ as shown in [Figure 51](#) bounds an immersed disk with a positive self-intersection in ∂X . This disk can be seen as the track of the null-homotopy shown in [Figure 52](#) which unhooks the clasp. A 4-dimensional neighborhood of the immersed disk can be identified with a Casson handle with a single positive self-plumbing. Note that the double point loop of the intersection point of the immersed disk is isotopic to the companion l , as shown in the middle of [Figure 52](#). Further, by the choice of twisting, this double point loop is zero-framed on the surface. If l is itself a Whitehead double of a curve in the boundary, this double point loop is again null-homotopic in the boundary.²⁸ Consequently, we can put another Casson tower stage on this curve. After one further stage, we have built a height 3 untwisted Casson tower, with each stage's core containing a single positive intersection point. Freedman [[Fre88](#)], in his proof that the Whitehead double of one component of the Whitehead link is slice, showed that this simplest Casson tower of height 3 contains a topologically locally flat embedded disk for the boundary curve. Compare also with the discussion in [[CP16](#), Footnote on p. 2], and see [[GS99](#), Sec. 6.1] for an explanation of the plumbings in the stages of the Casson tower in terms of Kirby diagrams. Observe that the Casson tower lives in a neighborhood of the original companion curve k , and does not interact with the 2-handles of X . In our language, this topological disk is a topological shallow disk in $\partial X \times [0, 1]$ for the knot $\text{Wh}_+(\text{Wh}_+(\text{Wh}_+(k, 0), 0), 0)$.

Obstructing shallow smooth sliceness in $\partial X \times [0, 1]$: Hedden's formula [Theorem 9.8](#) can be applied in the $\mathbb{Z}H\mathbb{S}^3$ L-space ∂X to the i -fold iterated 0-twisted Whitehead double $\text{Wh}_+^{(i)}(k, \vec{0})$, where $\text{Wh}_+^{(1)}(k, \vec{0}) =$

²⁸ Observe that thus the Wall-Schneiderman μ -invariant vanishes already for 2-fold iterated Whitehead doubles $\text{Wh}_+(\text{Wh}_+(k))$.

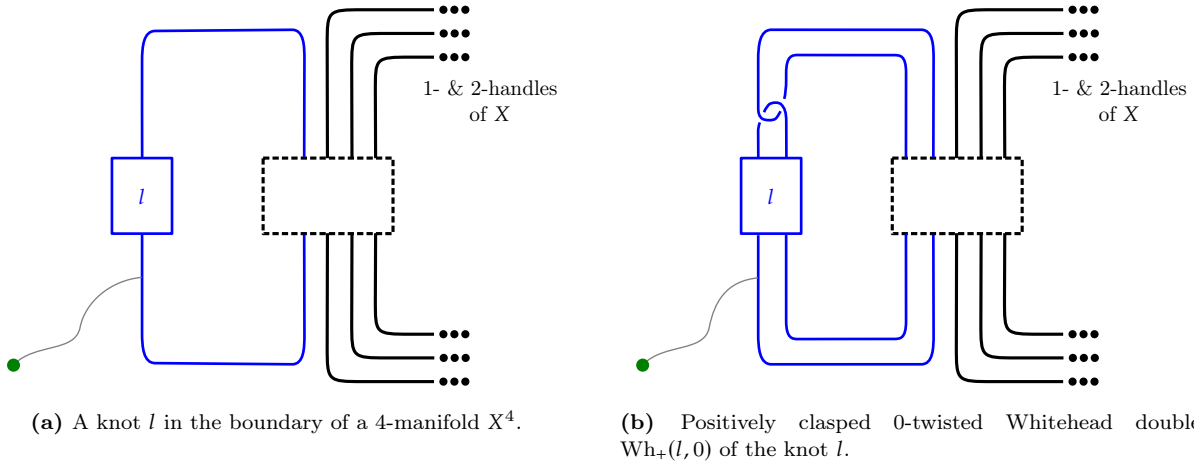


Figure 51. Whitehead double of a knot in the boundary of the 4-manifold X^4 , whose 1-handles and 2-handles are shown in black. The dashed unlabeled boxes containing both black and blue strands indicates that l (and its Whitehead doubles) might link with the curves describing the handles of X^4 . This is a more general version of Figure 34.

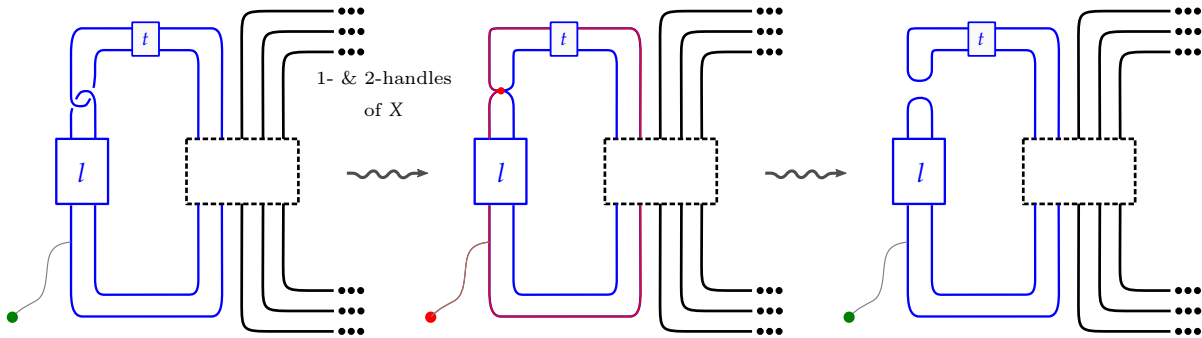


Figure 52. Another picture of the null-homotopy of the t -twisted Whitehead double $Wh_+(l, t)$ of the curve l in ∂X . The double point loop is drawn in red, observe that it is isotopic to the original knot l . Compare also with Figure 35.

$Wh_+(k, 0)$ and inductively $Wh_+^{(i)}(k, \vec{0}) = Wh_+(Wh_+^{(i-1)}(k, \vec{0}), 0)$. In particular, starting with a knot k such that $\tau(\partial X, k) > 0$, we can see iteratively that $\tau(\partial X, Wh_+^{(i)}(k, \vec{0})) = 1$. We conclude from the genus bound in [HR21b, Prop. 5.14] that the iterated Whitehead doubles are not smoothly shallow slice in $\partial X \times [0, 1]$, and thus have to be smoothly deep slice in X^4 . \square

Remark 9.17. Given an integral homology 3-sphere Y^3 , Freedman [Fre82, Thm. 1.4'] observed the existence of a compact, contractible topological 4-manifold bounding Y . An alternative construction by Freedman-Quinn appears in [FQ90]. Freedman's topological h -cobordism theorem implies that the compact contractible 4-manifold bounding Y is unique up to homeomorphism fixing the boundary, for the argument see for example [Beh+21, Rem. 21.2].

Now given additionally a knot K with Alexander polynomial 1 in Y^3 an $\mathbb{Z}H\mathbb{S}^3$, it is topologically slice in the Freedman contractible manifold V^4 bounding Y^3 . The knot K is even \mathbb{Z} -slice in V^4 , which means that there exists a topologically locally flat slice disk whose complement in V^4 has infinite cyclic fundamental group. We can wonder whether the Freedman-Quinn proof [FQ90, Sec. 11.7], [GT04] (with another exposition in [Beh+21, Thm. 1.14]) produces a topological slice disk in a collar $Y \times [0, 1]$. This is not the case.

For example, the 0-twisted Whitehead double of the dual curve \widetilde{K} in the Poincaré homology sphere P has a genus 1 Seifert surface, from which we can determine its Alexander polynomial to be $\Delta_{\text{Wh}_+(\widetilde{K},0)}(t) = 1$. Here Alexander polynomials for knots k in integral homology spheres, which automatically bound a Seifert surface F , can be computed from a Seifert matrix S of the Seifert form $S: H_1(F; \mathbb{Z}) \otimes H_1(F; \mathbb{Z}) \rightarrow \mathbb{Z}$, $S(\alpha, \beta) = \text{lk}(\alpha^+, \beta)$ via the usual formula $\Delta_k(t) = \det(tS - S^T)$. See [Remark 9.11](#) for discussion of linking numbers in general 3-manifolds.

Let V^4 be the compact contractible topological 4-manifold with $\partial V = P$, then by Freedman-Quinn $\text{Wh}_+(\widetilde{K}, 0)$ is topologically slice in V . But Schneiderman's $\mu(\text{Wh}_+(\widetilde{K}, 0))$ is non-trivial, so it cannot bound a topological disk in the collar $P \times [0, 1]$.

9.3.2 The dual knot in the Poincaré homology sphere. We now return to the explicit example of the dual knot in the Poincaré homology sphere and its Whitehead doubles to check that they satisfy the required properties. Hedden-Levine’s filtered mapping cone formula [HL21] can be used to compute the full Knot Floer complex $\text{CFK}^\infty(\mathbb{S}_{+1}^3(K), \widetilde{K})$ of the dual knot in a surgery, and from this in particular its τ -invariant. Zhou [Zho20, Thm. 3.2] computes the τ -invariant of the dual curve in the (+1)-surgery on $T_{2,4m-1}$, here we recall the results of his computations in the case $m = 1$. We verify this computation independently via the Generalized Slice-Bennequin inequality in Section 9.3.3.

PROPOSITION 9.18 (Application of [Zho20, Thm. 3.2]). *The τ -invariant of the dual knot in the Poincaré homology sphere with reverse orientation, is*

$$\tau(\mathbb{S}_{+1}^3(T_{2,3}), \widetilde{T_{2,3}}) = -1.$$

where $\mathbb{S}_{+1}^3(T_{2,3})$ is (+1)-surgery on the right handed trefoil $T_{2,3}$.

Proof. We will apply [Zho20, Thm. 3.2] to the L-space knot $K = T_{2,3}$ whose knot complex has 3 generators, and which has $n(K) = 1$. The generators of the $\mathbb{Z} \oplus \mathbb{Z}$ -filtered full knot Floer complex of the dual knot $\text{CFK}^\infty(\mathbb{S}_{+1}^3(K), \widetilde{K})$ after quotienting out acyclic $\mathbb{F}[U, U^{-1}]$ -summands is given in below. Each generator spanning a 1-dimensional \mathbb{F} -vector space is shown in the plane with coordinates (i, j) ; here an x at (i, j) corresponds to the generator $U^{-i} \cdot x$. In other words, an element of the form $U^i \cdot x$ is placed at the coordinate $(-i, A(U^i \cdot x)) = (-i, A(x) - i)$ where A is the Alexander grading. One coordinate j is induced from the Alexander filtration, while the other i records the negative of the U exponent. Arrows denote a nontrivial differential, and the homological grading is not shown in the picture.

$$\begin{array}{ccc} \mathbb{F}\langle a \rangle_{(0,1)} & & \\ \downarrow & & \\ \mathbb{F}\langle b \rangle_{(0,0)} & \longleftarrow & \mathbb{F}\langle U^{-1}c \rangle_{(1,0)} \end{array}$$

More precisely, these are the generators over $\mathbb{F}[U, U^{-1}]$, where U^{-1} is an inverse of the formal variable U . Thus the complete picture consists of infinitely many copies of the diagram above, shifted appropriately according to the action of U . In other words, the full complex appears by tensoring the above complex with $\mathbb{F}[U, U^{-1}]$ as below, where we skip writing the coefficient \mathbb{F} .

$$\begin{array}{ccccc} & & & & \langle U^{-1}a \rangle_{(1,2)} \\ & & & & \downarrow \\ & & & & \langle U^{-1}b \rangle_{(1,1)} \longleftarrow \langle U^{-2}c \rangle_{(2,1)} \\ & & \langle a \rangle_{(0,1)} & & \\ & & \downarrow & & \\ & & \langle b \rangle_{(0,0)} \longleftarrow \langle U^{-1}c \rangle_{(1,0)} & & \\ & \langle Ua \rangle_{(-1,0)} & & & \\ & \downarrow & & & \\ \langle U^2a \rangle_{(-2,-1)} & \langle Ub \rangle_{(-1,-1)} \longleftarrow \langle c \rangle_{(0,-1)} & & & \\ \downarrow & & & & \\ \langle U^2b \rangle_{(-2,-2)} \longleftarrow \langle Uc \rangle_{(-1,-2)} & & & & \end{array}$$

The knot Floer complex of the dual curve in the Poincaré sphere after quotienting acyclic summands coincidentally agrees with $\text{CFK}^\infty(\mathbb{S}^3, -T_{2,3})$, the full knot Floer homology of the left-handed trefoil in the 3-sphere.

To read off the τ -invariant we can restrict to the smaller $\widehat{\text{CFK}}$ -complex, which only considers the elements with $i = 0$ and the differentials that preserve the (i, j) -grading. Then the τ -invariant has yet another definition as

$$\tau(Y, K) = \min\{s \mid \widehat{\text{CFK}}(K)\{j \leq s\} \rightarrow \widehat{\text{CFK}}(K) \text{ is non-trivial in homology}\}.$$

In our case, we see that $\widehat{\text{CFK}}$ is generated by the three elements a, b, c . The element c has lowest Alexander filtration equal to -1 and it maps to the non-trivial generator in homology. \square

Remark 9.19. For later, we record that the ε -invariant is $\varepsilon(\mathbb{S}_{+1}^3(T_{2,3}), \widehat{T_{2,3}}) = -1 = \varepsilon(\mathbb{S}^3, -T_{2,3})$. This can be read off from our CFK^∞ complex (which has a particularly convenient choice of basis) by looking at the unique generator which has no incoming or outgoing vertical arrows. In this case, this generator is c and it lies at the tail of a horizontal arrow, which implies that the ε -invariant is -1 .

Also observe that when we begin the iterated Whitehead doubling process, in our case in the first step the Y_2 piece in the bordered Floer decomposition will be the complement of a knot in the 3-sphere, and

$$\widehat{\text{CFK}}(\mathbb{S}_{-1}^3(T_{2,-3}), \widehat{T_{2,-3}}) \simeq \widehat{\text{CFA}}(\mathbb{S}^1 \times \mathbb{D}^2, \widehat{T_{2,-3}}) \boxtimes \widehat{\text{CFD}}(\mathbb{S}^3 - \nu(T_{2,-3})).$$

But in the subsequent steps of the doubling, we take a satellite of a knot in the 3-manifold $Y = \mathbb{S}_{-1}^3(T_{2,-3})$ which is not \mathbb{S}^3 .

PROPOSITION 9.20. *For every $n \in \mathbb{N}$, the n -fold iterated Whitehead double of the dual curve $\text{Wh}_\pm^{(n)}(\widetilde{K}, \vec{t})$ with any choice of twisting $\vec{t} = (t_1, \dots, t_n)$ and sign of clasps in (± 1) -surgery on a non-trivial prime knot $K \subset \mathbb{S}^3$ is not a local knot.*

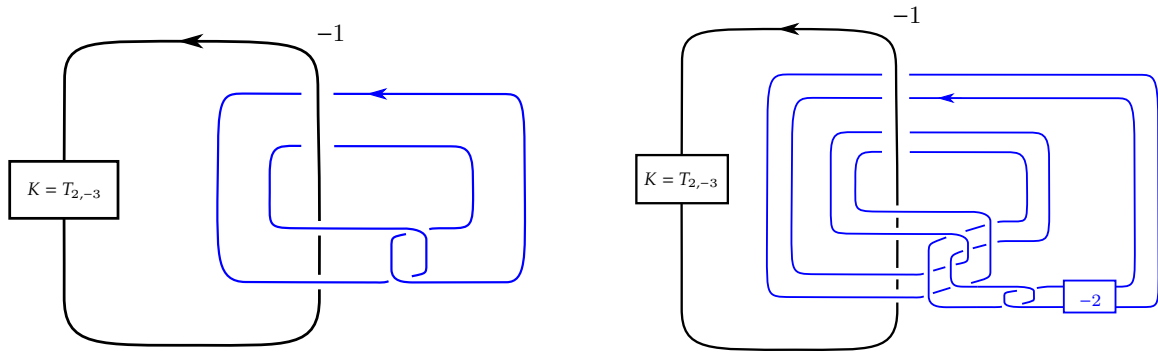
Proof. Without loss of generality, we will prove this for the (-1) -surgery $\mathbb{S}_{-1}^3(K)$. To arrive at a contradiction, assume that there is an embedded 3-ball $\mathbb{D}^3 \hookrightarrow \mathbb{S}_{-1}^3(K)$ which contains the knot $\text{Wh}_\pm^{(n)}(\widetilde{K}, \vec{t})$. We will use the JSJ-decomposition of the exterior

$$\mathbb{S}_{-1}^3(K) - \bar{\nu}(\text{Wh}_\pm^{(n)}(\widetilde{K}, \vec{t}))$$

and an innermost disk argument to show that the boundary of the 3-ball cannot enclose the closed tubular neighborhood $\bar{\nu}(\text{Wh}_\pm^{(n)}(\widetilde{K}, \vec{t}))$ on one side. For background on these 3-manifold techniques, see for example [Sch14, Sec. 3.8, 3.9].

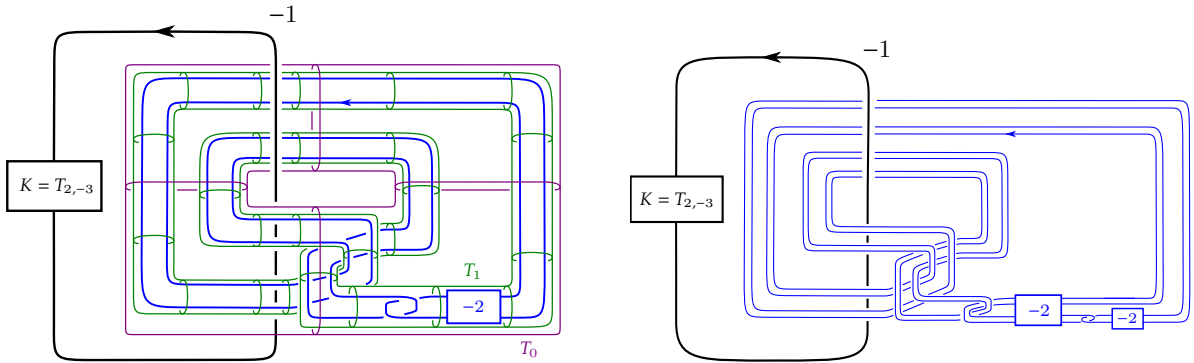
We now argue that the satellite tori in the iterated Whitehead double construction of $\text{Wh}_\pm^{(n)}(\widetilde{K}, \vec{t})$ are incompressible. The boundary of the closed tubular neighborhood of the dual curve $\partial\bar{\nu}(\widetilde{K})$ is incompressible in $\mathbb{S}_{-1}^3(K) - \bar{\nu}(\widetilde{K}) \cong \mathbb{S}^3 - \bar{\nu}(K)$ since we assumed that the knot $K \subset \mathbb{S}^3$ is non-trivial. Let $\text{Wh} \subset \mathbb{S}^1 \times \mathbb{D}^2$ be the positively or negatively clasped Whitehead pattern in a solid torus. The meridian $p \times \partial\mathbb{D}^2$ is not null-homotopic in the complement $\mathbb{S}^1 \times \mathbb{D}^2 - \text{Wh}$ of the pattern [Rol90, 3.G.4]. This implies that the Whitehead pattern in the solid torus is geometrically essential [Rol90, p. 4.D.3], which in turn implies that the map of $\pi_1(\partial(\mathbb{S}^1 \times \mathbb{D}^2)) \rightarrow \pi_1(\mathbb{S}^1 \times \mathbb{D}^2 - \text{Wh})$ is injective, proving incompressibility of the boundary of $(\mathbb{S}^1 \times \mathbb{D}^2 - \text{Wh})$. Due to the symmetry of the Whitehead link, the peripheral torus of the Whitehead pattern is incompressible in $\mathbb{S}^1 \times \mathbb{D}^2 - \text{Wh}$ as well. This argument also holds for twisted Whitehead patterns in the solid torus. Moreover, each component of the 3-manifold obtained by cutting along the collection of satellite tori is Seifert fibered or atoroidal, confirming that this is indeed the JSJ-decomposition; for the piece $\mathbb{S}^3 - \bar{\nu}(K)$ this uses that the knot K is prime.

We abuse notation and reuse the letter $S: \partial\mathbb{D}^3 \hookrightarrow \mathbb{S}_{-1}^3(K) - \text{Wh}_\pm^{(n)}(\widetilde{K}, \vec{t})$ to denote the embedding of the 2-sphere in every step of the following cut-and-paste argument. Label the tori in the JSJ-decomposition T_0, T_1, \dots, T_n from outermost to innermost in the iterated Whitehead doubling procedure, see Figure 53c. In the following, “inside” and “outside” will refer to the side of T_i towards the increasing and decreasing index respectively. Assume that (after possibly an isotopy) S is transverse to the collection of tori, and



(a) $(+1)$ -twisted positive Whitehead double $\text{Wh}_+(\tilde{K}, +1)$ of the dual curve.

(b) 0 -twisted double of $(+1)$ -twisted double (all positive) $\text{Wh}_+(\text{Wh}_+(\tilde{K}, +1), 0)$ of the dual curve.



(c) JSJ-tori in the complement of the iterated double $\text{Wh}_+(\text{Wh}_+(\tilde{K}, +1), 0)$.

(d) Taking another 0 -twisted Whitehead double yields $\text{Wh}_+(\text{Wh}_+(\text{Wh}_+(\tilde{K}, +1), 0), 0)$.

Figure 53. Iterated doubles of the dual curve \tilde{K} in $\mathbb{S}^3_{-1}(T_{2,-3})$. All of the framings are written in terms of the ambient 3-manifold $Y = \mathbb{S}^3_{-1}(T_{2,-3})$. The diagram of the Whitehead pattern has writhe equal to 2 in \mathbb{S}^3 , thus to take (iterated) 0 -framed doubles in Y we have to include the (-2) -twist boxes at each stage. We do not draw the last Whitehead doubling operation that is performed in the proof of **Theorem 9.1**.

intersects T_i in a non-empty collection of circles, but has already been made disjoint from the T_j for $j > i$. Take an intersection curve which is innermost on S , then it will bound a disk on one of the sides of T_i , and because of the incompressibility also on the torus itself. This disk in T_i can be used to surger S into a disjoint union of 2-spheres, where the boundary of the closed tubular neighborhood of $\text{Wh}_\pm^{(n)}(\tilde{K}, \vec{t})$ can only be enclosed in one of them. This 2-sphere is our new S , and observe that its number of intersection circles with the JSJ-tori has decreased.

Thus, inductively, we can find a 2-sphere S disjoint from the JSJ decomposition containing $\bar{v}(\text{Wh}_\pm^{(n)}(\tilde{K}, \vec{t}))$. This sphere S has to live inside of the solid torus bounded by the innermost JSJ torus, and contain the Whitehead pattern, which is impossible because the pattern is geometrically essential. \square

Remark 9.21 (Concordance to local knots). The dual curve $\tilde{K} = \widetilde{T_{2,-3}} \subset \mathbb{S}^3_{-1}(T_{2,-3})$ itself is non-trivial in homotopy,²⁹ and thus not even concordant to a local knot in $\mathbb{S}^3_{-1}(T_{2,-3}) \times [0, 1]$.

The one-fold Whitehead double of the dual curve $\text{Wh}_\pm(\tilde{K}, t)$, with any sign of the clasp and twisting t , has Schneiderman's invariant $\text{Wh}_\pm(\tilde{K}, t) = m$ nontrivial. Therefore it is not concordant to a local knot either.

²⁹ after choosing a whisker to the basepoint

Question 9.22. Is $\text{Wh}_+^{(2)}(\widetilde{K}, 0)$ or $\text{Wh}_+^{(3)}(\widetilde{K}, 0)$ or any of $\text{Wh}_+^{(n)}(\widetilde{K}, 0)$, $n \geq 4$ concordant to a local knot in $\mathbb{S}_{-1}^3(T_{2,-3}) \times [0, 1]$?

For knots in the 3-sphere³⁰, the ε -invariant vanishing implies that the τ -invariant has to be zero as well [Hom14, Prop. 3.6]. The failure of knots to satisfy this implication was used in [HLL18] as an obstruction to being homology concordant to any knot in the 3-sphere. An explicit example in Hom-Levine-Lidman is the dual knot in +1 surgery on the $(2, 3)$ -cable of the left handed trefoil, which has $\varepsilon(Y, K) = 0$ but $\tau(Y, K) = -1$.

Since both τ and ε of the dual knot in the Poincaré sphere with reverse orientation are equal to -1 , we cannot use this technique to obstruct it from being (homology) concordant to a local knot.

THEOREM 9.23. *The 2-handlebody $X^4 = X_{-1}(T_{2,-3})$ given by attaching a (-1) -framed 2-handle to the 4-ball along the left-handed trefoil knot contains a non-local null-homotopic knot in the boundary which is topologically shallow slice, but smoothly deep slice in X^4 .*

Proof of Theorem 9.23. Apply Lemma 9.16 to $k = \text{Wh}_+(\widetilde{K}, +1)$, the $(+1)$ -twisted positively clasped Whitehead double of the dual curve \widetilde{K} in the 3-manifold $Y = \mathbb{S}_{-1}^3(K)$, which is the boundary of the (-1) -trace of the left-handed trefoil $K = T_{2,-3}$. This boundary is the reverse of $(+1)$ -surgery on the right handed trefoil knot, i.e. $\mathbb{S}_{+1}^3(T_{2,3})$ with opposite orientation. The dual curve \widetilde{K} in $Y = \mathbb{S}_{-1}^3(K)$ has positive τ -invariant according to Proposition 9.18 and the behavior of τ under orientation change of the ambient 3-manifold, $\tau(-Y, \widetilde{K}) = -\tau(Y, \widetilde{K})$. Taking a $(+1)$ -twisted Whitehead double with the Y -framing yields a curve k that, if we draw it in the surgery diagram, appears untwisted. Thus by forgetting about the surgery curve, we see that it is unknotted in the 3-sphere and bounds a smooth disk into the 0-handle. Since k has linking number 0 with the surgery curve, its 0-framing in the surgery agrees with the 0-framing in \mathbb{S}^3 .

For companions with $\tau(Y, C) = +1$, such as the dual curve \widetilde{K} in the Poincaré sphere, Hedden's formula Theorem 9.8 computes

$$\tau(Y, \text{Wh}_+(C, t)) = \begin{cases} 0 & \text{for } t \geq 2\tau(Y, C) = 2 \\ 1 & \text{for } t < 2\tau(Y, C) = 2 \end{cases}$$

The result for twisting $t = +1$ in our case is $\tau(Y, \text{Wh}_+(\widetilde{K}, +1)) = +1$.

Therefore by Lemma 9.16 the knot $\text{Wh}_+^{(3)}(k, 0) \subset \mathbb{S}_{-1}^3(K)$ is null-homotopic in the boundary of the 2-handlebody $X_{-1}(K)$, topologically shallow slice and smoothly deep slice. Moreover, these Whitehead doubled knots are non-local by Proposition 9.20. \square

Remark 9.24. We were not able to determine the minimal number of 0-twisted Whitehead doubling steps required to obtain a topological slice disk in $Y \times [0, 1]$, starting with the seed knot $k = \text{Wh}_+(\widetilde{K}, +1)$ in the Poincaré sphere Y . For example after the first zero twisted doubling, the knot $\text{Wh}_+(\text{Wh}_+(\widetilde{K}, +1), 0)$ is Alexander polynomial 1, but we do not know whether the topological slice disk in the contractible 4-manifold from Remark 9.17 lives in the collar $Y \times [0, 1]$. The μ -invariant $\mu(\text{Wh}_+(\text{Wh}_+(\widetilde{K}, +1), 0)) = 1$ is trivial in this case, since the double point loop is itself the Whitehead pattern from the $(+1)$ -twisted doubling.

Adding one further doubling we see that $\text{Wh}_+(\text{Wh}_+(\text{Wh}_+(\widetilde{K}, +1), 0), 0)$ does bound a height 3 Casson tower, but its top stage is twisted with the top immersed disk corresponding to the first twisted doubling, see the schematic Figure 54. For this reason, in the statement of the general Lemma 9.16 we added another 3-fold iterated double to the knot, in this manner obtaining a height three untwisted tower for which we could apply Freedman's result [Fre88].

³⁰ and more generally, in an ZHS^3 L-space Y

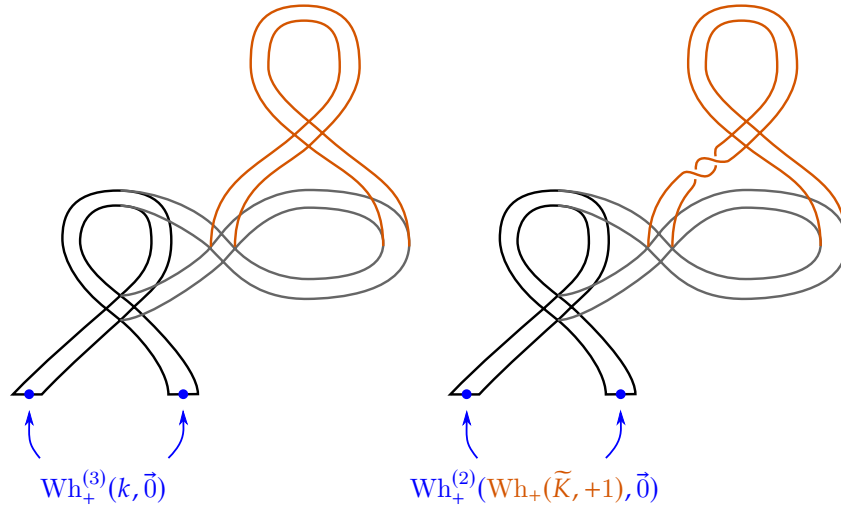


Figure 54. Schematic of a height 3 untwisted Casson tower (**left**) and a height 3 Casson tower whose topmost stage is twisted (**right**). In each stage, there is a single, positive self-plumbing. Casson towers are 4-dimensional objects with a framed embedded circle in its boundary, whose closed tubular neighborhood $\mathbb{S}^1 \times \mathbb{D}^2$ is called the attaching region. The attaching circle on the left is a 3-fold untwisted Whitehead double, while on the right the first doubling operation is twisted.

9.3.3 Generalized Slice-Bennequin inequality for $\mathbb{S}_{-1}^3(T_{2,-3}) \times [0, 1]$. Here we discuss the Generalized Slice-Bennequin inequality [HR21a] for contact manifolds with non-vanishing Ozsváth-Szabó contact invariant in the example of the dual curve in the Poincaré sphere $Y = \mathbb{S}_{-1}^3(T_{2,-3})$. This will lead to an alternative and independent computation of the τ -invariants of the dual curve $\tau(Y, \tilde{K}) = +1$ and its (+1)-twisted Whitehead double $\tau(Y, Wh_+(\tilde{K}, +1)) = +1$.

We first elaborate on orientation conventions. A common description of the Poincaré sphere is as the Brieskorn sphere $Y = \Sigma(2, 3, 5)$ with its positive orientation coming from the link of the algebraic curve $\{x^2 + y^3 + z^5 = 0\}$ in \mathbb{C}^3 . We take (Y, ξ) to be our contact manifold, where ξ is the unique³¹ tight positive³² contact structure on the Poincaré sphere with the usual positive orientation. Resolving the link of this complex surface singularity shows that the tight contact structure on Y is Stein fillable by the resolution which is an E_8 -plumbing of 2-spheres with Euler number -2 . In fact, every Stein filling of Y is homeomorphic to the E_8 -manifold [Sti02]. The Poincaré homology sphere with reversed orientation $-Y = -\Sigma(2, 3, 5)$ does not admit a positive tight contact structure by [EH01].³³ According to [KS79], attaching a (+1)-framed 2-handle to the 4-ball along the right handed trefoil knot $T_{2,3}$ yields a complex manifold, whose oriented boundary is $-\Sigma(2, 3, 5)$.

Hedden [Hed08] defines a contact version $\tau_\xi(Y, K)$ of the τ -invariant by recording the Alexander filtration of the first appearance of the *contact invariant* $c(\xi) \in \widehat{HF}(-Y)$. The contact invariant takes values in \widehat{HF} of the 3-manifold with reversed orientation, which is indicated by the minus sign above. In general (Y, ξ) Stein fillable implies $c(\xi) \in \widehat{HF}(-Y)$ is nontrivial. Since the Poincaré homology sphere with its tight contact structure is Stein fillable, its contact invariant $c(\xi) \in \widehat{HF}(-Y) \cong \mathbb{F}$ is nontrivial. The contact τ_ξ -invariant related to the generalized τ_α -invariant associated to a Floer class $\alpha \in \widehat{HF}(Y)$ as follows: If $c(\xi) \neq 0 \in \widehat{HF}(-Y)$, then $\tau_{c(\xi)}(-Y, K) = -\tau_\xi(Y, K)$. A *Legendrian* knot is a smooth knot in the 3-manifold

³¹ The uniqueness of the positive tight contact structure on the Poincaré sphere is due to Ghiggini-Schönenberger, for this and more classification results see [Sch01; GS03]. A family of fibered knots in Y which support the tight contact structure and have lens space surgeries is discussed in [Bak20].

³² *Positive* means that the contact structure is given by a 1-form α with $\alpha \wedge d\alpha > 0$

³³ There are also infinitely many examples known of closed, oriented, irreducible 3-manifolds with no tight contact structure [LS07].

tangent to the contact structure. For background on contact structures and the *Thurston-Bennequin number* $\text{tb}(\mathcal{K})$ and the *rotation number* $\text{rot}(\mathcal{K})$ (the classical invariants) of Legendrian knots see [Etn05].

Let $\Sigma \subset Y \times [0, 1]$ be a smoothly embedded surface with Legendrian boundary $\partial\Sigma \subset Y \times \{1\}$. The proof of Hedden-Raoux's [HR21a, Thm. 1] slice-Bennequin inequality comes from the following chain of inequalities. In general we need to assume that the contact invariant $c(\xi) \in \widehat{\text{HF}}(-Y)$ is non-zero, which we saw is true for the Poincaré sphere Y .

$$\text{tb}_\xi(\partial\Sigma) + |\text{rot}_{[\Sigma]}(\partial\Sigma)| \leq 2\tau_\xi(Y, \partial\Sigma) - 1 = -2\tau_{c(\xi)}(-Y, \partial\Sigma) - 1 \leq -\chi(\Sigma)$$

The rotation number $\text{rot}_{[\Sigma]}$ depends on the homology class $[\Sigma] \in H_2(Y \times [0, 1]; \mathbb{Z})$ and the Legendrian isotopy class of the boundary $\partial\Sigma \subset Y \times \{1\}$. We will need that for a Legendrian knot \mathcal{K} in the 3-sphere, the Thurston-Bennequin number $\text{tb}(\mathcal{K})$ and the rotation number $\text{rot}(\mathcal{K})$ can be computed from a Legendrian front diagram \mathcal{K} via the following formulas:

$$\begin{aligned} \text{tb}(\mathcal{K}) &= \text{writhe}(\mathcal{K}) - \frac{1}{2}(\#\text{cusps}) \\ \text{rot}(\mathcal{K}) &= \frac{1}{2}(\#\text{down cusps} - \#\text{up cusps}) \end{aligned}$$

In the case that $\partial\Sigma = \widetilde{K}$ is the dual knot in the Poincaré sphere with reversed orientation $-Y = -\mathbb{S}_{-1}^3(T_{2,-3}) = \mathbb{S}_{+1}^3(T_{2,3})$, we computed in Proposition 9.18 that $\tau_{c(\xi)}(-Y, \widetilde{K}) = -1$. As an alternative to Heegaard-Floer techniques, we now obtain lower bounds for the τ -invariant of the dual curve and of its (+1)-twisted Whitehead double from the slice-Bennequin inequality.

Warning: Our first goal is producing a contact surgery diagram of the tight contact structure on the Poincaré sphere. Let \mathcal{LHT} be a Legendrian representative of the left handed trefoil knot $T_{2,-3}$ with $\text{tb}(\mathcal{LHT}) = -6$ and $\text{rot}(\mathcal{LHT}) = -1$. If we perform the surgery on \mathbb{S}^3 to the Poincaré sphere Y with topological surgery coefficient $r_{\text{top}} = -1$ on \mathcal{LHT} , this corresponds to a *contact surgery coefficient* of $r_{\text{cont}} = +5$. By definition, this contact surgery coefficient is measured with respect to the *contact longitude* of the component, which is obtained from the Legendrian pushoff of the component; *topological surgery coefficients* are measured with respect to the Seifert longitude. In general, the topological $r_{i,\text{top}}$ and contact surgery coefficient $r_{i,\text{cont}}$ of a Legendrian component L_i in a contact surgery diagram are related via $r_{i,\text{top}} = r_{i,\text{cont}} + \text{tb}(L_i)$. But this (+5)-contact surgery on $\mathcal{LHT} \subset \mathbb{S}^3$ gives an overtwisted contact surgery on the Poincaré sphere, and in fact it is not possible to obtain the tight positive contact structure on Y via contact surgery on a single component [EKO22].

We reproduce a three-component contact surgery diagram of the tight structure on the Poincaré sphere from [EKO22] in Figure 55a. Each surgery component is a Legendrian unknot with $\text{tb} = -1$, thus the topological and contact surgery numbers differ by 1. Since all of the contact coefficient are negative, this is a tight contact structure on the Poincaré sphere [Wan15], compare [Keg16, Thm. 3.2.6], which is unique as stated in the above construction. We also show in gray the image of the dual curve of the left-handed trefoil in this three-component diagram. It is convenient to use the KLO software [Swe21] for following the dual curve through the Kirby moves, Rolfsen twists and slam dunks which transform the diagrams into each other.

Now in Figure 55b we find a Legendrian representative ℓ of this curve, heuristically chosen³⁴ so that the tb -number in the standard tight structure $(\mathbb{S}^3, \xi_{\text{std}})$ on the 3-sphere is as large as possible. We compute

³⁴ Part of this can be automated: Use the PLink editor to manually import the link created by KLO into SnapPy [Cul+21] and convert it into a braid word. Import this braid word into Gridlink [Cul07] and use its simplify function, then the output can be converted into a front projection by hand. See [Rup21a] for more detailed instructions.

the classical invariants of the diagram d considered in $(\mathbb{S}^3, \xi_{\text{std}})$ and obtain

$$\begin{aligned}\text{tb}_{(\mathbb{S}^3, \xi_{\text{std}})}(d) &= (-1) - \frac{1}{2}(4) = -3 \\ \text{rot}_{(\mathbb{S}^3, \xi_{\text{std}})}(d) &= \frac{1}{2}(2 - 2) = 0.\end{aligned}$$

The formulas from [DK16; Keg16] allow computations of classical invariants of null-homologous knot in contact surgery diagrams from their front projections. For the diagrams in Figure 55, the topological linking-framing matrix B and the result Q of multiplying its columns with the surgery denominators $q = (4, 2, 2)$ is given below.

$$B = \begin{pmatrix} \frac{-5}{4} & 1 & 0 \\ 1 & -\frac{3}{2} & 1 \\ 0 & 1 & -\frac{3}{2} \end{pmatrix}; \quad Q = \begin{pmatrix} -5 & 2 & 0 \\ 4 & -3 & 2 \\ 0 & 2 & -3 \end{pmatrix}$$

The gray dual curve d has linking numbers with the surgery curves given by the vector $l = (+1, -2, +2)$. The last ingredient for computing the classical invariants is the integral solution $a = (-1, -2, -2)$ of the equation $l = Q \cdot a$. With this preliminary work, and the vector $\text{rot} = (0, 0, 0)$ of rotation numbers of the surgery link, we can now apply the conversion formulas:

$$\begin{aligned}\text{tb}_{(Y, \xi)}(d) &= \text{tb}_{(\mathbb{S}^3, \xi_{\text{std}})}(d) - \sum a_i q_i l_i = (-3) - (-4) = +1 \\ \text{rot}_{(Y, \xi)}(d) &= \text{rot}_{(\mathbb{S}^3, \xi_{\text{std}})}(d) - \sum a_i q_i \text{rot}_i = 0\end{aligned}$$

Now from the Slice-Bennequin inequality in $Y \times [0, 1]$ we obtain

$$+1 = \text{tb}_{(Y, \xi)}(d) + |\text{rot}_{[\Sigma]}(d)| \leq -2\tau_{c(\xi)}(-Y, \partial\Sigma) - 1$$

which implies $\tau_{c(\xi)}(-Y, d) \leq -1$, confirming our earlier Heegaard-Floer computation in Proposition 9.18. We want to emphasize that the previous discussion merely gives bounds on the classical invariants of the topological type of the dual curve, and in principle there might exist “better” Legendrian representatives that could be used for the slice-Bennequin bound.

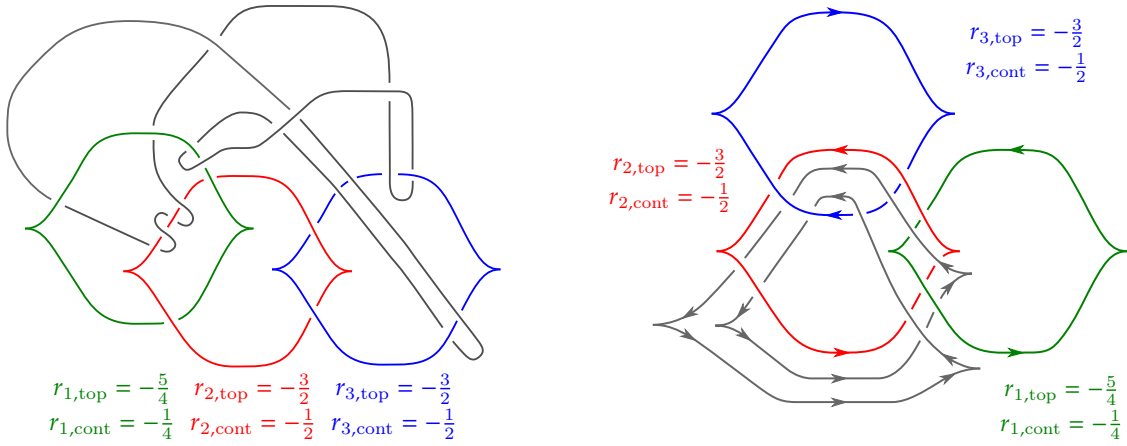
We want to go one step further and construct a Legendrian representative of the (+1)-twisted Whitehead double of the dual curve, where the twisting $t = +1$ is with respect to the framing in Y . Conveniently, the Legendrian pushoff d^{leg} shown in Figure 56a has linking number -3 in the 3-sphere with our diagram of the dual curve d . Using Hoste’s formula Remark 9.11, the linking number of d with this pushoff in Y is $\text{lk}_Y(d, d^{\text{leg}}) = \text{lk}_{\mathbb{S}^3}(d, d^{\text{leg}}) - l \cdot B^{-1} \cdot l^T = (-3) - (-4) = +1$. Thus to build a Legendrian front projection of a Legendrian representative of the (+1)-twisted Whitehead double with respect to the Y -framing we only need to insert a positive clasp between d and d^{leg} to obtain $\mathcal{W}h_+(d, +1)$. By counting signed crossings and cusps in the diagram, we compute

$$\begin{aligned}\text{tb}_{(\mathbb{S}^3, \xi_{\text{std}})}(\mathcal{W}h_+(d, +1)) &= (+6) - \frac{1}{2}(10) = +1 \\ \text{rot}_{(\mathbb{S}^3, \xi_{\text{std}})}(\mathcal{W}h_+(d, +1)) &= \frac{1}{2}(5 - 5) = 0.\end{aligned}$$

The Whitehead curve (and all of its iterates) has linking numbers with the surgery curves given by the zero vector $l' = (0, 0, 0)$, and an integral solution of the equation $l' = Q \cdot a'$ is $a' = (0, 0, 0)$.

$$\begin{aligned}\text{tb}_{(Y, \xi)}(\mathcal{W}h_+(d, +1)) &= \text{tb}_{(\mathbb{S}^3, \xi_{\text{std}})}(\mathcal{W}h_+(d, +1)) - 0 = (+1) - 0 = +1 \\ \text{rot}_{(Y, \xi)}(\mathcal{W}h_+(d, +1)) &= \text{rot}_{(\mathbb{S}^3, \xi_{\text{std}})}(\mathcal{W}h_+(d, +1)) - 0 = 0\end{aligned}$$

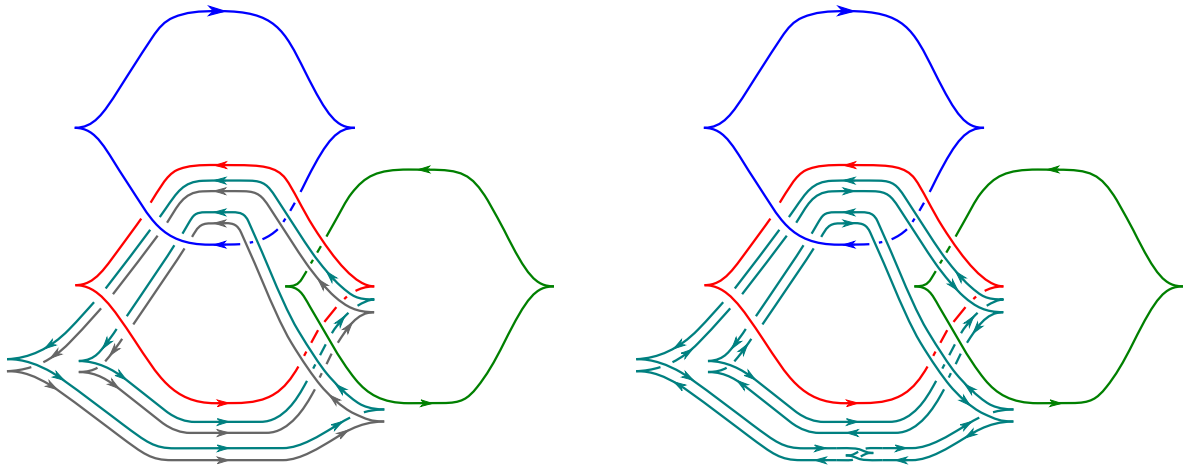
Again this leads to the Slice-Bennequin estimate $\tau_{c(\xi)}(-Y, \mathcal{W}h_+(d, +1)) \leq -1$. Since we know that the 3-genus of a Whitehead double is at most 1, this implies $\tau_{c(\xi)}(-Y, \mathcal{W}h_+(d, +1)) = -1$, confirming what we computed using Hedden’s formula for the (+1)-twisted case. Further discussion of Legendrian satellite operations and their classical invariants appears for example in [Coc+13] and [Ray15].



(a) Topological representative of the dual curve after transforming (-1) -surgery on the left handed trefoil to the contact surgery description on a 3-component link.

(b) Simplified Legendrian representative d of the dual curve, with $\text{writhe}(d) = -1$, and 2 up cusps and 2 down cusps.

Figure 55. The dual curve in contact surgery diagrams of the tight contact structure on the Poincaré homology sphere $Y = \mathbb{S}_{-1}^3(T_{2,-3})$.



(a) Legendrian parallel of the dual curve d in teal. In \mathbb{S}^3 , the linking number of d with the Legendrian parallel is -3 , which by Hoste's formula implies that the linking number in the surgery Y is $+1$.

(b) Thus we can build a Legendrian representative of $Wh_+(d, +1)$, the $(+1)$ -twisted Whitehead double with respect to the Y -framing, by inserting a positive clasp.

Figure 56. $(+1)$ -parallel and positive Whitehead double of the dual curve in $Y = \mathbb{S}_{-1}^3(T_{2,-3})$.

9.4 An infinite family of examples

The goal of this section is to extend the previous argument and find an infinite family of knots in the boundary of $X_{-1}(T_{2,-3})$, each of which exhibits the difference between topological and smooth deep and shallow sliceness.

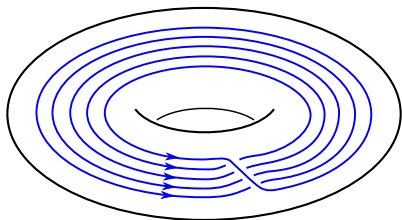


Figure 57. $(p, 1)$ -pattern in the solid torus, here for $p = 5$.

The examples will appear as $(p, 1)$ -cables of the knots constructed in [Section 9](#). A (p, q) -cable, $p, q \in \mathbb{Z}$ coprime³⁵, of a framed knot $J \subset Y^3$ in a 3-manifold is the satellite knot with companion J and pattern a (p, q) -torus knot. We can describe the resulting $J_{p,q}$ by placing a (p, q) -torus knot onto the boundary of a closed tubular neighborhood of J , where we use the framing to identify it with a standard torus $\mathbb{S}^1 \times \mathbb{S}^1$. The pattern knot will go p times around the longitudinal direction and q times around the meridian.

We will always assume $p > 1$, because the cable pattern with $p = 1$ is unknotted in the solid torus so $J_{1,q} = J$, and the sign of p can be changed by reversing the orientation of the cabled knot since $rK_{p,q} = K_{-p,-q}$, where r denotes reversing the orientation of a knot. Observe that both $T_{p,-q}$ and $T_{-p,q}$ are mirror images of $T_{p,q}$, and $T_{-p,-q} = rT_{p,q}$ is the original torus knot with reversed orientation.

In [\[Hom14\]](#) the formula is stated for knots in the 3-sphere, but again it holds more generally in $\mathbb{Z}H\mathbb{S}^3$ s which are also L-spaces. The reason once more is that bordered Floer homology and the other ingredients for Hom's proof work the same in integral homology 3-sphere L-spaces as for \mathbb{S}^3 .

THEOREM 9.25 (Generalization of [\[Hom14\]](#)). *For knots $J \subset Y^3$ in an integral homology 3-sphere L-space the τ -invariant of the (p, q) -cable knot is determined as follows:*

- If $\varepsilon(Y, J) = 1$, then $\tau(Y, J_{p,q}) = p \cdot \tau(Y, J) + \frac{(p-1)(q-1)}{2}$.
- If $\varepsilon(Y, J) = -1$, then $\tau(Y, J_{p,q}) = p \cdot \tau(Y, J) + \frac{(p-1)(q+1)}{2}$.
- If $\varepsilon(Y, J) = 0$, then³⁶ $\tau(Y, J) = 0$ and $\tau(Y, J_{p,q}) = \tau(\mathbb{S}^3, T_{p,q})$ agrees with the τ -invariant of torus knots.

Here we will not give a proof of [Theorem 9.25](#) in full generality, but only focus on the case of $(p, 1)$ -cables where we can emulate Chen's strategy using immersed curves. The $(p, 1)$ -cable pattern is shown in [Figure 57](#). Hom's formula specializes to the following for $(p, 1)$ -cables (remember that $p > 1$): If $\varepsilon(Y, J) = 1$, then $\tau(Y, J_{p,1}) = p \cdot \tau(K)$ and if $\varepsilon(Y, J) = -1$, then $\tau(Y, J_{p,1}) = p \cdot \tau(K) + (p - 1)$. Recall that reversing the orientation of the ambient 3-manifold changes the sign of the ε -invariant, $\varepsilon(-Y, J) = -\varepsilon(Y, J)$.

Watson-Hanselman [\[HW19\]](#) investigate the behavior of immersed curves under cabling in general, describing how the immersed curves for $\widehat{HF}(Y - \nu(J_{p,q}))$ can be obtained from the immersed curves for $\widehat{HF}(Y - \nu(J))$.

Proof of [Theorem 9.25](#) for $(p, 1)$ -cables. We begin by observing that $(p, 1)$ cable patterns are $(1, 1)$ links; in Schubert's normal form they correspond to $b(2p, 2)$. Again we can use [\[Che19, Thm. 5.4\]](#) in the other direction to conclude that the cable pattern link $b(2p, 2)$ admits a bordered Heegaard diagram whose

³⁵ We require $\gcd(p, q) = 1$ so that the pattern is actually a knot and not a link.

³⁶ This implication can be false in general 3-manifolds, i.e. the ε -invariant vanishing does not necessarily imply that the τ -invariant vanishes for $K \subset Y^3$, as shown in [\[HLL18\]](#).

β -curve has $r = 1$ loop and $s = p - 2|r| = p - 2$ stripes. Such a bordered doubly pointed Heegaard diagram for the $(p, 1)$ cable pattern is shown in [Figure 58](#), similar diagrams appear in [[Hom14](#), Fig. 6] and [[Dey19](#), Fig. 3].

The immersed curve encoding knot Floer homology of the companion knot determines the τ and ε invariant as discussed in [Section 9.2](#). Recall that $\tau(Y, C)$ is the height of the first intersection point of the distinguished component with the vertical axis $\{x = 0\}$, and $\varepsilon(Y, C)$ is determined by the direction in which it curves immediately after this first intersection point.

Assume $\tau(Y, C) \neq 0$ for now. We will argue the $\tau(Y, C) = 0$ case at the end of the proof. There are four possibilities of combinations of signs for $\tau(Y, C)$ and $\varepsilon(Y, C)$ of the companion, and the final intersection point together with its Alexander grading is indicated in [Figure 63](#). We now go through some of the cases with explicit examples, to argue why the cancellations occur in the specified order and result in the given intersection point. It is necessary to distinguish these cases because they influence the Whitney disks which occur in the picture.

For the first case of the proof, assume that $\tau(Y, C) > 0$ and $\varepsilon(Y, C) = +1$. Thus starting from the left, the distinguished component of the immersed curve has positive slope, intersects the vertical axis at some height and then turns downwards. The expected answer in that case is $\tau(Y, C_{p,1}) = p \cdot \tau(Y, C)$, and we indicate the remaining intersection point with its Alexander filtration in [Figure 64](#). Observe that the β -curve consists of a sequence of vertically stacked ‘fingers’, a certain number of which interact with the α -curve. This implies the following pattern for the Alexander filtrations of the intersection points: When following the β -curve from bottom to top, we start with intersection points of highest filtration, and the detour to the left decreases the filtration by one each time we walk over a line segment $\delta_{w,z}$. Arriving at the leftmost end of the finger, the filtration has decreased by p , which we call the length of the finger. We now turn around and go back to the right slightly above the row of $\delta_{w,z}$ -segments, and thus the filtration is constant on this horizontal part. Now we are back on the short vertical segments of the β -curve and continue on with the next finger.

In the following, we describe how the cancellation of intersections proceeds. For the Whitehead double in [Theorem 9.8](#), it was enough to cancel intersections with Alexander grading difference one. For cabling, however, we do need to remove disks connecting intersection points with higher Alexander grading differences. Thus we first remove those disks of Alexander grading difference 1, and then those of 2, then those of 3, and so on, up to the length of the finger in the β -curve, which is the cabling parameter p . The τ -invariant of the companion knot determines how many fingers interact with the immersed curve of the knot through the height of the first intersection with the vertical axis. Thus, for $\varepsilon(Y, C) = +1$ the Alexander filtration of the remaining intersection point depends multiplicatively on both $\tau(Y, C)$ and the parameter p .

Let us go through an explicit example where we compute $\tau((T_{2,3})_{5,1})$ of the $(5, 1)$ -cable of the $(2, 3)$ -torus knot and then explain why this technique works more generally. The pairing diagram of a $(p, 1)$ pattern with the immersed curves of the companion complement in the universal cover is shown in [Figure 59](#). Drawing a single lift of each curve, we indicate the Alexander filtrations of the intersection points and see the first collection of Whitney moves in [Figure 60](#). The first collection of moves removes intersection points of filtration difference zero in this case. In [Figure 61](#) we illustrate various Whitney moves at once, which strictly speaking occur one after another according to their filtration difference. Each consecutive step reduces the length of the blue ‘ β -fingers’ by one, until we reach the rightmost edge of the blue pattern. At this point, a final collection of Whitney moves is necessary as in [Figure 62](#), moving the blue curve over the z -basepoints until a single interaction either with the τ - or ε -determining part of the α -curve

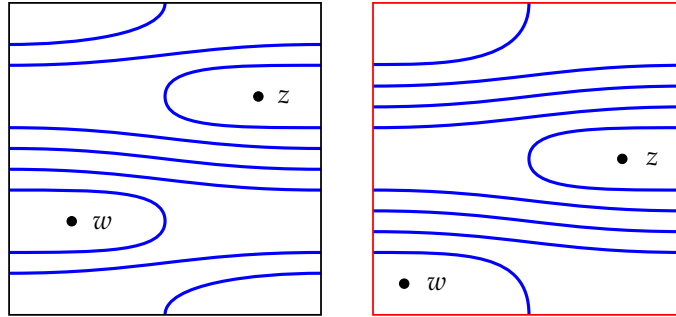


Figure 58. Bordered Heegaard diagram with β -curve for $(p, 1)$ cable pattern, in the case $p = 5$. On the left, the normal form with $r = 1$ loop and $s = p - 2$ stripes. On the right the fundamental domain is shifted to move the w -basepoint into the bottom left corner.

remains.

In this case of $\tau(Y, C) > 0$ and $\varepsilon(Y, C) = +1$ the intersection lies at the bottom of the peg-connecting segment with filtration $p \cdot \tau(Y, C)$.

For the second case, assume that $\tau(Y, C) < 0$ and $\varepsilon(Y, C) = -1$. That means starting from the left the distinguished curve has negative slope, and turns upwards after going over the meridian peg line. The expected answer is $\tau(Y, C_{p,1}) = p \cdot \tau(Y, C) + (p - 1)$, with the surviving generator shown in [Figure 65](#). We explain in the figure caption why this intersection point has Alexander filtration $p \cdot \tau(Y, C) + (p - 1)$. Looking from right to left instead, this intersection point occurs in the downward-curving part of the α -curve near the top.

We now handle the case of mixed signs for τ and ε , and start with positive $\tau(Y, C) > 0$ and $\varepsilon(Y, C) = -1$.³⁷ The expected answer is $\tau(Y, C_{p,1}) = p \cdot \tau(Y, C) + (p - 1)$. In the caption of [Figure 66](#) we give further details on why the remaining intersection point is of this filtration in the case that the signs of the τ and ε -invariants differ.

The case with $\tau(Y, C) < 0$ and $\varepsilon(Y, C) = +1$ is similar to the case with positive $\tau(Y, C) > 0$ and negative $\varepsilon(Y, C) = -1$, and we will not go through this argument again.

In the case $\tau(Y, C) = 0$ but possibly $\varepsilon(Y, C) \neq 0$, the final intersection occurs in the horizontal segment with filtration level zero, so $\tau(Y, C_{p,1}) = 0$. If $\varepsilon(Y, C) = 0$, then also $\tau(Y, C) = 0$, and thus the answer for the cable is zero as well. \square

Remark 9.26. For our purposes, we do not need the full power of Hom’s formulas for the τ -invariant of cables. It will be sufficient to have lower and upper bounds which show they are not equal to zero. Such

³⁷ For obtaining explicit examples, in the proof of [[Hom14](#), Cor. 3] Hom observes the following (modulo fixing a small typo): The cable $K_n^- = (T_{2,-3})_{2,2n+3}$ of the left-handed trefoil knot has $\tau(\mathbb{S}^3, K_n^-) = n$ and $\varepsilon(\mathbb{S}^3, K_n^-) = -1$. Taking $n = 1$, the knot $(T_{2,-3})_{2,5}$ has differing signs for the τ and ε invariant. Also note [[Hom14](#), Cor. 4] (attributed to Livingston): If the τ -invariant detects the smooth 4-genus, $g_4^{\text{sm}}(K) = |\tau(K)|$, then the sign of the ε -invariant agrees with that of the τ -invariant, $\varepsilon(K) = \text{sign } \tau(K)$.

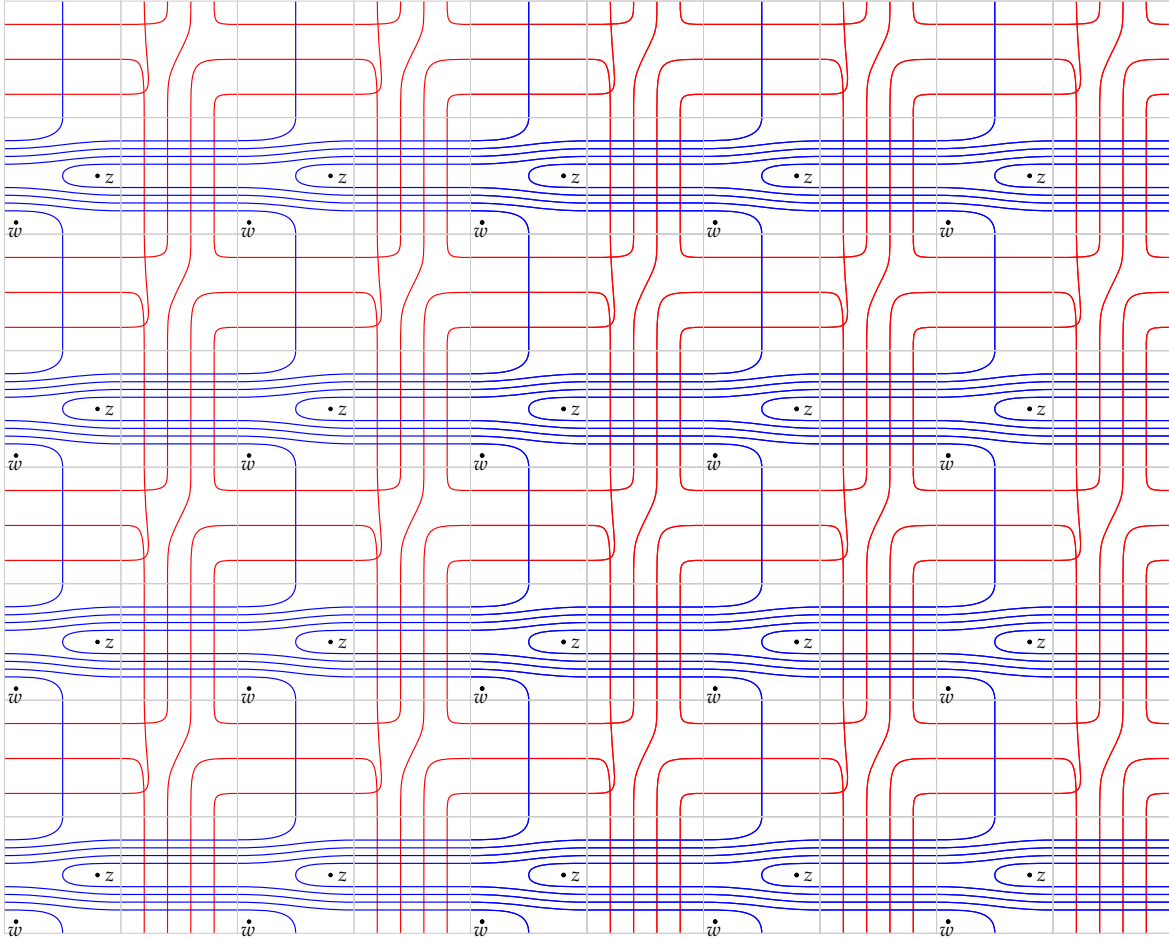


Figure 59. Pairing diagram of the blue β -curve of the $(p, 1)$ -pattern for $p = 5$ in Figure 58 with the red immersed α -curve for $T_{2,3}$ in the universal cover.

bounds were found by van Cott [Van10, Cor. 3] resulting from formal properties of the τ -invariant and Hedden's computations [Hed09] for $(p, pn + 1)$ -cablings. From this, for any nontrivial knot $K \subset \mathbb{S}^3$ and relatively prime integers p, q the τ -invariant of the (p, q) -cable satisfies

$$p \cdot \tau(K) + \frac{(p-1)(q-1)}{2} \leq \tau(K_{p,q}) \leq p \cdot \tau(K) + \frac{(p-1)(q+1)}{2}$$

Moreover, $\tau(K) = g_3(K)$ implies the lower bound to be an equality and for $\tau(K) = -g_3(K)$ the upper bound is sharp. Extending these bounds to knots in integral homology 3-sphere L-spaces would suffice for the following argument to go through.

In particular, this avoids the necessity to compute the ε -invariant of the iterated Whitehead double of the dual curve. We can be slightly more precise by observing that the ε -invariant of the iterated Whitehead double is non-zero, since the τ -invariant of the iterated Whitehead double is non-zero and the ambient 3-manifold is an integral homology 3-sphere L-space.

THEOREM 9.27. *There is an infinite family $J_{p,1}$ of null-homotopic non-local knots in the boundary of $X^4 = X_{-1}(T_{2,-3})$ the (-1) -trace of the left handed trefoil knot which are topologically shallow slice, but smoothly deep slice in X^4 . Moreover, the examples $J_{p,1}$ are all in different concordance classes in the collar $\partial X \times [0, 1]$.*

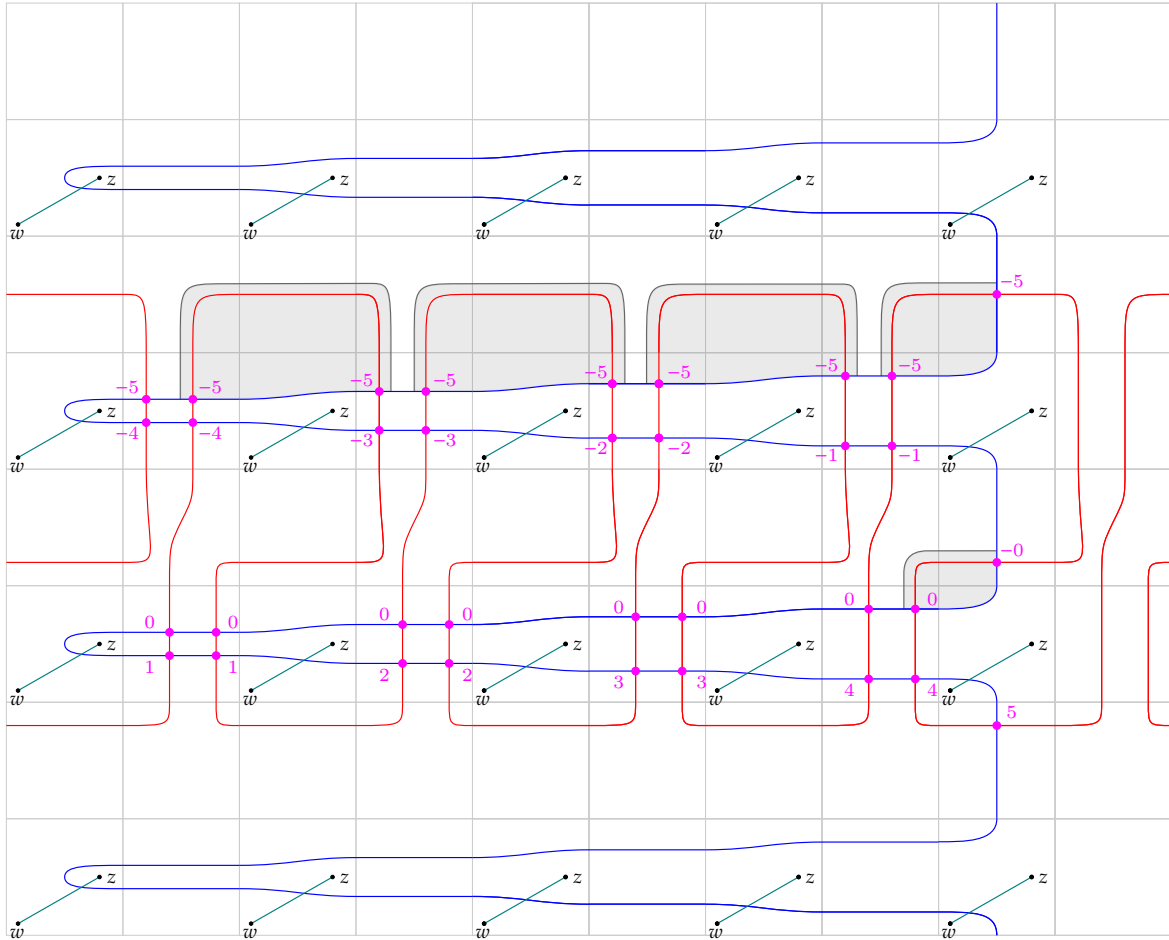


Figure 60. Pairing diagram of the $(p, 1)$ -pattern with the immersed curves of the companion, with a single lift of α and β from Figure 59. We also draw line segments $\delta_{w,z}$ (teal) between the basepoint, and calculate (differences between) the Alexander filtration of the intersection points (fuchsia). Shaded in gray is a first collection of Whitney moves removing pairs with filtration difference zero.

Proof. The infinite family comes from taking for $p \in \mathbb{N}$ the $(p, 1)$ -cable of the knots

$$J = \text{Wh}_+^{(3)}(\text{Wh}_+(\tilde{K}, +1), 0) \subset \mathbb{S}_-^3(T_{2,-3}) = Y$$

constructed in the proof of Theorem 9.1.

The $(p, 1)$ -pattern placed in a standard solid torus is unknotted in \mathbb{S}^3 , so the following properties are preserved. Again note that the 0-framing in the 3-sphere and the 0-framing in Y agree for the companion knot J , thus all of the satellite operations are 0-twisted.

- If J is topologically shallow slice in $Y \times [0, 1]$, then so is $J_{p,1}$ by taking the cable of the topological shallow slice disk.
- If J bounds a smooth slice disk in the 0-handle of X , then so does $J_{p,1}$, again by cabling the smooth slice disk. The framing on the boundary of the disk in the 0-handle is identical to the zero-framing in the boundary.

The τ -invariant will obstruct the $J_{p,1}$ from being smoothly shallow slice, and from being concordant to each other. By van Cott’s bounds in Remark 9.26, or Theorem 9.25, and our computation of $\tau(Y, J) = +1$,

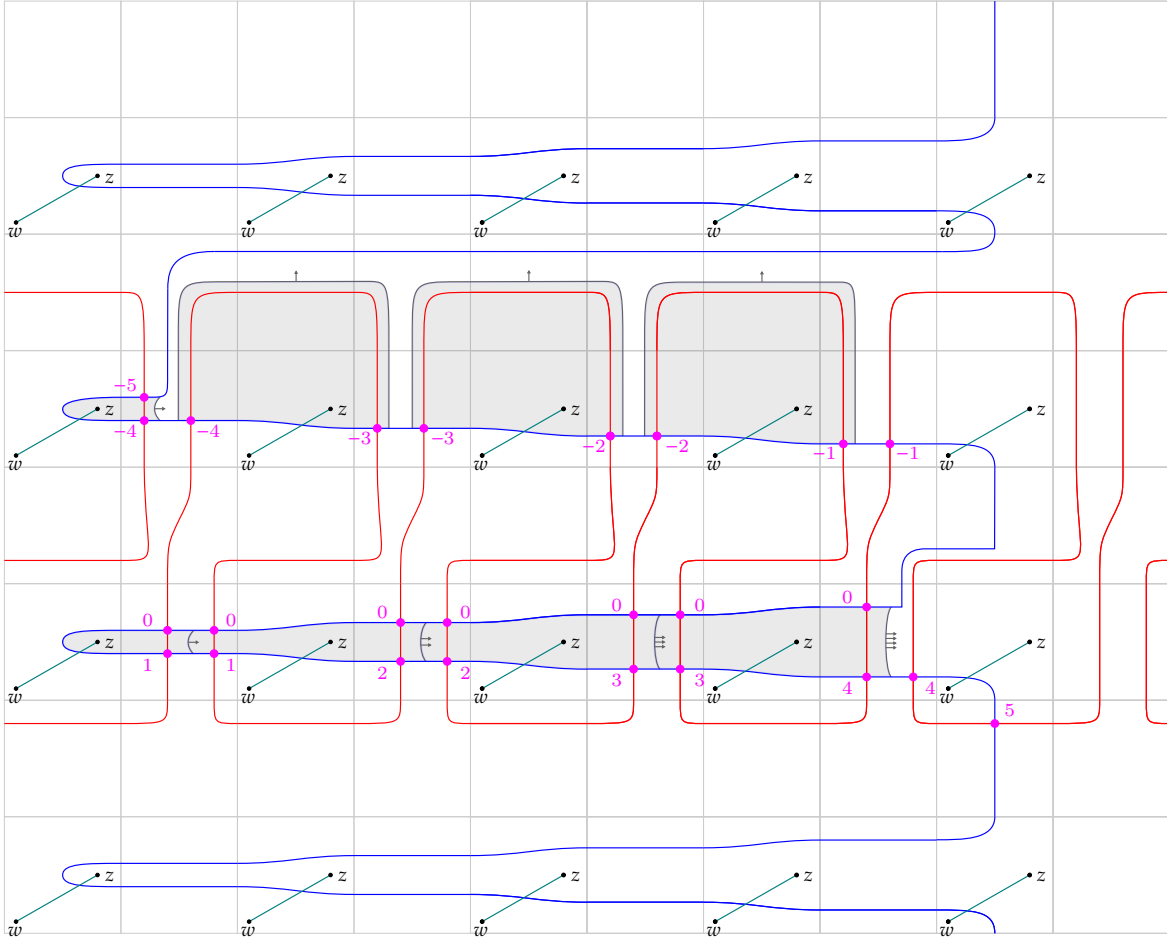


Figure 61. Following Figure 60, further cancellations of intersection points with filtration difference 1, followed by cancellation with difference 2, then 3 and then 4. We do not show all the Whitney moves, but remember that they are supposed to occur consecutively and ordered according to the filtration difference. Again the little arrows attached to the β -curve help with recording these differences.

we conclude that

$$p = p \cdot \tau(Y, J) \leq \tau(Y, J_{p,1}) \leq p \cdot \tau(Y, J) + (p - 1) = 2p - 1$$

Thus the τ -invariant $\tau(Y, J_{p,1})$ can grow arbitrarily large, and we can find an infinite sequence of $p_i, i \in \mathbb{N}$ where it takes different values.

These cables are not local either, by an adaptation of the argument in Proposition 9.20. The JSJ-decomposition of the complement of the knot $J_{p,1}$ is extended with an additional piece, obtained by cutting along the incompressible torus from the $(p, 1)$ -cabling construction. Here observe that the $(p, 1)$ -pattern is geometrically essential in the solid torus because it has non-trivial winding number, thus it cannot be contained in a solid ball, which is used to complete the last induction step. \square

Remark 9.28. Since the absolute value of the τ -invariant additionally gives a lower bound on the smooth slice genus in products of a 3-manifold with an interval, the proof of Theorem 9.27 shows that the $(p, 1)$ -cables of the 3-fold iterated Whitehead double of the dual curve give examples of the following: There exist knots in the boundary of the 2-handlebody $X^4 = X_{-1}(T_{2,-3})$ which are smoothly deep slice in X , topologically shallow slice, but which can have arbitrarily large smooth slice genus in $\partial X \times [0, 1]$.

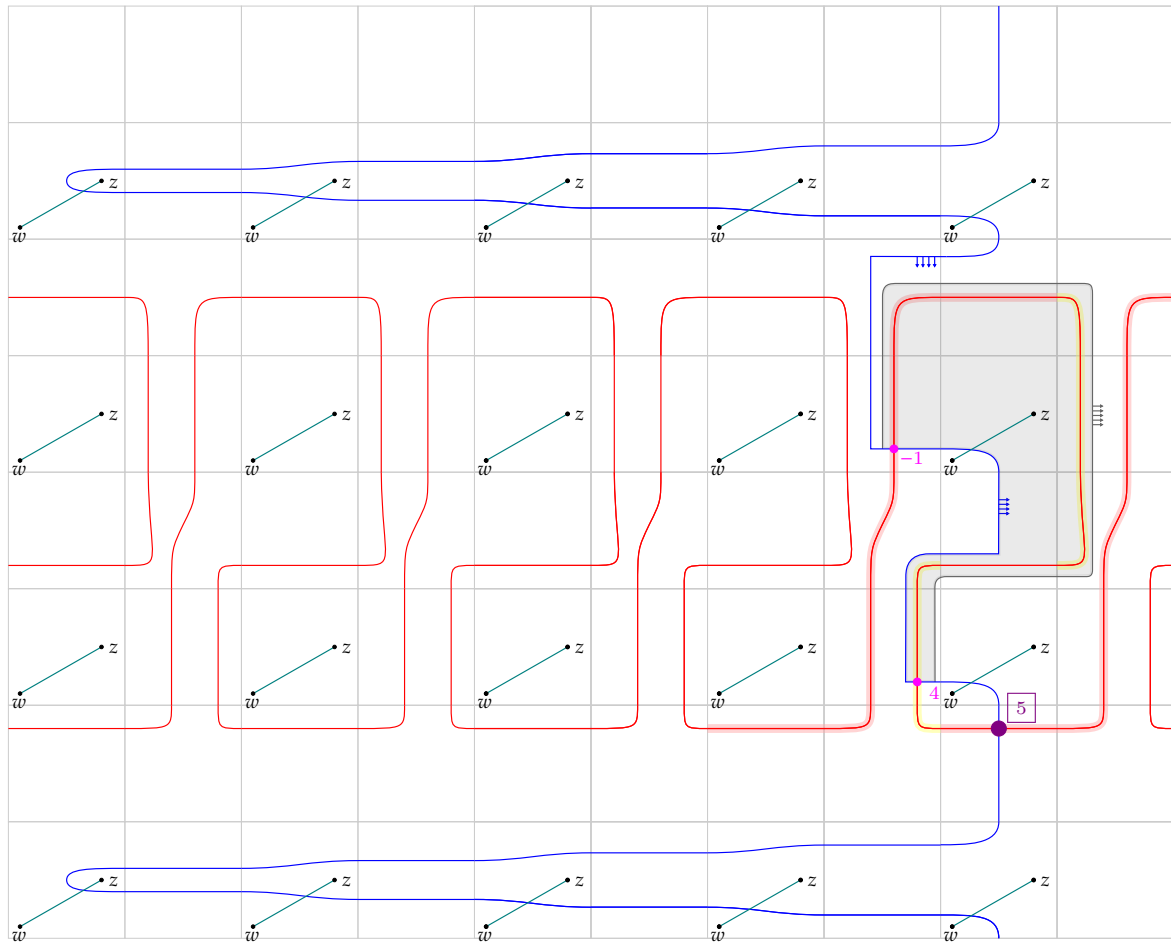


Figure 62. After Figure 61, we have a final Whitney move removing a pair of intersection points with filtration difference 5. The remaining intersection point of Alexander filtration 5 is marked with a thick purple dot at the bottom. The same cancellation process works for general p , which leads to longer blue ‘fingers’, and implies that $\tau(\mathbb{S}^3, (T_{2,3})_{p,1}) = p \cdot \tau(\mathbb{S}^3, T_{2,3}) = p$. In fact, the final answer only depends on the segments of the α -curve shaded in light red (which has positive slope because of the positive τ -invariant of the companion) and the segment shaded in yellow (which curves as in the picture since the ε -invariant of the companion is +1).

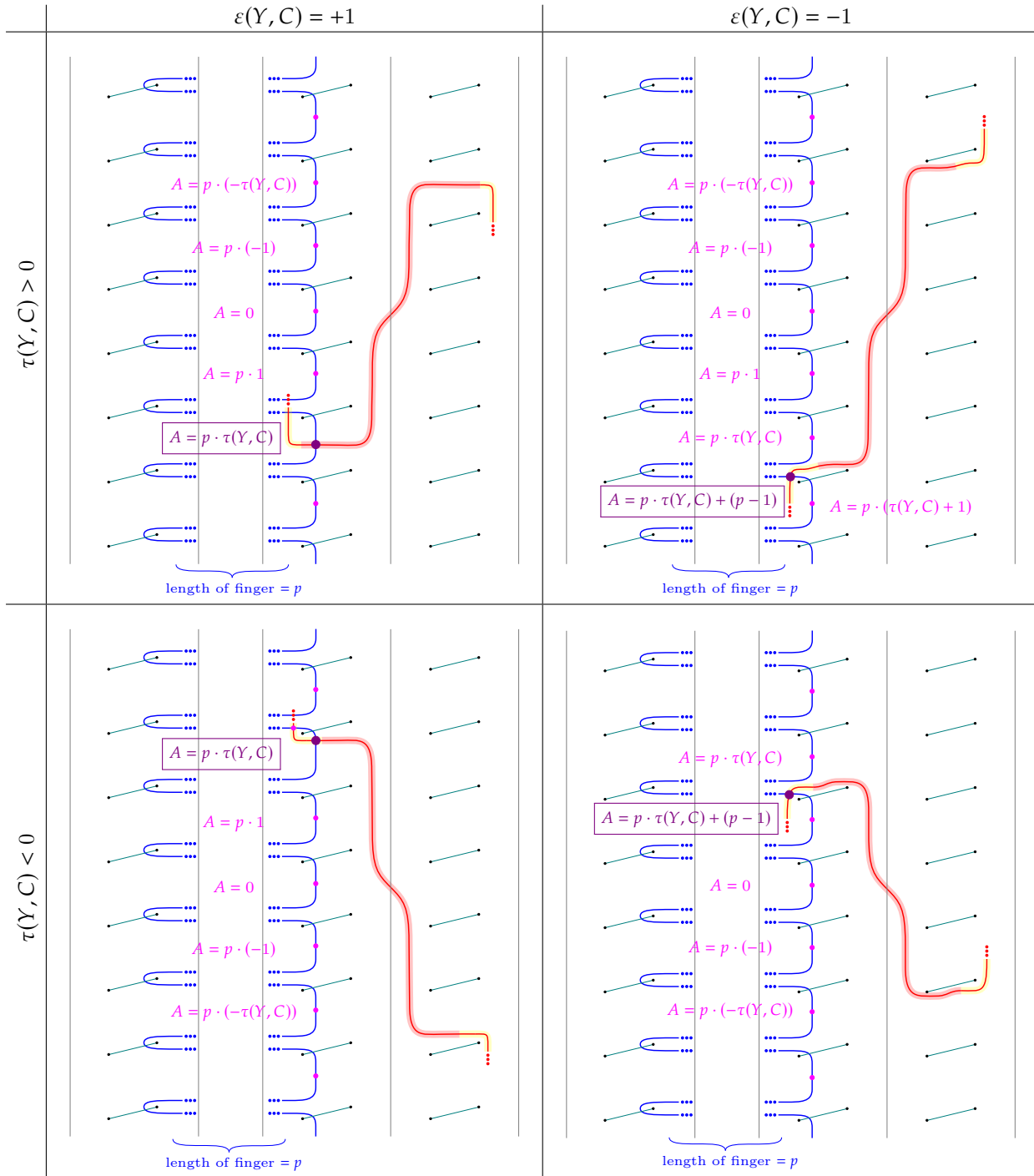


Figure 63. The remaining intersection points together with their Alexander filtration, for all possible combinations of signs for $\tau \neq 0$ and $\varepsilon \neq 0$ of the companion. Highlighted in red and yellow are the parts of the α -curve determining the τ -invariant and ε -invariant of the companion respectively. We also indicate the Alexander filtration of (hypothetical) intersection points that lie at the rightmost edge of the β -curve of the $(p, 1)$ -pattern.

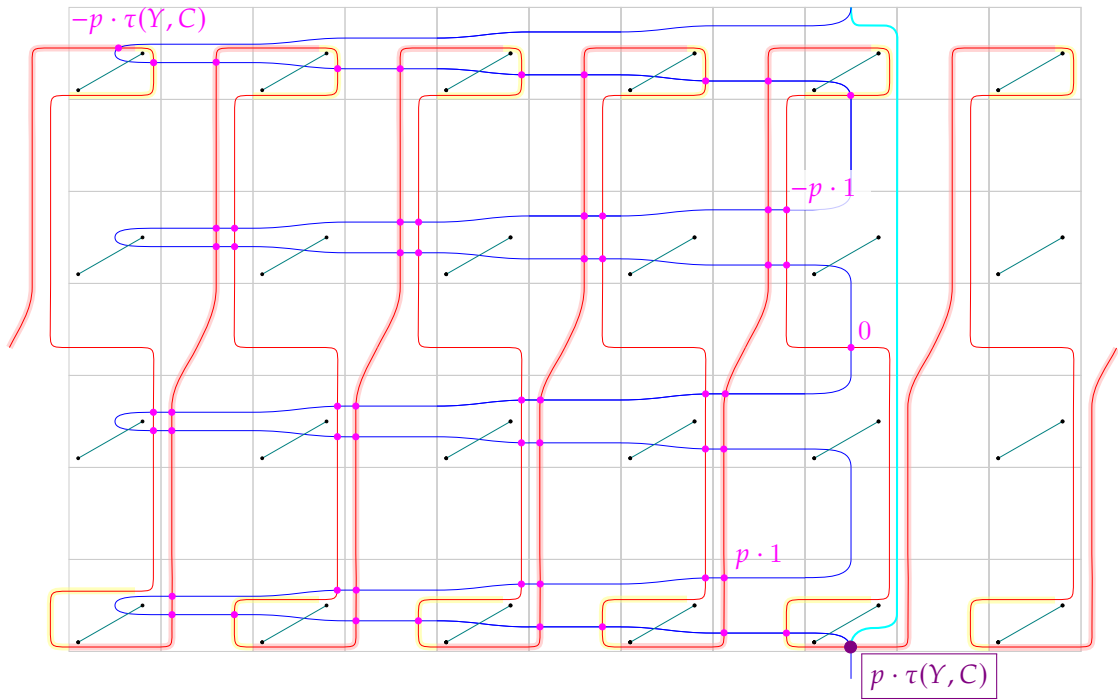


Figure 64. For $\tau(Y, C) > 0$ and $\varepsilon(Y, C) = +1$ the remaining intersection point is at the very bottom, and its absolute Alexander filtration is the τ -invariant of the companion knot times the length of the blue ‘ β fingers’, which is equal to p . In light blue we indicate the position of the β -curve after all of the cancellations. This leads to the expected final answer $\tau(Y, C_{p,1}) = p \cdot \tau(Y, C)$.

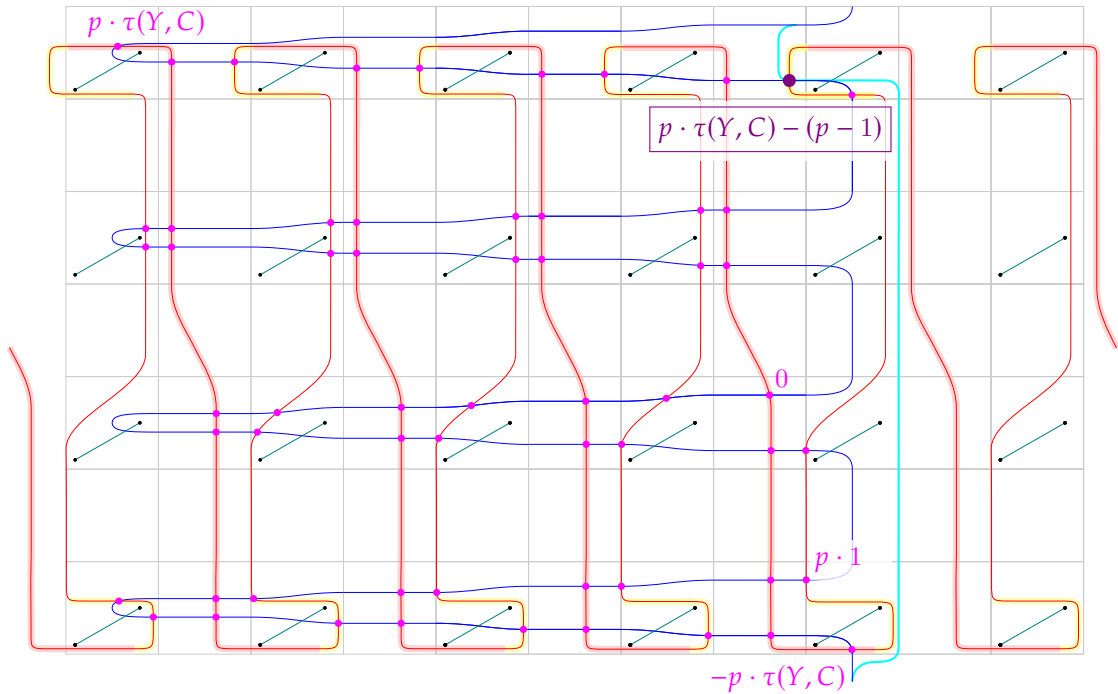


Figure 65. For $\tau(Y, C) < 0$ and $\varepsilon(Y, C) = -1$ the remaining intersection point is near the top of the horizontal segment going down from the height of the τ -invariant of the companion, at the bottom part of the blue ‘ β finger’ going through the downwards curving part determined by the negative epsilon invariant. Its absolute Alexander grading is the τ -invariant of the companion knot times the length of the blue ‘ β fingers’ plus the length of the finger but one. This leads to the expected final answer $\tau(Y, C_{p,1}) = p \cdot \tau(Y, C) + (p - 1)$.

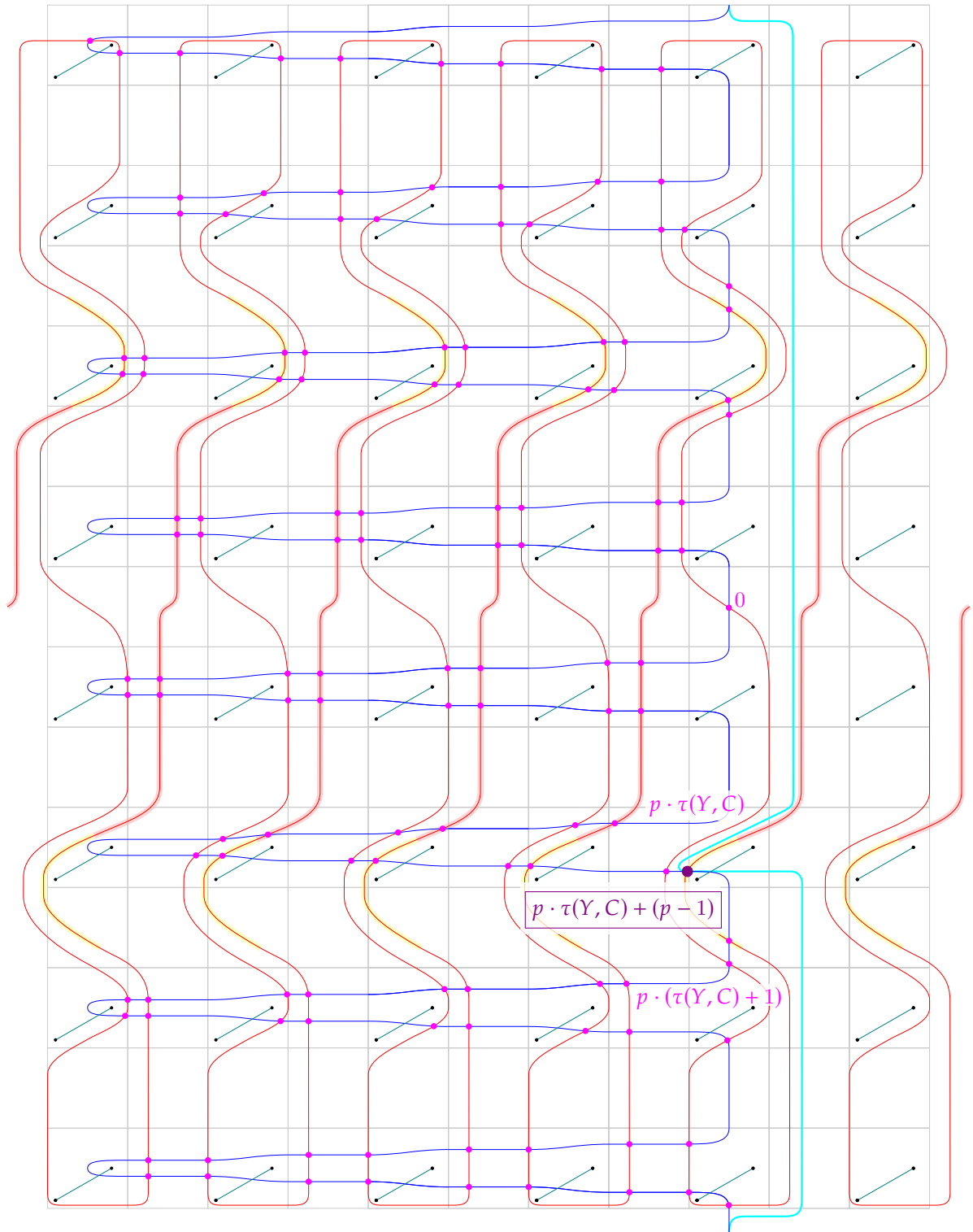


Figure 66. We draw the initial position of the β -curve in dark blue and its final placement after the Whitney moves in lighter blue. For $\tau(Y, C) > 0$ and $\varepsilon(Y, C) = -1$ the remaining intersection point is at the bottom part of the ‘ β finger’ going through the downwards curving part determined by the negative epsilon invariant. Its absolute Alexander grading is the τ -invariant of the companion knot times the length of the blue ‘ β fingers’ plus the length of the finger but one. This leads to the expected final answer $\tau(Y, C_{p,1}) = p \cdot \tau(Y, C) + (p - 1)$. Here the red α -immersed curve represents the companion knot $(T_{2,-3})_{2,5}$ and we are computing the τ -invariant of a further $(5, 1)$ -cable to be $\tau(\mathbb{S}^3, ((T_{2,-3})_{2,5})_{5,1}) = 9$.

10 DEEP SLICE LINKS

In this section we will investigate the difference between deep and shallow sliceness for links in the boundaries of 4-manifolds.

Two ordered links with the same number n of components in a 3-manifold $L, J \subset M^3$ are strong CAT concordant if there is a collection of disjoint, properly embedded CAT-annuli $\coprod^n \mathbb{S}^1 \times [0, 1] \hookrightarrow M \times [0, 1]$ with boundary $L \subset M \times \{0\}$ and $J \subset M \times \{1\}$. As a special case for concordances to the split unlink, a link $J = \bigcup J_i \subset \partial X$ is called CAT *strong slice* in X if it bounds a collection of disjoint CAT disks $\bigcup \Delta_i: \bigcup \mathbb{D}^2 \hookrightarrow X^4$, one for each component of J . A link whose components bound a collection of disjoint Seifert surfaces is called a *boundary link*.

Shallow slice knots are automatically null-homotopic in the boundary, in other words they are homotopic to a split local unknot. There is an analogous notion of homotopy for links. Two links $L, J \subset M$ in an ambient 3-manifold are *link homotopic* if all of the corresponding components are homotopic through homotopies which keep the different components disjoint throughout (but each component is allowed to pass through itself). Strong topological link concordance in a 3-manifold M^3 implies link homotopy [Gif79], [Gol79]. For this conclusion the ambient 3-manifold does not need to be orientable. In particular, if a link is topologically strong slice in $M \times [0, 1]$, it is link homotopic to a local unlink (split from the curves in a surgery diagram of M^3).

10.1 Existence of deep slice links

We now discuss a link analogue of Proposition 8.3, in which we constructed a null-homotopic deep slice knot in the boundary of every 2-handlebody X^4 with non-trivial $\pi_1(\partial X, *)$. Please see the caveat in Remark 10.2 on the homotopy class of the link of the following proposition.

PROPOSITION 10.1. *Let X^4 be a 2-handlebody with non-simply connected boundary, $\pi_1(\partial X, *) \neq \{1\}$. Then there exists a 2-component link $J \subset \partial X$ in the boundary with local, unknotted components which is topologically deep strong slice in X^4 .*

Proof. Fix a handle decomposition and Kirby diagram of the 2-handlebody X . Let $m \subset \partial X$ be a based meridian of one of the 2-handle attaching circles L_i such that m is non-trivial in $\pi_1(\partial X, *)$. Then the Bing double $J = \text{BD}(m)$ with respect to the blackboard framing of the boundary of the 0-handle is the 2-component link in Figure 67, where each of the two components J_1 and J_2 is an unknot split from the attaching link of the 2-handlebody.

Each individual component of the Bing double is a split unknot component and thus smoothly shallow slice. By going into the 0-handle of the 2-handlebody, i.e. forgetting about the attaching link L of the 2-handles, we see that J is strong slice in X because in the 0-handle \mathbb{D}^4 the Bing double J appears as a 2-component unlink. Observe that for this part of the argument it was important to take the Bing double with respect to the blackboard framing in the boundary 3-sphere of the 0-handle.³⁸

We will now argue why the link J is not topologically strong shallow slice. For the sake of contradiction, suppose that there exists disjoint topological shallow slice disks $\Delta_1 \cup \Delta_2 \hookrightarrow \partial X \times [0, 1]$. The fusion band pictured in Figure 68 between the two components results in the blackboard framed Whitehead double $\text{Wh}(m)$ of the meridian. The band sum of the strong slice disks results in a shallow disk $\Delta_1 \natural_b \Delta_2 \hookrightarrow \partial X \times [0, 1]$. But Schneiderman's μ -invariant shows that such a shallow disk does not exist, as in the proof of Proposition 8.11. \square

³⁸ In particular, this framing might not agree with the 0-framing of the dual curve m in the boundary ∂X of the 2-handlebody, see the discussion in Remark 9.11.

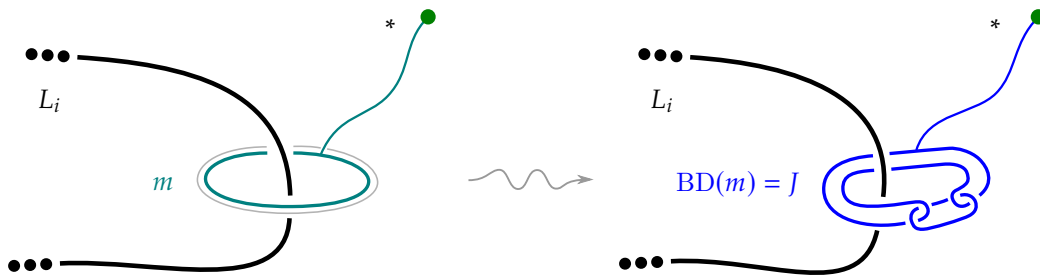


Figure 67. Bing double of a nontrivial meridian m with blackboard framing given as a parallel in gray, which does not have to agree with the 0-framing in the surgery on L .

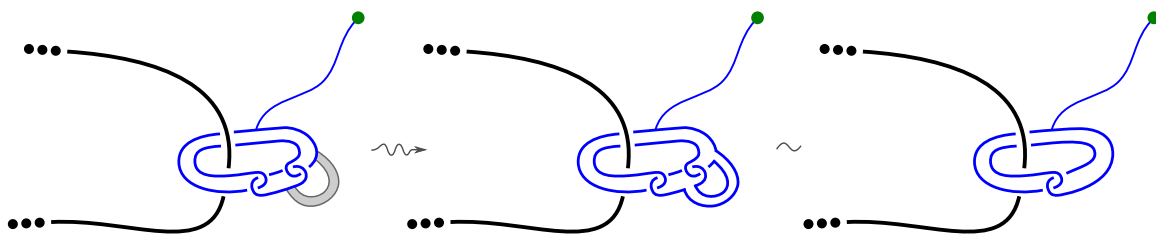


Figure 68. Fusion band from the Bing double to the Whitehead double.

Remark 10.2 (Link homotopy class of the Bing double). Unfortunately, the Bing double of the meridian constructed in the proof of [Proposition 10.1](#) often turns out to not be link null-homotopic in the boundary. If this Bing double is not link homotopic to a local unlink in the boundary, the Giffen-Goldsmith result gives an alternative obstruction to topological shallow sliceness, which does not use the μ -invariant.

For example, if m is the meridian to a (-1) -framed 2-handle, the resulting link $BD(m)$ is a $(+1)$ -twisted double in the ambient 3-manifold and closely related to the $(+1)$ -twisted Bing double of the unknot in the 3-sphere, which is the Whitehead link in \mathbb{S}^3 . The non-triviality of the Whitehead link on the 3-sphere can be detected with the repeating Milnor invariant $\mu_{1122}(Wh) = 1$. Tree-valued invariants for twisted Whitney towers from [\[CST14\]](#) should generalize to ambient 3-manifolds which are integral homology 3-spheres. In this language, the $(+1)$ -twisted Bing double of the meridian in (-1) -surgery on a knot has associated tree with twisted root and two leaves labeled 1 and 2, which is a non-trivial element. For a short overview of Milnor invariants see [\[Mei18\]](#), and for link-homotopy classes of string links in the 3-sphere see Habegger-Lin [\[HL90\]](#).

It would be interesting to find examples which are link null-homotopic in non-simply connected boundaries of 2-handlebodies, ideally with arbitrarily many components. We were not able to adapt a covering link argument which will be used later in [Section 10.2](#) to find such examples of links in 2-handlebodies with arbitrary non-simply connected boundary, since we do not know whether Schneiderman’s μ -invariant is well-defined under concordances in rational homology cobordisms. The independence of $\mu(K)$ from the choice of singular null-concordance in [\[Sch03\]](#) depends on the fact that in a product $M^3 \times [0, 1]$ of a 3-manifold with an interval, elements of $\pi_2(M^3 \times [0, 1])$ are representable by embedded 2-spheres. The proof of this fact does not immediately generalize to arbitrary $\mathbb{Q}H(M \times [0, 1])$.

Remark 10.3 (Obstructing shallow weak sliceness of the Bing double). If we try the same strategy to obstruct the weak shallow sliceness of the Bing double $BD(m)$ we run into the following problem. Suppose that $BD(m)$ is weakly slice in the collar, that is, assume there is an annulus $\mathbb{S}^1 \times \mathbb{D}^1 \hookrightarrow \partial X \times [0, 1]$ with boundary in $X \times \{0\}$ the two components of the Bing double. Adding the same fusion band as in [Figure 68](#),

we constructed a punctured torus bounding the Whitehead double $\text{Wh}(m)$. But such a genus 1 surface exists even in the 3-manifold ∂X already, thus we do not arrive at a contradiction.

Remark 10.4 (Case with simply connected boundary). If we try to apply a Bing doubling approach to the question of existence of deep slice links in 2-handlebodies with simply connected boundary, we run into the following problem. Following the proof idea in [Proposition 8.3](#), let J be a link in the boundary $\partial X = \mathbb{S}^3$ which is smoothly deep strong slice in X , but no band sum can be shallow slice since this would violate Rohlin's genus bound in [Theorem 8.5](#). If we were to Bing double every component of J , we would obtain a link with unknotted components which is still smoothly deep strong slice in X by Bing doubling the slice disks. But now the algebraic sum of these Bing doubled disks represent the zero element in $H_2(X; \mathbb{Z})$, since each Bing double contributes a positive and negative homology generator of the companion curve. As a consequence, we cannot use the genus bound obstruction since the zero element is always representable by a smoothly embedded sphere. We are left with asking the following.

Question 10.5. Let X^4 be a 2-handlebody with simply connected boundary and $n \in \mathbb{N}$. Does there exist an n -component link J in the boundary $\partial X \cong \mathbb{S}^3$ such that J is link null-homotopic, every proper sublink of J is smoothly shallow slice (or unlinked, i.e. J is Brunnian), but J itself is smoothly (or even topologically) deep strong slice in X^4 ?

Usually iterated, 'pure' Bing doubling does not produce null-homotopic links, but we can try to mix in Whitehead doubles to trivialize the link homotopy class of individual components or the entire link. The following lemma will allow us to construct deep slice null-homotopic boundary links for 2-handlebodies whose boundary is integral homology sphere (and not \mathbb{S}^3). We shall start with a curve in the boundary 3-manifold with a specific framing, so that the determinant of the resulting link can be used as a topological shallow sliceness obstruction.

PROPOSITION 10.6. *Let X^4 be a 2-handlebody with boundary ∂X an integral homology sphere given as an n -component integral framed link $L \subset \mathbb{S}^3$, with unimodular linking-framing matrix $B \in \text{GL}(n \times n; \mathbb{Z})$. Let $l = (l_1, \dots, l_n) \in \mathbb{Z}^n$ be a vector of linking numbers such that $-l \cdot B^{-1} \cdot l^T = k \in \mathbb{Z}$ is an integer with $|-16k + 1|$ not a perfect square. Then for every loop $\alpha \subset \mathbb{S}^3 - L \subset \partial X$ away from the surgery curves L , which is unknotted in \mathbb{S}^3 and realizes the \mathbb{S}^3 -linking numbers recorded in the vector l with the components of L , the following construction applies; see [Figure 69](#).*

The 2-component link $J = \text{Wh}_{+,1}(\text{BD}(\alpha, 0), 0) \subset \partial X$, the 0-twisted Whitehead double of the first component of the 0-twisted Bing double of the loop α (where all framings are taken with respect to the boundary \mathbb{S}^3 of the 0-handle of X), satisfies the following properties:

- J is link homotopic to the split unlink in the boundary;
- J is Brunnian in the boundary, i.e. every proper sublink of J is unlinked and thus smoothly shallow strong slice;
- J bounds smooth strong slice disks in the 2-handlebody X ;
- J is a boundary link in ∂X (in particular, all Milnor invariants, including the repeating ones, vanish for J);
- J is not topologically shallow strong slice in $\partial X \times [0, 1]$, and so J is topologically strong deep slice in X .

For a 2-handlebody the matrix B represents the intersection form of X , and its boundary ∂X is a rational homology sphere if and only if $\det(B) \neq 0$. The boundary is an integral homology sphere if and only

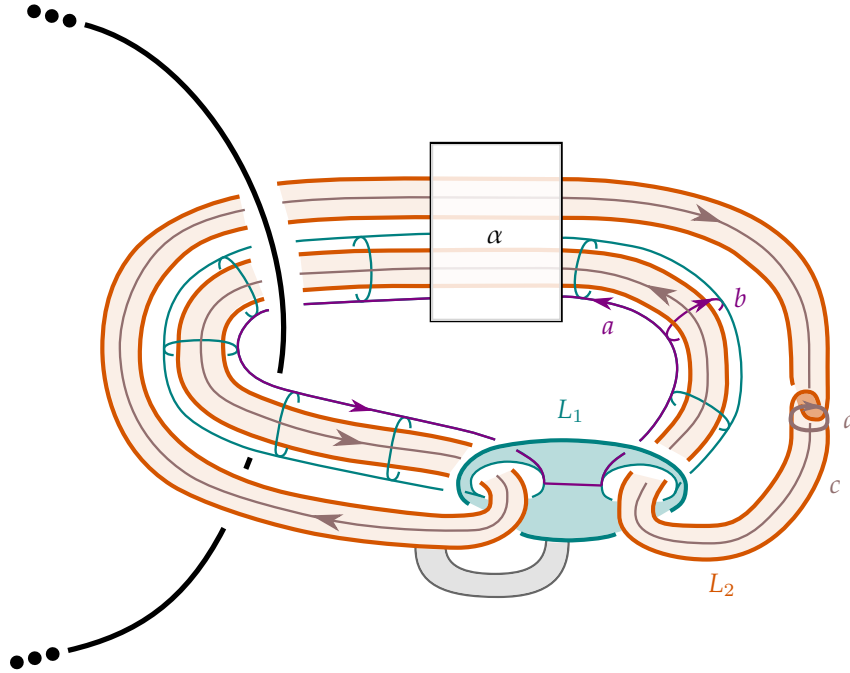


Figure 69. Disjoint Seifert surfaces with a choice of basis for the components of $J = \text{Wh}_{+,1}(\text{BD}(\alpha, 0), 0)$. We illustrate a single 2-handle of X^4 in black on the left, but remember that the curve α might link multiple components of the surgery link.

if B is unimodular, i.e. $\det(B) = \pm 1$. Given a vector of linking numbers $l = (l_1, \dots, l_n) \in \mathbb{Z}^n$, we can construct a loop α as required as follows: Take oriented parallel meridians of the link components, where the number and orientation of the copies is as recorded in the vector, and trivially band sum them in the complement of L so that the result is unknotted in the 3-sphere. Note that given a unimodular matrix B , it is not always possible to find a vector l such that its norm in the quadratic form is $l \cdot B^{-1} \cdot l^T = \pm 1$, for example there are no norm 1 vectors in the Leech lattice of rank 24.

Proof. By undoing the clasp in the Whitehead component, we see that $J = \text{Wh}_{+,1}(\text{BD}(\alpha, 0), 0)$ is link null-homotopic in ∂X . The Brunnian property is easily observed. Moving into the interior of the 0-handle of X amounts to forgetting about the attaching link L of the 2-handles, and since the companion α was unknotted and 0-framed with respect to the 4-ball boundary, without the surgery curves J is an unlink. Thus we find smooth strong slice disks for J in the 0-handle of X .

We draw disjoint Seifert surfaces for the components of J in **Figure 69**, and will now compute the Seifert form of the knot K obtained by trivially band summing the components as shown in the figure. In the Seifert form, the linking numbers are taken in ∂X . The condition on the linking numbers of α with the surgery link arranges the following The \mathbb{S}^3 -framed blackboard pushoff α^{bb} has linking number $\text{lk}_{\partial X}(\alpha, \alpha^{\text{bb}}) = \text{lk}_{\mathbb{S}^3}(\alpha, \alpha^{\text{bb}}) - l \cdot B^{-1} \cdot l^T = k$ with α in the boundary of the 2-handlebody. This is also the framing of the homology basis element a in **Figure 69**. The linking numbers of the other basis elements yield the same answer when computed in \mathbb{S}^3 or in ∂X , and the Seifert form is

$$S = \begin{pmatrix} k & 1 & 0 & 0 \\ 0 & 0 & 1 & 0 \\ 0 & 1 & 0 & 0 \\ 0 & 0 & 1 & 1 \end{pmatrix}$$

with $\det(S + S^T) = -16k + 1$.

The determinant of a knot $K \subset \partial X$ obstructs topological shallow sliceness for ∂X an integral homology sphere, as follows: If $K \subset \partial X$ bounds a topological slice disk in $\partial X \times [0, 1]$ then the Fox-Milnor condition [FM66] (see also [Lic97] in the topologically locally flat case) implies that the Alexander polynomial of K is of the form $\Delta_K(t) = f(t) \cdot f(t^{-1})$ for some integral polynomial $f(t) \in \mathbb{Z}[t]$. In that case, the absolute value of the determinant of K is a perfect square, $|\det(K)| = |\Delta_K(-1)| = |f(-1)|^2$.

Therefore, the link J is not topologically shallow strong slice in $\partial X \times [0, 1]$ for $k \in \mathbb{Z}$ such that $|\det(J)| = |-16k + 1|$ is not a perfect square. \square

COROLLARY 10.7. *Every 2-handlebody X^4 with boundary an integral homology 3-sphere $\neq \mathbb{S}^3$ contains a topologically deep slice link in the boundary, which is Brunnian, link null-homotopic, and a boundary link.*

Proof. Fix a handle decomposition and Kirby diagram of X . By unimodularity of the linking-framing matrix B of X , there has to be a link component with framing non-zero. Then there exists a multiple of its meridian with framing $-l \cdot B^{-1} \cdot l^T = k$ such that $|-16k + 1| \in \mathbb{N}$ is not a perfect square (because the difference between consecutive squares is the n th odd number, and grows larger than the difference $|-16k + 1| - |-16(k + 1) + 1|$). Use this multiple of the meridian as the pattern in Proposition 10.6 to construct the topologically deep slice link. \square

10.2 Topological shallow versus smooth deep slice for links

The difference between the topological and smooth category also manifests itself for deep and shallow slice links. We now construct a topologically shallow slice link whose proper sublinks are smoothly shallow slice, but which itself is smoothly deep slice. I.e. this link as a whole exhibits the difference between smooth and topological deep sliceness, but each component in itself does not.

THEOREM 10.8. *There exists a 2-component link J in the boundary $Y = \partial X$ of the 2-handlebody $X = X_{-1}(T_{2,-3})$ with the following properties:*

- J is not a local link in the boundary;
- J is link homotopic to the split unlink in the boundary;
- J is a boundary link in $Y = \partial X$ (in particular, all Milnor invariants, including the repeating ones, vanish for J);
- J is Brunnian in the boundary, i.e. every proper sublink of J is unlinked and thus smoothly shallow strong slice;
- J bounds smooth strong slice disks in the 2-handlebody X ;
- J is topologically shallow strong slice in $Y \times [0, 1]$;
- J is **not** smoothly shallow strong slice in $Y \times [0, 1]$.

The smooth shallow slice obstruction will be based on a covering link calculus argument, and we quickly introduce this method now. For examples of covering links of iterated Bing doubles see [CK08]. Levine [Lev12] used a covering link argument to show that for a knot $K \subset \mathbb{S}^3$ with $\tau(K) > 0$, the all positive Whitehead double of an iterated Bing double (with at least one Bing doubling iteration) of K is not smoothly slice. By Freedman-Quinn [FQ90, Sec. 11.7], the Whitehead double of any boundary link is topologically slice. Since Bing doubles are boundary links, this implies that the links studied by Levine are topologically slice. Additionally, he observed that the all-positive Whitehead double of the Borromean rings is not smoothly slice.

A *covering move* on a link $L \subset Y$ in a rational homology sphere is a sequence of the following two moves, see for example [CK08]:

- (1) Pass to a sublink $L' \subset L$.
- (2) Choose a component of $L \subset Y$ with trivial self-linking number in Y . Then a prime-power p^n -fold branched cover over this component is a rational homology sphere again, and we consider the preimage L' of the link L in the cover.

If we take a q -fold branched cover over a local unknotted component of $L \subset Y$, the resulting 3-manifold is a q -fold connected sum $\#^p Y$. To see this, think of the local unknot in an \mathbb{S}^3 -summand of $Y \cong \mathbb{S}^3 \# Y$ and remember that a branched cover over an unknot in the 3-sphere is a 3-sphere again, while the connected sum sphere lifts to q -many copies in the cover.

It is a folklore fact that a prime-power branched cover over a null-homologous knot in a rational homology sphere is again a rational homology sphere, see for example [Liv02, Sec. 3]. Branched covering over a slice disk in a rational homology ball yields a rational homology ball again, see for example [Kau87, p. 346] for this standard argument. Our slice disks live in collars $Y \times [0, 1]$, where taking such a branched cover over one of the disks produces a $\mathbb{Q}H(Y \times [0, 1])$ in turn. In particular if a link contained in a rational homology sphere Y is strong CAT slice in a rational homology $Y \times [0, 1]$, and we perform the second covering move on a component L_0 , we can lift the slice disks to the branched cover over the disk of L_0 , and thus obtain a CAT strong slice in a $\mathbb{Q}H(Y \times [0, 1])$. Thus an approach to obstructing smooth sliceness in $Y \times [0, 1]$ for $L \subset Y$ is finding a knot which is a covering link of L and whose sliceness can be obstructed in a rational homology $Y \times [0, 1]$.

We will use that a non-zero τ -invariant is a smooth sliceness obstruction for a knot in a rational homology 4-ball [OS03]; moreover τ is invariant under smooth concordances in $\mathbb{Q}H(\mathbb{S}^3 \times [0, 1])$ [Coc+13, Prop. 4.8]. We want to point to [Rao20] again for more details on the τ -invariants in rational homology 3-spheres, but this generality will not be necessary in our case where the boundaries Y are all integral homology spheres.

Proof of Theorem 10.8. The link in $\partial X = \mathbb{S}_{-1}^3(K)$, $K = T_{2,-3}$ with the required properties is

$$J = \text{Wh}_{+,1}^{(3)}(\text{BD}(\tilde{K}, 0), 0),$$

the 3-fold iterated 0-twisted Whitehead double of the first component of the Bing double of the dual curve \tilde{K} . All the twisting parameters are written in terms of the framing in the boundary of the 0-handle. In the Y -framing, the first Bing double is (+1)-twisted, but the subsequent iterated Whitehead doubles of the first component are 0-twisted in Y because the resulting curves have linking number zero with the surgery link, as explained in Remark 9.13.

Most of the properties of J follow from variations of previous arguments, which we quickly summarize now: The non-localness can be confirmed from the JSJ-decomposition of the complement as in Proposition 9.20, while an explicit link null-homotopy comes from unclasping the iterated Whitehead doubled component, compare Figure 52. To check the boundary link property we can find Seifert surfaces similar to the ones in Figure 69, which are of genus 1 for both components. The link J is Brunnian in the boundary, and also becomes unlinked when forgetting the surgery curve, where we can now observe the smooth slice disks in the 0-handle. Additionally, as in the proof of Lemma 9.16, the 3-fold Whitehead doubled component bounds a height three untwisted Casson tower with a single positive self-intersection in each stage, which contains a topological slice disk for that component in $Y \times [0, 1]$. This slice is disjoint from the surgery curve and the other Bing component, which can be capped off with its own slice disk in the product.

To complete the argument, we construct a covering link where we double branch cover over the second, non-Whitehead doubled component L_2 of the Bing double, as in Figure 70. For clarity of exposition,

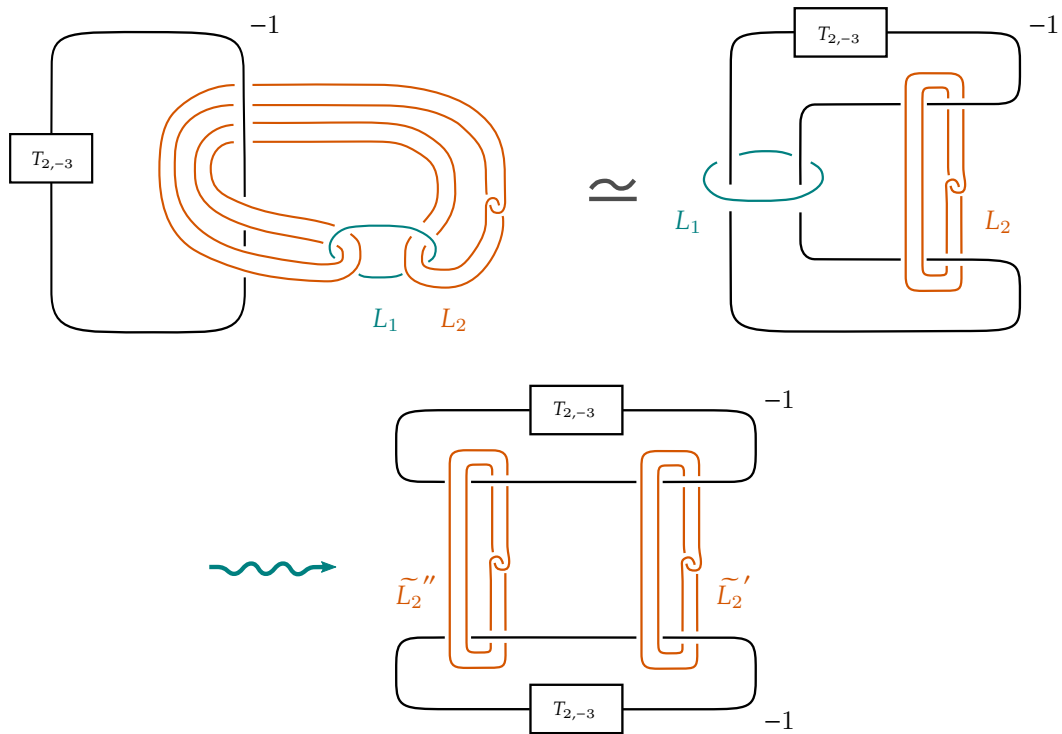


Figure 70. **Top row:** Isotopy of the link and surgery curve. **Bottom row:** Double branched cover over the component L_1 . The surgery coefficients are -1 for both lifts of the trefoil because the surgery curve does not have a self-clasp.

we will first compute a covering link of $\text{Wh}_{+,1}(\text{BD}(\tilde{K}, 0), 0)$, and explain how the additional iterated Whitehead doubles fit into the picture later. Since the branching component is a local unknot, the cover is $Y \# Y$, which we can draw explicitly by the lifted surgery description in the figure. Forget one of the lifts \tilde{L}_1' of the Whitehead component. The remaining lift \tilde{L}_1'' is a Whitehead double of the connected sum $(Y, \tilde{K}) \# (Y, \tilde{K})$ of two dual curves in the Poincaré sphere Y . By additivity this companion has $\tau((Y, \tilde{K}) \# (Y, \tilde{K})) = \tau(Y, \tilde{K}) + \tau(Y, \tilde{K}) = 2$, and we can compute the framing of the blackboard pushoff via Hoste's formula in [Remark 9.11](#) as $+2$. Using Hedden's formula [Theorem 9.8](#) we are in the case $+2 = t < 2\tau((Y, \tilde{K}) \# (Y, \tilde{K})) = +4$, which tells us that the framing of the lift of the Whitehead double is equal to $+1$.

In particular, this lift of the Whitehead curve cannot be smoothly slice in a rational homology $Y \times [0, 1]$. Now returning to the link $J = \text{Wh}_{+,1}^{(3)}(\text{BD}(\tilde{K}, 0), 0)$ which originated from further Whitehead doubles, these will lift in the double branched cover over L_2 to give iterated Whitehead doubles \tilde{L}_1'' . All of these are zero twisted both with respect to the blackboard framing in the boundary of the 0-handle, and also in $Y \# Y$. Therefore another application of Hedden's formula tells us the τ -invariant of the iterated doubles is equal to $+1$, obstructing them from being slice in a $\text{QH}(\mathbb{S}^3 \times [0, 1])$ as well. This is our contradiction to the shallow strong sliceness of the link J . \square

We can obtain infinitely many 2-component examples in $X_{-1}(T_{2,-3})$ by further iterating the Whitehead double. With each additional Whitehead double, the properties of the link are preserved for the same reasons as outlined in the proof of [Theorem 10.8](#). The additional Whitehead doubling steps lift to the covering link, thus we apply Hedden's formula iteratively again and again, computing the τ -invariant of the lift to be equal to $+1$. There are various other directions in which the theorem might generalize:

Question 10.9. Do such links as in [Theorem 10.8](#) exist in the boundary of every 2-handlebody?

Again this question can be split into two cases, for simply connected boundaries and non-simply connected boundaries. Additionally in our argument, we used both the computation of the τ -invariant of the dual knot in $\mathbb{S}_{-1}^3(T_{2,-3})$, and the \mathbb{ZHS}^3 L-space condition for the Whitehead double τ -computation, so the argument appears to be specific to the Poincaré sphere for now.

Question 10.10. Are there n -component examples with the properties as in [Theorem 10.8](#) for every $n \in \mathbb{N}$?

It appears possible, but technically challenging, to emulate an iterated covering link argument as in [\[CK08; Lev12\]](#). We can use the band move trick from the Bing to the Whitehead double in [Figure 68](#) to make a 3-component example by Bing doubling the iterated Whitehead component. This is still link homotopic to the unlink, since we Bing doubled a component with Whitehead pattern and we can link-homotope its clasp away with a band pass. The boundary link and Brunnian properties are preserved. It is topological shallow strong slice by Bing doubling the shallow disk for the Whitehead component; and smooth strong slice in the 2-handlebody by Bing doubling the smooth disk. The framing is zero both in 4-ball boundary and in Y because we had a Whitehead companion. The link is not smoothly shallow strong slice, because if so we could band together Bing components to go to Whitehead double of the Whitehead component. One more iteration of Hedden’s formula shows that the τ -invariant is equal to $+1$ for the resulting link component as well, which gives the smooth slice obstruction.

11 THE NORMAN-SUZUKI-TRICK AND UNIVERSAL SLICING PROBLEMS

The following paragraphs are reproduced from [\[KR21\]](#). As a convention until the end of this section, properly embedded slice disks $\Delta^2 \subset X^4$ in a 4-manifold are always required to be null-homologous, i.e. we only consider H -slice disks as in [Definition 7.1](#). We will still add the qualifier “ H -slice” in the statements to emphasize this point. For slicing in arbitrary 4-manifolds, we here restrict to null-homologous disks to exclude constructions as in the Norman-Suzuki trick. Since our obstructions work in the topologically locally flat category, we will formulate everything in this more general setting.

One approach to studying sliceness of a knot K in \mathbb{D}^4 is approximating the 4-ball by other 4-manifolds X^4 . By restricting to simply connected 4-manifolds X and fixing an intersection form this gives rise to various filtrations of the knot concordance group, notably the (n) -solvable filtration \mathcal{F}_n of Cochran-Orr-Teichner [\[COT03\]](#) and its positive and negative variants $\mathcal{P}_n, \mathcal{N}_n$ [\[CHH13\]](#).

Recall the discussion of slice disk constructions in [Section 9](#). In view of $(\mathbb{S}^2 \times \mathbb{S}^2)^\circ$ where every knot in the boundary bounds a disk (which is rarely null-homologous) and $(\#^p \mathbb{C}\mathbb{P}^2 \#^q \overline{\mathbb{C}\mathbb{P}^2})^\circ$, in which we find plenty of null-homologous disks (but only know how many summands p, q we need after fixing a knot on the boundary) a natural question concerns the existence of a *universal slicing manifold*. Is there a fixed compact, smooth, oriented 4-manifold V^4 with $\partial V = \mathbb{S}^3$ such that any knot $K \subset \mathbb{S}^3$ is slice in V via a null-homologous disk? It turns out that a signature estimate shows such a universal solution cannot exist.

THEOREM 11.1 ([\[KR21\]](#)). *Every compact oriented topological 4-manifold V^4 with $\partial V = \mathbb{S}^3$ contains a knot in its boundary that is not topologically H -slice in V^4 .*

If we relax the H -slice requirement, this leads to interesting open questions. Yasuhara [\[Yas91\]](#) observes that the torus knot $T_{2,-15}$ is not slice in $\mathbb{C}\mathbb{P}^2$, where there is no restriction on the homology class of the disk. Based on this, Manolescu-Marengon-Piccirillo [\[MMP20, Qn. 6.1\]](#) ask whether there is a knot which is not slice (again no assumption on homology class) in an indefinite 4-manifold, such as the K3 surface.

Remark 11.2. In a punctured infinite connected sum of projective planes

$$\mathbb{D}^4 \#^\infty (\mathbb{C}\mathbb{P}^2 \# \overline{\mathbb{C}\mathbb{P}^2})$$

we can slice every knot, but this is not compact. But for every fixed knot on the boundary its compact slice disk is contained in a finite stage

$$\mathbb{D}^4 \#^k \mathbb{C}\mathbb{P}^2 \#^l \overline{\mathbb{C}\mathbb{P}^2} \# \mathbb{D}^4 \subset \mathbb{D}^4 \#^\infty (\mathbb{C}\mathbb{P}^2 \# \overline{\mathbb{C}\mathbb{P}^2}).$$

The remainder of this section is concerned with a proof of [Theorem 11.1](#). As preparation, let us specialize a result [[CN20](#), Thm. 3.8], which is a generalization of the Murasugi-Tristram inequality for links bounding surfaces in 4-manifolds, to the case of knots. Here $\sigma_\omega(K)$ is the *Levine-Tristram signature* of the knot K , defined as the signature of the hermitian matrix $(1 - \omega)V + (1 - \overline{\omega})V^T$, where V is a Seifert matrix of K and ω a unit complex number not equal to 1. References for the knot signature include [[Lev69](#)], [[Tri69](#)] and the recent survey [[Con21](#)]. The following inequality only holds for specific values of ω , and will adopt the notation \mathbb{S}_1^1 for unit complex numbers $\omega \in \mathbb{S}^1 - \{1\}$ which do not appear as a zero of an integral Laurent polynomial $p \in \mathbb{Z}[t, t^{-1}]$ with $p(1) = \pm 1$.

THEOREM 11.3 ([[CN20](#), Special case of Thm. 3.8]). *Let X be a closed oriented topological 4-manifold with $H_1(X; \mathbb{Z}) = 0$. If $\Sigma \subset (\mathbb{S}^3 \times [0, 1]) \# X$ is a null-homologous topological cobordism between two knots $K \subset \mathbb{S}^3 \times \{0\}$ and $-K' \subset -(\mathbb{S}^3 \times \{1\})$, each contained in one of the two boundary component \mathbb{S}^3 's of $(\mathbb{S}^3 \times [0, 1]) \# X$, then*

$$|\sigma_{K'}(\omega) - \sigma_K(\omega) + \text{sign}(X)| - \chi(X) + 2 \leq -\chi(\Sigma)$$

for all $\omega \in \mathbb{S}_1^1$.

For $K \subset \partial X^\circ$ which is H -slice in X and Σ an annulus, we can further simplify:

COROLLARY 11.4. *Let X be a closed topological 4-manifold with $H_1(X; \mathbb{Z}) = 0$. If the knot $K \subset \mathbb{S}^3$ is topologically H -slice in X° then for $\omega \in \mathbb{S}_1^1$ we have*

$$|\sigma_K(\omega) + \text{sign}(X)| - \chi(X) + 2 \leq 0$$

To prove [Theorem 11.1](#) it will be enough to obstruct the sliceness of a single knot in the boundary. The strategy is to first use surgery to trivialize H_1 , then pick the knot K in the original manifold boundary and arrive at a contradiction to [Corollary 11.4](#) in the surgered manifold if K started out H -slice.

Proof of [Theorem 11.1](#). Let V be a compact topological 4-manifold with boundary \mathbb{S}^3 , we want to find a knot in its boundary which is not H -slice. Pick a set of disjointly embedded loops $\gamma_1, \dots, \gamma_l$ in V whose homology classes generate $H_1(V)$. If V already satisfies $H_1(V) = 0$, set $l = 0$ for the remainder of the proof and omit the surgery altogether. Let K be a knot in \mathbb{S}^3 whose signature (at the unit complex number $\omega = -1$) satisfies

$$|\sigma_K(-1)| \geq |\text{sign}(V)| + |\chi(V)| + 2l.$$

Note that the constant on the right hand side only depends on the signature, Euler characteristic, and number of generators of $H_1(V)$, and not on the knot K . For example, since signature is additive under connected sum, the self-sum $K_n = \#^n K$ with n large enough has arbitrarily high signature at $\omega = -1$ if we start with a K that has positive signature $\sigma_K(-1)$ (for example, taking K to be the left-handed trefoil knot).

Suppose that K is slice in V via a null-homologous disk Δ . Being null-homologous in the relative second homology group means geometrically that there is a locally flat embedded 3-manifold M^3 with boundary the slice disk Δ union a Seifert surface for K in the boundary \mathbb{S}^3 , see [[Lic97](#), Lem. 8.14]. We can remove the closed components from M , what remains is a 3-manifold with non-empty boundary in V . Generically the embedded circles $\gamma_1, \dots, \gamma_l$ will intersect the 3-manifold M in points, but we can push these intersection

points off the boundary of M via an isotopy of the curves in V . We will still keep the notation $\gamma_1, \dots, \gamma_l$ for the isotoped curves which are now disjoint from M . Essentially, this finger move supported in a neighborhood of M is guided by pairwise disjoint arcs in M connecting the intersections points to the boundary.

Perform surgery on the loops $\gamma_1, \dots, \gamma_l$, i.e. for each γ_i remove an open tubular neighborhood $\nu(\gamma_i) \cong \mathbb{S}^1 \times \text{int } \mathbb{D}^3$ and glue copies of $\mathbb{D}^2 \times \mathbb{S}^2$ to the new $\mathbb{S}^1 \times \mathbb{S}^2$ boundary components via the identity map $\mathbb{S}^1 \times \mathbb{S}^2 \rightarrow \mathbb{S}^1 \times \mathbb{S}^2$. After this surgery we have a compact 4-manifold V' with $H_1(V') = 0$, and the original disk Δ survives into V' in which we will call it Δ' . Observe that this ‘new’ disk Δ' is still null-homologous in V' , since the 3-manifold is still present after the surgery. Each circle surgery in a 4-manifold increases the Euler characteristic by 2, thus $\chi(V') = \chi(V) + 2l$. By construction, the 4-manifolds V and V' are cobordant, and so their signatures $\text{sign}(V') = \text{sign}(V)$ agree.

Starting with a knot K with large enough signature, if there existed a null-homologous Δ' , since $H_1(V') = 0$ we would have

$$|\sigma_K(-1) + \text{sign}(V')| - \chi(V') + 2 = |\sigma_K(-1) + \text{sign}(V)| - (|\chi(V)| + 2l) + 2 > 0$$

which contradicts the inequality in [Corollary 11.4](#). Therefore the H -slice Δ for K cannot exist. \square

Remark 11.5. Earlier sources for results in the smooth category include Gilmer and Viro’s [\[Gil81\]](#) version of the Murasugi-Tristram inequality for the classical signature as stated in [\[Yas96, Thm. 3.1\]](#). Our preference for using [\[CN20\]](#) in the proof of [Theorem 11.1](#) comes from the result being stated in the topological locally flat category.

12 CONCLUSION AND OPEN QUESTIONS RELATED TO DEEP SLICENESS

In [Theorem 9.27](#) we found infinitely many non-local knots in the boundary of $X_{+1}(K)$ exhibiting the difference between topological and smooth deep sliceness. We can trivially extend this to an infinite family in infinitely many 2-handlebodies, by taking a boundary connected sum $(X_{+1}(K), J_{p,1}) \natural (X', U)$ with a local unknot $U \subset \partial X'$ in the boundary of another 2-handlebody. This connected sum has no influence on the topological shallow sliceness and the smooth deep slice disk. Moreover, since the τ -invariant is additive under connected sums, it still obstructs deep shallow sliceness of the knot $J_{p,1} = J_{p,1} \# U \subset \partial X_{+1}(K) \# \partial X'$. The examples are still non-local, as can be seen from a similar cut-and-paste argument now including the connected sum sphere as a piece of the decomposition.

In particular, by taking $X' = (-X_{+1}(K), U)$ we find infinitely many smoothly deep and topologically shallow slice knots in the boundary $\mathbb{S}_{+1}^3 \# -\mathbb{S}_{+1}^3$ of the integral homology 4-ball $X_{+1}(K) \natural -X_{+1}(K)$.

Recent work of Manolescu-Marengon-Piccirillo [\[MMP20\]](#) investigates H -sliceness in indefinite 4-manifolds. For example, in [\[MMP20, Cor. 1.7\]](#) they observe that there exists a knot $K_{\text{DV}} \subset \mathbb{S}^3$ (originally constructed by Donald-Vafaee [\[DV16\]](#)) which is topologically shallow H -slice in a bounded punctured K3-surface X , but is not smoothly H -slice in X . Iida-Mukherjee-Taniguchi [\[IMT22\]](#) improved this by building an infinite family which are topologically shallow H -slice, not smoothly H -slice in X , but which are smoothly slice in X , i.e. these are local examples of topologically shallow and smoothly deep slice knots in a bounded punctured K3-surface X .

In [Theorem 8.1](#), we found smoothly deep slice knots in the boundary of every 2-handlebody. It would be interesting to find an example for the difference between smooth and topological deep sliceness in every 2-handlebody as well.

Question 12.1. Does every 2-handlebody whose boundary is not a 3-sphere contain a non-local topologically shallow and smoothly deep slice knot in its boundary?

Freedman's theorem on iterated Whitehead doubles is a powerful way to construct topological slices in collars of the boundary. This technique shows for any curve in the boundary of the 2-handlebody, its 3-fold iterated Whitehead double is topologically shallow slice. But extending our results from [Section 9](#) obstructing the smooth shallow sliceness runs into two problems: There is an absence of example of knots in 3-manifolds with non-trivial τ -invariant. Additionally, it is not clear how to generalize Hedden's Whitehead doubling formula [Theorem 9.8](#) and Hom's satellite formula [Theorem 9.25](#) if the 3-manifold containing the knots is not an integral homology 3-sphere or an L-space.

Another interesting direction for further study is the difference between shallow and deep slice links, as started in [Section 10](#), where additional variations of the questions are possible, e.g. by distinguishing weak and strong sliceness.

PART III

TRISECTING GROUPS OF KNOTTED SURFACE COMPLEMENTS

In this part, we study smoothly embedded surfaces in bridge position in a trisected 4-manifold from a group-theoretic perspective. The algebraic decomposition of the fundamental group of the complement contains comprehensive information about the bridge trisection of the surfaces.

We will begin [Section 13](#) by rapidly recalling the terminology of trisections of smooth closed 4-manifolds. This way of decomposing smooth 4-manifolds into a triple of 4-dimensional 1-handlebodies was introduced by Gay and Kirby [[GK16](#)]. Then, inspired by the Abrams-Gay-Kirby [[AGK18](#)] group trisections for closed smooth 4-manifolds, we will introduce group trisections for knotted surfaces in bridge position.

As an interlude in [Section 14](#), we will recap the setup and main result of the forthcoming article [[BKKLR22](#)], which is joint work in progress with Sarah Blackwell, Rob Kirby, Michael Klug and Vincent Longo. This extends the theory of group trisections of closed 4-manifolds to bridge trisected knotted surfaces in trisected 4-manifolds. In the simplest setting of bridge trisected surfaces in the genus 0 trisection of the 4-sphere, this sets up a map from group trisections of knotted surface type to bridge trisections of surfaces.

The remaining sections contain computational results, partly obtained by using the author's SageMath module [[Rup21a](#)], whose main functions are documented in [Section 15.2](#). Using the triplane diagrams for twist-spun knots in [[MZ17](#)], we calculate the group trisections of certain twist spins of torus knots in [Section 16](#). We continue by finding bridge positions of Suciuc's ribbon 2-knots R_k in [Section 17](#), and discuss the resulting group trisections. In particular, the group trisections of the members of Suciuc's family all correspond to the trefoil knot group, but are not isomorphic as group trisections of knotted surface type.

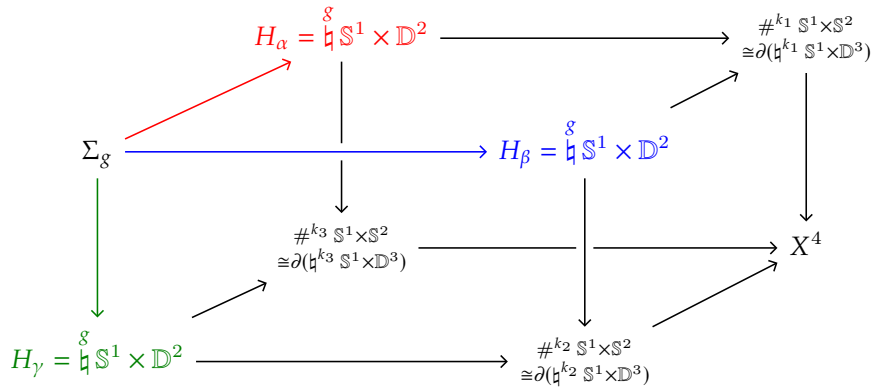


Figure 71. The pieces in the definition of a (parameterized) trisection of X^4 as a diagram of topological spaces.

13 GROUP TRISECTIONS OF CLOSED 4-MANIFOLDS AND BRIDGE TRISECTIONS

A *trisection* of a smooth compact orientable closed 4-manifold is a decomposition into three standard 4-dimensional 1-handlebodies

$$X = X_1 \cup X_2 \cup X_3$$

with conditions on the pairwise and triple overlaps as follows. The 4-dimensional 1-handlebodies are diffeomorphic to the boundary connected sums $X_i \cong \natural^{k_i} \mathbb{S}^1 \times \mathbb{D}^3$, with triple intersection $X_1 \cap X_2 \cap X_3 \cong \Sigma_g$ the *central genus g surface*, or *core*, of the trisection. Further, the pairwise intersections $X_i \cap X_{i+1} \cong \natural^g \mathbb{S}^1 \times \mathbb{D}^2$ (the indices taken modulo 3) are 3-dimensional handlebodies. For each i , the pairwise union of the 3-dimensional handlebodies adjacent to X_i makes up a Heegaard splitting of $\partial X_i \cong \#^{k_i} \mathbb{S}^1 \times \mathbb{S}^2$. The pieces of a trisection, together with the gluing information, are illustrated in the commutative cube of topological spaces in Figure 71.

Gay-Kirby [GK16] show that every closed connected oriented 4-manifold has a trisection, which is unique up to a stabilization operation that increases the genus of the central surface and of the handlebodies. We only consider balanced trisections where $k = k_1 = k_2 = k_3$. This is without loss of generality since every trisection can be made balanced by enough stabilizations. The most important example for us is the unique genus 0 trisection of the 4-sphere, which we can describe using the standard open book decomposition of \mathbb{S}^4 with binding an unknotted \mathbb{S}^2 and whose pages are 3-balls, as follows: Cut the 4-ball into the three sectors consisting of the union of pages

$$X_1 = \mathbb{D}^3_{[0, \frac{2\pi}{3}]}, X_2 = \mathbb{D}^3_{[\frac{2\pi}{3}, \frac{4\pi}{3}]} \text{ and } X_3 = \mathbb{D}^3_{[\frac{4\pi}{3}, 0]}.$$

Their pairwise intersections are in the extremal 3-ball pages, unions of which give genus 0 Heegaard splittings of the 3-sphere.

Bridge trisections are a 4-dimensional generalization of bridge splittings of links in 3-manifolds. A *bridge splitting* of a link in a 3-manifold is a decomposition of the link into an endpoint union of a pair of trivial tangles in handlebodies. A *genus g handlebody H* is a compact oriented 3-manifold whose boundary is a oriented closed genus g surface, with the property that H can be cut along properly embedded 2-dimensional disks such that the resulting space is a collection of 3-dimensional balls; in particular, a 3-ball $B \cong \mathbb{D}^3$ is a handlebody. A *b -bridge trivial tangle T* in a handlebody H is a collection of b properly embedded arcs in H such that all of the arcs can be simultaneously isotoped into the boundary of H , while fixing ∂T . Given two handlebodies containing trivial tangles (H_1, T_1) and (H_2, T_2) with the

property that $\partial H_1 = \partial H_2$ and $\partial T_1 = \partial T_2$, we say that (H_1, T_1) and (H_2, T_2) are *equivalent* if there exists a diffeomorphism $H_1 \rightarrow H_2$ mapping T_1 to T_2 that is the identity on ∂H_1 .

A *bridge trisection* of a smoothly embedded closed surface³⁹ $F \subset \mathbb{S}^4$ is a decomposition into a union of three trivial 2-disk systems,

$$(\mathbb{S}^4, F) = (X_1, D_1) \cup (X_2, D_2) \cup (X_3, D_3),$$

where the pairwise and triple intersections are required to be of a special form, as we now explain. The $X_i \cong \mathbb{D}^4$ are the 4-balls of the previously discussed trisection of \mathbb{S}^4 , and each $D_i: \coprod^{c_i} \mathbb{D}^2 \hookrightarrow \mathbb{D}^4$ is a properly embedded *trivial disk system*. Trivial means that the disks are simultaneously isotopic into the 3-dimensional boundary ∂X_i , fixing the boundary ∂D_i point-wise. The boundary of the disks is further assumed to be an endpoint-union of b -bridge trivial tangles in 3-balls, each tangle living in one half of the boundary $\partial X_i \cong \mathbb{D}^3 \cup_{\mathbb{S}^2} \mathbb{D}^3$. These tangles are usually called the α -, β - and γ -tangle, and each pairwise endpoint-union $T_\mu \cup_\partial T_\nu$ forms an unlink $\mathcal{U}_{\mu \cup \nu}$ in one of the 3-spheres $\partial X_i \cong \mathbb{S}^3$. The bridge trisection has four parameters $(b; c_1, c_2, c_3)$, where b is the *bridge number*, and c_i is the number of trivial disks in the disk system of that sector, which is sometimes called the *patch number*.

The pieces of a bridge trisection and their interactions are illustrated in the commutative cube of pairs of topological spaces in [Figure 72](#). These bridge trisections exist more generally for every smoothly knotted, not necessarily orientable surface embedded in a trisected connected orientable closed smooth 4-manifold [\[MZ18\]](#). In this thesis, we will only study knotted surfaces in the standard genus 0 trisection of the 4-sphere, as in the original bridge trisection paper [\[MZ17\]](#).

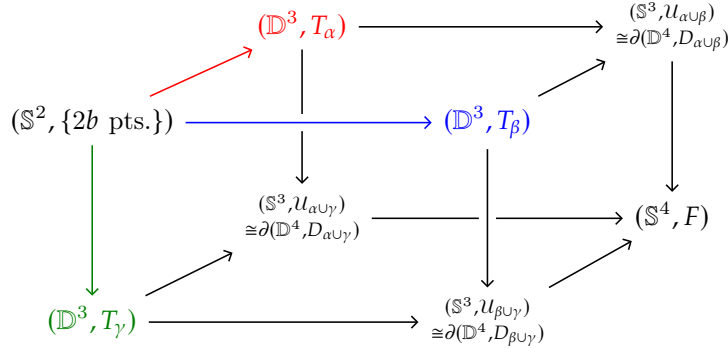


Figure 72. The pieces of a (parameterized) b -bridge trisection of a smoothly embedded closed surface F in the 4-sphere, as a commutative cube of pairs of topological spaces.

13.1 Definition of group trisections of knotted surface type

Convention (Basepoints). We once and for all choose a basepoint $*$ in the standard genus g oriented surface Σ_g . This basepoint choice on the central surface of the trisection of a closed manifold (or on the bridge surface of a bridge trisection, where $*$ should lie in the complement of the bridge points) will induce basepoints for all the other pieces of the decomposition. In the following, we usually will not indicate the basepoint in the various fundamental groups of the spaces involved.

Let $(\mathbb{D}^2, \{p_1, \dots, p_{2b}\}, *)$ be the unit disk with $2b$ marked points p_i and a basepoint $* \in \partial \mathbb{D}^2$ in the complement of the marked points. By taking the quotient which crushes the boundary to a point, we obtain the genus 0 oriented surface \mathbb{S}^2 with basepoint $*$ and marked points p_1, \dots, p_{2b} as in [Figure 73](#). We will fix once and for all this based model for a 2-sphere with $2b$ marked points.

³⁹ The surface F may be disconnected or non-orientable.

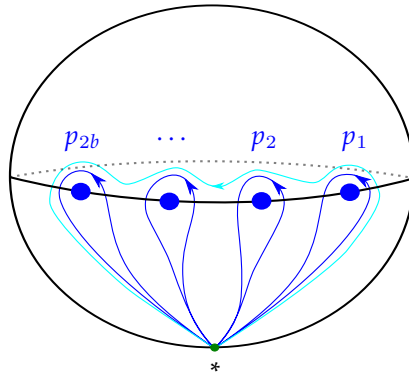


Figure 73. Sphere with $2b$ marked points p_1, \dots, p_{2b} and an associated system of generators (dark blue) for $\pi_1(\mathbb{S}^2 - p_1, \dots, p_{2b}, *)$, the fundamental group of the complement of the punctures, with the relation $p_1 \cdots p_{2b} = 1$ (light blue).

With this basepoint convention in place, a *parameterized trisection* is a trisection with fixed diffeomorphisms from its pieces to the *standard models* respecting the basepoint and inclusions. This means there are identifications from the sectors $(X_i, *)$ to $(\mathfrak{h}^k \mathbb{S}^1 \times \mathbb{D}^3, *)$, from the 3-dimensional handlebodies $(X_i \cap X_{i+1}, *)$ to $(\mathfrak{h}^8 \mathbb{S}^1 \times \mathbb{D}^2, *)$ and from $(X_1 \cap X_2 \cap X_3, *)$ to $(\Sigma_g, *)$. Similarly, a *parameterized bridge trisection* is a bridge trisection with fixed identifications of $(X_1, D_1, *) \cap (X_2, D_2, *) \cap (X_3, D_3, *)$ with the standard model of the central surface $(\mathbb{S}^2, \{p_1, \dots, p_{2b}\}, *)$, of the pairwise overlaps $(X_i, D_i, *) \cap (X_{i+1}, D_{i+1}, *)$ with the standard model of a trivial tangle in the 3-ball $(\mathbb{D}^2 \times \mathbb{D}^1, \{p_1, \dots, p_{2b}\} \times \mathbb{D}^1)$, and of the patches $(X_i, D_i, *)$ with the standard trivial disk system in the 4-ball $(\mathbb{D}^2 \times \mathbb{D}^1 \times \mathbb{D}^1, \{p_1, \dots, p_{2b}\} \times \mathbb{D}^1 \times \mathbb{D}^1)$.

These parametrizations are equivalent to compatible choices of *spines* for each handlebody or tangle complement. Here a spine is an embedded graph that the handlebody or tangle complement deformation retracts to. After fixing a handle decomposition, an efficient way to construct a spine is by connecting the cores of the 1-handles to a common point in the interior of the 0-handle, which yields a wedge of circles. After picking orientations of the edges we can naturally choose generators of the fundamental groups as loops that start at the common point and traverse each lobe of the wedge in the positive direction. We comment on the spines for tangle complements further in [Lemma 14.2](#), see also the lecture notes [\[Joh06\]](#) and [\[Isl21, Sec. 3\]](#).

On \mathbb{S}^2 we choose a simple system of rays r_i , connecting $*$ to each point in $\{p_1, \dots, p_{2b}\}$, and indexed so that a small circle around $*$ oriented by the 2-sphere intersects the r_i in order of increasing subscripts.⁴⁰ The choice of arcs $\{r_i\}$ and orientations identifies generators of $\pi_1(\mathbb{S}^2 - \{p_1, \dots, p_{2b}\}, *)$, where each generator corresponds to a loop that runs out along r_i , goes around the endpoint p_i in a positive direction, and returns along the arc r_i . We abuse notation and let p_1, \dots, p_{2b} also denote these fundamental group elements. Then we have

$$\pi_1(\mathbb{S}^2 - \{p_1, \dots, p_{2b}\}, *) = \langle p_1, \dots, p_{2b} \mid p_1 \cdots p_{2b} = 1 \rangle.$$

This is a free group on $2b - 1$ generators, but picking out these free generators involves an arbitrary choice of basis that we want to avoid.

Let $F \subset \mathbb{S}^4$ be a smoothly embedded connected orientable or non-orientable surface in the 4-sphere. Groups of the form $\pi_1(\mathbb{S}^4 - F, *)$ are called *knotted surface groups*. Put the surface F into bridge trisected position. We can use the Seifert-van Kampen theorem to describe how the groups of the complements of the bridge trisection pieces assemble into the group of the complement of the surface, which leads to

⁴⁰ This is also known as a Hurwitz arc system [\[Kam02, Sec. 2.3\]](#) and is a standard method of fixing generators for the fundamental group of punctured genus 0 surfaces (potentially with boundary).

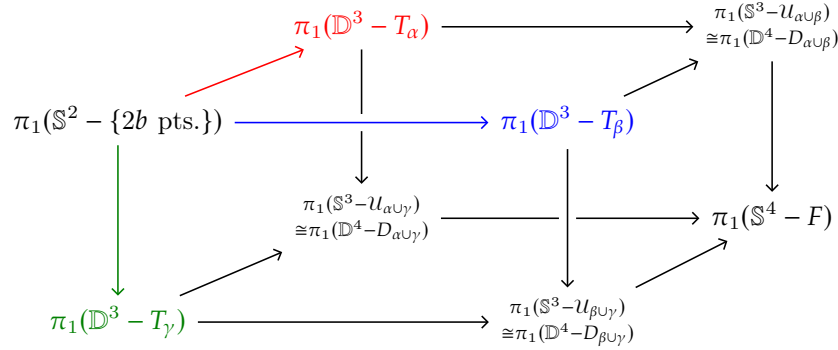


Figure 74. Applying the Seifert-van Kampen theorem to obtain three compatible decompositions of the knot group. The resulting diagram is a commutative cube of surjective group homomorphisms such that each face is a pushout.

the commutative cube of group homomorphisms in [Figure 74](#). Note that all of the topological spaces are implicitly based at $*$ as in the convention; also compare with the set-up in [[Jos+21](#), Sec. 4]. In the case of a parameterized bridge trisection, we can identify explicit bases for the various free groups appearing in the corners of the group trisection cube by determining them on the standard models. This is a justification for the diagram in the definition of group trisections of knotted surface type in [Figure 75](#). First we include some additional motivation, highlighting the difficulty of using the fundamental group for studying knotted surfaces.

In the 3-sphere, the knot group, together with the peripheral information⁴¹ of the conjugacy classes of a positively oriented longitude and a meridian, determines the isotopy type of a classical knot $\mathbb{S}^1 \hookrightarrow \mathbb{S}^3$ [[Wal68](#); [GL89](#)].

Knotted surfaces in the 4-sphere exhibit more complicated behavior. In particular, there are many cases in which the group of the complement of a surface does not determine the smooth isotopy class of the knotted surface. As a sampler, we discuss certain twist-spun torus knots in [Section 16](#) and Suciú’s ribbon 2-knots R_k in [Section 17](#). For an example with positive genus, there exist infinitely many stabilizations of the 6-twist spun trefoil $\tau^6 T_{2,3}$ which share the same group but are all mutually non-isotopic [[KK94](#)]. There even exist pairs of non-isotopic knotted surfaces of arbitrary genus with isomorphic knot quandles [[Tan07](#)], thus with isomorphic groups and the same conjugacy class of a meridian.

It is known that for knotted 2-spheres in the 4-sphere, there are at most two non-equivalent⁴² knots which share homeomorphic exteriors, and these knots appear from the exterior by re-gluing $\mathbb{S}^2 \times \mathbb{D}^2$ along a map $\mathbb{S}^2 \times \mathbb{S}^1 \rightarrow \mathbb{S}^2 \times \mathbb{S}^1$ of the boundary. This gluing map might differ by a Gluck twist, and there are known cases where this leads to equivalent knots, as well as cases where the results are non-equivalent [[Gor76](#)]. Examples of non-equivalent n -knots $\mathbb{S}^n \hookrightarrow \mathbb{S}^{n+2}$ with homeomorphic exterior for ambient dimension $n + 2 \geq 5$ were already constructed in [[CS76](#)].

Our motivation for introducing *group trisections of knotted surface type* is defining a stronger algebraic invariant that, additionally to the fundamental group of the complement $\pi_1(\mathbb{S}^4 - F)$, contains a decomposition of the group into free groups reflecting the data of a bridge trisection. Compare this with the main result for group trisections of closed 4-manifolds [[AGK18](#)]: For a given finitely presented group G there are infinitely many closed smooth compact orientable 4-manifolds with fundamental group isomorphic to G , but a group trisection of G determines a unique parameterized trisection and in turn a unique smooth 4-manifold.

We first define an algebraic version of the map induced by a trivial tangle on fundamental groups. Additional justification for this definition is given in [Lemma 14.2](#).

⁴¹ Recall the definition of peripheral subgroups in [Definition 3.5](#).

⁴² Here, two smooth knots are called *equivalent* if there is a diffeomorphism of \mathbb{S}^4 taking one to the other.

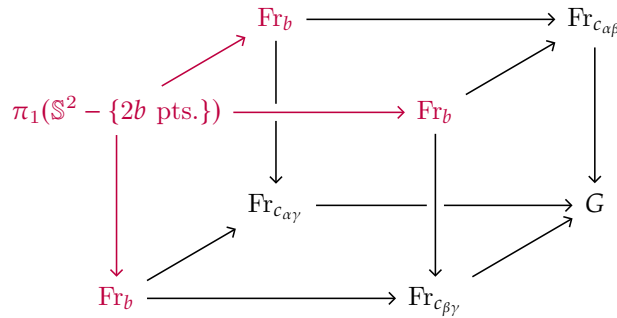


Figure 75. Definition of a group trisection of knotted surface type.

Definition 13.1 (Trivial tangle homomorphism). A *trivial tangle homomorphism* is an epimorphism from a punctured sphere group to a free group

$$\phi: \pi_1(\mathbb{S}^2 - \{p_1, \dots, p_{2b}\}, *) \rightarrow \langle t_1, \dots, t_b \rangle$$

with a fixed choice of basis, such that the homomorphism satisfies the following property. Each p_i maps to a conjugate of one of the $t_j^{\pm 1}$, where each of t_j and its inverse t_j^{-1} appears exactly once as the central letter in the cancellation-free word in the free group describing p_i 's image. More precisely, there exists a bijection

$$f: \{p_1, \dots, p_{2b}\} \rightarrow \{t_1, t_1^{-1}, \dots, t_b, t_b^{-1}\}$$

and there exist group elements $g_i \in \langle t_1, \dots, t_b \rangle$ with $\phi(p_i) = g_i f(p_i) g_i^{-1}$.

In the upcoming discussion, the p_i are the generators around the punctures, while the t_i are tangle complement generators. For an example of a trivial tangle homomorphism, see Equation (15.1) (here indexing starts at 0, and the p_i are renamed to x_i , and t_i are renamed to a_i).

Example 13.2 (Non-example). Consider the following map with $b = 2$.

$$\begin{aligned} \langle p_1, p_2, p_3, p_4 \mid p_1 p_2 p_3 p_4 = 1 \rangle &\rightarrow \langle t_1, t_2 \rangle \\ p_1 &\mapsto t_1^2 \\ p_2 &\mapsto t_1^3 \\ p_3 &\mapsto t_2 \\ p_4 &\mapsto t_2^{-1} t_1^{-5} \end{aligned}$$

The map is surjective, since $p_2^{-1} p_1$ and p_3 map to generators of the co-domain. But it does not satisfy the conjugate condition on a trivial tangle homomorphism. This can already be observed from the homological information obtained by abelianizing the map. For example, in first homology the element p_1 maps to twice a generator. Δ

Definition 13.3. A *group trisection of knotted surface type* of a finitely presented group G is a commutative cube of group epimorphisms as in Figure 75 such that the three maps out of the punctured sphere group are trivial tangle homomorphisms. Additionally, all the faces of the cube are pushouts, and the first pushouts are required to produce free groups, as shown in the diagram.

From the pushout property, we see that the group trisection is already determined by the data of the triple of maps with source the punctured sphere group. A *morphism* of group trisections of knotted surface type is a collection of group homomorphisms between the corresponding corners of the cubes such that all of the diagrams formed by the edges commute. In an *isomorphism* of group trisections, all of the maps between the corners are group isomorphisms; in particular, such an isomorphism sends meridians

of the punctures in $\pi_1(\mathbb{S}^2 - \{p_1, \dots, p_{2b}\})$ to meridians.

In the context of closed 4-manifolds, functoriality of group trisections is discussed in [Klu18].

13.1.1 Related literature. It is a folklore fact that every epimorphism from a (closed) surface group to a free group can be realized geometrically by a handlebody bounding the surface, a proof sketch appears for example in [LR02, Lem. 2.2]. Another exposition of this result from the Morse theory perspective is given in [MM21], where the authors relate epimorphisms from the fundamental group of a manifold to systems of framed hypersurfaces. Their cobordism arguments are analogous to the band summing operations in the last step of our algorithm in the proof of [Theorem 14.5](#).

Equivalence classes of homomorphisms from surface groups to free groups under pre- and post-composition with automorphisms have been studied in the literature, and a summary of some of the results appears in [GKZ92]. Stallings core graphs introduced in [Sta83] are in one to one correspondence with conjugacy classes of subgroups of finitely generated free groups. The concept of core graphs is extended to subgroups of surface groups in [MP21a].

Remark 13.4 (Warning: group trisection of knotted surface type \neq group trisection of a knotted surface group). A group trisection of knotted surface type is not the same as a group trisection in the sense of [AGK18] of a closed 4-manifold whose fundamental group is a knotted surface group $\pi_1(\mathbb{S}^4 - F, *)$. The difference is that for trisections of closed 4-manifolds, the group in the leftmost corner of the cube comes from the central trisection surface, thus is the fundamental group of an orientable closed surface. In our case, the group in the corner comes from a $2b$ times punctured sphere, which is free of rank $2b - 1$.

13.2 The free group characterizes unlinks

In this short section, we discuss some background on unlinks which will be convenient for studying the endpoint-unions of trivial tangles in a bridge trisection.

There exist non-trivial links $L \subset \#^k \mathbb{S}^1 \times \mathbb{S}^2$ whose fundamental group of the complement is free (but which is not free of the same rank as the complement of the local unlink). For example, the core curve of one of the Heegaard tori in the standard genus 1 splitting of $\mathbb{S}^1 \times \mathbb{S}^2$ has complement homotopy equivalent to the other solid torus, i.e. the fundamental group of its complement is free on one generator. On the other hand, the complement of the unknot $U \subset \mathbb{S}^1 \times \mathbb{S}^2$ has $\pi_1(\mathbb{S}^1 \times \mathbb{S}^2 - U)$ free on two generators, which can be taken to be the meridian of the unknot and the generator of $\pi_1(\mathbb{S}^1 \times \mathbb{S}^2)$.

We want to warn the reader that the usage of the word ‘link group’ is not consistent in the literature. In the context of this thesis, we use it to describe the fundamental group of a link complement in a 3-manifold.

LEMMA 13.5. *The fundamental group detects the unlink in the connected sum $\#^k \mathbb{S}^1 \times \mathbb{S}^2$. That is, if $L = L_1 \sqcup \dots \sqcup L_n \hookrightarrow \#^k \mathbb{S}^1 \times \mathbb{S}^2$ is an n -component link with $\pi_1(\mathbb{S}^1 \times \mathbb{S}^2 - L) \cong \text{Fr}_{n+k}$ a free group of rank $n + k$, then L is the n -component unlink.*

Proof. This proof is a generalization of the argument in [Hil81, Thm. 1], which was applied to unlinks in the 3-sphere. The meridian-longitude generators of the peripheral torus around a link component of L span an abelian subgroup in the free $\pi_1(\mathbb{S}^1 \times \mathbb{S}^2 - L)$. Any abelian subgroup of a free group is cyclic. By the assumptions on the rank of the group of the complement, the meridians of the link components have to generate a rank k submodule of the first homology of the link complement. Therefore we conclude that the longitudes are nullhomotopic in the link exterior. Now we apply the loop theorem to obtain disjointly embedded disks spanning each link component, thus recognizing the split unlink. \square

Remark 13.6. An analogous statement to [Lemma 13.5](#) is false for higher dimensional links. Cochran [\[Coc83\]](#) exhibited links of 2-spheres in the 4-sphere whose groups are free (but not freely generated by their meridians).

13.2.1 Decidability questions. Recognizing whether a given finitely presented group is the group of the complement of a closed orientable knotted surface in the 4-sphere is not algorithmic, this follows from the case $\mathcal{A} = \mathcal{G}, \mathcal{B} = \mathcal{K}_2$ in [\[GGS10, Thm. 1.1\]](#). It was known previously [\[Gor95\]](#) that it is undecidable whether a given finite presentation describes an n -knot group $\pi_1(\mathbb{S}^{n+2} - \mathbb{S}^n, *)$ for $n \geq 3$. As a corollary of the combination of [\[GGS10, Thm. 1.1\]](#) and our [Corollary 14.6](#), it is an undecidable problem to find a trisection of knotted surface type for a given finitely presented group G or show that none exists. The problem is unsolvable because such a procedure would decide whether G is a knotted surface group.

Given a finite presentation of a group G and a solution to the word problem of G , there is an algorithm to decide whether G is a free group [\[GW09, Cor. 4.3\]](#). As a consequence of Geometrization, we know that 3-manifold groups are residually finite and thus have decidable word problems; for this see e.g. [\[AFW15\]](#). So, given a triple of trivial tangle homomorphisms, there exists an algorithm for deciding whether the groups appearing in the corners of the induced pushout cube are free groups.

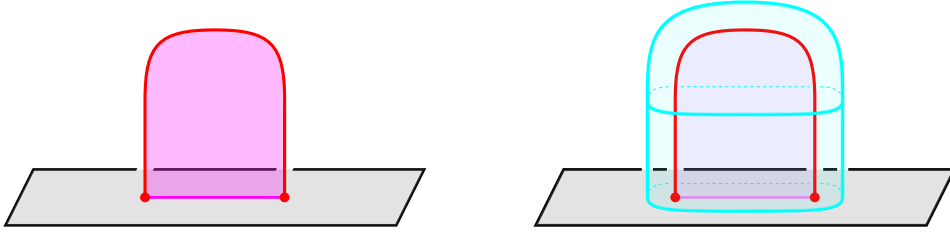


Figure 76. A bridge disk (left in fuchsia) and a bubble disk (right in light blue).

14 TRIVIAL TANGLES IN THE 3-BALL FROM GROUP EPIMORPHISMS

This section is summarizing a special case of the main construction in joint work in progress with Sarah Blackwell, Rob Kirby, Michael Klug and Vincent Longo.

Recall our terminology for tangles in 3-balls: A b -bridge *trivial tangle* T in the 3-ball is a collection of b properly embedded arcs in $B \cong \mathbb{D}^3$ such that all of the arcs can be simultaneously isotoped into the boundary of B . Given two 3-balls containing trivial tangles (\mathbb{D}^3, T_1) and (\mathbb{D}^3, T_2) with the property that $\partial T_1 = \partial T_2$, we say that (\mathbb{D}^3, T_1) and (\mathbb{D}^3, T_2) are *equivalent* if there exists a diffeomorphism $\mathbb{D}^3 \rightarrow \mathbb{D}^3$ mapping T_1 to T_2 that is the identity on $\partial \mathbb{D}^3$.

We will be concerned with the set of equivalence classes of trivial tangles (\mathbb{D}^3, T) such that $\partial \mathbb{D}^3 = \mathbb{S}^2$ and $\partial T = \{p_1, \dots, p_{2b}\}$. Any equivalence class of such a trivial tangle can be described by a *shadow diagram* \mathcal{D} on the surface \mathbb{S}^2 , made up of an embedded collection of b pairwise disjoint arcs $S = \{S_1, \dots, S_b\}$ whose endpoints are $\{p_1, \dots, p_{2b}\}$. For trivial tangles in higher genus handlebodies, there is an additional collection of cut system curves in the diagram, and in [MZ18] this is referred to as a ‘curve-and-arc system’. For more background on shadow diagrams, see for example [MTZ20].

We can think of \mathbb{D}^3 as appearing from taking a thickening $\mathbb{S}^2 \times [0, 1]$, and attaching a 3-ball to the 2-sphere boundary component on the interior. Given a shadow diagram, a trivial tangle in the resulting genus 0 handlebody can be constructed by taking the arcs of the tangle to be the union of $\{p_1, \dots, p_{2b}\} \times [0, \frac{1}{2}]$ together with the arcs S_1, \dots, S_b in the shadow diagram considered as arcs in $\mathbb{S}^2 \times \{\frac{1}{2}\}$. Conversely, given a 3-ball and a trivial tangle T we can obtain a diagram \mathcal{D} for (\mathbb{D}^3, T) by taking an isotopy relative to the boundary of T into \mathbb{S}^2 and letting the shadow diagram S denote the end result of this isotopy.

We refer to disjoint properly embedded disks that are the endpoint union of a shadow arc and the associated tangle component as *bridge disks*. One choice for these bridge disks is the track $S_i \times [0, \frac{1}{2}]$. A *bubble disk* in $\mathbb{D}^3 - T$ is a properly embedded disk which encloses a bridge disk of the tangle strand. It can be built from the bridge disk by taking a positive and negative parallel push-off, connected with an annulus following the tangle strand; see Figure 76.

Definition 14.1 (Topological realization). A *topological realization* of a trivial tangle homomorphism

$$\phi: \pi_1(\mathbb{S}^2 - \{p_1, \dots, p_{2b}\}, *) \rightarrow \langle t_1, \dots, t_b \rangle$$

is a trivial tangle T in a 3-ball B with $\partial B = \mathbb{S}^2$ and $\partial T = \{p_1, \dots, p_{2b}\}$ such that there is an isomorphism $\psi: \pi_1(B - T, *) \xrightarrow{\cong} \langle t_1, \dots, t_b \rangle$ that makes the following diagram commute:

$$\begin{array}{ccc}
 & & \pi_1(B - T, *) \\
 & \nearrow \iota_* & \downarrow \psi \\
 \pi_1(\mathbb{S}^2 - \{p_1, \dots, p_{2b}\}, *) & & \cong \\
 & \searrow \phi & \downarrow \\
 & & \langle t_1, \dots, t_b \rangle
 \end{array}$$

Here $\iota_*: \pi_1(\mathbb{S}^2 - \{p_1, \dots, p_{2b}\}, *) \rightarrow \pi_1(B - T, *)$ is induced by the inclusion $\iota: \mathbb{S}^2 - \{p_1, \dots, p_{2b}\} \rightarrow B - T$.

Now we will set up some notation in preparation for the following lemma. Let \mathcal{D} be a shadow diagram for a trivial tangle (\mathbb{D}^3, T) with $\partial \mathbb{D}^3 = \mathbb{S}^2$ and $\partial T = \{p_1, \dots, p_{2b}\}$, together with an ordering of the arcs S_1, \dots, S_b in the diagram, and a choice of an orientation for each of the S_j . Observe that cutting the surface \mathbb{S}^2 along the shadow arcs creates a connected, planar surface, and thus we will be able to choose *dual loops* t_j as follows.

For each arc S_j , choose a loop t_j based at $*$ that intersects S_j in exactly one point and does not intersect any of the other arcs. Orient t_j so that at the point of intersection of t_j and S_j , the orientation of t_j followed by the orientation of S_j agrees with the ambient orientation of \mathbb{S}^2 . Therefore, we now have $t_j \in \pi_1(\mathbb{S}^2 - \{p_1, \dots, p_{2b}\}, *)$; see **Figure 77a**.

LEMMA 14.2. *Using the notation defined above, we have the following.*

- (1) *The loops representing t_j are well-defined in $\pi_1(\mathbb{D}^3 - T, *)$, independent of choices.*
- (2) *The map*

$$\begin{aligned}
 \psi_{\mathcal{D}}: \pi_1(\mathbb{D}^3 - T, *) &\rightarrow \langle t_1, \dots, t_b \rangle \\
 t_j &\mapsto t_j
 \end{aligned}$$

is an isomorphism.

- (3) *The composition of the map induced by inclusion and $\psi_{\mathcal{D}}$*

$$\phi: \pi_1(\mathbb{S}^2 - \{p_1, \dots, p_{2b}\}, *) \xrightarrow{\iota_*} \pi_1(\mathbb{D}^3 - T, *) \xrightarrow{\psi_{\mathcal{D}}} \langle t_1, \dots, t_b \rangle$$

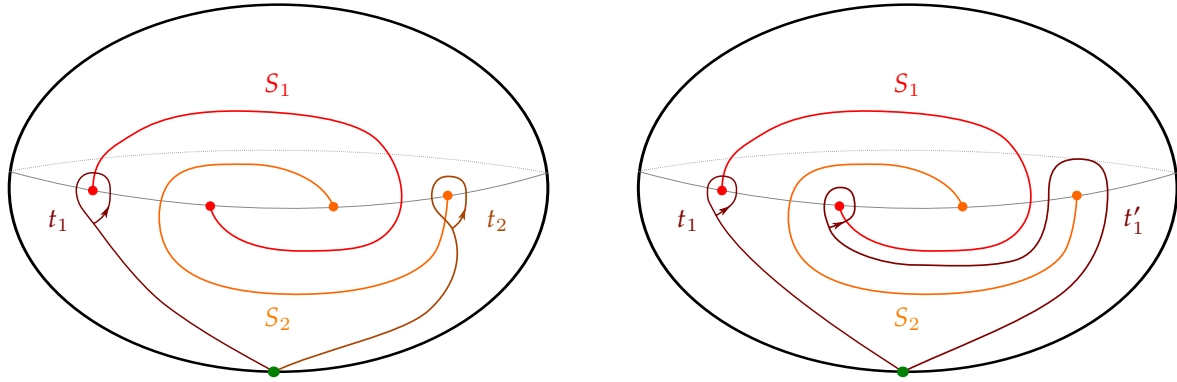
*on an element $\gamma \in \pi_1(\mathbb{S}^2 - \{p_1, \dots, p_{2b}\}, *)$ is computed as follows. Represent γ by a based, closed, immersed curve on \mathbb{S}^2 that is transverse to the shadow arcs S_i . We call this curve again γ . The image of γ under this composition of maps is given by traversing γ and building a word in the elements t_1, \dots, t_b and their inverses as follows. Start with the empty word. For each intersection between S_j and γ we concatenate $t_j^{\pm 1}$ on the right, where the sign is determined by the sign of the intersection of the oriented curves as in **Figure 78a**.*

- (4) *The map ϕ in (3) is a trivial tangle homomorphism, and with the choice of isomorphism $\psi_{\mathcal{D}}$, the trivial tangle (\mathbb{D}^3, T) is a topological realization of ϕ .*

Proof. Part (1): Observe that the choices of these elements t_j are not unique when considered as elements in $\pi_1(\mathbb{S}^2 - \{p_1, \dots, p_{2b}\}, *)$; see **Figure 77b**. However, we now prove that they are unique in the group $\pi_1(\mathbb{D}^3 - T, *)$. By choosing a collection of disjoint bridge disks, and cutting $\mathbb{D}^3 - T$ along these disks, we obtain a 3-ball as in **Figure 79**. From this it follows that the choices t_j are unique as elements of $\pi_1(\mathbb{D}^3 - T, *)$, because there is a unique homotopy class of curves connecting points in a 3-ball.

Part (2): Now define the map

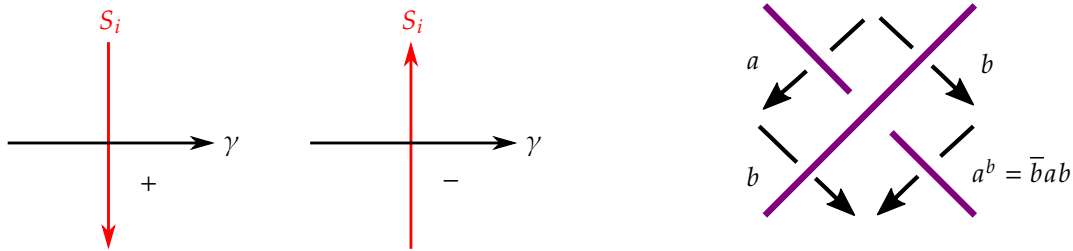
$$\langle t_1, \dots, t_b \rangle \rightarrow \pi_1(\mathbb{D}^3 - T, *)$$



(a) Finding loops t_j dual to the shadow arcs S_j .

(b) Inequivalent choices t_1 and t'_1 in the surface minus the points, which become isotopic (up to orientation) in the 3-ball minus the tangle determined by S_1, S_2 .

Figure 77. Shadow arcs and dual loops.



(a) Sign convention for intersection points, where the colored arrow is a shadow arc, and the black γ is an element in π_1 represented by a based closed immersed curve on the surface.

(b) Wirtinger relation at a crossing of a triplane diagram.

Figure 78. Sign conventions in shadow diagrams and Wirtinger relation in triplane diagram.

by sending $t_j \mapsto t_j$ (we abuse notation by taking the same letter on both sides). We argue that this map is an isomorphism. First observe that $\pi_1(\mathbb{D}^3 - T, *)$ is a free group of rank b , because $\mathbb{D}^3 - T$ deformation retracts onto a spine obtained in the following way. As above, cutting along (a choice of) bridge disks results in a 3-ball, thus the t_i make up a spine for the tangle complement $\mathbb{D}^3 - T$. This also means that the homomorphism above is surjective, and since free groups are Hopfian, it must be an isomorphism.

Part (3): Using the spine from the proof of Part (2), we apply the ‘cut system-spine’ duality, see e.g. [Joh06], to see that the image of an element $\gamma \in \pi_1(\mathbb{S}^2 - \{p_1, \dots, p_{2b}\}, *)$ under these maps can be computed by recording intersections of γ with the bridge disks. This is since traversing an edge in the spine corresponds to intersecting its dual disk. For curves γ that live on the surface \mathbb{S}^2 , these intersections occur precisely on a half-boundary of the bridge disks; see Figure 79.

Part (4): For checking the conditions on a trivial tangle homomorphism, recall that we used the following curves to represent the generators $p_i \in \pi_1(\mathbb{S}^2 - \{p_1, \dots, p_{2b}\}, *)$. We choose as Hurwitz arc system a simple system of rays r_i connecting $*$ to each point in $\{p_1, \dots, p_{2b}\}$. Then p_i corresponds to a loop that runs out along r_i , goes around the endpoint p_i in a positive direction, and returns along the arc r_i . The

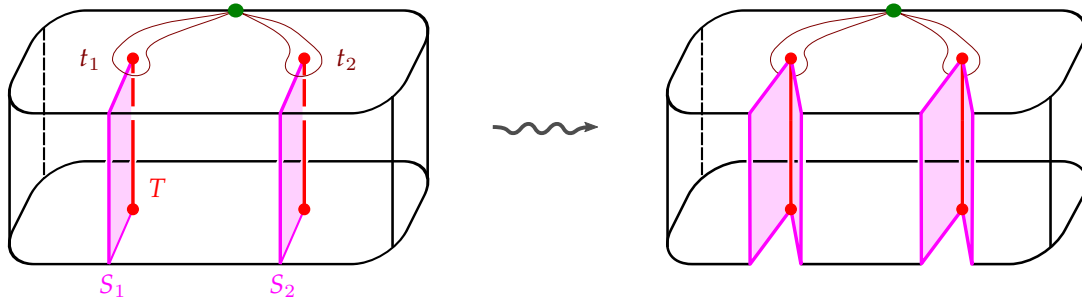


Figure 79. Cutting along a choice of bridge disks for the trivial tangle in a 3-ball results in a 3-ball again. The figure also shows how to build a spine of the tangle complement in the 3-ball: On the boundary, choose loops t_i on the punctured sphere which are dual to the shadow arcs S_i determined by the bridge disks. These can be pushed into the 3-ball, and in the cut 3-ball result in a pair of arcs which each connect one of the cutting disks' sides to the basepoint.

sequence in which the whisker of the loop around p_i intersects the tangle shadows reads off a word g_i in the free group. Then, running around the puncture concatenates one of the generators t_i , followed by returning to the base points contributing g_i^{-1} . Each tangle strand appears exactly twice as the central letter, once with each orientation.

The homomorphism $\pi_1(\mathbb{S}^2 - \{p_1, \dots, p_{2b}\}, *) \xrightarrow{\iota_*} \pi_1(\mathbb{D}^3 - T, *)$ is surjective, because we can build the tangle exterior from the exterior of the bridge points by attaching 2- and 3-handles. \square

LEMMA 14.3 (Uniqueness of realization). *Let (B_1, T_1) and (B_2, T_2) be two trivial tangles in 3-balls B_1, B_2 with $\partial B_1 = \mathbb{S}^2 = \partial B_2$ and $\partial T_1 = \{p_1, \dots, p_{2b}\} = \partial T_2$ so that there is an isomorphism ρ between the fundamental groups of the tangle complements which makes the following diagram commute:*

$$\begin{array}{ccc}
 & & \pi_1(B_1 - T_1, *) \\
 & \nearrow & \downarrow \rho \\
 \pi_1(\mathbb{S}^2 - \{p_1, \dots, p_{2b}\}, *) & & \pi_1(B_2 - T_2, *)
 \end{array}$$

Then (B_1, T_1) and (B_2, T_2) are equivalent.

Proof. We will construct a diffeomorphism $B_1 \rightarrow B_2$ mapping T_1 to T_2 that extends the identity on the boundary ∂B_1 , by defining it first on 2-cells in the complement of T_1 in B_1 , and then extending over 3-balls.

Fix shadow arcs for the tangle T_1 , and choose whiskers connecting each arc to the basepoint. Let η be the based boundary of a closed tubular neighborhood of one of the shadow arcs of T_1 . This curve bounds a bubble disk in $B_1 - T_1$; recall Figure 76. From commutativity of the diagram, we have that η is null-homotopic in $B_2 - T_2$, and thus by Dehn's lemma bounds a disk in the complement of T_2 . Use these disks to extend the map over all the bubble disks in $B_1 - T_1$.

To finish the construction, by the Alexander trick the map extends over the 3-cells in $B_1 - T_1$. Observe that each of the bubble disks cuts off a single tangle strand on one of its sides. Combined with the observation that there is a unique trivial 1-strand tangle in the 3-ball, this shows that the diffeomorphism $B_1 \rightarrow B_2$ we constructed can be arranged to map T_1 to T_2 . \square

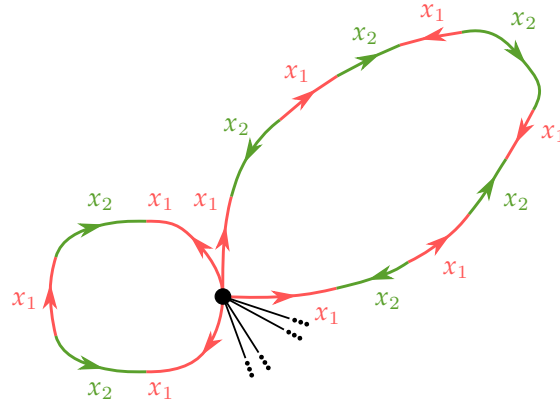


Figure 80. A directed graph Γ with edges labeled by elements of $\{x_1, \dots, x_n\}$, where Γ is topologically a wedge of k circles (only two lobes of which are shown in this picture completely) and each of the circles is subdivided and labeled according to the words w_1, \dots, w_k . In this example, reading counter-clockwise, $w_1 = x_1x_2^{-1}x_1^{-1}x_2x_1^{-1}$ and $w_2 = x_1x_2^{-1}x_1x_2x_1^{-1}x_2^{-1}x_1x_2^{-1}x_1^{-1}x_2x_1^{-1}$.

14.1 Stallings folding

We now discuss a technique due to Stallings called folding [Sta83] which in our context will be used as a step in the topological realization of trivial tangle homomorphisms and in studying generating systems for tangle complements. There are several applications of folding in the study of finitely generated free groups (e.g. for the membership problem, or determining the index and normality of a subgroup of a free group; see for example [CM17, Chpt. 4]). However, for our purposes we only need one application, namely that folding gives a convenient algorithmic method to determine if a set of elements $w_1, \dots, w_k \in \text{Fr}_n$ generates Fr_n , where Fr_n is the free group on the basis elements x_1, \dots, x_n .

We now describe this algorithm. Begin by forming a directed graph Γ with edges labeled by elements of $\{x_1, \dots, x_n\}$, where Γ is topologically a wedge of k circles and each of the circles is subdivided and labeled according to the words w_1, \dots, w_k as in Figure 80. We can change Γ by a move called a *fold* to obtain a new such graph as in Figure 81a.

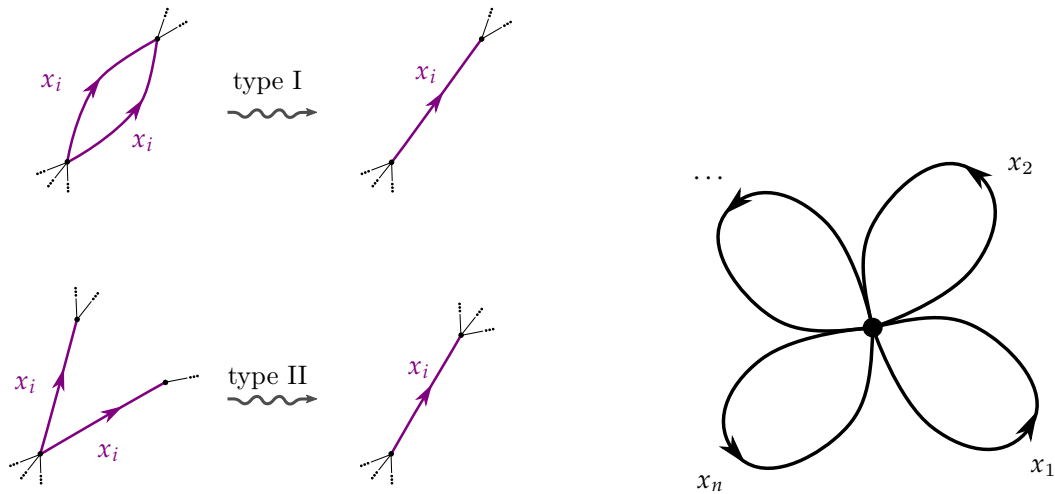
LEMMA 14.4 (Stallings). *The elements $w_1, \dots, w_k \in \text{Fr}_n$ generate the free group Fr_n if and only if the Stallings graph Γ given by w_1, \dots, w_k as in Figure 80 can be folded by any sequence of folds to the graph R_n in Figure 81b.*

THEOREM 14.5 ([BKCLR22]). *For every trivial tangle homomorphism*

$$\phi: \pi_1(\mathbb{S}^2 - \{p_1, \dots, p_{2b}\}, *) \rightarrow \langle t_1, \dots, t_b \rangle$$

there exists a topological realization, where the realizing tangle (\mathbb{D}^3, T) is unique by Lemma 14.3. Further, we can give an algorithm to construct a diagram for the topological realization.

Summary of the proof in [BKCLR22]. The plan is to describe a topological realization of ϕ by an explicit diagram that we will produce in such a way that Lemma 14.2 ensures that it is indeed a topological realization of ϕ . In the first stage, we produce a preliminary diagram \mathcal{D} that, if it were to consist of only the curves of a shadow diagram, would be a realization of ϕ . After this, in the second stage we will apply Stallings folding from Lemma 14.4 to guide band sums which eliminate the superfluous components of the preliminary diagram. An important step is to argue why the necessary bands always exist. We now describe the stages of the proof in more detail.



(a) Types of folds. The labels and orientations of the edges being folded must match. In particular, for fold II, the orientation of the edges can be either both in or both out of the shared vertex.

(b) The directed graph R_n is topologically a wedge of n circles, with each circle uniquely labeled by an element x_i .

Figure 81. Step and goal of Stallings folding.

In the first stage it is important to make a distinction between words in the generators and inverses of generators in a free group, and elements of the free group. For now, when we write $\phi(p_i)$, we mean the unique freely reduced words representing these elements. To produce \mathcal{D} look at the (not necessarily freely-reduced) word given by concatenating the freely-reduced $\phi(p_i)$, namely

$$w = \phi(p_1) \cdot \phi(p_2) \cdot \dots \cdot \phi(p_{2b})$$

and note that, since ϕ is a homomorphism, this word is equal to the trivial, i.e. empty word in $\langle t_1, \dots, t_b \rangle$. View the sphere as the plane with a point at infinity, place all of the punctures in a line, and place the basepoint at infinity. Mark the loops around each punctured point p_i on \mathbb{S}^2 with ‘oriented dashes’ labeled by the respective elements in $\phi(p_1), \dots, \phi(p_{2b})$.

The second step is to freely reduce the word w , and as cancellations occur in the free reductions, draw arcs between the corresponding dashes. The arcs retain the respective labelings and have orientations induced by the dashes. The loops around the punctures each intersect an odd number of dashes, which are now each part of an arc. Connect the middle dash to the punctured point, and connect the rest of the dashes in pairs that go around the opposite side of the puncture.

Similarly, by the conjugate condition in [Definition 13.1](#) of a trivial tangle homomorphism, we see that there is exactly one arc with label t_i for $i = 1, \dots, b$. However, in general \mathcal{D} might consist of additional closed curves with labels t_j . Suppose that at this stage there are no such additional curves in \mathcal{D} , namely, for each t_j there were no closed curves with that label. In this case, we know by [Lemma 14.2](#) that \mathcal{D} is a diagram for a topological realization of ϕ .

In the second stage, we will modify the preliminary diagram \mathcal{D} in steps by performing orientation- and label-preserving band sums between components in order to eliminate the extra closed curves.

The algorithm for finding these bands is as follows. Let Γ be the graph that is topologically a wedge of circles such that each circle is *colored* by the words $\phi(p_1), \dots, \phi(p_{2b})$. Add an additional *label* to each edge of Γ , namely label each edge of Γ with the corresponding closed curve or arc in the preliminary diagram \mathcal{D} . We will modify the graph Γ by folding and this will dictate how to modify the diagram \mathcal{D} by

band sums. At each stage, we will refer to the new graph again by Γ and the new diagram again by \mathcal{D} . Since the elements

$$\phi(p_1), \dots, \phi(p_{2b})$$

generate the free group $\langle t_1, \dots, t_b \rangle$, by [Lemma 14.4](#) there exists a sequence of foldings of the graph Γ to a wedge of b circles, where b is the rank of the free group. Choose a sequence of such foldings. Recall that foldings must occur between edges with the same *coloring*, but not necessarily the same *labels* (using the language of the previous paragraph). Whenever two edges of Γ with the same label are folded, the diagram \mathcal{D} is left unchanged and the edge of Γ resulting from the fold is given the same label as the edges it came from. Whenever two edges of Γ with different labels are folded, an orientation-preserving band between the two corresponding curves/arcs is chosen, disjoint from all of the other curves/arcs, and the diagram \mathcal{D} is modified by performing a band sum along this band. The edge of Γ resulting from the fold is given a new labeling that identifies the two curves/arcs which were banded together. Any other occurrences of the involved labels are modified as well.

Assuming for a moment that all the required bands do exist, since the graph Γ folds down to a wedge of circles R_g , in the final diagram there will be one arc for each edge of R_g . It then follows that there will be exactly b arcs in the final diagram \mathcal{D} . The preceding discussion then applies to see that the resulting diagram \mathcal{D} indeed does provide a topological realization of ϕ .

The existence of the bands follows from a careful analysis of the folding cases. □

COROLLARY 14.6. *Every group trisection of knotted surface type determines a unique parameterized bridge trisection of a closed smoothly knotted surface in the trisected 4-sphere.*

Proof. Apply the algorithm from [Theorem 14.5](#) three times, once to each trivial tangle homomorphism in the group trisection of knotted surface type, to obtain three trivial tangles. Each tangle is uniquely determined by its corresponding trivial tangle homomorphism, and by construction parameterized. These will make up the spine of the bridge trisection we are looking for, by placing these trivial tangles into the 3-balls $\mathbb{D}_0^3, \mathbb{D}_{\frac{2\pi}{3}}^3$ and $\mathbb{D}_{\frac{4\pi}{3}}^3$ of the open book decomposition of \mathbb{S}^4 . The endpoints of the tangle are joined at the common central 2-sphere.

The pairwise unions of the tangles glue to give links L in the 3-sphere with $\pi_1(\mathbb{S}^3 - L)$ a free group, since we are assuming that the pairwise pushouts in the group trisection of knotted surface type are free. Then by [Lemma 13.5](#) these have to be unlinks in the 3-sphere, which bound unique trivial disk systems (the patches) in each of the 4-balls of the trisection of \mathbb{S}^4 , as in [\[MZ17\]](#). □

In our geometric reconstruction, b is the number of strands in the trivial tangles, and $c_{\alpha\beta}, c_{\beta\gamma}, c_{\alpha\gamma}$ are the number of patches in each sector. If a surface F is in b -bridge position with patch numbers c_1, c_2, c_3 , its Euler characteristic is $\chi(F) = c_1 + c_2 + c_3 - b$. This puts restrictions on the numbers b and c_i which can appear in a group trisection of knotted surface type that can be realized geometrically. The patch numbers can be read off from the algebra as the ranks of the free groups given by the first stage of pushouts. The smoothly knotted closed surface may be disconnected or non-orientable. The number of components and orientability of the surface can be determined from the first homology of the surface complement, i.e. from the abelianization of the final knotted surface group. For complements of connected surfaces, this group is by Alexander duality isomorphic to \mathbb{Z} for orientable surfaces and $\mathbb{Z}/2$ for non-orientable surfaces.

15 COMPUTING EPIMORPHISMS FROM TRIPLANE DIAGRAMS

In this section, we recall triplane diagrams which encode the trivial tangles of a bridge trisection, and how the Wirtinger algorithm applies to these projections in [Section 15.1](#). Then we will describe our computer implementation as a SageMath module in [Section 15.2](#).

If $F \subset \mathbb{S}^4$ is a smoothly knotted closed surface in the trisected 4-sphere, a bridge trisection of F can be represented diagrammatically with a *triplane diagram* encoding the triple $(T_\alpha, T_\beta, T_\gamma)$ of trivial tangles. First, a diagram for a trivial tangle (\mathbb{D}^3, T) is a generic projection of the 3-ball to a 2-disk so that the image of T , together with crossing information at each double point, determines the isotopy class of the tangle. For an example of a 2-bridge trivial tangle diagram see [Figure 82](#). Two of these tangle diagrams containing the same number of strands can be glued together, using the fixed position of the tangle endpoints, which yields a classical diagram of a link in the 3-sphere. Then a *triplane diagram* is a triple $(P_\alpha, P_\beta, P_\gamma)$ of trivial tangle diagrams so that every pairwise union $P_\eta \cup \overline{P_\mu}$ of one of the diagrams with the mirror image of another results in a diagram for an unlink in the 3-sphere. Explicit examples of triplane diagrams appear in [Figures 90, 93 and 97](#).

Here the orientation conventions for triplane diagrams are responsible for the appearance of mirror images. The 3-dimensional intersection $B_{ij} = X_i \cap X_j$ inherits its orientation from ∂X_i . This orientation is opposite to the one which would come from restricting the orientation of ∂X_j . For a careful discussion of the setup using normal vector fields on the 3-balls which determine the types of crossings in the diagram, see [[MZ17](#), Sec. 2.3].

Recall that any two bridge trisections of F are related by a sequence of *perturbations*, *deperturbations*, and *isotopies*. On the level of diagrams, the triples of triplane diagrams of isotopic surfaces are related by a sequence of Reidemeister moves in the individual triplane diagrams, mutual braid transpositions, stabilizations and destabilizations. An alternative diagrammatic representation is in terms of triples of shadow diagrams on the central surface, which we discuss in [Section 14](#).

15.1 Choosing Wirtinger generating meridians for trivial tangles

We want to discuss a subtlety in the choice of generating sets of meridians for trivial tangle complements. This is illustrated by the example in [Figure 82](#). Here we denote the meridians to the punctures on the central 2-sphere by the letters x_0, x_1, x_2, x_3 . Additionally, we draw meridians to the two maxima, denoted by a_0, a_1 .

It is possible to start the Wirtinger process with two *seed strands* located at a_0 and a_1 , as indicated in [Figure 84](#). Here the *Wirtinger algorithm* proceeds as follows: If the meridian of a strand has already been labeled with a conjugate of a seed generator, it extends over all overcrossings contained in this strand. If both the overstrand and one of the understrands at a crossing in the diagram have been labeled, the other understrand is determined by the Wirtinger relation that is required to hold at that crossing. Note that the precise form of the relation depends on the orientations of the meridians coming together at the crossing, an example is indicated in [Figure 78b](#).

In particular, from the resulting list of conjugates at the bottom of the tangle in [Figure 84](#) we can read off the epimorphism from the punctured sphere group to the free group generated by a_0 and a_1 . Recall the usual notation for conjugates as $x^w = \overline{w}xw$, where overlines denote inverses $\overline{w} = w^{-1}$. Useful calculation

rules for the conjugate notation are the power laws $(x^w)^v = x^{wv}$ and $x^{(w^v)} = x^{\overline{v}wv}$.

$$\begin{aligned}
 \langle x_0, x_1, x_2, x_3 \mid x_0x_1x_2x_3 = 1 \rangle &\rightarrow \langle a_0, a_1 \rangle \\
 x_0 &\mapsto a_0^{\overline{a_1}a_0a_1\overline{a_0}a_1} \\
 x_1 &\mapsto a_1^{\overline{a_0}a_1a_0\overline{a_1}a_0a_1\overline{a_0}a_1} \\
 x_2 &\mapsto \overline{a_0}a_1\overline{a_0} \\
 x_3 &\mapsto \overline{a_1}a_0\overline{a_1}\overline{a_0}a_1\overline{a_0}
 \end{aligned} \tag{15.1}$$

The *Wirtinger number* of a diagram as the minimal number of generators in a Wirtinger system was introduced in [Bla+20a], see this reference for the precise terminology and definitions. The Wirtinger number can be extended to an invariant of links by taking the minimum of the Wirtinger number over all possible diagrams. In particular, Blair-Kjuchukova-Velazquez-Villanueva show that for links in the 3-sphere, the Wirtinger number agrees with the bridge number, and they investigate its relation to the meridional rank.

In our example, it is not possible to single out two meridians of the punctures and use them as seed strands for a successful Wirtinger procedure, as illustrated in Figure 83. For each choice, the Wirtinger algorithm fails at some point, because there are crossings where no conjugate could be associated to the overstrand. For example in Figure 83a, starting from the meridians x_0 and x_1 , the partial coloring by the meridians extends over the first two crossings on the left, but then has to dry up as both strands reach uncolored crossings as the understrand.

Moreover, we can use the Stallings folding sequence in Figure 85 to check that the images of x_0 and x_1 do not generate the free group $\langle a_0, a_1 \rangle$. Similarly, for the three other choices of pairs of punctures, the Stallings folding does not succeed. We show the most important steps in the folding of x_0, x_3 in Figure 86, of x_1, x_2 in Figure 87 and of x_2, x_3 in Figure 88. The shapes of the resulting graphs are not wedges of circles, as would be required by the Stallings folding procedure to conclude that they generate $\langle a_0, a_1 \rangle$. Counting the number of preimages of the basepoint, we prove the following:

PROPOSITION 15.1. *For the trivial tangle in Figure 82, none of the subgroups $\langle x_i, x_j \rangle$ for $i \neq j \in \{0, \dots, 3\}$ generate the rank 2 free group of the complement $\pi_1(\mathbb{D}^3 - T) \cong \langle a_0, a_1 \rangle$. Moreover, for the pairs x_i, x_j which include precisely one generator per tangle strand, we observe the following: The index of the subgroups $\langle x_0, x_1 \rangle$ and $\langle x_2, x_3 \rangle$ in the tangle group $\langle a_0, a_1 \rangle$ is equal to 3, for $\langle x_0, x_3 \rangle$ and $\langle x_1, x_2 \rangle$ the index is equal to 11.*

Recall that each such pair x_i, x_j , one for each strand, does indeed *normally* generate the group of the tangle complement.⁴³

⁴³ That is, products of conjugates generate the group.

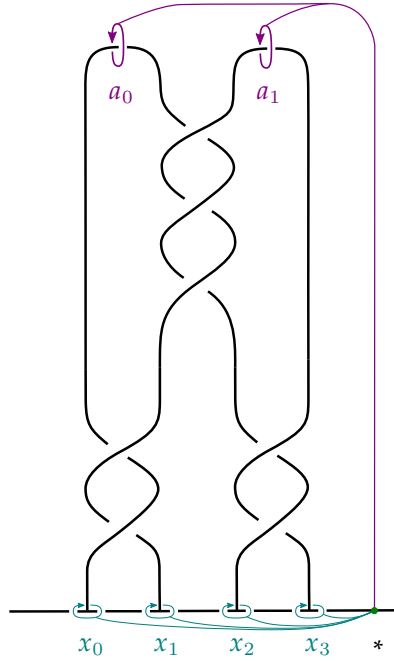


Figure 82. A trivial tangle T in the 3-ball \mathbb{D}^3 in Morse position, where the boundary 2-sphere of the 3-ball is the compactification of a horizontal plane at the bottom (only a horizontal line of which is shown). We give a choice of meridians at the maxima in purple, these generate the tangle complement group $\pi_1(\mathbb{D}^3 - T, *)$ which is free of rank 2 on a_0, a_1 . The collection of all meridians x_0, x_1, x_2, x_3 to the punctures on the 2-sphere provides another generating set of the tangle complement. We will observe that in this example, no two-element subset of the sphere punctures generates.

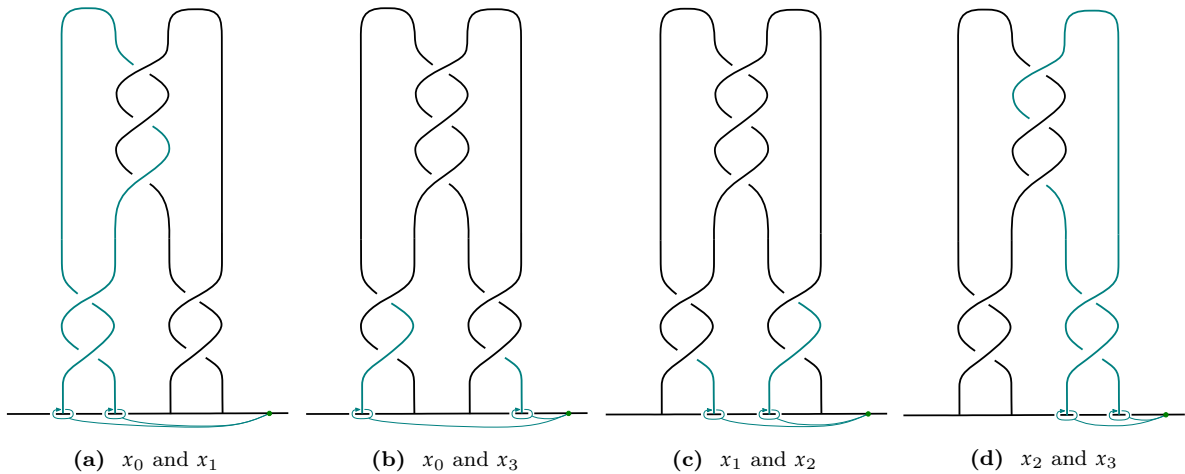


Figure 83. Unsuccessful runs of the Wirtinger algorithm with seed strands located at two of the punctures x_i, x_j . The partial coloring at the end of the process is drawn in teal, which indicates those meridians which can be expressed as conjugates of the seed strands.

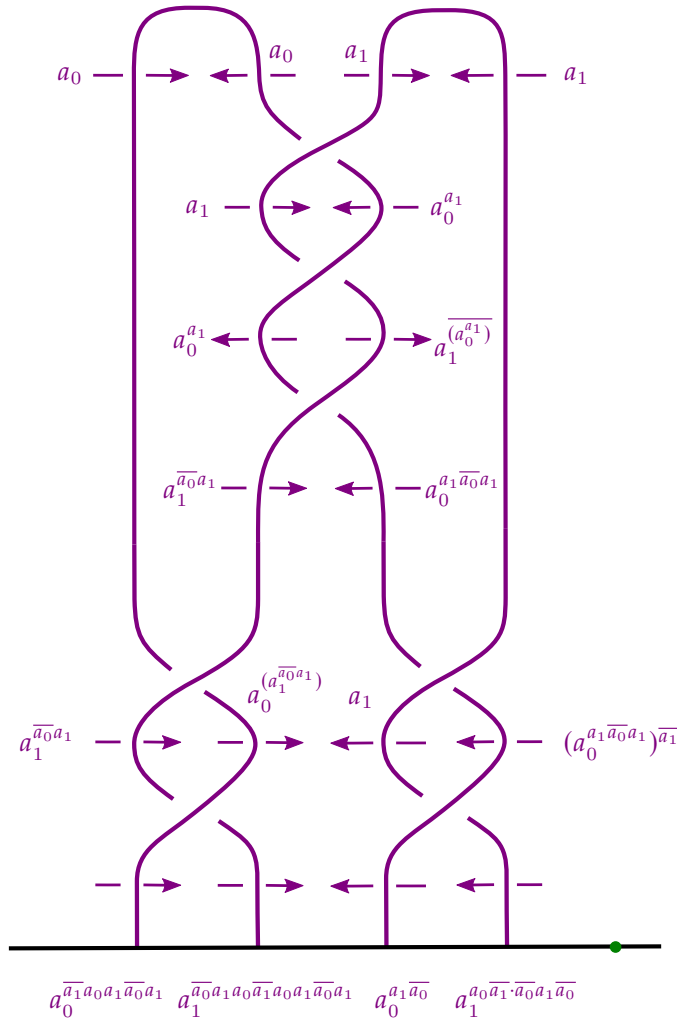


Figure 84. Running the Wirtinger process with seed strands located at the maxima a_0, a_1 . Each arrow denotes a based meridian to the strand. The basepoint is placed above the diagram, so the whiskers can run on top of all the other strands to the tail of the meridian arrow, around the strand following the orientation, and then back to the basepoint on top of everything else. The conjugates at the bottom determine the images of x_0, x_1, x_2, x_3 in the trivial tangle homomorphism from Equation (15.1).

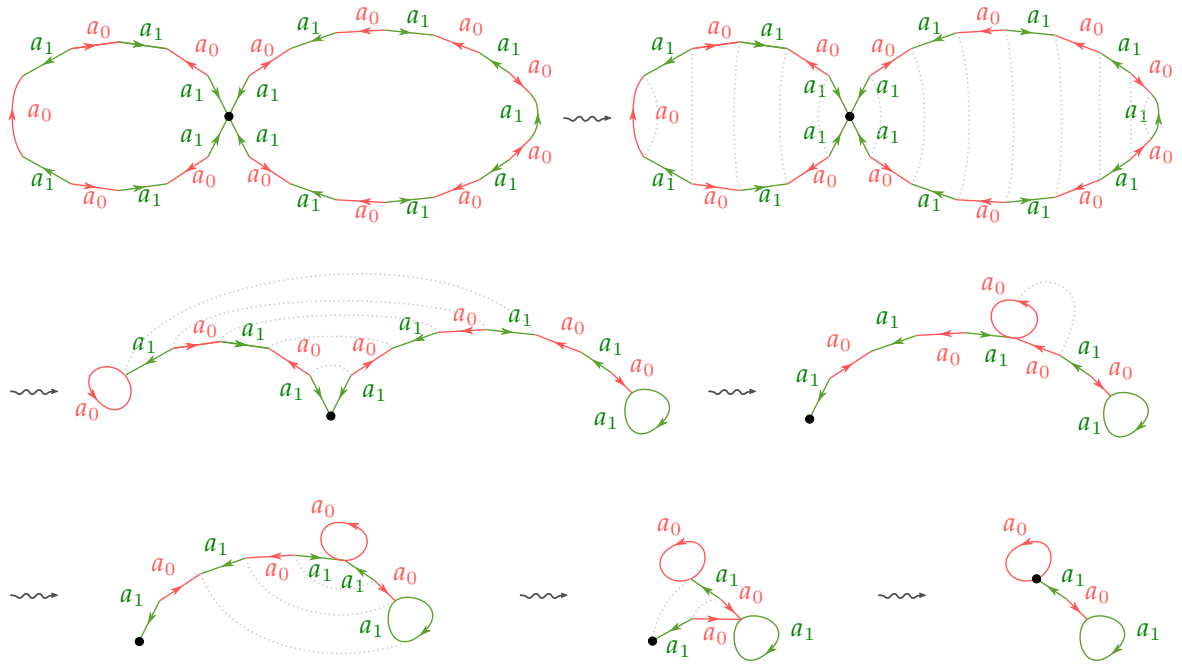


Figure 85. Stallings folding sequence for the images of $x_0 \mapsto a_0^{-1}a_0a_1\bar{a}_0a_1$ and $x_1 \mapsto a_1^{-1}a_1a_0\bar{a}_1a_0a_1\bar{a}_0a_1$.

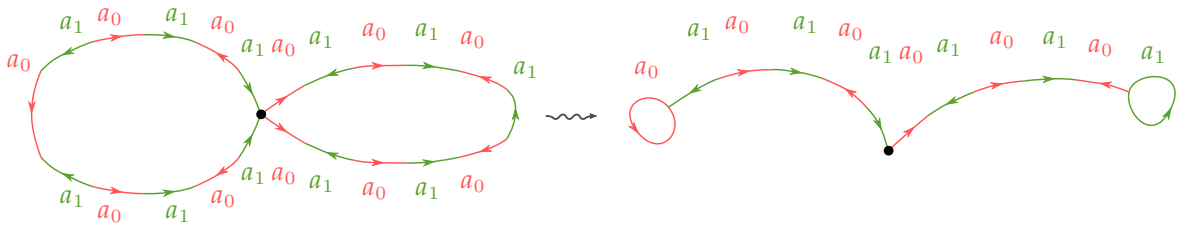


Figure 86. Stallings folding sequence for the images of $x_0 \mapsto a_0^{-1}a_0a_1\bar{a}_0a_1$ and $x_3 \mapsto a_1^{-1}a_1a_0\bar{a}_1a_0a_1\bar{a}_0$.

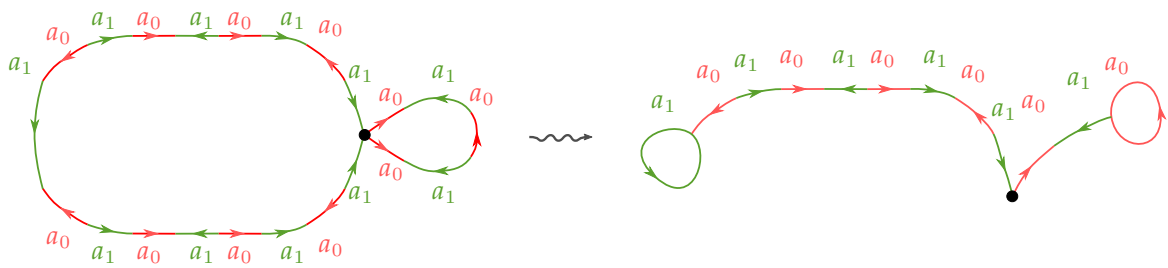


Figure 87. Stallings folding sequence for the images of $x_1 \mapsto a_1^{-1}a_1a_0\bar{a}_1a_0a_1\bar{a}_0a_1$ and $x_2 \mapsto a_0^{-1}a_1\bar{a}_0$.

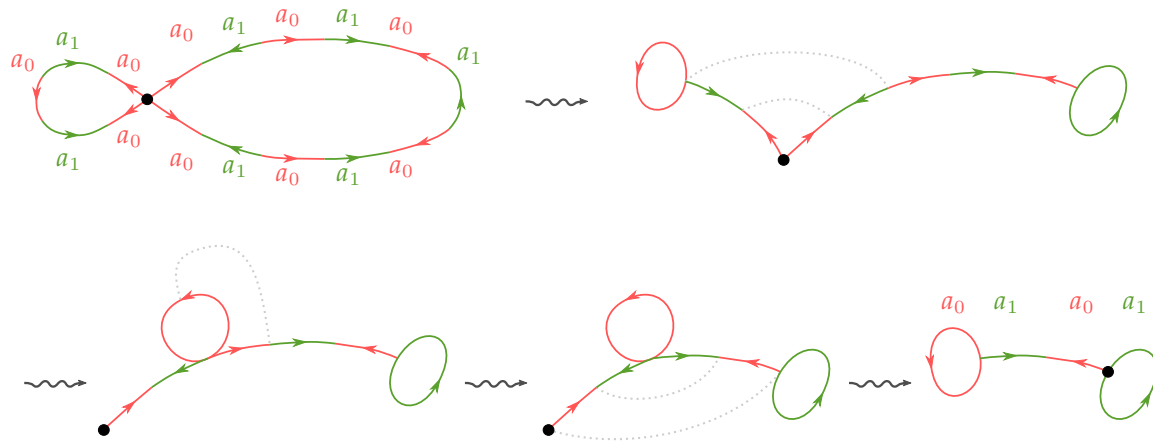


Figure 88. Stallings folding sequence for the images of $x_2 \mapsto \overline{a_1 a_0}$ and $x_3 \mapsto \overline{a_1^{a_0 a_1} \overline{a_0 a_1} \overline{a_0}}$.

```

1 def add_crossing(self, crossing : Braid_crossing):
2     """
3     Modifies self.generators_temp_list
4     with the Wirtinger rules according to the added crossing
5     """
6     self.braid_word.append(crossing)
7     if crossing.sign == +1:
8         # Positive crossing
9         overstrand_word = self.generators_temp_list[crossing.first_index]
10        new_understrand_word = overstrand_word * self.generators_temp_list[
11            crossing.second_index] * overstrand_word^(-1)
12        self.generators_temp_list[crossing.first_index] = new_understrand_word
13        self.generators_temp_list[crossing.second_index] = overstrand_word
14    elif crossing.sign == -1:
15        # Negative crossing
16        overstrand_word = self.generators_temp_list[crossing.second_index]
17        new_understrand_word = overstrand_word^(-1) * self.generators_temp_list[
18            crossing.first_index] * overstrand_word
19        self.generators_temp_list[crossing.first_index] = overstrand_word
20        self.generators_temp_list[crossing.second_index] = new_understrand_word
21    else:
22        raise Exception("Invalid value in sign of crossing")
23    # Uncomment to print intermediate steps
24    # print("generators_temp_list:", self.generators_temp_list)
25    return

```

Table 1. Code snippet of the `Trivial_tangle.add_crossing()` method, which appends a generalized braid crossing to `self.braid_word` and modifies `self.generators_temp_list` according to the new Wirtinger relation.

15.2 Documentation of the SageMath module

Calculating the trivial tangle homomorphisms $\pi_1(\mathbb{S}^2 - \{p_1, \dots, p_{2b}\}, *) \rightarrow \pi_1(\mathbb{D}^3 - T, *)$ induced by tangle complements requires a significant amount of bookkeeping of the conjugates in the Wirtinger algorithm. This can partly be automated using the author's SageMath module [Rup21a]. In particular, this program includes functions for computing the pieces of a group trisection, and putting these together via pushouts to build up the components of the Seifert-van Kampen cube in Figure 74. The user should be careful with a possible index shift in the naming of the generators when using [Rup21a], where the labels of the generators and tangle strands always start at zero.

The python class `Bridge_Trisection` is a container for a collection of three trivial tangle diagrams. For illustration, we take the object `tau_3_T_2_5` which encodes a bridge trisection of the 3-twist spin of the $(2, 5)$ -torus knot, $\tau^3 T_{2,5}$, see also Section 16.1.1. Each `Bridge_Trisection` contains three trivial tangles, which are instances of the class `Trivial_tangle`.

Trivial tangles are encoded as the upper plat closure of a *generalized braid word*. By the program's convention, the bridge points are labeled from left to right with the numbers 0 to $2b - 1$. The difference between usual braid words and generalized braid words is that in our trivial tangles, we allow maxima to occur at any height, which removes a pair of strands from the other braid strands which continue upwards. In particular, after such a maximum it becomes possible for strands labeled with non-consecutive indices to cross. We use the letter $\sigma_{i,j}$ to denote a positive crossing between the i th and j th strand, where $i < j$. The notation with overlines $\overline{\sigma_{i,j}} = \sigma_{i,j}^{-1}$ denotes the inverse, which is a negative crossing between the strands. For example, the green γ -tangle in the 3-twist spin of the $(2, 5)$ -torus knot has five half-twists between the strands with index 1 and 4, and so `tau_3_T_2_5.gre_tangle` can be constructed from the following list:

```
[ Braid_crossing(1, 4, +1), Braid_crossing(1, 4, +1), Braid_crossing(1, 4, +1),
  Braid_crossing(1, 4, +1), Braid_crossing(1, 4, +1) ]
```

The constructor of the `Trivial_tangle` class iteratively calls the `.add_crossing()` method, which appends a single generalized braid crossing to the tangle's `.braid_word`, and at the same time moves the Wirtinger generators further up in the sequence of crossings; see Table 1. By convention, for a 4-bridge tangle the generators at the bottom start off as the list `[x0, x1, x2, x3, x4, x5, x6, x7]` of elements of a `FinitelyPresentedGroup` without relations in SageMath. The object `xi` corresponds to the loop x_i as in Figure 82, which starts at the basepoint, goes under the tangle strand in the diagram numbered with i from left to right, and then returns to the basepoint. Internally, the list of current generators at the top is kept in memory, and depending on the strand indices and sign of the crossing, the Wirtinger conjugation is performed. The current list can be accessed via the field `tau_3_T_2_5.gre_tangle.generators_temp_list`, which for this specific γ -tangle ends up as the following at the top:

$$x_0, (x_1 x_4)^3 (x_1^{-1} x_4^{-1})^2 x_1^{-1}, x_2, x_3, (x_1 x_4)^2 x_1 (x_4^{-1} x_1^{-1})^2, x_5, x_6, x_7.$$

The strands at the maxima are joined in pairs, which are encoded as a list of tuples of indices. In our example of the γ -tangle these can be accessed in the following way:

```
tau_3_T_2_5.gre_tangle.strand_matching = [(0, 1), (4, 7), (2, 3), (5, 6)]
```

Now in the method `tau_3_T_2_5.gre_tangle.group()` the program will construct a SageMath object of type `FinitelyPresentedGroup` representing the group of the tangle complement; see Table 2. This group's generators are also called `x0, x1, x2, x3, x4, x5, x6, x7` and its relations come from setting pairs of conjugates from the first step equal according to the matching at the maxima. For this 4-bridge

γ -tangle we obtain the group presentation with 8 generators and 4 relations

$$\langle x_0, x_1, x_2, x_3, x_4, x_5, x_6, x_7 \mid x_0(x_1x_4)^3(x_1^{-1}x_4^{-1})^2x_1^{-1}, (x_1x_4)^2x_1(x_4^{-1}x_1^{-1})^2x_7, x_2x_3, x_5x_6 \rangle.$$

As we know from the topology of a 4-bridge trivial tangle complement, this is isomorphic to a free group on 4 generators, one for each tangle strand.

The SageMath command `tau_3_T_2_5.gre_tangle.group().simplification_isomorphism()` is usually able to compute a free basis of the group, and in this case returns the following map:

$$\begin{aligned} \langle x_0, \dots, x_7 \mid x_0(x_1x_4)^3(x_1^{-1}x_4^{-1})^2x_1^{-1}, (x_1x_4)^2x_1(x_4^{-1}x_1^{-1})^2x_7, x_2x_3, x_5x_6 \rangle &\rightarrow \langle t_0, t_2, t_5, t_7 \rangle \\ x_0 &\mapsto t_0; x_1 \mapsto (t_7t_0)^2(t_7^{-1}t_0^{-1})^2t_7^{-1}; x_2 \mapsto t_2; x_3 \mapsto t_2^{-1} \\ x_4 &\mapsto (t_7t_0)^2t_7(t_0^{-1}t_7^{-1})^3; x_5 \mapsto t_5; x_6 \mapsto t_5^{-1}; x_7 \mapsto t_7 \end{aligned}$$

In particular, the composition of the natural quotient map from the punctured sphere group to the tangle complement, followed by this isomorphism to a free group, is the trivial tangle homomorphism associated to this tangle.

Remark 15.2. For the trivial tangle in [Figure 84](#), as discussed in [Proposition 15.1](#), no pair of meridians of the punctures will generate the free group. SageMath is not able to find a two-generator meridional presentation, but manages to reduce the number of generators to three via the following isomorphism:

$$\begin{aligned} \langle x_0, x_1, x_2, x_3 \mid x_0x_1x_2x_3x_2x_3^{-1}x_2^{-1}x_0x_1x_0^{-1}x_2x_3x_2x_3^{-1}x_2^{-1}x_0x_1^{-1}x_0^{-1}x_2x_3x_2^{-1}x_3^{-1}x_2^{-1}x_0x_1^{-1}x_0^{-1}, \\ x_0x_1x_0^{-1}x_2x_3x_2x_3^{-1}x_2^{-1}x_0x_1x_0^{-1}x_2x_3x_2^{-1}x_3^{-1}x_2^{-1}x_0x_1^{-1}x_0^{-1}x_2x_3x_2^{-1} \rangle \\ \rightarrow \langle y_0, y_1, y_2 \mid y_1^{-1}y_0^{-1}y_2(y_0y_1)^2y_0^{-1}y_1^{-1}y_0^{-1}y_2y_0y_1y_0(y_1^{-1}y_0^{-1})^2y_2^{-1}y_0y_1y_0 \rangle \\ x_0 \mapsto y_0; x_1 \mapsto y_1; x_2 \mapsto y_2; x_3 \mapsto y_2^{-1}y_1^{-1}y_0^{-1} \end{aligned}$$

Let us zoom out again and consider the bridge trisection as a whole, assembled from three trivial tangles. The group presentation for the α -tangle from the method `tau_3_T_2_5.red_tangle.group()` is

$$\begin{aligned} \langle x_0, x_1, x_2, x_3, x_4, x_5, x_6, x_7 \mid x_0(x_1x_2x_3)^3(x_1x_2)^3x_1^{-1}x_2^{-1}x_1^{-1}(x_2^{-1}x_1^{-1}x_3^{-1})^3x_2^{-1}x_1^{-1}, \\ (x_1x_2x_3)^3(x_1x_2)^2x_1x_2^{-1}x_1^{-1}(x_2^{-1}x_1^{-1}x_3^{-1})^3x_2^{-1}x_1^{-1}x_7, \\ (x_1x_2x_3)^3(x_2^{-1}x_1^{-1}x_3^{-1})^2x_2^{-1}x_1^{-1}x_6, x_4x_5 \rangle. \end{aligned}$$

The group of the β -tangle can be accessed via `tau_3_T_2_5.blu_tangle.group()` which returns

$$\langle x_0, x_1, x_2, x_3, x_4, x_5, x_6, x_7 \mid x_0(x_1x_2)^3(x_1^{-1}x_2^{-1})^2x_1^{-1}, (x_1x_2)^2x_1(x_2^{-1}x_1^{-1})^2x_5, x_3x_4, x_6x_7 \rangle.$$

Putting all three of these together amounts to creating a group presentation with generators x_0, \dots, x_7 and relations given by the union of all of the relations for the α -, β - and γ -tangles. In the SageMath-program, this can be constructed with the `.group()` method applied to the bridge trisection. For example, the call `tau_3_T_2_5.group()` returns the following presentation of $\pi_1(\mathbb{S}^4 - \tau^3T_{2,5})$ with meridional generators:

$$\begin{aligned} \langle x_0, x_1, x_2, x_3, x_4, x_5, x_6, x_7 \mid x_0(x_1x_2x_3)^3(x_1x_2)^3x_1^{-1}x_2^{-1}x_1^{-1}(x_2^{-1}x_1^{-1}x_3^{-1})^3x_2^{-1}x_1^{-1}, \\ (x_1x_2x_3)^3(x_1x_2)^2x_1x_2^{-1}x_1^{-1}(x_2^{-1}x_1^{-1}x_3^{-1})^3x_2^{-1}x_1^{-1}x_7, \\ (x_1x_2x_3)^3(x_2^{-1}x_1^{-1}x_3^{-1})^2x_2^{-1}x_1^{-1}x_6, x_4x_5; \\ x_0(x_1x_2)^3(x_1^{-1}x_2^{-1})^2x_1^{-1}, (x_1x_2)^2x_1(x_2^{-1}x_1^{-1})^2x_5, x_3x_4, x_6x_7; \\ x_0(x_1x_4)^3(x_1^{-1}x_4^{-1})^2x_1^{-1}, (x_1x_4)^2x_1(x_4^{-1}x_1^{-1})^2x_7, x_2x_3, x_5x_6 \rangle \end{aligned} \tag{15.2}$$

```

1 def group(self):
2     """
3     Gives a presentation of the group of the tangle complement
4     (which is free on b generators)
5     with generators the meridians around the punctures
6     and relations from joining up the tangle strands at the top
7     """
8     relations = [self.generators_temp_list[a] * self.generators_temp_list[b]
9                 for (a, b) in self.strand_matching]
10    return self.F.quotient(relations)

```

Table 2. Code snippet of the `Trivial_tangle.group()` method, which computes the relations from the matching of the conjugates at the maxima, and constructs the corresponding quotient of a free group F .

Usually, these presentations can be simplified significantly, and SageMath can help in this process with the built-in method `.simplification_isomorphism()`.

$$\begin{aligned}
 \langle x_0, x_1, x_2, x_3, x_4, x_5, x_6, x_7 \mid \text{Relations}_{\tau^3 T_{2,5}} \rangle &\rightarrow \langle x_0, x_2 \mid x_0^{-3} x_2^{-1} x_0^3 x_2, (x_0^{-1} x_2)^2 x_0^{-1} (x_2^{-1} x_0)^2 x_2^{-1} \rangle \\
 x_0 &\mapsto x_0 \\
 x_1 &\mapsto x_0^{-1} \\
 x_2, x_4, x_6 &\mapsto x_2 \\
 x_3, x_5, x_7 &\mapsto x_2^{-1}
 \end{aligned}$$

Observe that this is the quotient of the meridional presentation of the trefoil group

$$\langle x_0, x_2 \mid (x_0^{-1} x_2)^2 x_0^{-1} (x_2^{-1} x_0)^2 x_2^{-1} \rangle,$$

where the relation $x_0^{-3} x_2^{-1} x_0^3 x_2$ implies that the third power x_0^3 of the meridian x_0 commutes with the other meridian x_2 , and thus is central in the group.

16 GROUP TRISECTIONS OF TWIST-SPUN TORUS KNOTS

THEOREM 16.1. *There exist at least three non-isomorphic group trisections of knotted surface type of $\mathbb{Z} \times \text{Dod}^*$, the product of the integers with the 120 element binary dodecahedral group; two of these have bridge number 4 and the third one has bridge number 7. Under topological realization, these group trisections of knotted surface type correspond to knotted genus 0 surfaces in \mathbb{S}^4 .*

Proof. Under topological realization from [Corollary 14.6](#), these three group trisections of knotted surface type correspond to the knotted spheres $\mathbb{S}^2 \hookrightarrow \mathbb{S}^4$ listed below. We will describe their constituent trivial tangle homomorphisms in the section which is indicated in the list.

- $\tau^3 T_{2,5}$, the 3-twist spin of the $(2, 5)$ -torus knot in [Section 16.1.1](#)
- $\tau^5 T_{2,3}$, the 5-twist spin of the $(2, 3)$ -torus knot in [Section 16.1.2](#)
- $\tau^2 T_{3,5}$, the 2-twist spin of the $(3, 5)$ -torus knot in [Section 16.2.1](#).

Now we argue that their group trisections of knotted surface type are not isomorphic.⁴⁴ This is a direct consequence of Gordon's theorem [[Gor73](#)] that the minimal exponent of a meridian's power which is central in the groups $\pi_1(\mathbb{S}^4 - \tau^i T_{j,k}, *)$ has to divide the twisting parameter, as we now explain.

Pick a generator p of the punctured sphere group and follow it through the group trisection cube, we call its image in the final knotted sphere group p as well. Observe that the image of p is a meridional generator, and thus the smallest power of p that lands this elements in the center is an invariant distinguishing the group-, and consequently the bridge trisections.

All three of these groups $\pi_1(\mathbb{S}^4 - \tau^i T_{j,k}, *)$ are abstractly isomorphic to a direct product $\mathbb{Z} \times \text{Dod}^*$ of the integers with the binary dodecahedral group Dod^* ; see [[Zee65](#)]. \square

Presentations for the knot groups are for instance

$$\pi_1(\mathbb{S}^4 - \tau^2 T_{3,5}) \cong \langle x, y \mid x^3 = y^5, [a^2, x] = 1, [a^2, y] = 1 \rangle$$

where $a = a(x, y)$ is a meridian of $T_{3,5}$ expressed as a word in the non-meridional generators x, y coming from the genus 1 Heegaard decomposition of the 3-sphere. Recall that this Heegaard splitting leads to the presentation $\pi_1(\mathbb{S}^3 - T_{3,5}) \cong \langle x, y \mid x^3 = y^5 \rangle$ of the group of the torus knot complement. If we write the first homology of the complement multiplicatively generated by $H_1(\mathbb{S}^4 - \tau^2 T_{3,5}) \cong \langle t \rangle$, then under abelianization the generators of the knot group map to $x \mapsto t^5, y \mapsto t^3$, and we pick our orientations so that the meridian maps to $a \mapsto t$.

To write down the presentations for the other knot groups, we will abuse notation and reuse the letters x, y for the generators of the torus knot complement and a for a choice of meridian. With this,

$$\pi_1(\mathbb{S}^4 - \tau^3 T_{2,5}) \cong \langle x, y \mid x^2 = y^5, [a^3, x] = 1, [a^3, y] = 1 \rangle$$

$$\pi_1(\mathbb{S}^4 - \tau^5 T_{2,3}) \cong \langle x, y \mid x^2 = y^3, [a^5, x] = 1, [a^5, y] = 1 \rangle.$$

Remark 16.2. [Theorem 16.1](#) generalizes; take coprime integers $p, q, r \geq 2$ and consider the following knotted 2-spheres:

- p -twist spin of the (q, r) -torus knot, $\tau^p T_{q,r}$
- q -twist spin of the (p, r) -torus knot, $\tau^q T_{p,r}$
- r -twist spin of the (p, q) -torus knot, $\tau^r T_{p,q}$

⁴⁴ The stronger statement that these group trisections of knotted surface type are not even *stably isomorphic* (where algebraic stabilization is a suitably defined algebraic version of the perturbation operation on bridge trisections) follows from the correspondence theorem in [[BKKLR22](#)] together with Gordon's observation that $\tau^3 T_{2,5}$, $\tau^5 T_{2,3}$ and $\tau^2 T_{3,5}$ are all distinct, non-isotopic 2-knots.

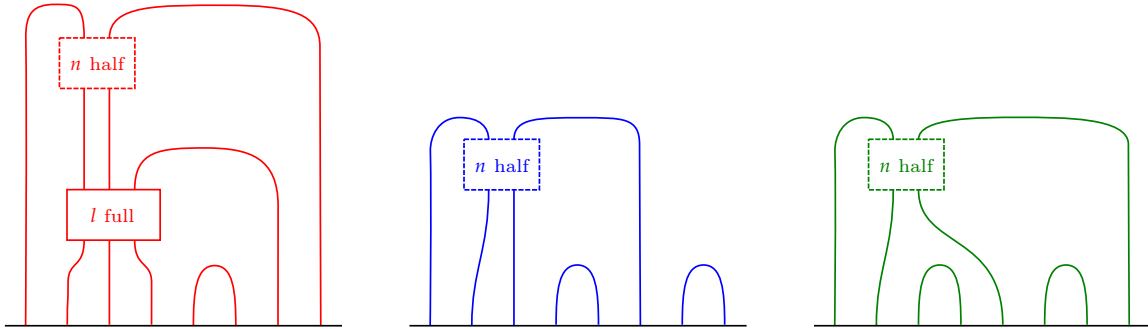


Figure 89. Triplane diagram of a 4-bridge trisection of an l -twist spin of the $(2, n)$ torus knot, $\tau^l T_{2,n}$, with $l \in \mathbb{Z}$ arbitrary and $n \in \mathbb{Z}$ not divisible by 2. The number of twisting l determines the number of full-twists in the red α -tangle, and the second parameter n of the torus knot the number of half-twists near the top of the three tangles.

Since p, q, r are pairwise coprime, all three of these knotted spheres $\tau^i T_{j,k}: \mathbb{S}^2 \hookrightarrow \mathbb{S}^4$ for $\{i, j, k\} = \{p, q, r\}$ have the same fundamental group for their complement $\pi_1(\mathbb{S}^4 - \tau^i T_{j,k}, *)$: By Zeeman [Zee65], all of them are fibered by the punctured bounded Brieskorn sphere $\Sigma(p, q, r)$, but these fibrations have monodromies with different periods. If the fiber is a homology sphere, one can show that the resulting groups of the 2-knots are abstractly isomorphic. The example for $(p, q, r) = (2, 3, 5)$ is also discussed by Boyle [Boy88], where he starts with Zeeman's observation that these twist spun 2-knots are fibered by a punctured Poincaré homology sphere $\Sigma(2, 3, 5)$. Even though they share the same group, these are non-isotopic 2-knots and one way to distinguish them is to look at the smallest power of a meridian which lies in the center of the knot group. This family of knots is further discussed in [Gor73].

16.1 Bridge trisections of twist spun 2-bridge torus knots

Both $\tau^3 T_{2,5}$ and $\tau^5 T_{2,3}$ are twist-spins of 2-bridge torus knots. Thus, they admit a bridge position with $b = 4$ and a particular general form for the three tangles. Using the recipe for twist spun knots from [MZ17], we can construct the triplane diagram for an l -twist spin of a $(2, n)$ -torus knot $\tau^l T_{2,n}$ in Figure 89. Here the number of full-twists $l \in \mathbb{Z}$ can be chosen arbitrarily and $n \in \mathbb{Z}$ is odd.

Now we can read off the generalized braid words for the three tangles as follows:

- $(\sigma_{1,2}\sigma_{2,3})^{3 \cdot l} \sigma_{1,2}^n$ for the red α -tangle with strand matching at the top $[(0, 1), (2, 7), (3, 6), (4, 5)]$,
- $\sigma_{1,2}^n$ for the blue β -tangle with strand matching at the top $[(0, 1), (2, 5), (3, 4), (6, 7)]$,
- $\sigma_{1,4}^n$ for the green γ -tangle with strand matching at the top $[(0, 1), (4, 7), (2, 3), (5, 6)]$.

16.1.1 3-twist spin of the $(2, 5)$ -torus knot, $\tau^3 T_{2,5}$. Since this is our first example for the twist-spun torus knots, we will give a detailed account of the group presentations of the individual pieces; this is also the same bridge trisection used in the example illustrating the SageMath program in Section 15.2. The description will be terser in the following sections. To illustrate this first example, we also draw the triplane diagram explicitly in Figure 90. The generalized braid words and conjugates at the maxima after the Wirtinger algorithm for each tangle are listed below:

- The generalized braid word for the red α -tangle is $(\sigma_{1,2}\sigma_{2,3}\sigma_{1,2}\sigma_{2,3}\sigma_{1,2}\sigma_{2,3})^3 \sigma_{1,2}^5 = (\sigma_{1,2}\sigma_{2,3})^9 \sigma_{1,2}^5$. This translates to three full-twists between the strands 1, 2, 3 followed by five half-twists between 1, 2. The α -tangle strand matching at the top is $[(0, 1), (2, 7), (3, 6), (4, 5)]$.

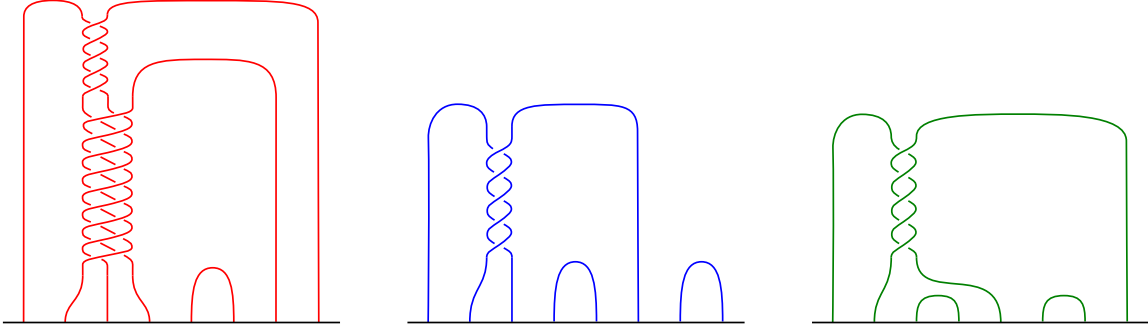


Figure 90. Triplane diagram of a 4-bridge trisection of the 3-twist spin of the $(2, 5)$ torus knot, $\tau^3 T_{2,5}$. This is the case $l = 3$, $n = 5$ of Figure 89.

The α -tangle conjugates at the top are (listed from left to right):

$$\begin{aligned} & x_0, (x_1 x_2 x_3)^3 (x_1 x_2)^3 x_1^{-1} x_2^{-1} x_1^{-1} (x_2^{-1} x_1^{-1} x_3^{-1})^3 x_2^{-1} x_1^{-1}, \\ & (x_1 x_2 x_3)^3 (x_1 x_2)^2 x_1 x_2^{-1} x_1^{-1} (x_2^{-1} x_1^{-1} x_3^{-1})^3 x_2^{-1} x_1^{-1}, (x_1 x_2 x_3)^3 (x_2^{-1} x_1^{-1} x_3^{-1})^2 x_2^{-1} x_1^{-1}, \\ & x_4, x_5, x_6, x_7 \end{aligned}$$

- The generalized braid word for the β -tangle is $\sigma_{1,2}^5$.
This translates to five half-twists between the strands 1, 2.
The β -tangle strand matching at the top is $[(0, 1), (2, 5), (3, 4), (6, 7)]$.
The β -tangle conjugates at the top are:

$$x_0, (x_1 x_2)^3 (x_1^{-1} x_2^{-1})^2 x_1^{-1}, (x_1 x_2)^2 x_1 (x_2^{-1} x_1^{-1})^2, x_3, x_4, x_5, x_6, x_7$$

- The generalized braid word for the γ -tangle is $\sigma_{1,4}^5$.
This translates to five half-twists between the strands 1, 4.
The γ -tangle strand matching at the top is $[(0, 1), (4, 7), (2, 3), (5, 6)]$.
The γ -tangle conjugates at the top are:

$$x_0, (x_1 x_4)^3 (x_1^{-1} x_4^{-1})^2 x_1^{-1}, x_2, x_3, (x_1 x_4)^2 x_1 (x_4^{-1} x_1^{-1})^2, x_5, x_6, x_7$$

We can now proceed by constructing presentations of the tangle complement groups with $2b$ generators and b relations by setting the matched conjugates equal to each other, as we have done in Section 15.2. In this example, we also want to discuss the unlinks which appear by putting pairs of the tangles together (where in each pair one of the diagrams is mirrored because of the orientation conventions). Via the method `tau_3_T_2_5.pairwise_pushout_relations()` we get a three element list containing the relations of all possible pairings of tangles. For example, the command

```
tau_3_T_2_5.F.quotient(tau_3_T_2_5.pairwise_pushout_relations()[0])
```

produces the group of the unlink $\pi_1(\mathbb{S}^3 - \mathcal{U}_{\alpha\cup\beta})$ with presentation

$$\begin{aligned} \langle x_0, x_1, x_2, x_3, x_4, x_5, x_6, x_7 \mid \text{Rel}_\alpha : & x_0(x_1 x_2 x_3)^3 (x_1 x_2)^3 x_1^{-1} x_2^{-1} x_1^{-1} (x_2^{-1} x_1^{-1} x_3^{-1})^3 x_2^{-1} x_1^{-1}, \\ & (x_1 x_2 x_3)^3 (x_1 x_2)^2 x_1 x_2^{-1} x_1^{-1} (x_2^{-1} x_1^{-1} x_3^{-1})^3 x_2^{-1} x_1^{-1} x_7, \\ & (x_1 x_2 x_3)^3 (x_2^{-1} x_1^{-1} x_3^{-1})^2 x_2^{-1} x_1^{-1} x_6, x_4 x_5; \\ \text{Rel}_\beta : & x_0(x_1 x_2)^3 (x_1^{-1} x_2^{-1})^2 x_1^{-1}, (x_1 x_2)^2 x_1 (x_2^{-1} x_1^{-1})^2 x_5 \\ & x_3 x_4, x_6 x_7 \rangle \end{aligned}$$

which is free on the two generators x_0, x_3 . This base change can be realized via the following isomorphism:

$$\begin{aligned} \pi_1(\mathbb{S}^3 - \mathcal{U}_{\alpha\cup\beta}) &\rightarrow \langle x_0, x_3 \rangle \\ x_0 &\mapsto x_0 \\ x_1 &\mapsto (x_3x_0)^2(x_3^{-1}x_0^{-1})^2x_3^{-1} \\ x_2 &\mapsto (x_3x_0)^2x_3(x_0^{-1}x_3^{-1})^3 \\ x_3, x_5 &\mapsto x_3 \\ x_4 &\mapsto x_3^{-1} \\ x_6 &\mapsto x_0^{-3}x_3^{-1}x_0^3 \\ x_7 &\mapsto x_0^{-3}x_3x_0^3 \end{aligned}$$

For completeness of this example, we also describe the remaining pairwise pushouts. The group of the union of the β - and γ -tangle is free on x_0, x_5 with presentation

$$\begin{aligned} \pi_1(\mathbb{S}^3 - \mathcal{U}_{\beta\cup\gamma}) &\cong \langle x_0, \dots, x_7 \mid \text{Rel}_\beta : x_0(x_1x_2)^3(x_1^{-1}x_2^{-1})^2x_1^{-1}, (x_1x_2)^2x_1(x_2^{-1}x_1^{-1})^2x_5, x_3x_4, x_6x_7; \\ &\quad \text{Rel}_\gamma : x_0(x_1x_4)^3(x_1^{-1}x_4^{-1})^2x_1^{-1}, (x_1x_4)^2x_1(x_4^{-1}x_1^{-1})^2x_7, x_2x_3, x_5x_6 \rangle. \end{aligned}$$

For the last pair, the group of the union of the γ - and α -tangle is free on x_1, x_4 with presentation

$$\begin{aligned} \pi_1(\mathbb{S}^3 - \mathcal{U}_{\gamma\cup\alpha}) &\cong \langle x_0, \dots, x_7 \mid \text{Rel}_\gamma : x_0(x_1x_4)^3(x_1^{-1}x_4^{-1})^2x_1^{-1}, (x_1x_4)^2x_1(x_4^{-1}x_1^{-1})^2x_7, x_2x_3, x_5x_6; \\ &\quad \text{Rel}_\alpha : x_0(x_1x_2x_3)^3(x_1x_2)^3x_1^{-1}x_2^{-1}x_1^{-1}(x_2^{-1}x_1^{-1}x_3^{-1})^3x_2^{-1}x_1^{-1}, \\ &\quad (x_1x_2x_3)^3(x_1x_2)^2x_1x_2^{-1}x_1^{-1}(x_2^{-1}x_1^{-1}x_3^{-1})^3x_2^{-1}x_1^{-1}x_7, \\ &\quad (x_1x_2x_3)^3(x_2^{-1}x_1^{-1}x_3^{-1})^2x_2^{-1}x_1^{-1}x_6, x_4x_5 \rangle. \end{aligned}$$

Finally, putting all three tangles together produces the presentation of $\pi_1(\mathbb{S}^4 - \tau^3T_{2,5})$ given in [Equation \(15.2\)](#).

16.1.2 5-twist spin of the (2, 3)-torus knot, $\tau^5T_{2,3}$. We obtain the generalized braid words by specializing the description at the beginning of the section to $l = 5$ and $n = 3$. Let us start by giving the presentation of the final pushout group $\pi_1(\mathbb{S}^4 - \tau^5T_{2,3})$ with 8 puncture generators and $3 \cdot 4$ relations, which are written in packs of four to indicate from which of the three tangles they originated.

$$\begin{aligned} \langle x_0, \dots, x_7 \mid \text{Rel}_\alpha : &x_0(x_1x_2x_3)^5(x_1x_2)^2x_1^{-1}(x_2^{-1}x_1^{-1}x_3^{-1})^5x_2^{-1}x_1^{-1}, \\ &(x_1x_2x_3)^5x_1x_2x_1(x_2^{-1}x_1^{-1}x_3^{-1})^5x_2^{-1}x_1^{-1}x_7, \\ &(x_1x_2x_3)^5(x_2^{-1}x_1^{-1}x_3^{-1})^4x_2^{-1}x_1^{-1}x_6, x_4x_5; \\ \text{Rel}_\beta : &x_0(x_1x_2)^2x_1^{-1}x_2^{-1}x_1^{-1}, x_1x_2x_1x_2^{-1}x_1^{-1}x_5, x_3x_4, x_6x_7; \\ \text{Rel}_\gamma : &x_0(x_1x_4)^2x_1^{-1}x_4^{-1}x_1^{-1}, x_1x_4x_1x_4^{-1}x_1^{-1}x_7, x_2x_3, x_5x_6 \rangle \end{aligned}$$

This is isomorphic via the map $x_0 \mapsto x_0$; $x_1 \mapsto x_0^{-1}$; $x_2, x_4, x_6 \mapsto x_2$; $x_3, x_5, x_7 \mapsto x_2^{-1}$ to the presentation

$$\langle x_0, x_2 \mid x_0^{-1}x_2x_0^{-1}x_2^{-1}x_0x_2^{-1}, x_2^5x_0^5 \rangle.$$

As expected, this is a quotient of the trefoil group $\langle x_0, x_2 \mid x_0^{-1}x_2x_0^{-1}x_2^{-1}x_0x_2^{-1} \rangle$ by the relation $x_2^5x_0^5$, which we now argue is equivalent to making the fifth power x_0^5 central in the trefoil group. If $x_0^5 = x_2^{-5}$, then x_0^5 commutes with x_2 (and obviously with itself). On the other hand, since x_0 and x_2 are conjugate in the knot group and x_0^5 is assumed to be central, we can write $x_0^5 = (w^{-1}x_2w)^5 = w^{-1}x_2^5w = x_2^5$.

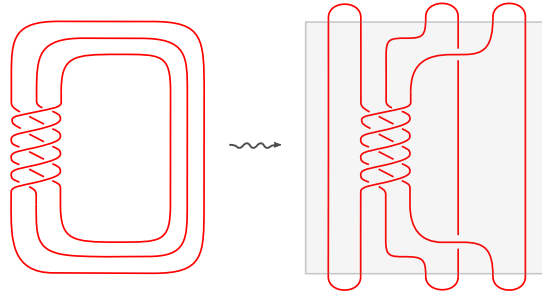


Figure 91. The $(3,5)$ torus knot as a 3-bridge plat closure.

One can construct the presentations for the individual tangles (and their associated trivial tangle homomorphisms) by taking a subset of the relations above, for example the group of the α -tangle has the presentation $\langle x_0, \dots, x_7 \mid \text{Rel}_\alpha \rangle$.

16.2 Bridge trisections of twist spun 3-bridge torus knots

The 2-knot $\tau^2 T_{3,5}$ is a twist-spin of a 3-bridge torus knot; again we can vary the twisting and torus knot parameters to obtain $\tau^l T_{3,n}$, where $l \in \mathbb{Z}$ can be chosen arbitrarily and $n \in \mathbb{Z}$ is coprime to 3. To apply the recipe for bridge trisections of twist spun knots from [MZ17], we first need to write 3-strand torus knots as a plat closure of a braid, which we demonstrate in Figure 91. Then the triplane diagram for an l -twist spin of a $(3,n)$ -torus knot $\tau^l T_{3,n}$ is depicted in Figure 92.

We can also give the generalized braid words for an l -twist spin of an $(3,n)$ -torus knot:

- $(\overline{\sigma_{7,8}} \cdot \overline{\sigma_{6,7}} \cdot \overline{\sigma_{8,9}} \cdot \overline{\sigma_{7,8}})(\sigma_{1,2}\sigma_{2,3}\sigma_{3,6}\sigma_{6,7})^l(\sigma_{7,8}\sigma_{8,9}\sigma_{6,7})(\sigma_{1,2}\sigma_{2,7})^n\sigma_{7,8}$ for the red α -tangle with strand matching at the top $[(0, 1), (2, 7), (3, 6), (4, 5), (8, 13), (9, 12), (10, 11)]$;
- $\overline{\sigma_{5,8}}(\sigma_{1,2}\sigma_{2,5})^n\sigma_{5,8}$ for the blue β -tangle with strand matching at the top $[(0, 1), (2, 5), (3, 4), (6, 7), (8, 11), (9, 10), (12, 13)]$;
- $\overline{\sigma_{7,10}}(\sigma_{1,4}\sigma_{4,7})^n\sigma_{7,10}$ for the green γ -tangle with strand matching at the top $[(0, 1), (2, 3), (4, 7), (5, 6), (8, 9), (10, 13), (11, 12)]$.

16.2.1 2-twist spin of the $(3,5)$ -torus knot, $\tau^2 T_{3,5}$. We illustrate this example explicitly in the triplane diagram Figure 93. The final pushout group $\pi_1(\mathbb{S}^4 - \tau^2 T_{3,5})$ has 14 puncture generators and $3 \cdot 7$ relations, written in packs of seven to indicate from which of the three tangles they originated. The complete presentation is written down in Figure 94.

This finishes our discussion of the group trisections of knotted surface type corresponding to the standard bridge trisections of twist-spun torus knots. We can simplify the presentation with the isomorphism in Figure 95.

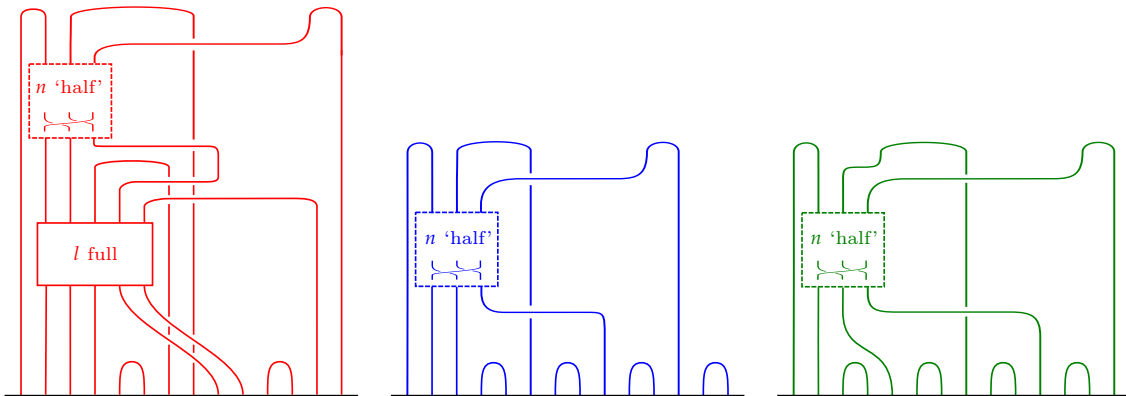


Figure 92. Triplane diagram of a 7-bridge trisection of an l -twist spin of the $(3, n)$ torus knot, $\tau^l T_{3,n}$, with $l \in \mathbb{Z}$ and $n \in \mathbb{Z}$ not divisible by 3. The number of twisting l determines the number of full-twists in the red α -tangle, and the second parameter n of the torus knot the number of times one of the strands crosses over all the others in the 3-bundle near the top.

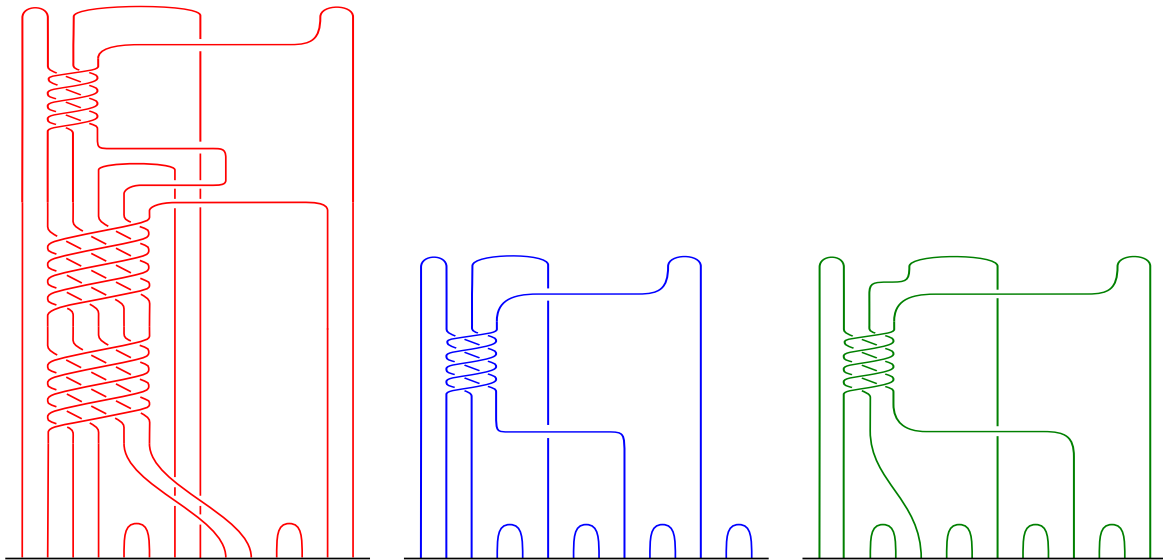


Figure 93. Triplane diagram of a 7-bridge trisection of the 2-twist spin of the $(3, 5)$ -torus knot, $\tau^2 T_{3,5}$. This is the case $l = 2$, $n = 5$ of Figure 92.

$$\begin{aligned}
\langle x_0, \dots, x_{13} \mid \text{Rel}_\alpha : & x_0(x_1x_2x_3x_8x_9)^2(x_1x_2x_8)^2x_2^{-1}x_1^{-1}x_8^{-1}(x_2^{-1}x_1^{-1}x_9^{-1}x_8^{-1}x_3^{-1})^2x_2^{-1}x_1^{-1}, \\
& (x_1x_2x_3x_8x_9)^2x_1x_2x_8x_1x_2x_8^{-1}x_2^{-1}x_1^{-1}(x_8^{-1}x_3^{-1}x_2^{-1}x_1^{-1}x_9^{-1})^2x_8^{-1}x_7 \\
& (x_8x_9x_1x_2x_3)^2x_8x_1x_2x_8x_1x_2^{-1}x_1^{-1}x_8^{-1}(x_2^{-1}x_1^{-1}x_9^{-1}x_8^{-1}x_3^{-1})^2x_2^{-1}x_1^{-1}, \\
& (x_1x_2x_3x_8x_9)^2x_2^{-1}x_1^{-1}x_9^{-1}x_8^{-1}x_3^{-1}x_2^{-1}x_1^{-1}x_9^{-1}x_8^{-1}x_6(x_8x_9x_1x_2x_3)^2(x_9^{-1}x_8^{-1}x_3^{-1}x_2^{-1}x_1^{-1})^2, \\
& x_4x_5, (x_1x_2x_3x_8x_9)^2x_1x_2x_8x_1x_2x_1^{-1}x_8^{-1}(x_2^{-1}x_1^{-1}x_9^{-1}x_8^{-1}x_3^{-1})^2x_2^{-1}x_1^{-1}x_{13}, \\
& (x_1x_2x_3x_8x_9)^2x_8^{-1}x_3^{-1}x_2^{-1}x_1^{-1}x_9^{-1}x_8^{-1}x_3^{-1}x_2^{-1}x_1^{-1}x_{12}, x_{10}x_{11}; \\
\text{Rel}_\beta : & x_0(x_1x_2x_8)^2x_2^{-1}x_1^{-1}x_8^{-1}x_2^{-1}x_1^{-1}, \\
& x_1x_2x_8x_1x_2x_8^{-1}x_2^{-1}x_1^{-1}x_8^{-1}x_5x_8x_1x_2x_8x_1x_2^{-1}x_1^{-1}x_8^{-1}x_2^{-1}x_1^{-1}, \\
& x_3x_4, x_6x_7, x_1x_2x_8x_1x_2x_1^{-1}x_8^{-1}x_2^{-1}x_1^{-1}x_{11}, x_9x_{10}, x_{12}x_{13}; \\
\text{Rel}_\gamma : & x_0(x_1x_4x_{10})^2x_4^{-1}x_1^{-1}x_{10}^{-1}x_4^{-1}x_1^{-1}, x_2x_3, \\
& x_1x_4x_{10}x_1x_4x_{10}^{-1}x_4^{-1}x_1^{-1}x_{10}^{-1}x_7x_{10}x_1x_4x_{10}x_1x_4^{-1}x_1^{-1}x_{10}^{-1}x_4^{-1}x_1^{-1}, \\
& x_5x_6, x_8x_9, x_1x_4x_{10}x_1x_4x_1^{-1}x_{10}^{-1}x_4^{-1}x_1^{-1}x_{13}, x_{11}x_{12} \rangle
\end{aligned}$$

Figure 94. Final pushout of the 7-bridge group trisection of knotted surface type of $\tau^2T_{3,5}$ corresponding to the bridge trisection in [Figure 93](#).

$$\begin{aligned}
\langle x_0, \dots, x_{13} \mid \text{Rel}_\alpha, \text{Rel}_\beta, \text{Rel}_\gamma \rangle & \rightarrow \langle x_1, x_2, x_8 \mid x_1^2x_8^{-1}x_1^{-2}x_8, x_2^{-1}x_1^{-2}x_2x_1^2, x_8^{-1}x_2^{-1}x_1x_8^{-1}x_1^{-1}x_2x_8x_1^{-1}x_2x_1, \\
& x_1x_2x_8x_1^{-1}x_2x_8^{-1}x_2^{-1}x_1^{-1}x_8^{-1}x_2 \rangle \\
x_0 & \mapsto x_1^{-1}x_2x_8x_1x_2x_1^{-1}x_8^{-1}x_2^{-1}x_1^{-1}x_8^{-1}x_1 \\
x_1 & \mapsto x_1 \\
x_2, x_4, x_6 & \mapsto x_2 \\
x_3, x_5, x_7 & \mapsto x_2^{-1} \\
x_8, x_{10}, x_{12} & \mapsto x_8 \\
x_9, x_{11}, x_{13} & \mapsto x_8^{-1}.
\end{aligned}$$

Figure 95. Simplification isomorphism of the group presentation for $\pi_1(\mathbb{S}^4 - \tau^2T_{3,5})$ in [Figure 94](#). The first two relations of the simplified presentation proclaim x_1^2 to commute with the other generators x_2, x_8 which makes this second power of a meridian central. The last two relations are from a Wirtinger presentation of the torus knot $T_{3,5}$ in the 3-sphere.

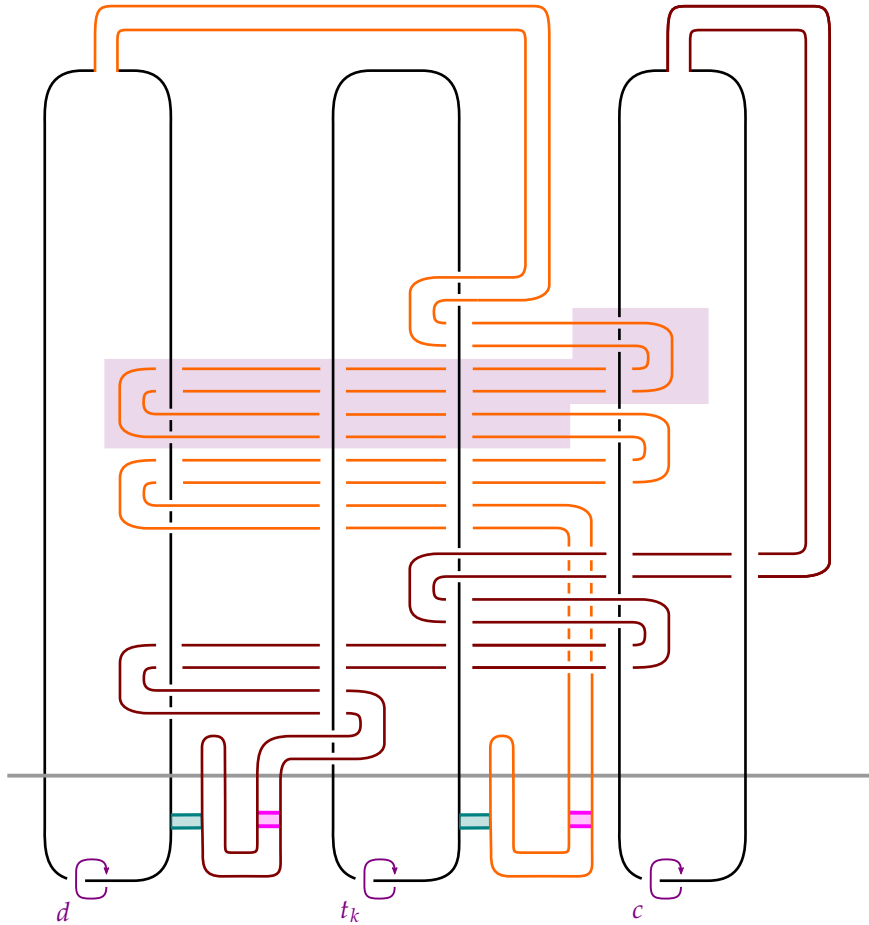


Figure 96. Banded bridge position of Suci's 2-knot $R_k: \mathbb{S}^2 \hookrightarrow \mathbb{S}^4$ for $k = 3$. The lightly shaded box indicates which part of the orange fusion band needs to be duplicated to increase the parameter k .

17 SUCIU'S TREFOIL GROUP

17.1 Bridge trisections of Suci's knots

In this section, starting from Suci's ribbon presentation [Suc85, Fig. 6] of R_k reproduced in Figure 22a, we construct 7-bridge trisections of the knotted spheres. We previously dualized one of each parallel saddle band to convert the equatorial cross-section into the banded unlink diagram Figure 22b. The algorithmic procedure from [MZ17] transforms this diagram into banded bridge trisected position, as in Figure 96.⁴⁵ For fusion number 2 ribbon presentations, this yields a $(7, 3, 3, 3)$ -bridge trisection (i.e. there are 7 bridges with 14 bridge points, and 3 patches in each sector). In our figures, we illustrate the banded bridge splitting and resulting bridge trisection for $k = 3$; increasing this parameter $k \in \mathbb{N}$ amounts to adding additional linking of the orange fusion band with the minima c and d .

The three triplane diagrams resulting from the banded bridge splitting are pictured in Figure 97. For the α -tangle we take the trivial tangle above the bridge sphere, for the β -tangle we use the tangle below the bridge sphere where we forget the bands, and for the γ -tangle we perform band surgery along the bands in the bottom tangle.

⁴⁵ For an alternative approach to this, compare the *ribbon bridge trisections* in the work of Joseph-Meier-Miller-Zupan [Jos+21].

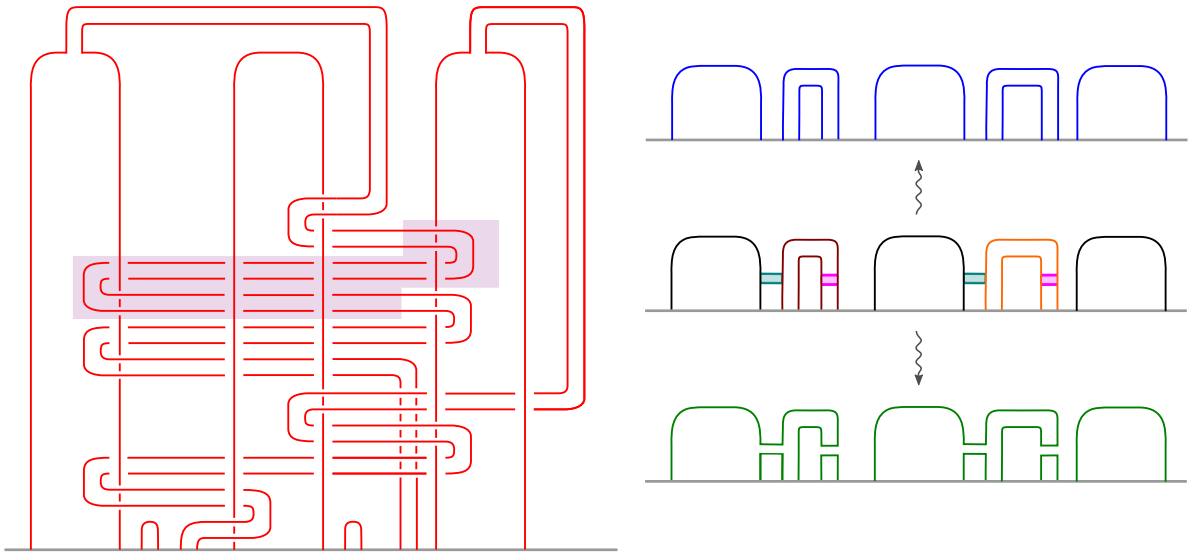


Figure 97. The three trivial tangles of a 7-bridge trisection of Suci's knot R_k , for $k = 3$. This is constructed from the banded bridge splitting in Figure 96 as follows: The red α -tangle (**left**) consists of the strands above the bridge sphere. For the blue β -tangle (**top right**) take the strands below the bridge sphere and forget the bands. Finally, the green γ -tangle (**bottom right**) is the result of performing band surgery on the strands below the bridge sphere. An additional isotopy would be needed to bring the γ -tangle into Morse position with 7 maxima. Different parameters $k \in \mathbb{N}_{\geq 2}$ can be achieved by repeating the shaded pattern in the α -tangle $k - 1$ times.

Remark 17.1. We can use a few tricks to decrease the number of crossings in a triplane diagram of a bridge splitting for R_k . For example, in Figure 98 we show an alternative banded bridge splitting in which we have made the minima t_k and c switch places horizontally. When increasing k , this does not add additional crossings between the orange fusion band and the t_k -minimum. Observe that the cores of the fusion bands still read off the same elements in the fundamental group of the minima unlink complement as before. This confirms that the picture is indeed describing Suci's ribbon knot R_k . Recall that in the banded unlink diagram, we can perform band passes between the orange and brown fusion bands without changing the isotopy class of the resulting knotted ribbon surface.

17.2 Group trisections of Suci's knots

THEOREM 17.2. *There exist infinitely many non-isomorphic 7-bridge group trisections of knotted surface type of the trefoil knot group.*

Proof. In the remainder of this section, we will describe how to obtain group trisections of knotted surface type from the bridge trisections of Suci's ribbon knots R_k . As there is no meridian-preserving isomorphism between the knot groups $\pi_1(\mathbb{S}^4 - R_k)$ for different k according to [Suc85], the knotted surface group trisection cubes cannot be isomorphic.⁴⁶ □

Meridians of the 14 punctures on the bridge sphere are called $x_0, x_1, x_2, \dots, x_{12}, x_{13}$, from left to right in the diagrams. The matching of the tangle strands at the maxima is independent of the parameter $k \in \mathbb{N}$, and is given below.

- α -tangle matching: $[(0, 7), (1, 6), (2, 3), (4, 5), (8, 9), (10, 13), (11, 12)]$;

⁴⁶ Again, this theorem can be strengthened and Suci's result obstructs stable isomorphism of the group trisections of knotted surface type, by using the techniques of [BKCLR22].

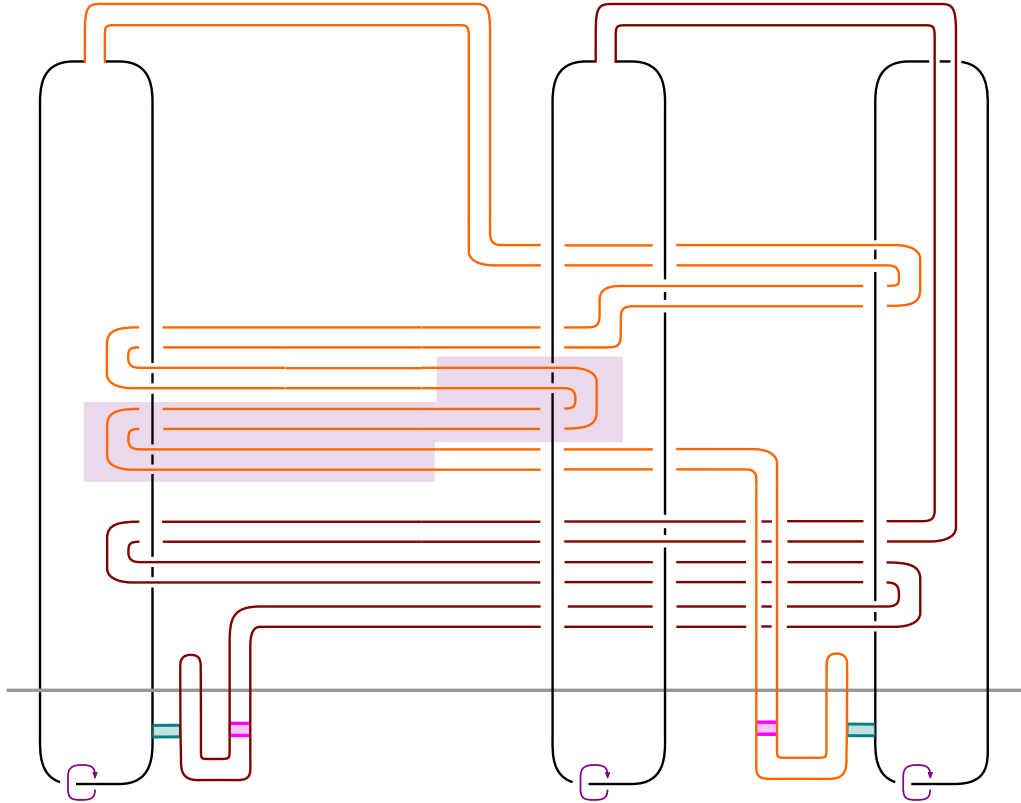


Figure 98. Alternative banded bridge position for Suciu’s knot R_k for $k = 3$. Compared with Figure 96, we have flipped the order in which the minima t_k and c are drawn. We again shaded the region in the orange band that has to be repeated $k - 1$ times to obtain other parameters $k \in \mathbb{N}_{\geq 2}$.

- β -tangle matching: $[(0, 1), (2, 5), (3, 4), (6, 7), (8, 11), (9, 10), (12, 13)]$;
- γ -tangle matching: $[(0, 3), (1, 2), (4, 5), (6, 9), (7, 8), (10, 11), (12, 13)]$.

Now we write down the generalized braid word for the α -tangle in R_k , note the repeating pattern depending on $k \in \mathbb{N}_{\geq 1}$ which is responsible for adding additional linking of the orange fusion band with the minima d and c :

$$\begin{aligned} & \sigma_{5,6}\sigma_{4,5}\sigma_{4,5}\sigma_{5,6}\sigma_{1,4}^{-1}\sigma_{4,5}^{-1}\sigma_{4,5}^{-1}\sigma_{1,4}^{-1}\sigma_{5,6}^{-1}\sigma_{4,5}^{-1}\sigma_{6,7}^{-1}\sigma_{5,6}^{-1} \\ & \sigma_{7,10}\sigma_{10,11}\sigma_{6,7}\sigma_{7,10}\sigma_{11,12}^{-1}\sigma_{10,11}^{-1}\sigma_{10,11}^{-1}\sigma_{11,12}^{-1}\sigma_{7,10}^{-1}\sigma_{10,11}^{-1}\sigma_{6,7}^{-1}\sigma_{7,10}^{-1} \\ & \sigma_{5,6}\sigma_{6,7}\sigma_{6,7}\sigma_{5,6}\sigma_{7,10}\sigma_{10,11}\sigma_{6,7}\sigma_{7,10}\sigma_{11,12}^{-1}\sigma_{10,11}^{-1}\sigma_{12,13}^{-1}\sigma_{11,12}^{-1} \\ & \sigma_{5,6}\sigma_{6,7}\sigma_{4,5}\sigma_{5,6}\sigma_{1,4}^{-1}\sigma_{4,5}^{-1}\sigma_{4,5}^{-1}\sigma_{1,4}^{-1}\sigma_{5,6}^{-1}\sigma_{4,5}^{-1}\sigma_{6,7}^{-1}\sigma_{5,6}^{-1}\sigma_{7,10}^{-1}\sigma_{6,7}^{-1}\sigma_{6,7}^{-1}\sigma_{7,10}^{-1} \\ & (\sigma_{5,6}\sigma_{6,7}\sigma_{4,5}\sigma_{5,6}\sigma_{1,4}^{-1}\sigma_{4,5}^{-1}\sigma_{4,5}^{-1}\sigma_{1,4}^{-1}\sigma_{5,6}^{-1}\sigma_{4,5}^{-1}\sigma_{6,7}^{-1}\sigma_{5,6}^{-1}\sigma_{7,10}^{-1}\sigma_{6,7}^{-1}\sigma_{6,7}^{-1}\sigma_{7,10}^{-1})^{k-1} \\ & \sigma_{5,6}\sigma_{6,7}\sigma_{6,7}\sigma_{5,6} \end{aligned}$$

Further, there are no crossings in the β - and γ -tangle of Suciu’s knots, thus the generalized braid word representing them is empty.

From the matching of the tangle strands, we obtain the relations for the tangle complement groups. Observe that the relations for the β - and γ -tangle complement are independent of k .

- The α -tangle corresponds to the following quotient of the punctured sphere group

$$\langle x_0, x_1, x_2, x_3, x_4, x_5, x_6, x_7, x_8, x_9, x_{10}, x_{11}, x_{12}, x_{13} \mid \text{Rel}_\alpha^0(k), \dots, \text{Rel}_\alpha^6(k) \rangle$$

where the 7 relations are listed in [Table 3](#) for the case $k = 3$. The SageMath program can be used to compute the relations for other $k > 3$, but the output gets unwieldy quickly because of the high number of additional crossings.

– Relations for the β -tangle complement:

$$\langle x_0, x_1, x_2, x_3, x_4, x_5, x_6, x_7, x_8, x_9, x_{10}, x_{11}, x_{12}, x_{13} \mid x_0x_1, x_2x_5, x_3x_4, x_6x_7, x_8x_{11}, x_9x_{10}, x_{12}x_{13} \rangle$$

– Relations for the γ -tangle complement:

$$\langle x_0, x_1, x_2, x_3, x_4, x_5, x_6, x_7, x_8, x_9, x_{10}, x_{11}, x_{12}, x_{13} \mid x_0x_3, x_1x_2, x_4x_5, x_6x_9, x_7x_8, x_{10}x_{11}, x_{12}x_{13} \rangle$$

In fact, all of the groups of the unlinks from the pairwise unions $\pi_1(\mathbb{S}^3 - \mathcal{U}_{\alpha\cup\beta})$, $\pi_1(\mathbb{S}^3 - \mathcal{U}_{\beta\cup\gamma})$ and $\pi_1(\mathbb{S}^3 - \mathcal{U}_{\gamma\cup\alpha})$ of the tangles are freely generated by $\langle x_0, x_6, x_{12} \rangle$. This aligns with our previous claim that the patch number is equal to 3 in each sector.

For every $k \geq 3$, the presentation for $\pi_1(\mathbb{S}^4 - R_k)$ can be simplified via the map

$$\begin{aligned} x_0, x_2, x_4 &\mapsto x_0; \quad x_1, x_3, x_5 \mapsto x_0^{-1}; \\ x_6, x_8, x_{10} &\mapsto x_6; \quad x_7, x_9, x_{11} \mapsto x_6^{-1}; \\ x_{12} &\mapsto x_{12}; \quad x_{13} \mapsto x_{12}^{-1} \end{aligned}$$

to the following presentation:

$$\begin{aligned} \langle x_0, \dots, x_{13} \mid \text{Rel}_\alpha(k), \text{Rel}_\beta, \text{Rel}_\gamma \rangle &\rightarrow \langle x_0, x_6, x_{12} \mid x_{12}x_6^{-1}x_{12}^{-1}x_0x_6x_0^{-1}x_6^{-1}x_0^{-1}x_{12}x_6, \\ &\quad x_0x_6^{-1}(x_{12}^{-1}x_0)^{k-1}x_6^{-1}(x_0^{-1}x_{12})^{k-1}x_6 \rangle \end{aligned}$$

Under the map $x_0 \mapsto d^{-1}$; $x_6 \mapsto t_k^{-1}$; $x_{12} \mapsto c^{-1}$ this corresponds to the fusion number 2 ribbon presentation of $\pi_1(\mathbb{S}^4 - R_k)$ we discussed in [Section 6.3](#):

$$\langle t_k, c, d \mid d^{-1} \cdot t_k(dc^{-1})^{-k+1} \cdot t_k \cdot (t_k(dc^{-1})^{-k+1})^{-1}; \quad c^{-1} \cdot t_kcd^{-1}t_k^{-1} \cdot d \cdot (t_kcd^{-1}t_k^{-1})^{-1} \rangle$$

18 CONCLUSION AND FURTHER DIRECTIONS FOR STUDYING GROUP TRISECTIONS OF KNOTTED SURFACE TYPE

Bridge trisections are particularly suited for studying covers of 4-manifolds branched over smoothly embedded surfaces. This is because a bridge trisection of the branching surface downstairs can be lifted to a trisection of the 4-manifold upstairs. Observe that a branched cover over a trivial tangle in a 3-dimensional handlebody is again a 3-dimensional handlebody (and similarly, a branched cover over a trivial disk system in a 4-dimensional 1-handlebody yields a 4-dimensional 1-handlebody). For examples of this, see [\[LM21\]](#) for branched covers over complex curves in the projective plane, and [\[Bla+20b\]](#) for dihedral branched covers over surfaces in the 4-sphere.

Upcoming joint work [\[ACMPR22\]](#) with Akram Alishahi, Patricia Cahn, Gordana Matic and Juanita Pinzón-Cañedo will describe a trisected version of the Reidemeister-Schreier algorithm. This algorithm computes presentations of subgroups of finitely presented groups, which can in particular be applied to the fundamental groups of covering spaces; see also [\[Fox62, Sec. 8\]](#).

Suciu's knots can be distinguished by the fundamental groups of their double branched covers [\[KS20\]](#). With the group trisection of the complement of Suciu's example constructed above, we can refine the detection result by applying the trisected Reidemeister-Schreier algorithm, which results in a group trisection of the branched cover (i.e. a group trisection of a closed 4-manifold). Unfortunately, since the complexity of the group trisection of Suciu's knots grows very quickly with the parameter $k \in \mathbb{N}$, this does not appear to be feasible without computer assistance. Nevertheless, using our computer implementation of the trisected Reidemeister-Schreier algorithm, we were able to confirm the results of [\[KS20\]](#); a detailed documentation will appear in [\[ACMPR22\]](#).

$$\text{Rel}_a^2(k=3) = x_2 x_3,$$

$$\begin{aligned} \text{Rel}_a^3(k=3) = & (x_4 x_5 x_6 x_5^{-1} x_4^{-1} x_7 x_{12}^{-1} x_7^{-1} x_6^{-1} x_5^{-1} x_4^{-1} x_1^{-1} x_4 x_5 x_6 x_4 x_5 x_6^{-1} x_5^{-1} x_4^{-1} x_1 x_4 x_5 x_6 x_7 x_{12} x_7^{-1} x_7^{-1} x_6^{-1} x_5^{-1} x_4^{-1} \\ & x_1^{-1} x_4 x_5 x_6 x_5^{-1} x_4^{-1} x_6^{-1} x_5^{-1} x_4^{-1} x_1 x_4 x_5 x_6 x_7 x_{12} x_7^{-1} x_{12}^{-1} x_7^{-1} x_6^{-1} x_5^{-1} x_4^{-1} x_1^{-1} x_4 x_5 x_6 x_5^{-1} x_4^{-1} x_6^{-1} x_5^{-1} x_4^{-1} x_1 x_4 x_5 \\ & x_6 (x_7 x_{12}^{-1} x_7^{-1} x_6^{-1} x_5^{-1} x_4^{-1} x_1^{-1} x_4 x_5 x_6 x_4 x_5 x_6^{-1} x_5^{-1} x_4^{-1} x_1 x_4 x_5 x_6 x_7 x_{12})^2 x_7^{-1} x_{12}^{-1} x_7^{-1} x_6^{-1} x_5^{-1} x_4^{-1} x_1^{-1} x_4 x_5 x_6 x_5^{-1} \\ & x_4^{-1} x_6^{-1} x_5^{-1} x_4^{-1} x_1 x_4 x_5 x_6 x_7 x_{12} x_7^{-1} x_6^{-1} x_5^{-1} x_4^{-1} x_1^{-1} x_4 x_5 x_6 x_4 x_5 x_6^{-1} x_5^{-1} x_4^{-1} x_1 x_4 x_5 x_6 x_7 x_{11}^{-1} x_{10}^{-1} x_7^{-1} x_6^{-1} x_5^{-1} \\ & x_4^{-1} x_1^{-1})^2 x_4 x_5 x_6 x_5^{-1} x_4^{-1} x_6^{-1} x_5^{-1} x_4^{-1} x_1^{-1} (x_4 x_5 x_6 x_4 x_5 x_6^{-1} x_5^{-1} x_4^{-1} x_1 x_4 x_5 x_6 x_7 x_{10} x_{11} x_7^{-1} x_6^{-1} x_5^{-1} x_4^{-1} x_1^{-1} x_4 x_5 x_6 \\ & x_5^{-1} x_4^{-1} x_6^{-1} x_5^{-1} x_4^{-1} x_1)^2 x_4 x_5 x_6 x_7 x_{12} x_7^{-1} x_6^{-1} x_5^{-1} x_4^{-1} x_1^{-1} x_4 x_5 x_6 x_4 x_5 x_6^{-1} x_5^{-1} x_4^{-1} x_1 x_4 x_5 x_6 x_7 x_{12} x_7 (x_{12}^{-1} x_7^{-1} \\ & x_6^{-1} x_5^{-1} x_4^{-1} x_1^{-1} x_4 x_5 x_6 x_5^{-1} x_4^{-1} x_6^{-1} x_5^{-1} x_4^{-1} x_1 x_4 x_5 x_6 x_7 x_{12} x_7^{-1})^2 x_6^{-1} x_5^{-1} x_4^{-1} x_1^{-1} x_4 x_5 x_6 x_4 x_5 x_6^{-1} x_5^{-1} x_4^{-1} x_1 x_4 \\ & x_5 x_6 x_7 x_{12} x_7 x_{12}^{-1} x_7^{-1} x_6^{-1} x_5^{-1} x_4^{-1} x_1^{-1} x_4 x_5 x_6 x_4 x_5 x_6^{-1} x_5^{-1} x_4^{-1} x_1 x_4 x_5 x_6 x_7 x_{12} x_7^{-1} x_{12}^{-1} x_7^{-1} x_6^{-1} x_5^{-1} x_4^{-1} x_1^{-1} x_4 x_5 x_6 \\ & x_5^{-1} x_4^{-1} x_6^{-1} x_5^{-1} x_4^{-1} x_1 x_4 x_5 x_6 x_7 x_{12} x_7^{-1} x_4 x_5 x_6^{-1} x_5^{-1} x_4^{-1} x_1 x_4 x_5 x_6 x_7 x_{10} x_{11} x_7^{-1} x_6^{-1} x_5^{-1} x_4^{-1} x_1^{-1} x_4 x_5 x_6 x_5^{-1} x_4^{-1} \\ & x_6^{-1} x_5^{-1} x_4^{-1} x_1 x_4 x_5 x_6 x_7 x_{12} x_7^{-1} x_6^{-1} x_5^{-1} x_4^{-1} x_1^{-1} x_4 x_5 x_6 x_4 x_5 x_6^{-1} x_5^{-1} x_4^{-1} x_1 x_4 x_5 x_6 x_7 x_{12} x_7 (x_{12}^{-1} x_7^{-1} x_6^{-1} x_5^{-1} x_4^{-1} \\ & x_1^{-1} x_4 x_5 x_6 x_5^{-1} x_4^{-1} x_6^{-1} x_5^{-1} x_4^{-1} x_1 x_4 x_5 x_6 x_7 x_{12} x_7^{-1})^2 x_6^{-1} x_5^{-1} x_4^{-1} x_1^{-1} x_4 x_5 x_6 x_4 x_5 x_6^{-1} x_5^{-1} x_4^{-1} x_1 x_4 x_5 x_6 x_7 x_{12} (x_7 \\ & x_{12}^{-1} x_7^{-1} x_6^{-1} x_5^{-1} x_4^{-1} x_1^{-1} x_4 x_5 x_6 x_4 x_5 x_6^{-1} x_5^{-1} x_4^{-1} x_1 x_4 x_5 x_6 x_7 x_{12} x_7 x_{12}^{-1} x_7^{-1} x_6^{-1} x_5^{-1} x_4^{-1} x_1^{-1} x_4 x_5 x_6 x_5^{-1} x_4^{-1} x_6^{-1} \\ & x_5^{-1} x_4^{-1} x_1 x_4 x_5 x_6 x_7 x_{12} x_7^{-1} x_{12}^{-1} x_7^{-1} x_6^{-1} x_5^{-1} x_4^{-1} x_1^{-1} x_4 x_5 x_6 x_5^{-1} x_4^{-1} x_6^{-1} x_5^{-1} x_4^{-1} x_1 x_4 x_5 x_6 (x_7 x_{12}^{-1} x_7^{-1} x_6^{-1} x_5^{-1} \\ & x_4^{-1} x_1^{-1} x_4 x_5 x_6 x_4 x_5 x_6^{-1} x_5^{-1} x_4^{-1} x_1 x_4 x_5 x_6 x_7 x_{12})^2 x_7^{-1} x_{12}^{-1} x_7^{-1} x_6^{-1} x_5^{-1} x_4^{-1} x_1^{-1} x_4 x_5 x_6 x_5^{-1} x_4^{-1} x_6^{-1} x_5^{-1} x_4^{-1} x_1 x_4 \\ & x_5 x_6 x_7 x_{12} x_7^{-1} x_6^{-1} x_5^{-1} x_4^{-1} x_1^{-1} x_4 x_5 x_6 x_4 x_5 x_6^{-1} x_5^{-1} x_4^{-1} x_1 x_4 x_5 x_6 x_7 x_{11}^{-1} x_{10}^{-1} x_7^{-1} x_6^{-1} x_5^{-1} x_4^{-1} x_1^{-1} x_4 x_5 x_6 x_5^{-1} x_4^{-1})^2 \\ & x_6^{-1} x_5^{-1} x_4^{-1} x_1^{-1} x_4 x_5 x_6 x_4 x_5 x_6^{-1} x_5^{-1} x_4^{-1} x_1 x_4 x_5 x_6 x_7 x_{11}^{-1} x_{10}^{-1} x_7^{-1} x_6^{-1} x_5^{-1} x_4^{-1} x_1^{-1} x_4 x_5 x_6 x_5^{-1} x_4^{-1} x_6^{-1} x_5^{-1} x_4^{-1} x_1 \\ & x_4 x_5 x_6 (x_4 x_5 x_6^{-1} x_5^{-1} x_4^{-1} x_1 x_4 x_5 x_6 x_7 x_{10} x_{11} x_7^{-1} x_6^{-1} x_5^{-1} x_4^{-1} x_1^{-1} x_4 x_5 x_6 x_5^{-1} x_4^{-1} x_6^{-1} x_5^{-1} x_4^{-1} x_1 x_4 x_5 x_6 x_7 x_{12}^{-1} x_7^{-1} \\ & x_6^{-1} x_5^{-1} x_4^{-1} x_1^{-1} x_4 x_5 x_6 x_4 x_5 x_6^{-1} x_5^{-1} x_4^{-1} x_1 x_4 x_5 x_6 x_7 x_{12} x_7 (x_{12}^{-1} x_7^{-1} x_6^{-1} x_5^{-1} x_4^{-1} x_1^{-1} x_4 x_5 x_6 x_5^{-1} x_4^{-1} x_6^{-1} x_5^{-1} x_4^{-1} x_1 \\ & x_4 x_5 x_6 x_7 x_{12} x_7^{-1})^2 x_6^{-1} x_5^{-1} x_4^{-1} x_1^{-1} x_4 x_5 x_6 x_4 x_5 x_6^{-1} x_5^{-1} x_4^{-1} x_1 x_4 x_5 x_6 x_7 x_{12} x_7 x_{12}^{-1} x_7^{-1} x_6^{-1} x_5^{-1} x_4^{-1} x_1^{-1} x_4 x_5 x_6 x_4 x_5 \\ & x_6^{-1} x_5^{-1} x_4^{-1} x_1 x_4 x_5 x_6 x_7 x_{12} x_7^{-1} x_{12}^{-1} x_7^{-1} x_6^{-1} x_5^{-1} x_4^{-1} x_1^{-1} x_4 x_5 x_6 x_5^{-1} x_4^{-1} x_6^{-1} x_5^{-1} x_4^{-1} x_1 x_4 x_5 x_6 x_7 x_{12} x_7^{-1})^2, \end{aligned}$$

$$\text{Rel}_a^4(k=3) = x_8 x_9$$

Table 4. Relations for the α -tangle in the group trisection of Suci's R_3 , continued.

REFERENCES

- [AGK18] A. ABRAMS, D. T. GAY, and R. KIRBY. Group trisections and smooth 4-manifolds. *Geom. Topol.* 22.3 (2018), pp. 1537–1545. ISSN: 1465-3060. DOI: [10.2140/gt.2018.22.1537](https://doi.org/10.2140/gt.2018.22.1537). arXiv: [1605.06731](https://arxiv.org/abs/1605.06731) [[math.GT](#)] ([↑ 11](#), [133](#), [137](#), [139](#)).
- [AGL17] P. ACETO, M. GOLLA, and K. LARSON. Embedding 3-manifolds in spin 4-manifolds. *J. Topol.* 10.2 (2017), pp. 301–323. ISSN: 1753-8416. DOI: [10.1112/topo.12010](https://doi.org/10.1112/topo.12010). arXiv: [1607.06388](https://arxiv.org/abs/1607.06388) [[math.GT](#)] ([↑ 10](#)).
- [Akb83] S. AKBULUT. *Unpublished observation at the CBMS conference held at Santa Barbara*. 1983 ([↑ 8](#)).
- [Akb10] S. AKBULUT. Cappell-Shaneson homotopy spheres are standard. *Ann. of Math. (2)* 171.3 (2010), pp. 2171–2175. ISSN: 0003-486X. DOI: [10.4007/annals.2010.171.2171](https://doi.org/10.4007/annals.2010.171.2171). arXiv: [0907.0136](https://arxiv.org/abs/0907.0136) [[math.GT](#)] ([↑ 7](#)).
- [Akb16] S. AKBULUT. *4-manifolds*. Vol. 25. Oxford Graduate Texts in Mathematics. Oxford University Press, Oxford, 2016, pp. xii+262. ISBN: 978-0-19-878486-9. DOI: [10.1093/acprof:oso/9780198784869.001.0001](https://doi.org/10.1093/acprof:oso/9780198784869.001.0001) ([↑ 8](#)).
- [ACMPR22] A. ALISHAHI, P. CAHN, G. MATIC, J. PINZÓN-CAICEDO, and B. RUPPIK. *Trisected Reidemeister-Schreier and dihedral branched covers*. In preparation. 2022 ([↑ 167](#)).
- [Art25] E. ARTIN. Zur Isotopie zweidimensionaler Flächen im \mathbb{R}^4 . *Abh. Math. Sem. Univ. Hamburg* 4.1 (1925), pp. 174–177. ISSN: 0025-5858. DOI: [10.1007/BF02950724](https://doi.org/10.1007/BF02950724) ([↑ 34](#)).
- [AFW15] M. ASCHENBRENNER, S. FRIEDL, and H. WILTON. Decision problems for 3-manifolds and their fundamental groups. In: *Interactions between low-dimensional topology and mapping class groups*. Vol. 19. Geom. Topol. Monogr. Geom. Topol. Publ., Coventry, 2015, pp. 201–236. DOI: [10.2140/gtm.2015.19.201](https://doi.org/10.2140/gtm.2015.19.201). arXiv: [1405.6274](https://arxiv.org/abs/1405.6274) [[math.GT](#)] ([↑ 140](#)).
- [BK20] S. BAADER and A. KJUCHUKOVA. Symmetric quotients of knot groups and a filtration of the Gordian graph. *Math. Proc. Cambridge Philos. Soc.* 169.1 (2020), pp. 141–148. ISSN: 0305-0041. DOI: [10.1017/s0305004119000136](https://doi.org/10.1017/s0305004119000136). arXiv: [1711.08144](https://arxiv.org/abs/1711.08144) [[math.GT](#)] ([↑ 48](#)).
- [Bak20] K. L. BAKER. The Poincaré homology sphere, lens space surgeries, and some knots with tunnel number two. *Pacific J. Math.* 305.1 (2020). With an appendix by Baker and Neil R. Hoffman, pp. 1–27. ISSN: 0030-8730. DOI: [10.2140/pjm.2020.305.1](https://doi.org/10.2140/pjm.2020.305.1). arXiv: [1504.06682](https://arxiv.org/abs/1504.06682) [[math.GT](#)] ([↑ 108](#)).
- [BS16] R. İ. BAYKUR and N. SUNUKJIAN. Knotted surfaces in 4-manifolds and stabilizations. *J. Topol.* 9.1 (2016), pp. 215–231. ISSN: 1753-8416. DOI: [10.1112/jtopol/jtv039](https://doi.org/10.1112/jtopol/jtv039). arXiv: [1504.04086](https://arxiv.org/abs/1504.04086) [[math.GT](#)] ([↑ 23](#), [25](#), [29](#), [34](#), [41](#), [44](#)).
- [Beh+21] S. BEHRENS, B. KÁLMAR, M. KIM, M. POWELL, and A. RAY. *The Disc Embedding Theorem*. OUP Oxford, 2021. ISBN: 9780192578389 ([↑ 102](#)).
- [BKCLR22] S. BLACKWELL, R. KIRBY, M. KLUG, V. LONGO, and B. RUPPIK. *Bisecting and trisecting groups of knots and manifolds*. In preparation. 2022 ([↑ 15](#), [133](#), [145](#), [157](#), [165](#)).
- [Bla+20a] R. BLAIR, A. KJUCHUKOVA, R. VELAZQUEZ, and P. VILLANUEVA. Wirtinger systems of generators of knot groups. *Comm. Anal. Geom.* 28.2 (2020), pp. 243–262. ISSN: 1019-8385. DOI: [10.4310/cag.2020.v28.n2.a2](https://doi.org/10.4310/cag.2020.v28.n2.a2). arXiv: [1705.03108](https://arxiv.org/abs/1705.03108) [[math.GT](#)] ([↑ 149](#)).
- [Bla+20b] R. BLAIR, P. CAHN, A. KJUCHUKOVA, and J. MEIER. *A note on three-fold branched covers of S^4* . 2020. arXiv: [1909.11788](https://arxiv.org/abs/1909.11788) [[math.GT](#)] ([↑ 167](#)).
- [BN17] H. U. BODEN and M. NAGEL. Concordance group of virtual knots. *Proc. Amer. Math. Soc.* 145.12 (2017), pp. 5451–5461. ISSN: 0002-9939. DOI: [10.1090/proc/13667](https://doi.org/10.1090/proc/13667). arXiv: [1606.06404](https://arxiv.org/abs/1606.06404) [[math.GT](#)] ([↑ 69](#)).
- [Boy88] J. BOYLE. Classifying 1-handles attached to knotted surfaces. *Trans. Amer. Math. Soc.* 306.2 (1988), pp. 475–487. ISSN: 0002-9947. DOI: [10.2307/2000807](https://doi.org/10.2307/2000807) ([↑ 21](#), [23](#), [44](#), [158](#)).
- [CS76] S. E. CAPPELL and J. L. SHANESON. There exist inequivalent knots with the same complement. *Ann. of Math. (2)* 103.2 (1976), pp. 349–353. ISSN: 0003-486X. DOI: [10.2307/1970942](https://doi.org/10.2307/1970942) ([↑ 137](#)).
- [CS98] J. S. CARTER and M. SAITO. *Knotted surfaces and their diagrams*. Vol. 55. Mathematical Surveys and Monographs. American Mathematical Society, Providence, RI, 1998, pp. xii+258. ISBN: 0-8218-0593-2. DOI: [10.1090/surv/055](https://doi.org/10.1090/surv/055) ([↑ 50](#)).

- [Cas86] A. J. CASSON. *Three lectures on new-infinite constructions in 4-dimensional manifolds*. Vol. 62. Progr. Math. With an appendix by L. Siebenmann. Birkhäuser Boston, Boston, MA, 1986, pp. 201–244 (↑ 4, 19, 23).
- [Cel18] D. CELORIA. On concordances in 3-manifolds. *J. Topol.* 11.1 (2018), pp. 180–200. ISSN: 1753-8416. DOI: [10.1112/topo.12051](https://doi.org/10.1112/topo.12051). arXiv: [1602.05476](https://arxiv.org/abs/1602.05476) [math.GT] (↑ 69, 79).
- [CK08] J. C. CHA and T. KIM. Covering link calculus and iterated Bing doubles. *Geom. Topol.* 12.4 (2008), pp. 2173–2201. ISSN: 1465-3060. DOI: [10.2140/gt.2008.12.2173](https://doi.org/10.2140/gt.2008.12.2173). arXiv: [0712.3762](https://arxiv.org/abs/0712.3762) [math.GT] (↑ 126, 127, 129).
- [CP16] J. C. CHA and M. POWELL. Casson towers and slice links. *Invent. Math.* 205.2 (2016), pp. 413–457. ISSN: 0020-9910. DOI: [10.1007/s00222-015-0639-z](https://doi.org/10.1007/s00222-015-0639-z). arXiv: [1411.1621](https://arxiv.org/abs/1411.1621) [math.GT] (↑ 101).
- [Che19] W. CHEN. *Knot Floer homology of satellite knots with (1,1)-patterns*. 2019. arXiv: [1912.07914](https://arxiv.org/abs/1912.07914) [math.GT] (↑ 9, 14, 65, 85, 86, 88–91, 93, 95, 112).
- [CM17] M. CLAY and D. MARGALIT. *Office hours with a geometric group theorist*. Princeton Univ. Press, Princeton, NJ, 2017, pp. 3–20. DOI: [10.2307/j.ctt1vwmg8g](https://doi.org/10.2307/j.ctt1vwmg8g) (↑ 145).
- [CL86] T. D. COCHRAN and W. B. R. LICKORISH. Unknotting information from 4-manifolds. *Trans. Amer. Math. Soc.* 297.1 (1986), pp. 125–142. ISSN: 0002-9947. DOI: [10.2307/2000460](https://doi.org/10.2307/2000460) (↑ 79).
- [Coc83] T. COCHRAN. Ribbon knots in S^4 . *J. London Math. Soc. (2)* 28.3 (1983), pp. 563–576. ISSN: 0024-6107. DOI: [10.1112/jlms/s2-28.3.563](https://doi.org/10.1112/jlms/s2-28.3.563) (↑ 13, 39, 40, 52, 140).
- [Coc+13] T. D. COCHRAN, B. D. FRANKLIN, M. HEDDEN, and P. D. HORN. Knot concordance and homology cobordism. *Proc. Amer. Math. Soc.* 141.6 (2013), pp. 2193–2208. ISSN: 0002-9939. DOI: [10.1090/S0002-9939-2013-11471-1](https://doi.org/10.1090/S0002-9939-2013-11471-1). arXiv: [1102.5730](https://arxiv.org/abs/1102.5730) [math.GT] (↑ 110, 127).
- [CHH13] T. D. COCHRAN, S. HARVEY, and P. HORN. Filtering smooth concordance classes of topologically slice knots. *Geom. Topol.* 17.4 (2013), pp. 2103–2162. ISSN: 1465-3060. DOI: [10.2140/gt.2013.17.2103](https://doi.org/10.2140/gt.2013.17.2103). arXiv: [1201.6283](https://arxiv.org/abs/1201.6283) [math.GT] (↑ 129).
- [COT03] T. D. COCHRAN, K. E. ORR, and P. TEICHNER. Knot concordance, Whitney towers and L^2 -signatures. *Ann. of Math. (2)* 157.2 (2003), pp. 433–519. ISSN: 0003-486X. DOI: [10.4007/annals.2003.157.433](https://doi.org/10.4007/annals.2003.157.433). arXiv: [math/9908117](https://arxiv.org/abs/math/9908117) [math.GT] (↑ 78, 129).
- [CST14] J. CONANT, R. SCHNEIDERMAN, and P. TEICHNER. Milnor invariants and twisted Whitney towers. *J. Topol.* 7.1 (2014), pp. 187–224. ISSN: 1753-8416. DOI: [10.1112/jtopol/jtt025](https://doi.org/10.1112/jtopol/jtt025). arXiv: [1102.0758](https://arxiv.org/abs/1102.0758) [math.GT] (↑ 123).
- [Con21] A. CONWAY. The Levine-Tristram signature: a survey. In: *2019-20 MATRIX annals*. Vol. 4. MATRIX Book Ser. Springer, Cham, 2021, pp. 31–56. DOI: [10.1007/978-3-030-62497-2_2](https://doi.org/10.1007/978-3-030-62497-2_2). arXiv: [1903.04477](https://arxiv.org/abs/1903.04477) [math.GT] (↑ 130).
- [CN20] A. CONWAY and M. NAGEL. Stably slice disks of links. *J. Topol.* 13.3 (2020), pp. 1261–1301. ISSN: 1753-8416. DOI: [10.1112/topo.12154](https://doi.org/10.1112/topo.12154). arXiv: [1901.01393](https://arxiv.org/abs/1901.01393) [math.GT] (↑ 78, 130, 131).
- [CP20] A. CONWAY and M. POWELL. *Embedded surfaces with infinite cyclic knot group*. To appear: Geometry & Topology. 2020. arXiv: [2009.13461](https://arxiv.org/abs/2009.13461) [math.GT] (↑ 2, 22).
- [Dav20] C. W. DAVIS. Concordance, crossing changes, and knots in homology spheres. *Canad. Math. Bull.* 63.4 (2020), pp. 744–754. ISSN: 0008-4395. DOI: [10.4153/s0008439519000791](https://doi.org/10.4153/s0008439519000791). arXiv: [1903.09225](https://arxiv.org/abs/1903.09225) [math.GT] (↑ 10).
- [Dav+18] C. W. DAVIS, M. NAGEL, J. PARK, and A. RAY. Concordance of knots in $S^1 \times S^2$. *J. Lond. Math. Soc. (2)* 98.1 (2018), pp. 59–84. ISSN: 0024-6107. DOI: [10.1112/jlms.12125](https://doi.org/10.1112/jlms.12125). arXiv: [1707.04542](https://arxiv.org/abs/1707.04542) [math.GT] (↑ 71).
- [Dey19] S. DEY. *Cable knots are not thin*. 2019. arXiv: [1904.11591](https://arxiv.org/abs/1904.11591) [math.GT] (↑ 113).
- [DV16] A. DONALD and F. VAFAEE. A slicing obstruction from the $\frac{10}{8}$ theorem. *Proc. Amer. Math. Soc.* 144.12 (2016), pp. 5397–5405. ISSN: 0002-9939. DOI: [10.1090/proc/13056](https://doi.org/10.1090/proc/13056). arXiv: [1508.07047](https://arxiv.org/abs/1508.07047) [math.GT] (↑ 131).
- [Don83] S. K. DONALDSON. An application of gauge theory to four-dimensional topology. *J. Differential Geom.* 18.2 (1983), pp. 279–315. ISSN: 0022-040X (↑ 8).
- [DK16] S. DURST and M. KEGEL. Computing rotation and self-linking numbers in contact surgery diagrams. *Acta Math. Hungar.* 150.2 (2016), pp. 524–540. ISSN: 0236-5294. DOI: [10.1007/s10474-016-0660-8](https://doi.org/10.1007/s10474-016-0660-8). arXiv: [1605.00795](https://arxiv.org/abs/1605.00795) [math.GT] (↑ 110).

- [EKO22] J. ETNYRE, M. KEGEL, and S. ONARAN. *Contact surgery numbers*. 2022. arXiv: [2201.00157](#) [[math.GT](#)] (↑ 109).
- [Etn05] J. B. ETNYRE. Legendrian and transversal knots. In: *Handbook of knot theory*. Elsevier B. V., Amsterdam, 2005, pp. 105–185. DOI: [10.1016/B978-044451452-3/50004-6](#) (↑ 109).
- [EH01] J. B. ETNYRE and K. HONDA. On the nonexistence of tight contact structures. *Ann. of Math. (2)* 153.3 (2001), pp. 749–766. ISSN: 0003-486X. DOI: [10.2307/2661367](#). arXiv: [math/9910115](#) [[math.GT](#)] (↑ 108).
- [FHR88] B. FINE, J. HOWIE, and G. ROSENBERGER. One-relator quotients and free products of cyclics. *Proc. Amer. Math. Soc.* 102.2 (1988), pp. 249–254. ISSN: 0002-9939. DOI: [10.2307/2045870](#) (↑ 6, 18).
- [Flo88] A. FLOER. Morse theory for Lagrangian intersections. *J. Differential Geom.* 28.3 (1988), pp. 513–547. ISSN: 0022-040X (↑ 82).
- [Fox62] R. H. FOX. A quick trip through knot theory. In: *Topology of 3-manifolds and related topics (Proc. The Univ. of Georgia Institute, 1961)*. Prentice-Hall, Englewood Cliffs, N.J., 1962, pp. 120–167 (↑ 167).
- [Fox66] R. H. FOX. Rolling. *Bull. Amer. Math. Soc.* 72 (1966), pp. 162–164. ISSN: 0002-9904. DOI: [10.1090/S0002-9904-1966-11467-2](#) (↑ 39).
- [FM66] R. H. FOX and J. W. MILNOR. Singularities of 2-spheres in 4-space and cobordism of knots. *Osaka Math. J.* 3 (1966), pp. 257–267. ISSN: 0388-0699 (↑ 126).
- [Fre+10] M. FREEDMAN, R. GOMPF, S. MORRISON, and K. WALKER. Man and machine thinking about the smooth 4-dimensional Poincaré conjecture. *Quantum Topol.* 1.2 (2010), pp. 171–208. ISSN: 1663-487X. DOI: [10.4171/QT/5](#). arXiv: [0906.5177](#) [[math.GT](#)] (↑ 7).
- [FK78] M. FREEDMAN and R. KIRBY. A geometric proof of Rochlin’s theorem. In: *Algebraic and geometric topology (Proc. Sympos. Pure Math., Stanford Univ., Stanford, Calif., 1976), Part 2*. Proc. Sympos. Pure Math., XXXII. Amer. Math. Soc., Providence, R.I., 1978, pp. 85–97 (↑ 78).
- [FQ90] M. FREEDMAN and F. QUINN. *Topology of 4-manifolds*. Vol. 39. Princeton Mathematical Series. Princeton University Press, Princeton, NJ, 1990, pp. viii+259. ISBN: 0-691-08577-3 (↑ 2, 8, 19, 22, 40, 42, 66, 71, 75, 78, 80, 102, 126).
- [Fre88] M. H. FREEDMAN. Whitehead₃ is a “slice” link. *Invent. Math.* 94.1 (1988), pp. 175–182. ISSN: 0020-9910. DOI: [10.1007/BF01394351](#) (↑ 8, 14, 101, 107).
- [Fre82] M. H. FREEDMAN. The topology of four-dimensional manifolds. *J. Differential Geometry* 17.3 (1982), pp. 357–453. ISSN: 0022-040X (↑ 2, 73, 102).
- [Fri+19] S. FRIEDL, M. NAGEL, P. ORSON, and M. POWELL. Satellites and concordance of knots in 3-manifolds. *Trans. Amer. Math. Soc.* 371.4 (2019), pp. 2279–2306. ISSN: 0002-9947. DOI: [10.1090/tran/7313](#). arXiv: [1611.09114](#) [[math.GT](#)] (↑ 79).
- [FO15] S. FRIEDL and P. ORSON. Twist spinning of knots and metabolizers of Blanchfield pairings. *Ann. Fac. Sci. Toulouse Math. (6)* 24.5 (2015), pp. 1203–1218. ISSN: 0240-2963. DOI: [10.5802/afst.1481](#). arXiv: [1312.1934](#) [[math.GT](#)] (↑ 39).
- [Fuk17] M. FUKUDA. Branched twist spins and knot determinants. *Osaka J. Math.* 54.4 (2017), pp. 679–688. ISSN: 0030-6126 (↑ 39).
- [Gab20] D. GABAI. The 4-dimensional light bulb theorem. *J. Amer. Math. Soc.* 33.3 (2020), pp. 609–652. ISSN: 0894-0347. DOI: [10.1090/jams/920](#). arXiv: [1705.09989](#) [[math.GT](#)] (↑ 6, 19, 22, 41, 42).
- [GAP21] GAP GROUP. *GAP - Groups, Algorithms, and Programming, Version 4.11.1*. <https://www.gap-system.org>. 2021 (↑ 54).
- [GT04] S. GAROUFALIDIS and P. TEICHNER. On knots with trivial Alexander polynomial. *J. Differential Geom.* 67.1 (2004), pp. 167–193. ISSN: 0022-040X. arXiv: [math/0206023](#) [[math.GT](#)] (↑ 8, 78, 80, 102).
- [GK16] D. GAY and R. KIRBY. Trisecting 4-manifolds. *Geom. Topol.* 20.6 (2016), pp. 3097–3132. ISSN: 1465-3060. DOI: [10.2140/gt.2016.20.3097](#). arXiv: [1205.1565](#) [[math.GT](#)] (↑ 133, 134).
- [GM18] D. GAY and J. MEIER. *Doubly pointed trisection diagrams and surgery on 2-knots*. 2018. arXiv: [1806.05351](#) [[math.GT](#)] (↑ 81).
- [GS03] P. GHIGGINI and S. SCHÖNENBERGER. On the classification of tight contact structures. In: *Topology and geometry of manifolds (Athens, GA, 2001)*. Vol. 71. Proc. Sympos. Pure Math. Amer. Math.

- Soc., Providence, RI, 2003, pp. 121–151. DOI: [10.1090/pspum/071/2024633](https://doi.org/10.1090/pspum/071/2024633). arXiv: [math/0201099](https://arxiv.org/abs/math/0201099) [[math.GT](#)] ([↑ 108](#)).
- [Gif79] C. H. GIFFEN. Link concordance implies link homotopy. *Math. Scand.* 45.2 (1979), pp. 243–254. ISSN: 0025-5521. DOI: [10.7146/math.scand.a-11839](https://doi.org/10.7146/math.scand.a-11839) ([↑ 122](#)).
- [Gil81] P. M. GILMER. Configurations of surfaces in 4-manifolds. *Trans. Amer. Math. Soc.* 264.2 (1981), pp. 353–380. ISSN: 0002-9947. DOI: [10.2307/1998544](https://doi.org/10.2307/1998544) ([↑ 131](#)).
- [GMM05] H. GODA, H. MATSUDA, and T. MORIFUJI. Knot Floer homology of $(1, 1)$ -knots. *Geom. Dedicata* 112 (2005), pp. 197–214. ISSN: 0046-5755. DOI: [10.1007/s10711-004-5403-2](https://doi.org/10.1007/s10711-004-5403-2). arXiv: [math/0311084](https://arxiv.org/abs/math/0311084) [[math.GT](#)] ([↑ 89](#)).
- [Gol79] D. L. GOLDSMITH. Concordance implies homotopy for classical links in M^3 . *Comment. Math. Helv.* 54.3 (1979), pp. 347–355. ISSN: 0010-2571. DOI: [10.1007/BF02566279](https://doi.org/10.1007/BF02566279) ([↑ 122](#)).
- [GK78] D. L. GOLDSMITH and L. H. KAUFFMAN. Twist spinning revisited. *Trans. Amer. Math. Soc.* 239 (1978), pp. 229–251. ISSN: 0002-9947. DOI: [10.2307/1997855](https://doi.org/10.2307/1997855) ([↑ 39](#)).
- [GG73] M. GOLUBITSKY and V. GUILLEMIN. *Stable mappings and their singularities*. Graduate Texts in Mathematics, Vol. 14. Springer-Verlag, New York-Heidelberg, 1973, pp. x+209 ([↑ 19](#)).
- [GS99] R. E. GOMPF and A. I. STIPSICZ. *4-manifolds and Kirby calculus*. Vol. 20. Graduate Studies in Mathematics. American Mathematical Society, Providence, RI, 1999, pp. xvi+558. ISBN: 0-8218-0994-6. DOI: [10.1090/gsm/020](https://doi.org/10.1090/gsm/020) ([↑ 53](#), [74](#), [101](#)).
- [GGS10] F. GONZÁLEZ-ACUÑA, C. M. GORDON, and J. SIMON. Unsolvable problems about higher-dimensional knots and related groups. *Enseign. Math. (2)* 56.1-2 (2010), pp. 143–171. ISSN: 0013-8584. DOI: [10.4171/LEM/56-1-5](https://doi.org/10.4171/LEM/56-1-5). arXiv: [0908.4009](https://arxiv.org/abs/0908.4009) [[math.GT](#)] ([↑ 140](#)).
- [Gor73] C. M. GORDON. Some higher-dimensional knots with the same homotopy groups. *Quart. J. Math. Oxford Ser. (2)* 24 (1973), pp. 411–422. ISSN: 0033-5606. DOI: [10.1093/qmath/24.1.411](https://doi.org/10.1093/qmath/24.1.411) ([↑ 157](#), [158](#)).
- [Gor76] C. M. GORDON. Knots in the 4-sphere. *Comment. Math. Helv.* 51.4 (1976), pp. 585–596. ISSN: 0010-2571. DOI: [10.1007/BF02568175](https://doi.org/10.1007/BF02568175) ([↑ 137](#)).
- [Gor95] C. M. GORDON. Some embedding theorems and undecidability questions for groups. In: *Combinatorial and geometric group theory (Edinburgh, 1993)*. Vol. 204. London Math. Soc. Lecture Note Ser. Cambridge Univ. Press, Cambridge, 1995, pp. 105–110 ([↑ 140](#)).
- [GL89] C. M. GORDON and J. LUECKE. Knots are determined by their complements. *J. Amer. Math. Soc.* 2.2 (1989), pp. 371–415. ISSN: 0894-0347. DOI: [10.2307/1990979](https://doi.org/10.2307/1990979) ([↑ 137](#)).
- [Cul07] M. CULLER. *Gridlink, a tool for manipulating rectangular link diagrams, Version 2.0 (Revision: 1.75)*. <http://homepages.math.uic.edu/~culler/gridlink/>. 2007 ([↑ 109](#)).
- [GKZ92] R. I. GRIGORCHUK, P. F. KURCHANOV, and H. ZIESCHANG. Equivalence of homomorphisms of surface groups to free groups and some properties of 3-dimensional handlebodies. In: *Proceedings of the International Conference on Algebra, Part 1 (Novosibirsk, 1989)*. Vol. 131. Contemp. Math. Amer. Math. Soc., Providence, RI, 1992, pp. 521–530 ([↑ 139](#)).
- [GW09] D. GROVES and H. WILTON. Enumerating limit groups. *Groups Geom. Dyn.* 3.3 (2009), pp. 389–399. ISSN: 1661-7207. DOI: [10.4171/GGD/63](https://doi.org/10.4171/GGD/63). arXiv: [0704.0989](https://arxiv.org/abs/0704.0989) [[math.GT](#)] ([↑ 140](#)).
- [HL90] N. HABEGGER and X.-S. LIN. The classification of links up to link-homotopy. *J. Amer. Math. Soc.* 3.2 (1990), pp. 389–419. ISSN: 0894-0347. DOI: [10.2307/1990959](https://doi.org/10.2307/1990959) ([↑ 123](#)).
- [HK88] I. HAMBLETON and M. KRECK. On the classification of topological 4-manifolds with finite fundamental group. *Math. Ann.* 280.1 (1988), pp. 85–104. ISSN: 0025-5831. DOI: [10.1007/BF01474183](https://doi.org/10.1007/BF01474183) ([↑ 3](#)).
- [HK93] I. HAMBLETON and M. KRECK. Cancellation of hyperbolic forms and topological four-manifolds. *J. Reine Angew. Math.* 443 (1993), pp. 21–47. ISSN: 0075-4102 ([↑ 74](#)).
- [HK18] I. HAMBLETON and M. KRECK. On the classification of topological 4-manifolds with finite fundamental group: corrigendum [MR0928299]. *Math. Ann.* 372.1-2 (2018), pp. 527–530. ISSN: 0025-5831. DOI: [10.1007/s00208-018-1656-1](https://doi.org/10.1007/s00208-018-1656-1) ([↑ 3](#)).
- [HT97] I. HAMBLETON and P. TEICHNER. A non-extended Hermitian form over $\mathbf{Z}[\mathbf{Z}]$. *Manuscripta Math.* 93.4 (1997), pp. 435–442. ISSN: 0025-2611. DOI: [10.1007/BF02677483](https://doi.org/10.1007/BF02677483) ([↑ 22](#)).
- [HRW17] J. HANSELMAN, J. RASMUSSEN, and L. WATSON. *Bordered Floer homology for manifolds with torus boundary via immersed curves*. 2017. arXiv: [1604.03466](https://arxiv.org/abs/1604.03466) [[math.GT](#)] ([↑ 9](#), [14](#), [65](#), [85](#), [86](#)).

- [HRW18] J. HANSELMAN, J. RASMUSSEN, and L. WATSON. *Heegaard Floer homology for manifolds with torus boundary: properties and examples*. 2018. arXiv: [1810.10355 \[math.GT\]](#) (↑ 85–88).
- [HW15] J. HANSELMAN and L. WATSON. *A calculus for bordered Floer homology*. 2015. arXiv: [1508.05445 \[math.GT\]](#) (↑ 88).
- [HW19] J. HANSELMAN and L. WATSON. *Cabling in terms of immersed curves*. 2019. arXiv: [1908.04397 \[math.GT\]](#) (↑ 88, 112).
- [Har+22] S. HARVEY, J. JOSEPH, H. JUNG, and S. KIM. *Fusion numbers and determinants of ribbon 2-knots*. In preparation. 2022 (↑ 54, 59).
- [Hed07] M. HEDDEN. Knot Floer homology of Whitehead doubles. *Geom. Topol.* 11 (2007), pp. 2277–2338. ISSN: 1465-3060. DOI: [10.2140/gt.2007.11.2277](#). arXiv: [math/0606094 \[math.GT\]](#) (↑ 8, 9, 14, 65, 80, 84).
- [Hed08] M. HEDDEN. An Ozsváth-Szabó Floer homology invariant of knots in a contact manifold. *Adv. Math.* 219.1 (2008), pp. 89–117. ISSN: 0001-8708. DOI: [10.1016/j.aim.2008.04.007](#). arXiv: [0708.0448 \[math.GT\]](#) (↑ 108).
- [Hed09] M. HEDDEN. On knot Floer homology and cabling. II. *Int. Math. Res. Not. IMRN* 12 (2009), pp. 2248–2274. ISSN: 1073-7928. DOI: [10.1093/imrn/rnp015](#). arXiv: [0806.2172 \[math.GT\]](#) (↑ 115).
- [HKL16] M. HEDDEN, S.-G. KIM, and C. LIVINGSTON. Topologically slice knots of smooth concordance order two. *J. Differential Geom.* 102.3 (2016), pp. 353–393. ISSN: 0022-040X. arXiv: [1212.6628 \[math.GT\]](#) (↑ 84).
- [HL21] M. HEDDEN and A. S. LEVINE. *A surgery formula for knot Floer homology*. 2021. arXiv: [1901.02488 \[math.GT\]](#) (↑ 104).
- [HR21a] M. HEDDEN and K. RAOUX. Four-dimensional aspects of tight contact 3-manifolds. *Proc. Natl. Acad. Sci. USA* 118.22 (2021), Paper No. e2025436118, 6. ISSN: 0027-8424. DOI: [10.1073/pnas.2025436118](#). arXiv: [2010.13162 \[math.GT\]](#) (↑ 108, 109).
- [HR21b] M. HEDDEN and K. RAOUX. *Knot Floer homology and relative adjunction inequalities*. 2021. arXiv: [2009.05462 \[math.GT\]](#) (↑ 9, 65, 100, 102).
- [Hil81] J. A. HILLMAN. *Alexander ideals of links*. Vol. 895. Lecture Notes in Mathematics. Springer-Verlag, Berlin-New York, 1981, pp. v+178. ISBN: 3-540-11168-9 (↑ 139).
- [HK95] J. A. HILLMAN and A. KAWAUCHI. Unknotting orientable surfaces in the 4-sphere. *J. Knot Theory Ramifications* 4.2 (1995), pp. 213–224. ISSN: 0218-2165. DOI: [10.1142/S0218216595000119](#) (↑ 22).
- [Hir59] M. W. HIRSCH. Immersions of manifolds. *Trans. Amer. Math. Soc.* 93 (1959), pp. 242–276. ISSN: 0002-9947. DOI: [10.2307/1993453](#) (↑ 19).
- [Hit79] L. R. HITT. Examples of higher-dimensional slice knots which are not ribbon knots. *Proc. Amer. Math. Soc.* 77.2 (1979), pp. 291–297. ISSN: 0002-9939. DOI: [10.2307/2042654](#) (↑ 52, 53).
- [Hom14] J. HOM. Bordered Heegaard Floer homology and the tau-invariant of cable knots. *J. Topol.* 7.2 (2014), pp. 287–326. ISSN: 1753-8416. DOI: [10.1112/jtopol/jtt030](#). arXiv: [1202.1463 \[math.GT\]](#) (↑ 9, 14, 65, 87, 88, 107, 112–114).
- [HLL18] J. HOM, A. S. LEVINE, and T. LIDMAN. *Knot concordance in homology cobordisms*. 2018. arXiv: [1801.07770 \[math.GT\]](#) (↑ 10, 88, 107, 112).
- [HK79] F. HOSOKAWA and A. KAWAUCHI. Proposals for unknotted surfaces in four-spaces. *Osaka Math. J.* 16.1 (1979), pp. 233–248. ISSN: 0388-0699 (↑ 21, 23).
- [HMS79] F. HOSOKAWA, T. MAEDA, and S. SUZUKI. Numerical invariants of surfaces in 4-space. *Kobe Mathematics seminar notes* 7(2) (1979), pp. 409–420 (↑ 4, 23).
- [Hos86] J. HOSTE. A formula for Casson’s invariant. *Trans. Amer. Math. Soc.* 297.2 (1986), pp. 547–562. ISSN: 0002-9947. DOI: [10.2307/2000539](#) (↑ 98).
- [HKM21] M. HUGHES, S. KIM, and M. MILLER. *Band diagrams of immersed surfaces in 4-manifolds*. 2021. arXiv: [2108.12794 \[math.GT\]](#) (↑ 28).
- [HKM20] M. C. HUGHES, S. KIM, and M. MILLER. Isotopies of surfaces in 4-manifolds via banded unlink diagrams. *Geom. Topol.* 24.3 (2020), pp. 1519–1569. ISSN: 1465-3060. DOI: [10.2140/gt.2020.24.1519](#). arXiv: [1804.09169 \[math.GT\]](#) (↑ 54).
- [IMT22] N. IIDA, A. MUKHERJEE, and M. TANIGUCHI. *An adjunction inequality for the Bauer-Furuta type invariants, with applications to sliceness and 4-manifold topology*. 2022. arXiv: [2102.02076 \[math.GT\]](#) (↑ 131).

- [Isl21] G. ISLAMBOULI. Nielsen equivalence and trisections. *Geom. Dedicata* 214 (2021), pp. 303–317. ISSN: 0046-5755. DOI: [10.1007/s10711-021-00617-y](https://doi.org/10.1007/s10711-021-00617-y). arXiv: [1804.06978](https://arxiv.org/abs/1804.06978) [math.GT] (↑ 136).
- [Joh06] J. JOHNSON. *Notes on Heegaard splittings*. 2006 (↑ 136, 143).
- [Jos19] J. JOSEPH. *0-concordance of knotted surfaces and Alexander ideals*. 2019. arXiv: [1911.13112](https://arxiv.org/abs/1911.13112) [math.GT] (↑ 17, 28).
- [Jos20] J. JOSEPH. “Applications of Alexander ideals to knotted surfaces in 4-space”. PhD thesis. University of Georgia, 2020 (↑ 17).
- [Jos+21] J. JOSEPH, J. MEIER, M. MILLER, and A. ZUPAN. *Bridge trisections and classical knotted surface theory*. 2021. arXiv: [2112.11557](https://arxiv.org/abs/2112.11557) [math.GT] (↑ 21, 59, 137, 164).
- [JP21] J. JOSEPH and P. PONGTANAPAIAN. *Bridge numbers and meridional ranks of knotted surfaces and welded knots*. 2021. arXiv: [2111.09233](https://arxiv.org/abs/2111.09233) [math.GT] (↑ 18).
- [JKRS20] J. M. JOSEPH, M. R. KLUG, B. M. RUPPIK, and H. R. SCHWARTZ. Unknotting numbers of 2-spheres in the 4-sphere. *J. Topol.* 14.4 (2021), pp. 1321–1350. DOI: [10.1112/topo.12209](https://doi.org/10.1112/topo.12209). arXiv: [2007.13244](https://arxiv.org/abs/2007.13244) [math.GT] (↑ 3, 13, 17–19, 22, 23, 26–29, 34–36, 41–43, 46, 47, 50).
- [JMZ20a] A. JUHÁSZ, M. MILLER, and I. ZEMKE. Knot cobordisms, bridge index, and torsion in Floer homology. *J. Topol.* 13.4 (2020), pp. 1701–1724. ISSN: 1753-8416. DOI: [10.1112/topo.12170](https://doi.org/10.1112/topo.12170). arXiv: [1904.02735](https://arxiv.org/abs/1904.02735) [math.GT] (↑ 4, 23).
- [JMZ20b] A. JUHÁSZ, M. MILLER, and I. ZEMKE. *Transverse invariants and exotic surfaces in the 4-ball*. 2020. arXiv: [2001.07191](https://arxiv.org/abs/2001.07191) [math.GT] (↑ 30, 36).
- [JZ18] A. JUHÁSZ and I. ZEMKE. *Stabilization distance bounds from link Floer homology*. 2018. arXiv: [1810.09158](https://arxiv.org/abs/1810.09158) [math.GT] (↑ 4, 22, 29, 34, 41).
- [KY10] T. KADOKAMI and Z. YANG. An integral invariant from the knot group. *Osaka J. Math.* 47.4 (2010). <http://projecteuclid.org/euclid.ojm/1292854314>, pp. 965–976. ISSN: 0030-6126 (↑ 36).
- [Kam89] S. KAMADA. Nonorientable surfaces in 4-space. *Osaka J. Math.* 26.2 (1989), pp. 367–385. ISSN: 0030-6126 (↑ 21, 23).
- [Kam02] S. KAMADA. *Braid and knot theory in dimension four*. Vol. 95. Mathematical Surveys and Monographs. American Mathematical Society, Providence, RI, 2002, pp. xiv+313. ISBN: 0-8218-2969-6. DOI: [10.1090/surv/095](https://doi.org/10.1090/surv/095) (↑ 136).
- [Kam14] S. KAMADA. Cords and 1-handles attached to surface-knots. *Bol. Soc. Mat. Mex. (3)* 20.2 (2014), pp. 595–609. ISSN: 1405-213X. DOI: [10.1007/s40590-014-0022-x](https://doi.org/10.1007/s40590-014-0022-x). arXiv: [1403.0690](https://arxiv.org/abs/1403.0690) [math.GT] (↑ 21).
- [Kam17] S. KAMADA. *Surface-knots in 4-space, An introduction*. Springer Monographs in Mathematics. Springer, Singapore, 2017, pp. xi+212. DOI: [10.1007/978-981-10-4091-7](https://doi.org/10.1007/978-981-10-4091-7) (↑ 71).
- [Kan96] T. KANENOBU. Weak unknotting number of a composite 2-knot. *Journal of Knot Theory and Its Ramifications* 5.02 (1996), pp. 161–166. ISSN: 0218-2165. DOI: [10.1142/S0218216596000126](https://doi.org/10.1142/S0218216596000126) (↑ 27, 28).
- [Kan00] T. KANENOBU. An unknotting operation on ribbon 2-knots. *J. Knot Theory Ramifications* 9.8 (2000), pp. 1011–1028. ISSN: 0218-2165. DOI: [10.1142/S021821650000608](https://doi.org/10.1142/S021821650000608) (↑ 50).
- [KK94] T. KANENOBU and K.-I. KAZAMA. The peripheral subgroup and the second homology of the group of a knotted torus in S^4 . *Osaka J. Math.* 31.4 (1994), pp. 907–921. ISSN: 0030-6126 (↑ 137).
- [KS20] T. KANENOBU and T. SUMI. Suciu’s ribbon 2-knots with isomorphic group. *J. Knot Theory Ramifications* 29.7 (2020), pp. 2050053, 9. ISSN: 0218-2165. DOI: [10.1142/S0218216520500534](https://doi.org/10.1142/S0218216520500534) (↑ 7, 53, 59, 167).
- [KNR21] D. KASPROWSKI, J. NICHOLSON, and B. RUPPIK. *Homotopy classification of 4-manifolds whose fundamental group is dihedral*. To appear: Algebraic & Geometric Topology. 2021. arXiv: [2011.03520](https://arxiv.org/abs/2011.03520) [math.GT] (↑ 3, 15).
- [Kas+22] D. KASPROWSKI, M. POWELL, A. RAY, and P. TEICHNER. *Embedding surfaces in 4-manifolds*. 2022. arXiv: [2201.03961](https://arxiv.org/abs/2201.03961) [math.GT] (↑ 19).
- [KPR20] D. KASPROWSKI, M. POWELL, and B. RUPPIK. *Homotopy classification of 4-manifolds with finite abelian 2-generator fundamental groups*. 2020. arXiv: [2005.00274](https://arxiv.org/abs/2005.00274) [math.GT] (↑ 3, 15).
- [KPT21] D. KASPROWSKI, M. POWELL, and P. TEICHNER. *Algebraic criteria for stable diffeomorphism of spin 4-manifolds*. 2021. arXiv: [2006.06127](https://arxiv.org/abs/2006.06127) [math.GT] (↑ 3).

- [Kau87] L. H. KAUFFMAN. *On knots*. Vol. 115. Annals of Mathematics Studies. Princeton University Press, Princeton, NJ, 1987, pp. xvi+481. ISBN: 0-691-08434-3 (↑ 127).
- [KF08] L. H. KAUFFMAN and J. FARIA MARTINS. Invariants of welded virtual knots via crossed module invariants of knotted surfaces. *Compos. Math.* 144.4 (2008), pp. 1046–1080. ISSN: 0010-437X. DOI: [10.1112/S0010437X07003429](https://doi.org/10.1112/S0010437X07003429). arXiv: [0704.1246](https://arxiv.org/abs/0704.1246) [math.GT] (↑ 50).
- [Kaw96] A. KAWAUCHI. *A survey of knot theory*. Translated and revised from the 1990 Japanese original by the author. Birkhäuser Verlag, Basel, 1996, pp. xxii+420. ISBN: 3-7643-5124-1 (↑ 51).
- [Kaw12] A. KAWAUCHI. On the Alexander polynomials of knots with Gordian distance one. *Topology Appl.* 159.4 (2012), pp. 948–958. ISSN: 0166-8641. DOI: [10.1016/j.topol.2011.11.017](https://doi.org/10.1016/j.topol.2011.11.017) (↑ 45).
- [KSS82] A. KAWAUCHI, T. SHIBUYA, and S. SUZUKI. Descriptions on surfaces in four-space. I. Normal forms. *Math. Sem. Notes Kobe Univ.* 10.1 (1982), pp. 75–125. ISSN: 0385-633x (↑ 71).
- [KK08] C. KEARTON and V. KURLIN. All 2-dimensional links in 4-space live inside a universal 3-dimensional polyhedron. *Algebr. Geom. Topol.* 8.3 (2008), pp. 1223–1247. ISSN: 1472-2747. DOI: [10.2140/agt.2008.8.1223](https://doi.org/10.2140/agt.2008.8.1223) (↑ 54).
- [Keg16] M. KEGEL. “Legendrian knots in surgery diagrams and the knot complement problem”. PhD thesis. Universität zu Köln, 2016 (↑ 14, 109, 110).
- [Ker65] M. A. KERVAIRE. Les nœuds de dimensions supérieures. *Bull. Soc. Math. France* 93 (1965), pp. 225–271. ISSN: 0037-9484 (↑ 52).
- [KM61] M. A. KERVAIRE and J. W. MILNOR. On 2-spheres in 4-manifolds. *Proc. Nat. Acad. Sci. U.S.A.* 47 (1961), pp. 1651–1657. ISSN: 0027-8424. DOI: [10.1073/pnas.47.10.1651](https://doi.org/10.1073/pnas.47.10.1651) (↑ 74).
- [Kim06] H. J. KIM. Modifying surfaces in 4-manifolds by twist spinning. *Geom. Topol.* 10 (2006), pp. 27–56. ISSN: 1465-3060. DOI: [10.2140/gt.2006.10.27](https://doi.org/10.2140/gt.2006.10.27). arXiv: [math/0411078](https://arxiv.org/abs/math/0411078) [math.GT] (↑ 30, 31, 36–38).
- [KS79] R. C. KIRBY and M. G. SCHARLEMANN. Eight faces of the Poincaré homology 3-sphere. In: *Geometric topology (Proc. Georgia Topology Conf., Athens, Ga., 1977)*. Academic Press, New York-London, 1979, pp. 113–146 (↑ 108).
- [Kir95] R. KIRBY. Problems in low-dimensional topology. In: *Proceedings of Georgia Topology Conference, Part 2*. ftp://math.berkeley.edu/pub/Preprints/Rob_Kirby/Problems/problems.ps.gz. 1995 (↑ 67).
- [Kir89] R. C. KIRBY. *The topology of 4-manifolds*. Vol. 1374. Lecture Notes in Mathematics. Springer-Verlag, Berlin, 1989, pp. vi+108. ISBN: 3-540-51148-2. DOI: [10.1007/BFb0089031](https://doi.org/10.1007/BFb0089031) (↑ 23).
- [Kju+21] A. KJUCHUKOVA, A. N. MILLER, A. RAY, and S. SAKALLI. *Slicing knots in definite 4-manifolds*. 2021. arXiv: [2112.14596](https://arxiv.org/abs/2112.14596) [math.GT] (↑ 79).
- [Swe21] F. SWENTON. *KLO/Kirby Calculator, Version 0.970 alpha*. <https://community.middlebury.edu/~mathanimations/klo/>. 2021 (↑ 109).
- [Klu18] M. KLUG. Functoriality of group trisections. *Proc. Natl. Acad. Sci. USA* 115.43 (2018), pp. 10875–10879. ISSN: 0027-8424. DOI: [10.1073/pnas.1717167115](https://doi.org/10.1073/pnas.1717167115) (↑ 139).
- [KR21] M. KLUG and B. RUPPIK. Deep and shallow slice knots in 4-manifolds. *Proc. Amer. Math. Soc. Ser. B* 8 (2021), pp. 204–218. DOI: [10.1090/bproc/89](https://doi.org/10.1090/bproc/89). arXiv: [2009.03053](https://arxiv.org/abs/2009.03053) [math.GT] (↑ 3, 13, 65, 68, 69, 71, 73, 75–77, 129).
- [KM93] P. B. KRONHEIMER and T. S. MROWKA. Gauge theory for embedded surfaces. I. *Topology* 32.4 (1993), pp. 773–826. ISSN: 0040-9383. DOI: [10.1016/0040-9383\(93\)90051-V](https://doi.org/10.1016/0040-9383(93)90051-V) (↑ 34, 74).
- [KM13] P. B. KRONHEIMER and T. S. MROWKA. Gauge theory and Rasmussen’s invariant. *J. Topol.* 6.3 (2013), pp. 659–674. ISSN: 1753-8416. DOI: [10.1112/jtopol/jtt008](https://doi.org/10.1112/jtopol/jtt008). arXiv: [1110.1297](https://arxiv.org/abs/1110.1297) [math.GT] (↑ 7).
- [Lam20] P. LAMBERT-COLE. Bridge trisections in $\mathbb{C}P^2$ and the Thom conjecture. *Geom. Topol.* 24.3 (2020), pp. 1571–1614. ISSN: 1465-3060. DOI: [10.2140/gt.2020.24.1571](https://doi.org/10.2140/gt.2020.24.1571). arXiv: [1807.10131](https://arxiv.org/abs/1807.10131) [math.GT] (↑ 74).
- [LM21] P. LAMBERT-COLE and J. MEIER. Bridge trisections in rational surfaces. *Journal of Topology and Analysis* 0.0 (2021), pp. 1–54. DOI: [10.1142/S1793525321500047](https://doi.org/10.1142/S1793525321500047). arXiv: [1810.10450](https://arxiv.org/abs/1810.10450) [math.GT] (↑ 167).
- [LW97] R. LEE and D. M. WILCZYŃSKI. Representing homology classes by locally flat surfaces of minimum genus. *Amer. J. Math.* 119.5 (1997), pp. 1119–1137. ISSN: 0002-9327 (↑ 74).

- [LR02] C. J. LEININGER and A. W. REID. The co-rank conjecture for 3-manifold groups. *Algebr. Geom. Topol.* 2 (2002), pp. 37–50. ISSN: 1472-2747. DOI: [10.2140/agt.2002.2.37](https://doi.org/10.2140/agt.2002.2.37). arXiv: [math.GT/0202261](https://arxiv.org/abs/math.GT/0202261) [[math.GT](#)] ([↑ 139](#)).
- [Lev12] A. S. LEVINE. Slicing mixed Bing-Whitehead doubles. *J. Topol.* 5.3 (2012), pp. 713–726. ISSN: 1753-8416. DOI: [10.1112/jtopol/jts019](https://doi.org/10.1112/jtopol/jts019). arXiv: [0912.5222](https://arxiv.org/abs/0912.5222) [[math.GT](#)] ([↑ 126, 129](#)).
- [Lev69] J. LEVINE. Invariants of knot cobordism. *Invent. Math.* 8 (1969), 98–110, addendum, *ibid.* 8 (1969), 355. ISSN: 0020-9910. DOI: [10.1007/BF01404613](https://doi.org/10.1007/BF01404613) ([↑ 130](#)).
- [Lic97] W. B. R. LICKORISH. *An introduction to knot theory*. Vol. 175. Graduate Texts in Mathematics. Springer-Verlag, New York, 1997, pp. x+201. ISBN: 0-387-98254-X. DOI: [10.1007/978-1-4612-0691-0](https://doi.org/10.1007/978-1-4612-0691-0) ([↑ 126, 130](#)).
- [LOT18] R. LIPSHITZ, P. S. OZSVÁTH, and D. P. THURSTON. Bordered Heegaard Floer homology. *Mem. Amer. Math. Soc.* 254.1216 (2018), pp. viii+279. ISSN: 0065-9266. DOI: [10.1090/memo/1216](https://doi.org/10.1090/memo/1216). arXiv: [0810.0687](https://arxiv.org/abs/0810.0687) [[math.GT](#)] ([↑ 9, 81, 84, 86, 87](#)).
- [LS07] P. LISCA and A. I. STIPSICZ. Ozsváth-Szabó invariants and tight contact three-manifolds. II. *J. Differential Geom.* 75.1 (2007), pp. 109–141. ISSN: 0022-040X. arXiv: [math/0404136](https://arxiv.org/abs/math/0404136) [[math.GT](#)] ([↑ 108](#)).
- [Lit79] R. A. LITHERLAND. Deforming twist-spun knots. *Trans. Amer. Math. Soc.* 250 (1979), pp. 311–331. ISSN: 0002-9947. DOI: [10.2307/1998993](https://doi.org/10.2307/1998993) ([↑ 39](#)).
- [Lit81] R. A. LITHERLAND. The second homology of the group of a knotted surface. *Quart. J. Math. Oxford Ser. (2)* 32.128 (1981), pp. 425–434. ISSN: 0033-5606. DOI: [10.1093/qmath/32.4.425](https://doi.org/10.1093/qmath/32.4.425) ([↑ 21](#)).
- [Liv02] C. LIVINGSTON. Seifert forms and concordance. *Geom. Topol.* 6 (2002), pp. 403–408. ISSN: 1465-3060. DOI: [10.2140/gt.2002.6.403](https://doi.org/10.2140/gt.2002.6.403). arXiv: [math/0101035](https://arxiv.org/abs/math/0101035) [[math.GT](#)] ([↑ 127](#)).
- [MQ06] J. MA and R. QIU. A lower bound on unknotting number. *Chinese Ann. Math. Ser. B* 27.4 (2006), pp. 437–440. ISSN: 0252-9599. DOI: [10.1007/s11401-004-0390-z](https://doi.org/10.1007/s11401-004-0390-z) ([↑ 27](#)).
- [Mae77] T. MAEDA. On a composition of knot groups. II. Algebraic bridge index. *Math. Sem. Notes Kobe Univ.* 5.3 (1977), pp. 457–464. ISSN: 0385-633x ([↑ 61](#)).
- [MP21a] M. MAGEE and D. PUDEK. *Core Surfaces*. 2021. arXiv: [2108.00717](https://arxiv.org/abs/2108.00717) [[math.GR](#)] ([↑ 139](#)).
- [Man16] C. MANOLESCU. An introduction to knot Floer homology. In: *Physics and mathematics of link homology*. Vol. 680. Contemp. Math. Amer. Math. Soc., Providence, RI, 2016, pp. 99–135. DOI: [10.1090/conm/680](https://doi.org/10.1090/conm/680). arXiv: [1401.7107](https://arxiv.org/abs/1401.7107) [[math.GT](#)] ([↑ 81–83](#)).
- [MMP20] C. MANOLESCU, M. MARENGON, and L. PICCIRILLO. *Relative genus bounds in indefinite four-manifolds*. 2020. arXiv: [2012.12270](https://arxiv.org/abs/2012.12270) [[math.GT](#)] ([↑ 10, 66, 129, 131](#)).
- [MP21b] C. MANOLESCU and L. PICCIRILLO. *From zero surgeries to candidates for exotic definite four-manifolds*. 2021. arXiv: [2102.04391](https://arxiv.org/abs/2102.04391) [[math.GT](#)] ([↑ 10](#)).
- [MM21] W. MARZANTOWICZ and Ł. P. MICHALAK. *Relations between Reeb graphs, systems of hypersurfaces and epimorphisms onto free groups*. 2021. arXiv: [2002.02388](https://arxiv.org/abs/2002.02388) [[math.GT](#)] ([↑ 139](#)).
- [Mas69] W. S. MASSEY. Proof of a conjecture of Whitney. *Pacific J. Math.* 31 (1969), pp. 143–156. ISSN: 0030-8730 ([↑ 20](#)).
- [Mat86] Y. MATSUMOTO. An elementary proof of Rochlin’s signature theorem and its extension by Guillou and Marin. In: *À la recherche de la topologie perdue*. Vol. 62. Progr. Math. Birkhäuser Boston, Boston, MA, 1986, pp. 119–139. DOI: [10.1007/BF01585163](https://doi.org/10.1007/BF01585163) ([↑ 78](#)).
- [MTZ20] J. MEIER, A. THOMPSON, and A. ZUPAN. *Cubic graphs induced by bridge trisections*. 2020. arXiv: [2007.07280](https://arxiv.org/abs/2007.07280) [[math.GT](#)] ([↑ 141](#)).
- [MZ17] J. MEIER and A. ZUPAN. Bridge trisections of knotted surfaces in S^4 . *Trans. Amer. Math. Soc.* 369.10 (2017), pp. 7343–7386. ISSN: 0002-9947. DOI: [10.1090/tran/6934](https://doi.org/10.1090/tran/6934). arXiv: [1507.08370](https://arxiv.org/abs/1507.08370) [[math.GT](#)] ([↑ 11, 15, 133, 135, 147, 148, 158, 161, 164](#)).
- [MZ18] J. MEIER and A. ZUPAN. Bridge trisections of knotted surfaces in 4-manifolds. *Proc. Natl. Acad. Sci. USA* 115.43 (2018), pp. 10880–10886. ISSN: 0027-8424. DOI: [10.1073/pnas.1717171115](https://doi.org/10.1073/pnas.1717171115). arXiv: [1710.01745](https://arxiv.org/abs/1710.01745) [[math.GT](#)] ([↑ 11, 135, 141](#)).
- [Mei18] J.-B. MEILHAN. *Linking number and Milnor invariants*. 2018. arXiv: [1812.03319](https://arxiv.org/abs/1812.03319) [[math.GT](#)] ([↑ 123](#)).

- [MP19] A. N. MILLER and M. POWELL. Stabilization distance between surfaces. *Enseign. Math.* 65.3-4 (2019), pp. 397–440. ISSN: 0013-8584. DOI: [10.4171/lem/65-3/4-4](https://doi.org/10.4171/lem/65-3/4-4). arXiv: [1908.06701](https://arxiv.org/abs/1908.06701) [[math.GT](#)] ([↑ 26, 41](#)).
- [Mil58] J. MILNOR. On simply connected 4-manifolds. In: *Symposium internacional de topologia algebraica International symposium on algebraic topology*. Universidad Nacional Autónoma de México and UNESCO, Mexico City, 1958, pp. 122–128 ([↑ 3](#)).
- [Mil65] J. MILNOR. *Lectures on the h-cobordism theorem*. Notes by L. Siebenmann and J. Sondow. Princeton University Press, Princeton, N.J., 1965, pp. v+116 ([↑ 2](#)).
- [Miy86] K. MIYAZAKI. On the relationship among unknotting number, knotting genus and Alexander invariant for 2-knots. *Kobe J. Math.* 3.1 (1986), pp. 77–85. ISSN: 0289-9051 ([↑ 6, 18, 26, 46, 54](#)).
- [Mor84] J. W. MORGAN. The Smith conjecture. In: *The Smith conjecture (New York, 1979)*. Vol. 112. Pure Appl. Math. Academic Press, Orlando, FL, 1984, pp. 3–6. DOI: [10.1016/S0079-8169\(08\)61632-3](https://doi.org/10.1016/S0079-8169(08)61632-3) ([↑ 39](#)).
- [Nag+19] M. NAGEL, P. ORSON, J. PARK, and M. POWELL. Smooth and topological almost concordance. *Int. Math. Res. Not. IMRN* 1.23 (2019), pp. 7324–7355. ISSN: 1073-7928. DOI: [10.1093/imrn/rnx338](https://doi.org/10.1093/imrn/rnx338). arXiv: [1707.01147](https://arxiv.org/abs/1707.01147) [[math.GT](#)] ([↑ 69, 79](#)).
- [Nak81] Y. NAKANISHI. A note on unknotting number. *Math. Sem. Notes Kobe Univ.* 9.1 (1981), pp. 99–108. ISSN: 0385-633x ([↑ 26](#)).
- [NS20] P. NAYLOR and H. SCHWARTZ. *Gluck twisting roll spun knots*. 2020. arXiv: [2009.05703](https://arxiv.org/abs/2009.05703) [[math.GT](#)] ([↑ 29, 37](#)).
- [Nor69] R. A. NORMAN. Dehn’s lemma for certain 4-manifolds. *Invent. Math.* 7 (1969), pp. 143–147. ISSN: 0020-9910. DOI: [10.1007/BF01389797](https://doi.org/10.1007/BF01389797) ([↑ 10, 78](#)).
- [Ord06] P. ORDING. “On knot Floer homology of satellite (1,1) knots”. PhD thesis. Columbia University, 2006, p. 157. ISBN: 978-0542-64232-6 ([↑ 89](#)).
- [Ord13] P. ORDING. Constructing doubly-pointed Heegaard diagrams compatible with (1, 1) knots. *J. Knot Theory Ramifications* 22.11 (2013), pp. 1350071, 26. ISSN: 0218-2165. DOI: [10.1142/S0218216513500715](https://doi.org/10.1142/S0218216513500715). arXiv: [1110.5675](https://arxiv.org/abs/1110.5675) [[math.GT](#)] ([↑ 89](#)).
- [OS03] P. OZSVÁTH and Z. SZABÓ. Knot Floer homology and the four-ball genus. *Geom. Topol.* 7 (2003), pp. 615–639. ISSN: 1465-3060. DOI: [10.2140/gt.2003.7.615](https://doi.org/10.2140/gt.2003.7.615). arXiv: [math/0301149](https://arxiv.org/abs/math/0301149) [[math.GT](#)] ([↑ 8, 83, 127](#)).
- [OS04a] P. OZSVÁTH and Z. SZABÓ. Holomorphic disks and knot invariants. *Adv. Math.* 186.1 (2004), pp. 58–116. ISSN: 0001-8708. DOI: [10.1016/j.aim.2003.05.001](https://doi.org/10.1016/j.aim.2003.05.001). arXiv: [math/0209056](https://arxiv.org/abs/math/0209056) [[math.GT](#)] ([↑ 82, 83](#)).
- [OS04b] P. OZSVÁTH and Z. SZABÓ. Holomorphic disks and three-manifold invariants: properties and applications. *Ann. of Math. (2)* 159.3 (2004), pp. 1159–1245. ISSN: 0003-486X. DOI: [10.4007/annals.2004.159.1159](https://doi.org/10.4007/annals.2004.159.1159). arXiv: [math/0105202](https://arxiv.org/abs/math/0105202) [[math.GT](#)] ([↑ 82](#)).
- [OS04c] P. OZSVÁTH and Z. SZABÓ. Holomorphic disks and topological invariants for closed three-manifolds. *Ann. of Math. (2)* 159.3 (2004), pp. 1027–1158. ISSN: 0003-486X. DOI: [10.4007/annals.2004.159.1027](https://doi.org/10.4007/annals.2004.159.1027). arXiv: [math/0101206](https://arxiv.org/abs/math/0101206) [[math.GT](#)] ([↑ 81](#)).
- [OS06] P. OZSVÁTH and Z. SZABÓ. Lectures on Heegaard Floer homology. In: *Floer homology, gauge theory, and low-dimensional topology*. Vol. 5. Clay Math. Proc. Amer. Math. Soc., Providence, RI, 2006, pp. 29–70 ([↑ 81](#)).
- [OST08] P. OZSVÁTH, Z. SZABÓ, and D. THURSTON. Legendrian knots, transverse knots and combinatorial Floer homology. *Geom. Topol.* 12.2 (2008), pp. 941–980. ISSN: 1465-3060. DOI: [10.2140/gt.2008.12.941](https://doi.org/10.2140/gt.2008.12.941). arXiv: [math/0611841](https://arxiv.org/abs/math/0611841) [[math.GT](#)] ([↑ 83](#)).
- [Per03] G. PERELMAN. *Finite extinction time for the solutions to the Ricci flow on certain three-manifolds*. 2003. arXiv: [math/0307245](https://arxiv.org/abs/math/0307245) [[math.DG](#)] ([↑ 39, 69, 71](#)).
- [Pet09] T. PETERS. *On L-spaces and non left-orderable 3-manifold groups*. 2009. arXiv: [0903.4495](https://arxiv.org/abs/0903.4495) [[math.GT](#)] ([↑ 82](#)).
- [Plo84] S. P. PLOTNICK. Fibered knots in S^4 —twisting, spinning, rolling, surgery, and branching. In: *Four-manifold theory (Durham, N.H., 1982)*. Vol. 35. Contemp. Math. Amer. Math. Soc., Providence, RI, 1984, pp. 437–459. DOI: [10.1090/conm/035/780592](https://doi.org/10.1090/conm/035/780592) ([↑ 39](#)).

- [PRT21] M. POWELL, A. RAY, and P. TEICHNER. *The 4-dimensional disc embedding theorem and dual spheres*. 2021. arXiv: [2006.05209](https://arxiv.org/abs/2006.05209) [[math.GT](#)] (↑ 19).
- [Qui86] F. QUINN. Isotopy of 4-manifolds. *J. Differential Geom.* 24.3 (1986), pp. 343–372. ISSN: 0022-040X (↑ 19).
- [Rao20] K. RAOUX. τ -invariants for knots in rational homology spheres. *Algebr. Geom. Topol.* 20.4 (2020), pp. 1601–1640. ISSN: 1472-2747. DOI: [10.2140/agt.2020.20.1601](https://doi.org/10.2140/agt.2020.20.1601). arXiv: [1611.09415](https://arxiv.org/abs/1611.09415) [[math.GT](#)] (↑ 83, 127).
- [Ras10] J. RASMUSSEN. Khovanov homology and the slice genus. *Invent. Math.* 182.2 (2010), pp. 419–447. ISSN: 0020-9910. DOI: [10.1007/s00222-010-0275-6](https://doi.org/10.1007/s00222-010-0275-6). arXiv: [math/0402131](https://arxiv.org/abs/math/0402131) [[math.GT](#)] (↑ 7, 8).
- [Ras03] J. A. RASMUSSEN. “Floer homology and knot complements”. Thesis (Ph.D.)—Harvard University. PhD thesis. 2003, p. 126. ISBN: 978-0496-39374-9. arXiv: [math/0306378](https://arxiv.org/abs/math/0306378) [[math.GT](#)] (↑ 82).
- [Ray15] A. RAY. Satellite operators with distinct iterates in smooth concordance. *Proc. Amer. Math. Soc.* 143.11 (2015), pp. 5005–5020. ISSN: 0002-9939. DOI: [10.1090/proc/12625](https://doi.org/10.1090/proc/12625). arXiv: [1403.3883](https://arxiv.org/abs/1403.3883) [[math.GT](#)] (↑ 110).
- [RR17] A. RAY and D. RUBERMAN. Four-dimensional analogues of Dehn’s lemma. *J. Lond. Math. Soc. (2)* 96.1 (2017), pp. 111–132. ISSN: 0024-6107. DOI: [10.1112/jlms.12062](https://doi.org/10.1112/jlms.12062). arXiv: [1608.08654](https://arxiv.org/abs/1608.08654) [[math.GT](#)] (↑ 98).
- [Roh71] V. A. ROHLIN. Two-dimensional submanifolds of four-dimensional manifolds. *Funkcional. Anal. i Priložen.* 5.1 (1971). <https://www.maths.ed.ac.uk/~v1ranick/papers/rohlin2.pdf>, pp. 48–60. ISSN: 0374-1990 (↑ 71, 72).
- [Rol90] D. ROLFSEN. *Knots and links*. Vol. 7. Mathematics Lecture Series. Corrected reprint of the 1976 original. Publish or Perish, Inc., Houston, TX, 1990, pp. xiv+439 (↑ 26, 105).
- [Rup21a] B. M. RUPPIK. *Casson-Whitney unknotting, Group trisections and Suciu’s ribbon 2-knots in SageMath/GAP*. <https://github.com/ben300694/knot-theory>. Dec. 2021 (↑ 6, 12, 13, 15, 54, 58, 59, 109, 133, 154).
- [Rup21b] B. M. RUPPIK. *Concordances in (non-orientable 3-manifold) \times $[0, 1]$* . MATRIX-MFO Tandem Workshop: Invariants and Structures in Low-Dimensional Topology. To appear: Oberwolfach Report 2021-09. 2021 (↑ 13, 69).
- [Rus05] R. RUSTAMOV. *On plumbed L-spaces*. 2005. arXiv: [math/0505349](https://arxiv.org/abs/math/0505349) [[math.GT](#)] (↑ 81).
- [Sag21] SAGE DEVELOPERS. *SageMath, the Sage Mathematics Software System (Version 9.2)*. <https://www.sagemath.org>. 2021 (↑ 54).
- [Sat00] S. SATOH. Virtual knot presentation of ribbon torus-knots. *J. Knot Theory Ramifications* 9.4 (2000), pp. 531–542. ISSN: 0218-2165. DOI: [10.1142/S0218216500000293](https://doi.org/10.1142/S0218216500000293) (↑ 49, 50).
- [Sat04] S. SATOH. A note on unknotting numbers of twist-spun knots. *Kobe J. Math.* 21.1-2 (2004), pp. 71–82. ISSN: 0289-9051 (↑ 28, 34).
- [Sav12] N. SAVELIEV. *Lectures on the topology of 3-manifolds, An introduction to the Casson invariant*. revised. De Gruyter Textbook. Walter de Gruyter & Co., Berlin, 2012, pp. xii+207. ISBN: 978-3-11-025035-0. DOI: [10.1515/9783110806359](https://doi.org/10.1515/9783110806359) (↑ 98).
- [Sch85] M. G. SCHARLEMANN. Unknotting number one knots are prime. *Invent. Math.* 82.1 (1985), pp. 37–55. ISSN: 0020-9910. DOI: [10.1007/BF01394778](https://doi.org/10.1007/BF01394778) (↑ 18, 37).
- [Sch03] R. SCHNEIDERMAN. Algebraic linking numbers of knots in 3-manifolds. *Algebr. Geom. Topol.* 3 (2003), pp. 921–968. ISSN: 1472-2747. DOI: [10.2140/agt.2003.3.921](https://doi.org/10.2140/agt.2003.3.921). arXiv: [math/0202024](https://arxiv.org/abs/math/0202024) [[math.GT](#)] (↑ 8, 65, 71, 75, 76, 123).
- [ST19] R. SCHNEIDERMAN and P. TEICHNER. *Homotopy versus isotopy: spheres with duals in 4-manifolds*. 2019. arXiv: [1904.12350](https://arxiv.org/abs/1904.12350) [[math.GT](#)] (↑ 6, 41–44).
- [Sch01] S. SCHÖNENBERGER. *A manifold with unique tight contact structure*, Diplomarbeit—ETH Zürich. 2001 (↑ 108).
- [Sch14] J. SCHULTENS. *Introduction to 3-manifolds*. Vol. 151. Graduate Studies in Mathematics. American Mathematical Society, Providence, RI, 2014, pp. x+286. ISBN: 978-1-4704-1020-9. DOI: [10.1090/gsm/151](https://doi.org/10.1090/gsm/151) (↑ 105).
- [Sch19] H. R. SCHWARTZ. Equivalent non-isotopic spheres in 4-manifolds. *J. Topol.* 12.4 (2019), pp. 1396–1412. ISSN: 1753-8416. DOI: [10.1112/topo.12121](https://doi.org/10.1112/topo.12121). arXiv: [1806.07541](https://arxiv.org/abs/1806.07541) [[math.GT](#)] (↑ 42).

- [Sch21] H. R. SCHWARTZ. *A 4-dimensional light bulb theorem for disks*. 2021. arXiv: [2109.13397](https://arxiv.org/abs/2109.13397) [[math.GT](#)] ([↑ 21](#)).
- [Sin20] O. SINGH. Distances between surfaces in 4-manifolds. *J. Topol.* 13.3 (2020), pp. 1034–1057. ISSN: 1753-8416. DOI: [10.1112/topo.12148](https://doi.org/10.1112/topo.12148). arXiv: [1905.00763](https://arxiv.org/abs/1905.00763) [[math.GT](#)] ([↑ 4, 6, 22, 41, 42](#)).
- [Sma58] S. SMALE. A classification of immersions of the two-sphere. *Trans. Amer. Math. Soc.* 90 (1958), pp. 281–290. ISSN: 0002-9947. DOI: [10.2307/1993205](https://doi.org/10.2307/1993205) ([↑ 19](#)).
- [Cul+21] M. CULLER, N. M. DUNFIELD, M. GOERNER, and J. R. WEEKS. *SnapPy, a computer program for studying the geometry and topology of 3-manifolds*. <http://snappy.computop.org>. 2021 ([↑ 109](#)).
- [Sta83] J. R. STALLINGS. Topology of finite graphs. *Invent. Math.* 71.3 (1983), pp. 551–565. ISSN: 0020-9910. DOI: [10.1007/BF02095993](https://doi.org/10.1007/BF02095993) ([↑ 139, 145](#)).
- [Sti02] A. I. STIPSICZ. Gauge theory and Stein fillings of certain 3-manifolds. *Turkish J. Math.* 26.1 (2002), pp. 115–130. ISSN: 1300-0098 ([↑ 108](#)).
- [Sto94] R. STONG. Existence of π_1 -negligible embeddings in 4-manifolds. A correction to Theorem 10.5 of Freedmann and Quinn. *Proc. Amer. Math. Soc.* 120.4 (1994), pp. 1309–1314. ISSN: 0002-9939. DOI: [10.2307/2160253](https://doi.org/10.2307/2160253) ([↑ 42](#)).
- [Suc85] A. I. SUCIU. Infinitely many ribbon knots with the same fundamental group. *Math. Proc. Cambridge Philos. Soc.* 98.3 (1985), pp. 481–492. ISSN: 0305-0041. DOI: [10.1017/S0305004100063684](https://doi.org/10.1017/S0305004100063684) ([↑ 17, 53, 54, 56, 164, 165](#)).
- [Suz69] S. SUZUKI. Local knots of 2-spheres in 4-manifolds. *Proc. Japan Acad.* 45 (1969), pp. 34–38. ISSN: 0021-4280 ([↑ 10, 68, 78](#)).
- [Swe01] F. J. SWENTON. On a calculus for 2-knots and surfaces in 4-space. *J. Knot Theory Ramifications* 10.8 (2001), pp. 1133–1141. ISSN: 0218-2165. DOI: [10.1142/S0218216501001359](https://doi.org/10.1142/S0218216501001359) ([↑ 54](#)).
- [Tan07] K. TANAKA. Inequivalent surface-knots with the same knot quandle. *Topology Appl.* 154.15 (2007), pp. 2757–2763. ISSN: 0166-8641. DOI: [10.1016/j.topol.2007.05.010](https://doi.org/10.1016/j.topol.2007.05.010). arXiv: [math/0512099](https://arxiv.org/abs/math/0512099) [[math.GT](#)] ([↑ 137](#)).
- [Ter93] M. TERAGAITO. Roll-spun knots. *Math. Proc. Cambridge Philos. Soc.* 113.1 (1993), pp. 91–96. ISSN: 0305-0041. DOI: [10.1017/S0305004100075794](https://doi.org/10.1017/S0305004100075794) ([↑ 37–39](#)).
- [Ter94a] M. TERAGAITO. Corrigenda: “Roll-spun knots” [*Math. Proc. Cambridge Philos. Soc.* **113** (1993), no. 1, 91-96; MR1188820 (93k:57024)]. *Math. Proc. Cambridge Philos. Soc.* 116.1 (1994), p. 191. ISSN: 0305-0041. DOI: [10.1017/S0305004100072480](https://doi.org/10.1017/S0305004100072480) ([↑ 39](#)).
- [Ter94b] M. TERAGAITO. Twist-roll spun knots. *Proc. Amer. Math. Soc.* 122.2 (1994), pp. 597–599. ISSN: 0002-9939. DOI: [10.2307/2161054](https://doi.org/10.2307/2161054) ([↑ 13, 39](#)).
- [Tri69] A. G. TRISTRAM. Some cobordism invariants for links. *Proc. Cambridge Philos. Soc.* 66 (1969), pp. 251–264. ISSN: 0008-1981. DOI: [10.1017/s0305004100044947](https://doi.org/10.1017/s0305004100044947) ([↑ 73–75, 130](#)).
- [Van10] C. A. VAN COTT. Ozsváth-Szabó and Rasmussen invariants of cable knots. *Algebr. Geom. Topol.* 10.2 (2010), pp. 825–836. ISSN: 1472-2747. DOI: [10.2140/agt.2010.10.825](https://doi.org/10.2140/agt.2010.10.825). arXiv: [0803.0500](https://arxiv.org/abs/0803.0500) [[math.GT](#)] ([↑ 115](#)).
- [Var21] K. VARVAREZOS. *Heegaard Floer homology and chirally cosmetic surgeries*. 2021. arXiv: [2112.03144](https://arxiv.org/abs/2112.03144) [[math.GT](#)] ([↑ 85](#)).
- [Wal68] F. WALDHAUSEN. On irreducible 3-manifolds which are sufficiently large. *Ann. of Math. (2)* 87 (1968), pp. 56–88. ISSN: 0003-486X. DOI: [10.2307/1970594](https://doi.org/10.2307/1970594) ([↑ 137](#)).
- [Wal99] C. T. C. WALL. *Surgery on compact manifolds*. Second. Vol. 69. Mathematical Surveys and Monographs. Edited and with a foreword by A. A. Ranicki. American Mathematical Society, Providence, RI, 1999, pp. xvi+302. ISBN: 0-8218-0942-3. DOI: [10.1090/surv/069](https://doi.org/10.1090/surv/069) ([↑ 71](#)).
- [Wan15] A. WAND. Tightness is preserved by Legendrian surgery. *Ann. of Math. (2)* 182.2 (2015), pp. 723–738. ISSN: 0003-486X. DOI: [10.4007/annals.2015.182.2.8](https://doi.org/10.4007/annals.2015.182.2.8). arXiv: [1404.1705](https://arxiv.org/abs/1404.1705) [[math.GT](#)] ([↑ 109](#)).
- [Yaj62] T. YAJIMA. On the fundamental groups of knotted 2-manifolds in the 4-space. *J. Math. Osaka City Univ.* 13 (1962), pp. 63–71. ISSN: 0449-2773 ([↑ 49](#)).
- [Yas91] A. YASUHARA. (2,15)-torus knot is not slice in $\mathbb{C}P^2$. *Proc. Japan Acad. Ser. A Math. Sci.* 67.10 (1991), pp. 353–355. ISSN: 0386-2194 ([↑ 10, 72, 129](#)).
- [Yas92] A. YASUHARA. On slice knots in the complex projective plane. *Rev. Mat. Univ. Complut. Madrid* 5.2-3 (1992). <http://www.mat.ucm.es/serv/revista/vol5-23/vol5-23h.pdf>, pp. 255–276. ISSN: 0214-3577 ([↑ 72](#)).

- [Yas96] A. YASUHARA. Connecting lemmas and representing homology classes of simply connected 4-manifolds. *Tokyo J. Math.* 19.1 (1996), pp. 245–261. issn: 0387-3870. doi: [10.3836/tjm/1270043232](https://doi.org/10.3836/tjm/1270043232) (↑ 131).
- [Yil18] E. Z. YILDIZ. A note on knot concordance. *Algebr. Geom. Topol.* 18.5 (2018), pp. 3119–3128. issn: 1472-2747. doi: [10.2140/agt.2018.18.3119](https://doi.org/10.2140/agt.2018.18.3119). arXiv: [1707.01650](https://arxiv.org/abs/1707.01650) [math.GT] (↑ 75, 80).
- [Yos94] K. YOSHIKAWA. An enumeration of surfaces in four-space. *Osaka J. Math.* 31.3 (1994), pp. 497–522. issn: 0030-6126 (↑ 54).
- [Zee65] E. C. ZEEMAN. Twisting spun knots. *Trans. Amer. Math. Soc.* 115 (1965), pp. 471–495. issn: 0002-9947. doi: [10.2307/1994281](https://doi.org/10.2307/1994281) (↑ 31, 52, 157, 158).
- [Zho20] H. ZHOU. *Homology concordance and an infinite rank subgroup*. 2020. arXiv: [2009.05145](https://arxiv.org/abs/2009.05145) [math.GT] (↑ 14, 87, 104).

INDEX

- $(M^3 \times [0, 1])$ -4-genus, 69
- 2-knot, 18

- Alexander polynomial
 - in ZHS^3 , 103
- almost concordance, 79
- Arf invariant, 78
- associated graded, 82

- banded unlink diagram, 54
- basis
 - filtered, 86
 - simplified, 87
- Bing double, 122
- boundary link, 122
- bounded punctured, 66
- box tensor product, 84
- bridge
 - number, 135
 - trisection, 135

- cable knot, 112
- Casson-Whitney
 - length, 4, 22
 - number, algebraic, 26
 - number, geometric, 22
- central surface, 134
- concordance
 - for knots, 67
 - for links, 122
- covering move, 127
- cut system, 81

- determinant, 18
- diagram
 - shadow, 141
 - triplane, 148, 164
- disk
 - bridge, 141
- distinguished component, 88
- double point loop, 75
- dual curve, 98

- exotic, 2

- finger move, 19
 - trivial, 24
- fold, 145

- Fox p -coloring, 18
- fusion number, 46

- generalized braid word, 154
- Gordian distance, 5
- group trisection of knotted surface type, 138
- guiding arc, 24

- handle ribbon, 51
- handlebody, 135
- Heegaard diagram
 - bordered, 81, 85
 - doubly pointed, 81
- Heegaard Floer homology, 82
- homotopy
 - 4-ball, 2
 - 4-sphere, 2
 - arc-standard, 42
 - regular, 19

- integral homology 3-sphere, ZHS^3 , 80

- knot
 - stabilizing number, 78
 - trace, 71, 98
- Knot Floer complex
 - full, 83
 - minus, 83
- knotted surface group, 137

- L-space, 82
- Lagrangian Floer homology, 85
- Legendrian, 109
- link
 - group, 139
 - homotopy, 122
- linking number, 98
- local knot, 68
- locally flat, 66

- Ma-Qiu index $a(K)$, 27
- meridian, 24
- meridional rank, 27, 149

- Nakanishi index $m(K)$, 26
- normal generation, 149

- peripheral subgroup, 21
- Poincaré

- complex, 2
- conjecture, 2
- homology sphere, 82, 98
- quadratic 2-type, 3
- rational homology 3-sphere, $\mathbb{Q}HS^3$, 80
- reverse orientation, 98
- ribbon disk, 46
 - double, 46, 54
- ribbon surface, 46
- rim surgery
 - roll-twist, 37
 - twist, 29
- rotation number rot , 109
- satellite knot, 74
- seed strands, 148
- Seifert longitude, 84
- signature
 - Levine-Tristram, 130
- slice
 - H -slice, 66
 - deep slice, 66
 - shallow slice, 66
 - strong slice, 122
- spine, 136
- spun knot, 34
 - roll-twist, 37
 - twist, 34
- stabilization, 22
 - length, 41
 - number, algebraic, 26
 - number, geometric, 23
 - trivial, 24
- standard $\mathbb{R}P^2$, 59
- Thurston-Bennequin number tb , 109
- topological realization, 142
- trisection, 134
 - parameterized, 136
- trivial
 - disk system, 135
 - tangle, 135
 - tangle homomorphism, 138
- tube map, 50
- universal slicing manifold, 129
- unknotting number, 4
- Whitehead double, 76, 77
 - twisted, 84
- Whitney move, 19
- Wirtinger algorithm, 148

CURRICULUM VITAE

Personal Details

Name | BENJAMIN MATTHIAS RUPPIK

Education

2018 – 2022 | *Doctoral Student*,
RHEINISCHE FRIEDRICH-WILHELMS-UNIVERSITÄT, BONN, GERMANY.

2016 – 2018 | *Master of Science in Mathematics*,
RHEINISCHE FRIEDRICH-WILHELMS-UNIVERSITÄT, BONN, GERMANY.

2013 – 2016 | *Bachelor of Science in Mathematics*,
RHEINISCHE FRIEDRICH-WILHELMS-UNIVERSITÄT, BONN, GERMANY.

2007 – 2013 | *High School (Abitur)*,
GYMNASIUM HAUS OVERBACH, JÜLICH, GERMANY

Publications & Preprints

- 2021 | Klug, M., & Ruppik, B. (2021). Deep and shallow slice knots in 4-manifolds. Proceedings of the American Mathematical Society, Series B, 8(17), 204-218.
- 2021 | Joseph, J., Klug, M., Ruppik, B., & Schwartz, H. (2021). Unknotting numbers of 2-spheres in the 4-sphere. Journal of Topology, 14.4, 1321-1350.
- 2021 | Kasprowski, D., Nicholson, J., & Ruppik, B. (2021). Homotopy classification of 4-manifolds whose fundamental group is dihedral. To appear: Algebraic & Geometric Topology.
- 2021 | Ruppik, B. (2021). Concordances in $(\text{non-orientable } 3\text{-manifold}) \times [0, 1]$. MATRIX-MFO Tandem Workshop: Invariants and Structures in Low-Dimensional Topology, Oberwolfach Report 2021-09.
- 2020 | Kasprowski, D., Powell, M., & Ruppik, B. (2020). Homotopy classification of 4-manifolds with finite abelian 2-generator fundamental groups. [arXiv:2005.00274](https://arxiv.org/abs/2005.00274).

MAX-PLANCK-INSTITUT FÜR MATHEMATIK, BONN

Email address: bruppikmath@gmail.com